Mechanistic model-based drug development in the management of anticancer drugs resistance

Alexandre Sostelly

Université Claude Bernard Lyon 1

UNIVERSITÉ DE LYON

N° d'ordre : Année 2012

THÈSE DE L'UNIVERSITÉ DE LYON

délivrée par

L'UNIVERSITÉ CLAUDE BERNARD - LYON 1

EDISS

pour l'obtention du

DIPLÔME DE DOCTORAT

(arrêté du 7 août 2006)

soutenue publiquement le 2 novembre 2012 par

Alexandre SOSTELLY

Mechanistic model-based drug development in the management of anticancer drugs resistance

---

Composition du jury

M. Joseph Ciccolini	Rapporteur
M. Nicolas Simon	Rapporteur
M. Gilles Freyer	
M. Gilles Paintaud	
M. Michel Tod	Directeur de thèse

"We made science as we built houses; but an accumulation of facts is no more a science than a heap of stones is a house"

Henri POINCARE
La Science et l'hypothèse, 1908

UNIVERSITE CLAUDE BERNARD - LYON 1

Président de l'Université	**M. François-Noël GILLY**
Vice-président du Conseil d'Administration	M. le Professeur Hamda BEN HADID
Vice-président du Conseil des Etudes et de la Vie Universitaire	M. le Professeur Philippe LALLE
Vice-président du Conseil Scientifique	M. le Professeur Germain GILLET
Secrétaire Général	M. Alain HELLEU

COMPOSANTES SANTE

Faculté de Médecine Lyon Est – Claude Bernard	*Directeur* : M. le Professeur J. ETIENNE
Faculté de Médecine et de Maïeutique Lyon Sud – Charles Mérieux	*Administrateur provisoire* : M. le Professeur G. KIRKORIAN
UFR d'Odontologie	*Directeur* : M. le Professeur D. BOURGEOIS
Institut des Sciences Pharmaceutiques et Biologiques	*Directeur* : Mme la Professeure C. VINCIGUERRA
Institut des Sciences et Techniques de la Réadaptation	*Directeur* : M. le Professeur Y. MATILLON
Département de formation et Centre de Recherche en Biologie Humaine	*Directeur* : M. le Professeur P. FARGE

COMPOSANTES ET DEPARTEMENTS DE SCIENCES ET TECHNOLOGIE

Faculté des Sciences et Technologies	*Directeur* : M. le Professeur F. De MARCHI
Département Biologie	*Directeur* : M. le Professeur F. FLEURY
Département Chimie Biochimie	*Directeur* : Mme la Professeure H. PARROT
Département GEP	*Directeur* : M. N. SIAUVE
Département Informatique	*Directeur* : M. le Professeur S. AKKOUCHE
Département Mathématiques	*Directeur* : M. le Professeur A. GOLDMAN
Département Mécanique	*Directeur* : M. le Professeur H. BEN HADID
Département Physique	*Directeur* : Mme S. FLECK
Département Sciences de la Terre	*Directeur* : Mme la Professeure I. DANIEL
UFR Sciences et Techniques des Activités Physiques et Sportives	*Directeur* : M. C. COLLIGNON
Observatoire de Lyon	*Directeur* : M. B. GUIDERDONI
Polytech Lyon	*Directeur* : M. P. FOURNIER
Ecole Supérieure de Chimie Physique Electronique	*Directeur* : M. G. PIGNAULT
Institut Universitaire de Technologie de Lyon 1	*Directeur* : M. C. VITON
Institut Universitaire de Formation des Maîtres	*Directeur* : M. R. BERNARD
Institut de Science Financière et d'Assurances	*Directeur* : Mme la Professeure V. MAUME-DESCHAMPS

Preface

This Ph.D work has been carried out at the EMR3738, Chemotherapy Targeting in Oncology, University Claude Bernard Lyon 1 (Lyon, France) and at the Department of Pharmaceutical BioSciences, Uppsala University (Uppsala, Sweden). This collaboration has been made possible notably thanks to the support of the Explora'Doc grant program the Région Rhône-Alpes.

Abstract

Anticancer drug resistance is a major issue in the management of cancer disease. Efflux transporters contribute to the multidrug resistance by altering the intracellular disposition of cytotoxic drugs. In the past, the inhibition of P-gp efflux transporter essentially failed because of the lack of adequate methods to identify their mechanisms of action. Recently, new inhibitors of BCRP, one of the latest efflux transporter that have been discovered, have been developed that allow re-testing the multidrug resistance inhibition through efflux inhibition. Nevertheless, to avoid the same issues of development as for P-gp inhibitors, new methods have to be used.

This PhD work aims to demonstrate the benefits of mechanistic models to support the development of efflux transporter inhibitors and more generally of oncology compounds through two axes:

- The development of mechanistic models of the interaction between cytotoxic and efflux transporter inhibitors

- The development of quantitative tumour growth inhibition models to early evaluate oncology compounds and optimize patients' response

The results obtained with this approach allow the identification of key mechanisms of efflux transporter inhibitors and demonstrate the power of modelling and simulation to support oncology drug development.

Résumé

La résistance aux chimiothérapies anticancéreuses constitue un problème majeur dans la prise en charge du cancer. Les transporteurs d'efflux contribuent à ce phénomène de résistance en altérant l'accumulation intracellulaire des cytotoxiques. Dans le passé, l'inhibition du transporteur d'efflux P-gp n'a pas permis de surmonter ce phénomène notamment à cause du manque de méthodes adéquates pour identifier et quantifier la pharmacologie des inhibiteurs d'efflux. Récemment de nouveaux inhibiteurs de BCRP, l'un des derniers transporteurs d'efflux découverts, ont été synthétisés permettant de re-tester l'intérêt de l'inhibition de ces transporteurs dans la prise en charge de la résistance aux anticancéreux. Néanmoins, afin d'éviter les mêmes écueils que lors du développement des inhibiteurs de P-gp, il est nécessaire d'utiliser d'autres approches telles que la modélisation mathématique dès le début du développement préclinique de ces inhibiteurs. Cette thèse a pour but de montrer les bénéfices de la modélisation et de la simulation dans le développement préclinique des inhibiteurs de transporteurs d'efflux et plus largement dans le développement des molécules anticancéreuses. L'exemple utilisé au travers de ce travail concerne l'étude de l'interaction entre l'irinotecan, un cytotoxique largement utilisé dans le traitement du cancer colorectal, et le MBLI87, un nouvel inhibiteur de BCRP.

Deux principaux axes ont été abordés dans ce travail :

- Le développement de modèles (semi-) mécanistiques à effets mixtes pour identifier et quantifier les facteurs impactant l'efficacité de la combinaison irinotecan-MBLI87
- Le développement de modèles d'inhibition de la croissance tumorale à effets mixtes pour évaluer précocement ce type d'interaction de traitements et pour optimiser la réponse tumorale

Les résultats obtenus avec l'approche de modélisation ont permis d'identifier certains des mécanismes tumoraux impactant l'efficacité des inhibiteurs de transporteur d'efflux. De plus cette approche s'est révélée supérieure aux approches classiques dans l'évaluation de ces molécules et dans l'optimisation de la réponse tumorale démontrant la puissance de la modélisation et de la simulation comme outil de développement des molécules anticancéreuses.

List of Publications

This thesis is based on the following publications:

1. A template model for studying anticancer drug efflux transporter inhibitors *in vitro*
   Alexandre SOSTELLY, Léa PAYEN, Jérôme GUITTON, Attilio DI PIETRO, Pierre FALSON, Mylène HONORAT, Glaucio VALDAMERI, Annabelle GEZE , Ahcène BOUMENDJEL, Gilles FREYER, Michel TOD
   Accepted in Fundamental and Clinical Pharmacology

2. Characterization on the interaction between cytotoxic drug and efflux transporter inhibitor with a multiscale semi-mechanistic PKPD model
   Alexandre SOSTELLY, Léa PAYEN, Jérôme GUITTON, Attilio DI PIETRO, Pierre FALSON, Mylène HONORAT, Annabelle GEZE , Ahcène BOUMENDJEL, Gilles FREYER, Michel TOD
   In manuscript

3. Quantitative evaluation of the combination between cytotoxic drug and efflux transporter inhibitors based on a tumour growth inhibition model
   Alexandre SOSTELLY, Léa PAYEN, Jérôme GUITTON, Attilio DI PIETRO, Pierre FALSON, Mylène HONORAT, Annabelle GEZE , Ahcène BOUMENDJEL, Gilles FREYER, Michel TOD
   Acceptable in Fundamental and Clinical Pharmacology

4. Dose schedule optimization of anticancer drugs
   Alexandre SOSTELLY, Joakim NYBERG, Mats O. KARLSSON, Andrew C. HOOKER
   Submitted to AAPS Journal

Related paper:

1. Can we predict chemo-induced hematotoxicity in elderly patients treated with Pegylated Liposomal Doxorubicin? Results of a population-based model derived from the DOGMES phase II Trial of the GINECO
   Alexandre SOSTELLY, Emilie HENIN, Laure CHAUVENET, Anne-Claire HARDY-BESSARD, Véronique JESTIN-LE TALLEC, Sylvie KIRSHER, Cécile LEYRONNAS, Catherine LIGEZA-POISSON, Soraya RAMDANE, Jacques SALAVT, Sylvie VAN-HULT, Jean-Michel VANNETZEL, Gilles FREYER, Michel TOD, Claire FALANDRY
   Accepted in Journal of Geriatric Oncology

List of Communications

Oral communications

1. A template model for studying anticancer drug efflux inhibitors in-vitro
   SOSTELLY Alexandre, PAYEN Léa, GUITTON Jérôme, DI PETRO Attilio, FALSON Pierre, BOUMENDJEL Ahcène, FREYER Gilles, TOD Michel
   Young researcher session, GMP (Pharmacokinetic and Metabolism Group), October 2011, Paris (France)

2. Irinotecan intracellular penetration modeling in presence of BCRP inhibitors
   SOSTELLY Alexandre, PAYEN Léa, GUITTON Jérôme, DI PETRO Attilio, FALSON Pierre, BOUMENDJEL Ahcène, FREYER Gilles, TOD Michel
   Young researcher session, 13e journée du GPCO (Group of Clinical Pharmacology in Oncology), November 2010, Nîmes (France)

3. Optimization of the irinotecan, MBLI-87 combination for treating irinotecan resistant tumors
   SOSTELLY Alexandre, PAYEN Léa, RIBBA Benjamin, GIRARD Pascal, DI PETRO Attilio, FALSON Pierre, BOUMENDJEL Ahcène, FREYER Gilles, TOD Michel
   Non Clinical Statistics Conference, September 2010, Lyon (France)

Posters

1. Dose and dose schedule optimization of anticancer drugs
   SOSTELLY Alexandre, NYBERG Joakim, KARLSSON Mats O., HOOKER Andrew C.
   21st PAGE meeting, June 2012, Venice (Italy)

2. Tumor accessibility and composition play a major role on the efficiency of efflux transporter inhibitor – cytotoxic drug combination: Analysis with a mathematical model
   SOSTELLY Alexandre, PAYEN Léa, GUITTON Jérôme, DI PETRO Attilio, FALSON Pierre, BOUMENDJEL Ahcène, FREYER Gilles, TOD Michel
   103rd AACR Annual meeting, March 2012, Chicago (USA)
   Proceedings of the 103rd Annual Meeting of the American Association for Cancer Research; 2012 Mar 31-Apr 4; Chicago, IL. Philadelphia (PA): AACR; Cancer Res 2012; 72(8 Suppl): Abstract nr 3972.

3. Multiscale semi-mechanistic PKPD modeling of the interaction between irinotecan and ABCG2 inhibitors: A modeling tool to support preclinical development

SOSTELLY Alexandre, PAYEN Léa, GUITTON Jérôme, DI PETRO Attilio, FALSON Pierre, BOUMENDJEL Ahcène, FREYER Gilles, TOD Michel

GMP (Pharmacokinetic and Metabolism Group),
October 2011, Paris (France)

4. Characterization of the interaction between irinotecan, SN-38 and MBLI-87, a new BCRP inhibitor, with a multi-scale semi-mechanistic PKPD model

SOSTELLY Alexandre, PAYEN Léa, GUITTON Jérôme, DI PETRO Attilio, FALSON Pierre, BOUMENDJEL Ahcène, FREYER Gilles, TOD Michel

20th PAGE meeting, June 2011, Athens (Greece)

5. Predicting chemo-induced hematotoxicity in elderly metastatic breast patients treated by Pegylated Liposomal Doxorubicin (PLD): a population-based analysis on data coming from the DOGMES phase II GINECO study

SOSTELLY Alexandre, FALANDRY Claire, PUJADE-LAURAINE Eric, FREYER Gilles, TOD Michel

2011 ASCO meeting, June 2011, Chicago (USA)
J Clin Oncol 29: 2011 (suppl; abstr 19740)

6. Application of modeling and simulation to the development of MBLI-87, a new BCRP inhibitor

SOSTELLY Alexandre, PAYEN Léa, DI PETRO Attilio, FALSON Pierre, BOUMENDJEL Ahcène, FREYER Gilles, TOD Michel

102nd AACR Annual meeting, March 2011, Orlando (USA)

7. Optimization of the irinotecan, MBLI-87 combination with population modeling

SOSTELLY Alexandre, PAYEN Léa, DI PETRO Attilio, FALSON Pierre, BOUMENDJEL Ahcène, FREYER Gilles, TOD Michel

13e journée du GPCO (Group of Clinical Pharmacology in Oncology),
November 2010, Nîmes (France)

8. Modeling of the interaction between irinotecan and MBLI-87, a new BCRP inhibitor:

A K-PD tumor growth inhibition including an interaction pharmacodynamic component

SOSTELLY Alexandre, PAYEN Léa, RIBBA Benjamin, GIRARD Pascal, DI PETRO Attilio, FALSON Pierre, BOUMENDJEL Ahcène, FREYER Gilles, TOD Michel

19th PAGE meeting, June 2010, Berlin (Germany)

9. Simultaneous modeling of PSA in Prostatic Benign Hyperplasia (PBH) and prostatic adenocarcinoma patients treated by prostate surgery
SOSTELLY Alexandre, HENIN Emilie, YOU Benoit, GIRARD Pascal, KARLSSON Mats

18th PAGE meeting, June 2009, St-Petersburg (Russia)

Abbreviations

5-FU: 5-Fluoro-uracil
ABC: ATP Binding Cassette
ADP: Adenosine diphosphate
AML: Acute myeloid leukemia
AUC: Area under the curve
ATP: Adenosine triphosphate
BCRP: Breast Cancer Resistance Protein
BSA: Body Surface Area
CA125: Cancer Antigen 125
Cl: Clearance
CPT: Camptothecin
CPT11: Irinotecan
CYP: Cytochrome P
DNA: Deoxyribonucleic acid
EC_{50}: Half maximal effective concentration
FDA: Food and Drug Administration
FO: First order method
FOCE: Fist order conditional estimates method
FIM: Fisher Information Matrix
GI: Gastrointestinal
GoF: Goodness of fit
IC_{50}: Half maximal inhibitory concentration
IV: Intravenous
IIV: Inter-individual variability
IOV: Inter-occasion variability
IP: Intraperitonally
K_e: Elimination constant
kDa: kilo Dalton
MDR: Multidrug resistance
MRP: Multidrug resistance protein
NBD: Nucleotide binding domain
NSCLC: Non-small cell lung cancer
NLME: Non-linear mixed effects
NPDE: Normalized prediction distribution error
OC: Optimal control
ORR: Objective response rate
OS: Overall survival
PD: Pharmacodynamics
PFS: Progression free survival
P-gp: Permeability glycoprotein

PK: Pharmacokinetics
PSA: Prostate specific antigen
PoC: Proof of Concept
SLC: Solute carrier transporter
TGI: Tumour growth inhibition
TMD: Transmembrane domain
TV: Typical value
VPC: Visual predictive check
XME: Xenobiotic metabolization enzymes
WHO: World health organization

Table of contents

Introduction

Anticancer drug resistance is one of the main reason of treatment failures in cancer patients. In the past, the discovery of the function of efflux transporter in tumour resistance led to the development of various compounds that inhibit active cytotoxic efflux from tumour cells. Unfortunately, the development of P-gp inhibitors, the most widely studied efflux transporter, failed to inhibit multidrug resistance in patients despite promising results in animals. The question of overcoming multidrug resistance through the inhibition of others efflux transporters has rarely been addressed. Recently new BCRP inhibitors, one of the latest efflux transporters that have been discovered, have been synthesized. To avoid the same development issues as for P-gp inhibitors, it is necessary to use new methodologies from the beginning of their development.

The purpose of this PhD work was to use mechanistic models to support the development of new efflux inhibitors and more generally to show the benefits of the model-based development for oncology drugs.

After a presentation of the context of this work, three different parts are presented that all contain publications associated to this thesis. The first part deals with the mechanistic modelling of the interaction between cytotoxic and efflux transporter inhibitors *in vitro* and *in vivo*. In the second part, a tumour growth inhibition model of this interaction is presented and the last part shows the benefits of tumour growth inhibition models to optimize patients' response.

All the studies presented in the two first parts result from the collaboration between six different research teams. MBLI87 has been synthesized and formulated at the department of medicinal chemistry from the Joseph Fourier University in Grenoble (Pr. Ahcène Boumendjel, Dr. Annabelle Gèze). Cell cultures, *in vitro* tests and tumour growth

experiments have been carried out at the institute of biology and chemistry of proteins in Lyon (Dr. Attilio Di Pietro, Dr. Pierre Falson, Dr. Léa Payen). Dosages of MBLI87 and irinotecan have been performed at the biochemistry department of Lyon-Sud in Lyon (Pr. Jérôme Guitton, Dr. Léa Payen). Our team, EMR3738 Chemotherapy Targeting in Oncology (Pr. Gilles Freyer, Pr. Michel Tod) intervenes to model all the data generated from all the others teams.

Chapter I

Context of the research

1. Cancer

1.1. Cancer origins and development

Cancer is a generic appellation for a large group of diseases that can affect any parts of the body. According to the World Health Organization (WHO), cancer can be described as the rapid creation of abnormal cells that can invade adjoining parts of the body and spread to others organs (1).

Cancer cells become autocrine and lose their own specificity; they can thus grow beyond their usual boundaries. Modifications of normal cells into tumour cells result from the interaction between genetic factors and external agents, carcinogens (physical, chemical and biological carcinogens). Establishment of cancer disease follows three main phases:

- Initiation: occurrence of punctual DNA mutations resulting from the interaction between genetic factors and external carcinogens.
- Promotion: stimulation of mutated cells by external carcinogens
- Proliferation: escape of mutated cells from regulation system and beginning of proliferation without differentiation

Through the deregulation of genes regulating extracellular functions, tumour cells become able to evade form their primary site to join others organs. This process, called metastasis is an aggravating factor of the disease.

1.2. Cancer epidemiology

Cancer disease is a major public health issue. According to the World Health Organization, cancer causes 7.6 million of deaths worldwide in 2006. Global incidence of cancer disease increased around 60% between 1980 and 2000. Cancer deaths are projected to continue rising with a 13.1 million of deaths expected in 2030 (1).

The most common types of cancer are lung, stomach, liver, colon and breast cancers that together cause the most number of cancer deaths. Prostate and breast cancers are the most frequent cancers in male and female respectively.

The WHO defined five aggravating behavioural factors that explain around 30% of cancer diagnosis: high body mass index, low vegetable intake, lack of physical activity, use of alcohol and tobacco (1).

1.3. Cancer treatments

The choice for the most appropriate treatment depends on the tumour type, localization, development and also on the patient status.

1.3.1. Surgery

Historically, cancer treatment consisted in tumour excision through surgery. Nowadays, this invasive technique is mainly used at early stage of the disease and is always associated to others treatments such as radiotherapy or chemotherapy.

1.3.2. Radiotherapy

Radiotherapy consists in irradiating tissue to prevent cell division by altering their DNA. This loco-regional method targets cells that divide rapidly, such as tumour cells and is often associated to others treatments.

1.3.3. *Chemotherapy*

1.3.3.1. Principle

Chemotherapy is based on the administration of cytotoxic drugs that preferentially target cells that divide rapidly. Chemotherapeutic agents induce cell damage during cell division leading to the inhibition of cell growth and death. Chemotherapy is often envisaged in four therapeutic purposes:

- **Curative chemotherapy**
- **Neo-adjuvant chemotherapy** to reduce tumour burden before surgery or chemotherapy
- **Adjuvant chemotherapy** to prevent metastasis formation after surgery
- **Palliative chemotherapy** for cancer symptom relief

Solid tumours are rarely treatable with chemotherapy alone, but adjuvant chemotherapy is used to reduce relapse and death risks (2-5).

Chemotherapeutic agents affect non-specifically both tumour and normal cells that can lead to toxicities. Dose intensity of cytotoxic agents is thus often limited because of hematotoxicity, whereas the number of cycles is often limited because of cumulative toxicity such as cardiotoxicity following anthracyclines administration.

1.3.3.2. Main classes of chemotherapy

Chemotherapeutic drugs can be classified according to their mechanisms of action (Table 1).

Mechanisms of action	Chemotherapeutic agents
DNA alteration	Alkylating agents (chlomethine) Intercalating agents (daunorubicine, antibiotics) Topoisomerase I and II inhibitors (irinotecan, etoposide) Electrophilic intermediates (platinum derivatives)
Anti-metabolic	Antifolates (methotrexate) Analogues of purine base (6-mercaptopurine) Analogues of pyrimidine base (5-FU, gemcitabine)
Enzymatic inhibitors	Thymidylate synthetase inhibitor (raltitrexed) Ribonucleid diphosphatase reductase inhibitor (hydroxyurea) Dihydrofolate reductase inhibitor (methotrexate)
Cytokines	Interferon α
Anti-mitotic	Vinbastine, Taxanes (paclitaxel)
Tyrosine Kinase inhibitors	Imatinib, Gefitinib

Table 1: Main classes of chemotherapeutic agents

All the studies included in this thesis are focused on the chemotherapeutic agents, irinotecan, CPT11 and capecitabine, the oral pro-drug of 5-FU.

1.3.4. Irinotecan

Irinotecan (CPT11) is a semi-synthetic derivative of the alkaloid plant camptothecine (CPT, *Camptotheca acuminata*) (Figure 1) (7).

Figure 1: *Camptotheca acuminata*

CPT11 is converted by carboxylesterases into 7-ethyl-10-hydroxycamptothecine (SN38), its active metabolite. SN38 is conjugated to an inactive glucuronide (SN38G) by uridine

diphosphatase glucuronosyltransferase (6, 7). CPT11 presents also two inactive metabolites in plasma: 7-ethyl-10-[4-N-(5-aminopentanoic acid)-1-piperidino]-carboxylcamptothecin (APC), 7-ethyl-10-[4-amino-1-piperidino]-carboxylcamptothecin (NPC) resulting from the oxidation of the terminal piperidine ring of CPT11 by CYP450 3A4 (7, 8).

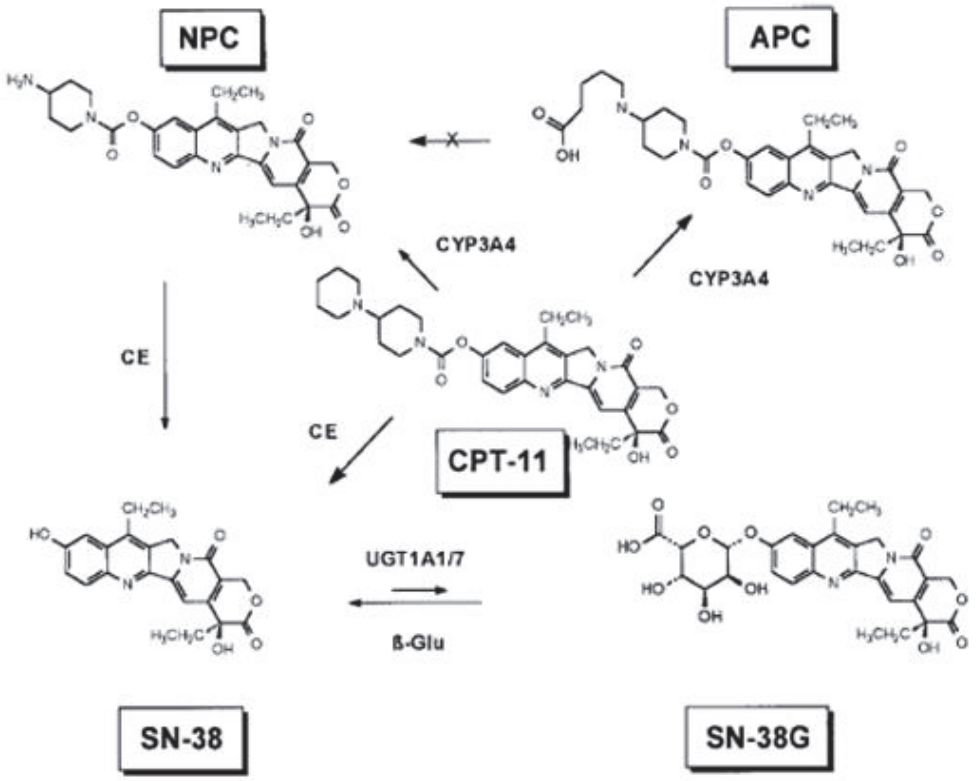

Figure 2: Irinotecan and its metabolites

1.3.4.1. Mechanism of action

CPT11 activity relies on the inhibition of the topoisomerase 1 enzyme. This enzyme plays a crucial role in DNA replication, transcription and repair. Topoisomerase 1 establishes a covalent bound with DNA to separate both DNA strands in order to ease the insertion of the RNA polymerase for DNA transcription.

Camptothecin-derivatives were the first compounds described to be able to stabilize this complex (9). The stabilization of the complex avoids the relegation of DNA strands after their opening resulting in cell death.

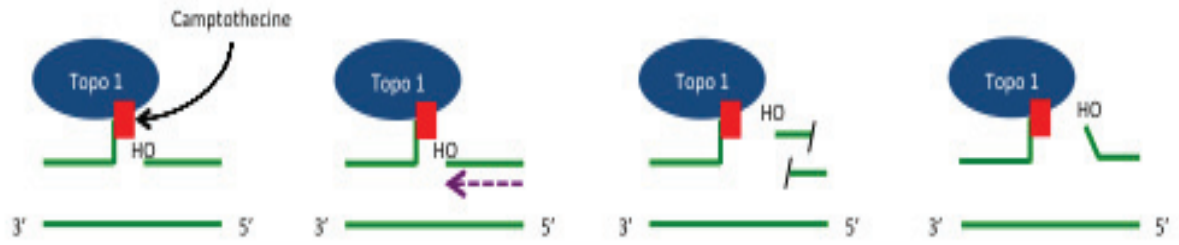

Figure 3: Mechanism of action of camptothecine

Topoisomerase 1 cleavage conversion into DNA damage by displacement of the cleaved strand 5'-OH extremity in DNA transcription (9)

1.3.4.2. Development

Camptothecin (CPT) was clinically tested during the 70s but first clinical trials did not conclude to a positive effect of CPT. The use of CPT was also associated to intolerable toxicities (hemorrhagic cystitis) that led to an immediate arrest of CPT clinical development.

In 1985, the topoisomerase 1 was identified as the target of CPT leading to a regain of interest for this drug. However, the natural CPT exhibits many formulation issues (CPT is bound more than 95% to serum albumin). Numerous studies were thus performed in order to improve CPT solubility and bioavailability. These studies showed that the incorporation of a lipophilic group at the 11th position decreases CPT affinity for serum albumin without reducing CPT cytotoxicity. This compound was thus called CPT11, irinotecan.

1.3.4.3. Pharmacokinetic properties

1.3.4.3.1. Animals

After intra-venous (IV) administration in mice, CPT11 shows a biphasic disposition in plasma with a terminal half-life ranging between 1.1 and 3h. CPT11 disposition is linear

at low doses but at high doses, over 40mg.kg^{-1}, its clearance decreases and AUC increases non-linearly with doses (10). Pharmacokinetic parameters of CPT11 and SN38 in plasma are similar after IV and intra-peritoneal (IP) administration (11).

1.3.4.3.2. Humans

After IV administration of 145mg.kg^{-1}, CPT11 disposition in plasma is biphasic with a terminal half-life of 8.8h. Its volume of distribution is estimated at 246L attesting its high tissue distribution. SN38 peaked between 1.5 and 3.6h from the infusion onset while SN38G T_{max} ranged between 1.7 and 6h. Metabolites concentration declines parallel to CP11. SN38G AUC is higher than SN38 AUC with a maximum ratio of 13. CPT11 and SN38 are found under two chemical forms: lactone and carboxylate that have different pharmacokinetic properties, *e.g.* higher clearance for the lactone form.

Secondary peaks of CPT11 and SN38 are observed suggesting entero-hepatic recycling.

CPT11, SN38 and SN38G elimination is mainly non-renal since urinary recovery represents only 14% and 0.2% of the administered dose for CPT11 and SN38 respectively.

No difference in CPT11 disposition in plasma was reported based on sex and race (12).

Xie *et al.* developed a population pharmacokinetic model of CPT11 and all of its metabolites that include both lactone and carboxylate forms (13). Authors showed that CPT11 hydrolysis was five times faster than the lactonization attesting that CPT11-carboxylate is the major form at equilibrium. The contrary was reported for SN38 with SN38-lactone dominating at equilibrium. For both CPT11 and SN38, clearance was higher for the lactone form (74.4L.h^{-1} compared to 12.4L.h^{-1} for CPT11-lactone and carboxylate respectively). SN38 and NPC are preferentially formed from CPT11-lactone, whereas APC is preferentially formed from CPT11-carboxylate.

1.3.4.4. Pharmacodynamic properties

CPT11 is well established as the first line therapy for the treatment of metastatic and advanced colorectal cancer (CRC) combined with 5-FU or alone after 5-FU failure (14). First clinical trials in Japan attested the efficacy of CPT11 administered every third week in advanced CRC (15). The first phase 2 trials indicated 22% of tumour response in patients refractory to standard 5-FU (16), results confirmed in several others studies .

The main dose-limiting toxicities of CPT11 include severe myelosuppression with an incidence of about 15-20% and delayed severe diarrhea that is observed in 20-25% of patients around five days after treatment onset (17). Severe diarrhea is impacted by the systemic and intestinal exposure of SN38 that accumulates into intestines.

The last study included in this thesis is focused on capecitabine, the oral pro-drug of 5-FU.

1.3.5. Capecitabine

Capecitabine is an orally administered tumour selective prodrug of 5-Fluorouracil (5-FU) that is approved in the management of colorectal and breast cancers.

After oral administration, capecitabine is well-absorbed and sequentially metabolized to 5-FU following three steps (Figure 4) (18):

- Capecitabine is converted to 5'-deoxy-5-fluorocytidine (5'-DFCR) by carboxylesterases
- 5'-DFCR is converted to 5'-doxy-5-fluoroudine (5'-DFUR) by cytidine deaminase
- 5'-DFUR is converted to 5-FU by thymidine phosphorylase (ThdPase)

Then, the active compound, 5-FU is first converted to dihydroxyfluorouracil (FUH_2) by dihydropyrimidine dehydrogenase (DPD). This step is followed by conversion to 5-fluoro-ureido-prorionic acid (FUPA) by dihydropyrimidine (DHP). The final step of 5-FU

metabolism consists in the conversion of FUPA to FBAL by the enzyme β-ureido-propionase (BUP) (19).

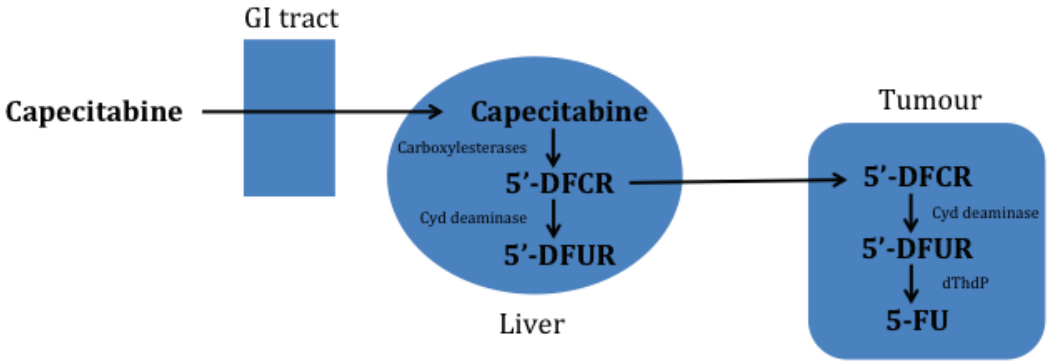

Figure 4: Metabolic pathway of capecitabine (18)

The biotransformation of capecitabine to 5'-DFCR occurs mainly in the liver to minimize the accumulation of 5-FU in plasma and healthy tissues. Conversion of 5'-DFCR to 5'-DFUR occurs via dThdPase which is more highly expressed in tumour tissues than in healthy tissues. Capecitabine is therefore expected to allow preferential exposure to 5-FU in tumour while limiting levels of circulating 5-FU (20).

Capecitabine development was subject to intensive modeling work so that it is an excellent candidate to evaluate new tools to optimize its current dosing schedule as it has been done in the following.

2. Anticancer drugs resistance

Chemotherapy is widely used for treating numerous cancer types. However, clinical resistance to cytotoxic chemotherapy is recognized as a major problem Tumour resistance is defined as the tumour cells cross-resistance to various compounds that are not structurally linked (21). Chemoresistance can result from different mechanisms that arise from three main types of events: alteration of drug uptake, efflux and biotransformation (22).

Chemoresistance can be classified into two types of mechanisms:

- Mechanisms related to tumour physiology
- Mechanisms related to tumour cells

2.1. Mechanisms related to tumour physiology

Teicher *et al.* were the first to describe the effect of tumour environment on tumour resistance (23). They exposed tumour cells to cytotoxic drugs *in vitro* and *in vivo*. While tumour cells *in vivo* exhibit resistance after weeks of treatment, the same cells do not present any resistance *in vitro*. The authors concluded that factors external to tumour cells were thus implied in the resistance development.

Brown *et al.* identified the two main external factors responsible for tumour resistance:

- Tumour vasculature
- Tumour oxygenation

2.1.1. Tumour vasculature

To ensure its development, tumour cells continuously produce pro-angiogenic factors to develop their own vascular network. The difference between the physiology of normal and tumour tissues stems from the tumour vasculature. Two types of vessels compose tumour tissues: existing blood vessels in normal tissue that the tumour has invaded and

tumour micro-vessels arising from neovascularization. Both types of vessels are highly irregular, give artery-venous shunts and have incomplete endothelial linings and basement membrane. Tumour blood flow is thus much more irregular than in normal tissue (24). Some zones of the tumour receive enough oxygen and nutriments to maintain their development whereas some others do not receive anything. This disparity on blood flow affects drug penetration into tumour (25).

Tumour vasculature became a new target in anticancer drug research with the development of anti-angiogenic drugs which tend to normalize the vascular network in order to ensure a well-balanced penetration of cytotoxic into tumour.

2.1.2. Tumour oxygenation

The unbalanced tumour vasculature also leads to the formation of hypoxic zones within the tumour tissue. Hypoxia has been recognized as a negative prognostic factor in cancer treatment. Given its central role in tumour progression and resistance to therapy, tumour hypoxia is now considered as a validated target in cancer treatment (26). Moreover, hypoxic cells grow slower than others cells (27), they are also more resistant to chemotherapeutic agents (28).

2.2. Mechanisms related to tumour cells

Healthy cells use various mechanisms to protect against toxins and xenobiotic. These mechanisms are also found in tumour cells and lead to drug resistance. Tumour resistance can appear at the beginning of the therapy (primary resistance) or after a period of response (secondary resistance).

In primary resistance, others oncoproteins that are not inhibited by the anticancer agents are implicated. To overcome this resistance, a new drug with a different mechanism of

action has to be used. Moreover, molecular diagnosis can avoid this type of resistance by identifying the correct target (29).

Two main steps lead to secondary resistance. The first step consists in the selection of resistant clones that have a state of dormancy; they are quiescent tumour cells with halted cell growth (30). In time, the resistance mechanisms can become more efficient and non-resistant clones can become resistant. In a second step, clonal evolution driven by genomic instability allows the appearance of resistant clones together with the development of drug- and target-independent resistance.

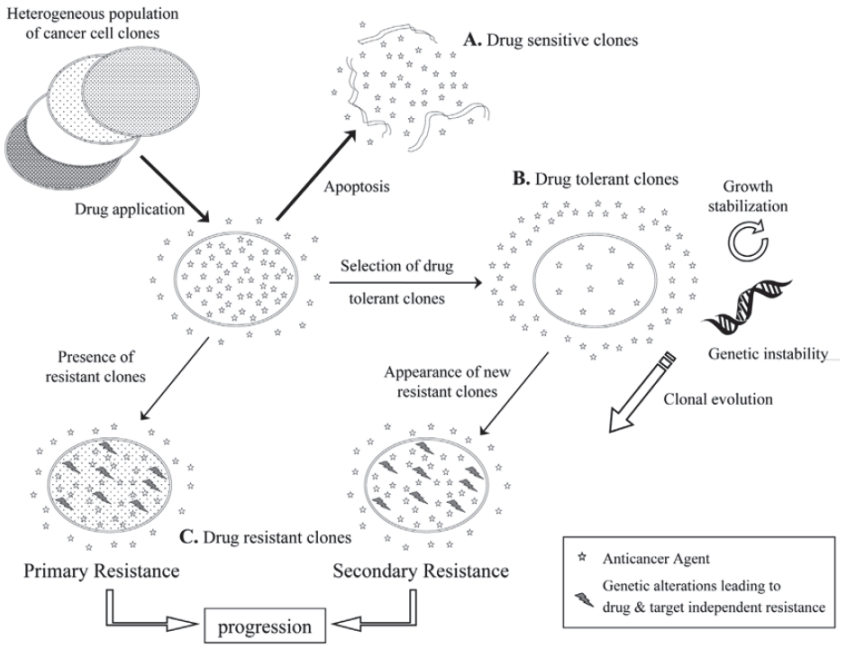

Figure 5: Resistance in cancer therapy (31)

In secondary resistance, resistant cell clones appear after a durable response to the treatment (**A**). It occurs in 2 steps. First, some clones can develop a tolerance to the drug (**B**). Tolerant clones have a halted growth. It can be caused by a suboptimal intracellular level of the therapeutic agent(s), mutations in the target protein or desensitization of apoptosis signalling. Secondly, new clones with increased growth appear. They have new genetic modifications and show resistance mechanisms which can be independent of the drug and its target(s) (**C**). Therefore, at the beginning of treatment, it is advisable to deliver the therapeutic agents inside the cancer cells as much as possible to impede clonal evolution and genetic instability

Rochat classified acquired cellular resistance in three categories: drug-dependent mechanisms, target-dependent mechanisms and drug- and target-independent mechanisms (31).

Category 1: Drug-dependent mechanisms due to the modification of drug disposition • Decrease of drug influx inside the cancer cell by lower expression of SLC isozymes • Modifications of drug biotransformation in the cans cells by XME isozymes • Increase od drug efflux out of the cancer cell by ABC isozymes • Decrease of drug disposition in the cancer cell by modulation of drug bioavailability in the systemic circulation
Category 2: Target-dependent mechanisms due to the desensitization of drug-target complex signalling • Mutations of the target protein • Amplification of the target protein • Alteration of drug-target complex signalling through coregulator proteins
Category 3: Drug- and target-independent mechanisms due to the complete escape of the drug-target complex signalling • Clonal evolution with new genetic aberrations • Increase of apoptotic signals • Decrease of survival signals

Table 2: Categories and main mechanisms of anticancer drug resistance in cancer cells (31)

2.2.1. Drug-dependent mechanisms

These mechanisms of resistance rely on the modification of intracellular drug disposition. Three main systems are involved in drug disposition in tumour cells: drug influx system by the Solute Carrier family (SLC), drug efflux system by the ATP-Binding Cassette family (ABC) and the xenobiotics metabolizing enzymes (XME) (Figure 5)

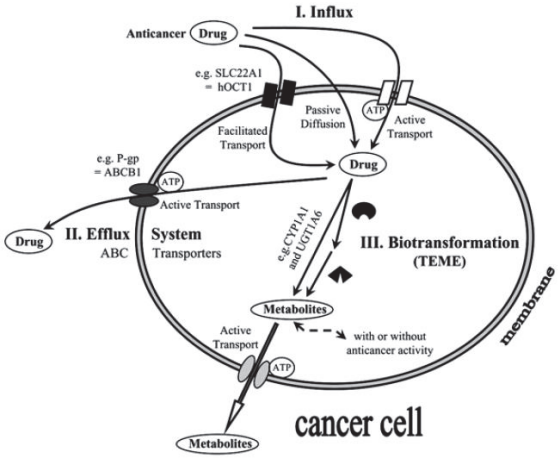

Figure 6: Drug dependent mechanisms of resistance (31)

The uptake of anticancer drugs involves three main families of SLC transporters: SLC21 (SLCO), the organic anion transporter family with 20 proteins (OATP); SLC22, the organic cation/anion/zwitterion transporter family with 18 proteins (OAT); SLC15, the proton oligopeptide co-transporter with 4 proteins (PEPT). Down-regulation of SLC transporters has been associated to the decrease uptake of platine derivatives (32). Effect of SLC transporters has been well characterized *in vitro* (33-36). However, their clinical implications in drug resistance have been clearly established for only a few compounds. As an example, patients treated with imatinib and having a poor expression of SLC22A1 have a significantly worse prognostic of overall survival (37).

Drug efflux system involve ATP-Binding Cassette (ABC) transporters. Three of these transporters have predominantly been linked to a potential role in drug resistance (ABCB1/P-gp, ABCG2/BCRP, ABCC1/MRP1). Overexpression of these transporters has been associated to negative chemo-sensitization of several anticancer agents (38). In renal carcinoma patients, high expression of P-gp is associated to a poor prognostic (39). However, several clinical studies have reported the failure of ABC transporters inhibitors in the management of drug resistance (12, 40-43). A more detailed review of the structure and role of ABC transporter is presented in the following.

Intracellular drug biotransformation mediated by XME enzymes is also involved in cellular drug resistance. The main XME enzymes involved in biotransformation of anticancer agents are CYP450 isoforms, UDP-glucuronosyl-transferases and glutathione S transferase (44-46). *In vitro*, CYP activity was found to decrease chemo-sensitivity of more than 50 compounds (47) highlighting its role in the modulation of anticancer drugs activity. As an example, CYP3A4 intracellular expression was found to be four times lower in patients responder to docetaxel compared to non-responders (48). Many examples establish the association between the XME expression and patients' survival (49-51) but

it is not completely established if XME activity responsible of these correlations is localized in tumour cells.

Coordinated regulations of SLC, XME and ABC enzymes have been described (52, 53). Their expression is regulated by similar nuclear receptors such as the constitutive androstane receptor (CAR). In addition, various data have identified overlapping substrates specificity for P-gp and CYP3A4 attesting that the drug metabolites are more expulsed out of the cells by ABC transporters. A good example is that hydroxyl groups included in SN38 structure helps its interaction with ABCG2 (54).

2.2.2. Target-dependent mechanisms

In case of target mutation, the drug cannot properly recognize the target that leads to a decrease of anticancer drug efficacy. The most well-known example concerns imatinib and its target Bcr-Abl protein kinase. Studies have detected mutations of Bcr-Abl in about 50% of patients with acquired resistance to imatinib (55-58). However, the Bcr-Abl mutation is not the only resistance mechanism to imatinib since the mutation only partially contributes to drug resistance because cancer cells carrying the mutant protein kinase are not invariably insensitive to imatinib (59).

In case of target amplification, drug amount is not sufficient to completely inhibit the target. An example is the overexpression of thymidylate synthetase promoter in homozygous patients that did not respond to 5-FU therapy (60).

2.2.3. Drug- and target- independent mechanisms

These mechanisms are neither related to the drug nor to the drug target. They concern the mutation and deregulation of oncogenes and the decrease of tumour cells apoptosis.

2.2.3.1. DNA repair

There are five recognized DNA repair pathways that protect cellular DNA from injury: nucleotide excision repair, mismatch repair, double-strand break repair, base excision

repair and direct repair. Alteration in the structure of the DNA molecule leads to cellular DNA damages recognition and repair which can result in the continued viability of cells resulting in resistance to drugs targeting DNA such as platinum-derivatives (61). Cancer cells DNA repair mechanisms are more efficient and faster than in normal cells (62). Nucleotide excision repair is a key pathway in cisplatine resistance. *In vitro* studies, using testicular carcinoma cell lines showed a deficiency in nucleotide excision repair and exhibit an important sensitivity to cisplatine (63). This finding has also been shown in multiple studies with human ovarian cell lines (64).

2.2.3.2. Decrease of apoptotic signals

The first association of the *bcl2* gene with human cancer was observed in human follicular lymphoma (65). *Bcl2* belongs to a distinct class of cancer related genes because it is neither an oncogene nor a tumour suppressor gene such as *Myc* or *p53*. It is defined as an apoptosis protection gene (66). *Bcl2* interacts directly with oncoproteins regulating the mitogenic cell signalling. It is thus involved in the regulation of the cell cycle by inhibiting apoptotic factors that delay the apoptosis and cause resistance (67, 68).

P53 protein is another important regulator of the cell cycle. It is activated after DNA damages. Tumour suppressive function of *p53* prevents the propagation of abnormal cells. Its role in the prevention of cancer has been demonstrated because *p53* is mutated in 50% of human cancers (69, 70). Tumour cells exhibiting mutated *p53* gene do not enter in apoptosis and become resistant.

3. ABC transporters

The ATP-Binding Cassette (ABC) superfamily of transporters is one of the largest protein families in biology (71). These transporters use the binding and hydrolysis of ATP to power the translocation across cell membrane of diverse substrates ranging from ions to macromolecules. Members of the ABC family are present in prokaryotes and eukaryotes (72). ABC exporters are present in both prokaryotes and eukaryotes; importers are exclusively present in prokaryotes. In *E. coli*, ABC transporters represent 5% of the genome (73). The human genome encodes 48 ABC transporters (74, 75) classified into seven families : ABCA, ABCB, ABCC, ABCD, ABCE, ABCF, ABCG.

3.1. Structure

ABC transporters have a characteristic architecture, which consists of four domains: two transmembrane domains (TMD) located in the membrane and two nucleotide binding domains (NBD) located in the cytoplasm (76). All the proteins that belong to the ABC family have the same structure (73, 77). This basic structure is duplicated in full transporter such as ABCB1 (P-gp) whereas half-transporters such as ABCG2 only have one NBD and one TMD.

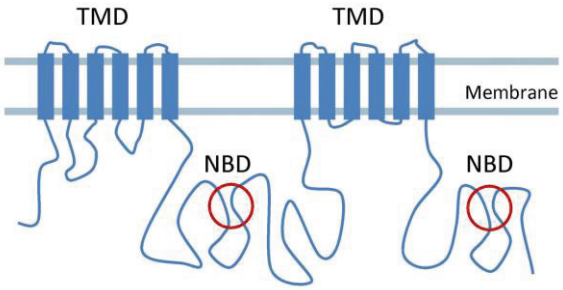

Figure 7: ABC transporters typical structure

3.1.1. Transmembrane domains

Transmembrane domains (TMD) are hydrophobic domains that are located in cell membrane. Each TMD is usually composed of six transmembrane helices (78). However, the transmembrane subunit can exhibit several variations with 5 to 11 transmembrane helices (79). TMD forms the permeation pathway for transport of substrates, even if the exact localization of the fixation site is not identified yet. Sequences of TMD are not well conserved throughout species because these domains are implied in substrate recognition.

3.1.2. Nucleotide binding domains

Nucleotide binding domains (NBD) are located in the cytoplasm where they hydrolyze ATP to power substrates transport.

NBD can be subdivided into two constituent domains: a catalytic core that contains the conserved P loop, Walker B motif, φ loop and switch region and an α-helical domain that contains the ABC signature motif (80).

The catalytic core is highly conserved in ABC transporters. P loop allows fixing ATP through binding of β and γ ATP phosphates. Φ loop located between P-loop and Walker B motif allows the binding between NBD and TMD. ABC signature doses not interact directly with nucleotide but its mutation prevents ATP hydrolysis (81). Switch region is located at the C-terminal extremity of NBD and participate to the modification of the conformation following ATP hydrolysis. This region binds the ATP-γ phosphate allowing to transfer ATP energy to TMD (82).

Motif	Functions
P-loop	ATP binding
Q-loop	NBD-TMD binding
ABC signature	ATP binding
Walker B	Mg^{2+} binding during ATP binding
Switch region	β, γ phosphates ATP binding

Table 3 : NBD motifs and functions

3.2. Mechanisms

ABC drug transport involves two interconnected cycles (83). A catalytic cycle of ATP hydrolysis that drives transport first occurs. Secondly, there is a substrate transport where substrates are moved from the cytoplasm to the extracellular side of the cell membrane.

Details of the catalytic and transport cycles, and how they are coupled, remain enigmatic. In many studies, P-gp appeared to behave as a symmetrical transporter with two equivalent NBDs and it is likely that the BCRP homodimer also functions symmetrically. However, there are many evidences that NBDs are not functionally equivalent (84).

The catalytic cycle involves binding of ATP to both NBDs, which induces formation of nucleotide dimer. One molecule of ATP become tightly bound (85) and is hydrolysed into ADP+P_i. ATP hydrolysis is the rate-limiting process for ATP transporter. After ATP hydrolysis, ADP and P_i are released from the NBD (82). The second round of ATP hydrolysis takes place on the other NBD.

Drug transport starts with the entry of substrates into the binding pocket on the cytoplasm side followed by the change in transporter conformation due to ATP hydrolysis. Substrates are finally released into the extracellular side of the cell membrane. Substrates initially interact with high affinity binding sites and moved then to low-affinity

site for release. The link between ATP hydrolysis and drug transport requires the communication between NBD and TMD that are linked by the conformational changes.

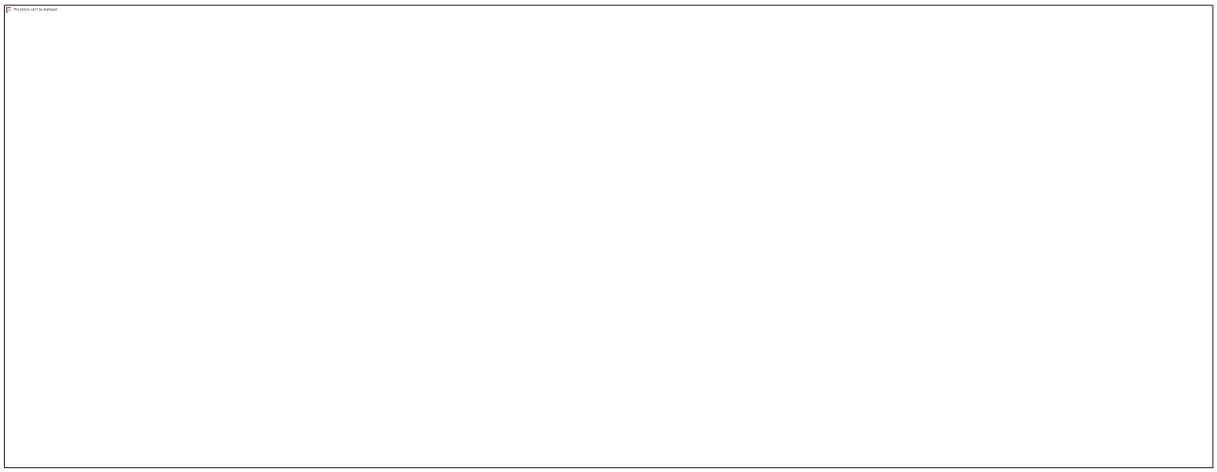

Figure 8: ABC transporters mechanism (86)

3.3. Human ABC transporters

Human genome encodes 48 ABC transporters. As shown in Table 4, these proteins are widely expressed.

Symbol	Expression	Symbol	Expression
ABCA1	Ubiquitous	ABCC2	Ubiquitous
ABCA2	Brain	ABCC3	Lung, intestine, liver
ABCA3	Lung	ABCC4	Prostate
ABCA4	Rod photoreceptors	ABCC5	Ubiquitous
ABCA5	Muscle, heart, testis	ABCC6	Kidney, liver
ABCA6	Liver	CFTR	Exocrine tissues
ABCA7	Spleen, thymus	ABCC8	Pancreas
ABCA8	Ovary	ABCC9	Heart, muscle
ABCA9	Heart	ABCC10	Ubiquitous
ABCA10	Muscle, heart	ABCC11	Ubiquitous
ABCA12	Stomach	ABCC12	Ubiquitous
ABCA13	Ubiquitous	ABCD1	Peroxisomes
ABCB1	Adrenal, kidney, brain	ABCD2	Peroxisomes
ABCB2	Ubiquitous	ABCD3	Peroxisomes
ABCB3	Ubiquitous	ABCD4	Peroxisomes
ABCB4	Liver	ABCE1	Ovary, testis, spleen
ABCB5	Ubiquitous	ABCF1	Ubiquitous
ABCB6	Mitochondria	ABCF2	Ubiquitous
ABCB7	Mitochondria	ABCF3	Ubiquitous
ABCB8	Mitochondria	ABCG1	Ubiquitous
ABCB9	Heart, brain	ABCG2	Placenta, intestine
ABCB10	Mitochondria	ABCG4	Liver
ABCB11	Liver	ABCG5	Liver, intestine
ABCC1	Ubiquitous	ABCG8	Liver, intestine

Table 4: Symbol and site of expression of human ABC transporters (74)

ABC transporters are classified into seven families (ABCA-ABCG) that are all involved in the transport of toxins and xenobiotic. ABC transporters are thus preferentially expressed in natural barrier (blood brain barrier, placenta, gut) (Figure 8). Some of them are particularly of interest because of their implications in human diseases.

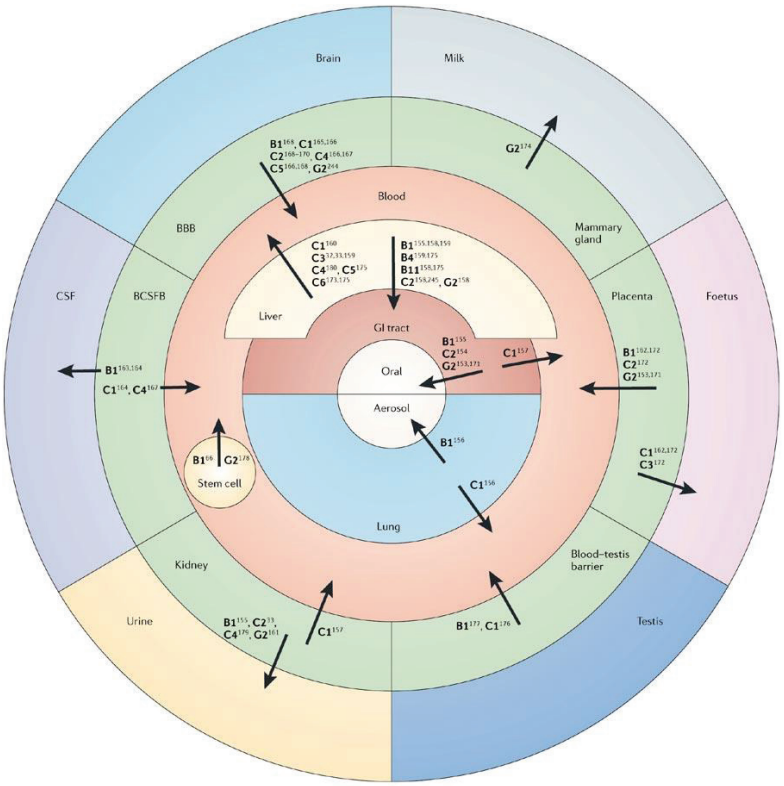

Figure 8: Localization of human ABC transporters (87)

3.3.1. ABC transporters in human diseases

ABC transporters can be involved in human diseases either because of their inactivation; where they are associated to genetic diseases, or because of their overexpression; where they are associated to drug resistance.

Ten ABC transporters have been identified in genetic disorders because of their inactivation (Table 5) (88).

The most famous example of diseases related to ABC inactivation is the ABCC7 inactivation in cystic fibrosis. Cystic fibrosis is an autosomal disease recessive genetic disorder affecting most critically lungs, pancreas, liver and intestine. It is characterized by abnormal transport of chloride and sodium across epithelium leading to viscous secretions. This disease is due to the mutation of the cystic fibrosis transmembrane

conductance regulator (CFTR/ABCC7) that encodes a chloride ion channel important in creating swear, digestive juices and mucus.

ABC transporter	Disease
ABCA1	Tangier disease
ABCA4	Stargardt disease
ABCB4	Progressive familial cholestasis 3
ABCB7	Anemia with ataxia
ABCB11	Progressive familial cholestasis 2
ABCC2	Dubin-Johnson syndrome
ABCC6	Pseudo-xanthoma elasticum
ABCC7	Cystic fibrosis
ABCD1	Adrenoleukodystrophy
ABCG5	Sitosterolemia
ABCG8	Sitosterolemia

Table 5: Human diseases associated to the inactivation of ABC transporters (88)

Overexpression of ABC transporters is associated to acquired drug resistance due to their abilities to extrude several classes of anticancer drugs from cell. This phenomenon was firstly described in cancer disease (89). Three main transporters have been clinically identified for their implications in anticancer drugs resistance: ABCB1 (P-gp-, ABCG2 (BCRP) and ABCC1 (MRP1) (90). The role of ABC proteins in resistance to anticancer drugs have been known for over 30 years (91).

Many drugs commonly used in in clinical therapy are transport substrates for P-gp, BCRP or MRP1. The ABC transporters play thus an important role in drug absorption, distribution and elimination *in vivo* since they can limit the uptake of many drugs. The presence of ABC transporters is a serious problem in drug discovery; many candidates may not be able to cross natural barriers *in vivo*, making them clinically useless. The presence of efflux pumps in the endothelial cells of the brain capillaries has an impact on pharmacotherapy of drugs that target the brain including cancer, AIDS, Parkinson's disease, epilepsy and schizophrenia (92). The presence of ABC transporters in the luminal

membrane of endothelial cells, where they immediately pump drugs back to the blood, thus reduces drugs accumulation into the brain.

3.4. P-glycoprotein

P-glycoprotein (ABCB1, P-gp) was originally discovered in colchicine selected Chinese hamster ovary (CHO) cells resistant to multiple natural drugs. P-gp was the first transporter discovered implied in drug resistance.

ABCB1 is a 170kDa single polypeptide that arises from an internal duplication and comprises two TMD and two NBD.

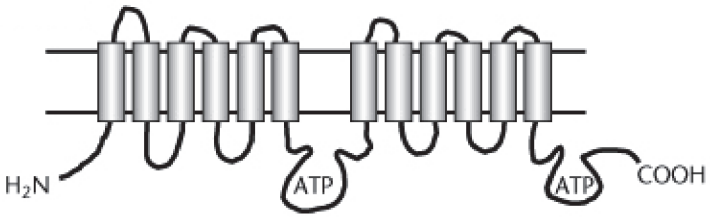

Figure X: ABCB1- P-gp structure (93)

It is preferentially located in the apical membrane of epithelial cells in wide types of tissues and preferentially at natural barriers. There is no doubt that ABCB1 is a key player in the defense of the body against xenobiotic and toxins (94). The most recent experiments on the defense role of P-gp are focused on three main barriers: the gut mucosa, the blood-brain barrier and the maternal foetal barrier.

3.4.1. Physiological roles

3.4.1.1. Gut mucosa

P-gp was known to be expressed in mucosal cells form its discovery. However, its function remains unclear, the transporter was deemed to interfere with the uptake of amphipathic drugs from the gut (95, 96).

P-gp can affect the oral bioavailability of its substrates. A good example is paclitaxel that is a very good P-gp substrate. Paclitaxel has to be administrated because intravenously of

its extremely poor oral availability that is related to P-gp function in gut (97). As a demonstration, paclitaxel oral bioavailability moved from 11% in wild-type mice to 35% in double knocked-out mice (Mdr1a$^{-/-}$).

3.4.1.2. Blood-brain barrier

Blood-brain barrier is composed of endothelial cells of brain capillaries linked together by tight junctions. Drugs getting into the brain have to cross endothelial cells and get by P-gp that is expressed at high levels in the apical membrane of these cells (94). The accumulation into the brain of a wide range of drugs (anticancer drugs, cardiac drugs, antidiarrheal drugs, immunosuppressant) is thus strongly decreased by P-gp action. Any P-gp substrates is affected unless compound diffuses rapidly through capillaries membrane like dexamethasone which is highly extruded at low concentrations but less affected at high concentrations (98).

3.4.1.3. Maternal-foetal barrier

Lankas *et al.* (99) found P-gp present in the foetus-derived epithelial cells. The transporter is expressed at the apical membrane of these cells facing maternal circulation in order to protect foetus against incoming toxins.

3.4.2. P-gp substrates

P-gp, as others ABC transporters, is able to transport a wide range of substrates that are structurally different and that include many therapeutic compounds (Table 6).

Anticancer drugs	**H2-receptor antagonists**	**HMG-CoA reductase inhibitors**
Vinca alkaloids (vinblastine, vincristine)	Cimetidine	Lovastine
Anthracyclines (doxrubicine, daunorubicine)	**Immunosuppressant**	Simvastatin
Taxanes (paclitaxel, docetaxel)	Cyclosporine A	**Antiemetics**
Epipodophylltoxins (epotoside, teniposide)	Tacrolimus	Ondansetron
Camptothecins (topotecan)	**Antiarrhythmic**	**Tyrosine kinase inhibitors**
Anthracenes (mitoxantrone, bisantrene)	Quinidine	Imatinib
HIV protease inhibitors	Amiodarone	Gefitinib
Ritovanir	Propafenone	**Cardiac glycosides**
Saquinavir	**Antiepileptic**	Digoxin
Nelfinavir	Felbamate	**Antihelminthics**
Analgesics	Topiramate	Ivermectin
Morphine	**Fluorescent compounds**	**Antibiotics**
Antihistamines	Calcein-AM	Erythromycin
Terfenadine	Hoechst 33342	Gramicidin A
Fexofenadine	**Calmodulin antagonists**	Antihypertensives
Calcium-channel blockers	Triluoperazine	Reserpine
Verapamil	Chlorpromazine	Propanolol
Nifedipine	Trans-flupentixol	**Steroids**
Azidopine	**Pesticides**	Corticosterone
Diltiazem	Methylparathion	Dexamethasone
Natural products	Endosulfan	Aldosterone
Curcumoids	Cypermethrin	**Antialcoholism drug**
Colchicine		Disurfiram

Table 6: Clinically relevant drugs and others compounds that interact with P-gp (93)

The substrate specificity of drug transporting P-gp is wide and not completely defined. P-gp prefers large amphipathic molecules that are neutral or weakly basic but it can also inefficiently transports anionic highly charged molecules such as methotrexate. Hydrophobicity, planar aromatic rings and the presence of amino groups favor the interaction with P-gp (100).

The ability of P-gp to extrude so many different substrates lies within its flexible central cavity that contains negatively charged residue in a hydrophobic environment. The cavity

allows multiple Van der Walls interactions and binding does not required precise positioning of the ligand (101).

3.4.3. Role in anticancer drug resistance

The Mdr1 gene that encoded P-gp is overexpressed in many human tumour from various histological origins. High expression of the transporter was observed prior to cytotoxic chemotherapy in many different tumour types including kidney, colon, liver, breast and ovarian cancers (102). In haematological malignancies, initial levels of P-gp expression increase after treatment onset. For Acute Myeloid Leukemia (AML), several studies have demonstrated a correlation between P-gp expression and poor prognostic or relapse (103). P-gp has been widely studied as a target to overcome multidrug resistance in cancer therapy. Despite intensive studies, efforts to overcome clinical resistance essentially failed. Initial attempts at P-gp reversal were based on experimental data showing that many compounds can inhibit P-gp *in vitro*. Laboratory observations were directly moved to the clinic and tested in small efficacy phase 2 trials with the hope that the same effects could have been met in patients. In the development of the three generations of P-gp inhibitors (Table 7), no emphasis was placed on the role of the transporter in tumour and the pharmacology of tested inhibitors was not considered (104).

1st generation of P-gp inhibitor
Verapamil
Cyclosporin A
Tamoxifen
2nd generation of P-gp inhibitors
PSC833 (valspodar)
VX-710 (biricodar)
3rd generation of P-gp inhibitors
LY335979 (zosuquidar)
XR9576 (tariquidar)
GF120918 (elacridar)
OC144-093

Table 7: Clinically relevant modulators that interact with P-gp (93)

There is thus still no good agreement on the usefulness of P-gp inhibitors in the treatment of human tumours overexpressing P-gp. Four factors may explain the development failures of P-gp inhibitors:

- Expression of P-gp in cancer cells was not correctly determined. It would have been necessary to focus trials with reversed agents on tumours in which P-gp is a real contributor of the tumour resistance. This problem was highlighted by Faneyte *et al.* (105). They showed by immunohistochemistry that P-gp in breast cancers is only present on the infiltrating macrophages and T cells and not in tumour cells.
- Early clinical trials with P-gp inhibitors were done with drugs and/or dosing regimens that not sufficiently inhibit the transporter. This makes these trials negative and not interpretable. Even the recent P-gp inhibitors valspodar used in many clinical trials did not completely inhibit P-gp (106).
- P-gp inhibitors also affect systemic drug disposition by decreasing P-gp mediated elimination or by interfering with drug metabolism through CYP450. If effective P-gp blockers are combined with drugs like doxorubicine or paclitaxel, patients are thus more exposed to the anticancer agents that can

lead to increased toxicity risk. The anticancer drug dose has to be decreased as it has been done in some clinical trials (107, 108).

- Tumours use any resistance mechanisms available. It is thus unknown how much P-gp contributes to the global observed resistance, since P-gp is certainly not the unique resistance mechanisms in tumour.

The potential contribution of P-gp to clinical drug resistance in cancer patients cannot be correctly assessed yet. However, it is quite unlikely that tumours would not use such a resistance mechanism (109, 110).

3.5. Breast Cancer Resistance Protein

Another phenotype similar but distinct from that found in cells overexpressing P-gp was reported in cells selected with mitoxantrone suggesting the presence of another efflux transporter. This transporter was first identified by Doyle *et al.* as the breast cancer resistance protein (BCRP), an half-size ABC transporter overexpressed in MCF7 breast cancer cells, and by Allikmets *et al.* as ABCP a transporter highly expressed in human placenta (111, 112). A third name, MXR (mitoxantrone resistance protein), was adopted by Miyake *et al.* (113). The BCRP/ABCP/MXR transporter belongs to the G subfamily of ABC transporters and was renamed ABCG2.

ABCG2 (BCRP) is a 72kDa protein composed of 655 amino-acids. It has N-terminal NMD and C-terminal TMD, a structure half the size and in inverse configuration to most of the ABC transporters. Because of it is a half transporter, it is believed to homodimerize or oligomerize in order to function.

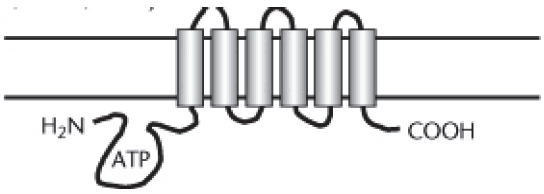

Figure 8: ABCG2 structure (93)

3.5.1. Physiological roles

ABCG2 mRNA is detectable in many tissues, with the highest levels in the placenta (112). The transporter was found in the apical membrane of placental syncytiotrophoblasts, hepatocytes, epithelial lining of small intestine and colon and in the ducts and lobules of the mammary gland (114). However, ABCG2 is absent in the heart, lung, muscles, kidney, pancreas, and peripheral blood leukocytes (115).

The localization of the transporter suggests that it could have an important defense function by limiting the uptake of drugs from the gut and preventing entry of drugs into the fetus.

3.5.1.1. Placenta

ABCG2 is highly expressed in the syncitiotrophoblasts of the chorionic villus where it protects the fetus from toxins through the extrusion of toxins from the foetal space (116-118). Experiments with pregnant mice receiving topotecan combined with the ABCG2 inhibitor GF120918 showed that the foetal plasma levels of topotecan were two-fold higher compared to those measured in maternal plasma supporting the theory that ABCG2 protects the developing fetus from toxins.

3.5.1.2. Blood Brain Barrier

Cooray *et al.* reported the localization of ABCG2 in microvessels endothelium of the brain on the luminal side suggesting the brain to blood ABCG2 transport and its role in brain protection (119). A three-fold higher levels of ABCG2 mRNA was found in the brain

capillaries of P-gp knock-out mice (Abcb1$^{-/-}$) indicating that ABCG2 compensate the lack of P-gp at the BBB (120). Both ABCG2 and P-gp contribute to the BBB. Deletion or inhibition of one of them will thus have a reduced effect.

Inhibition of both BCRP and P-gp results in a higher penetration of drugs in brain (121). As an example, brain penetration of topotecan was 3.7 fold higher in Abcb1/Abcg2$^{-/-}$ mice compared to wild type mice (122).

3.5.1.3. Gastrointestinal tract

ABCG2 expression is not well balanced along the GI tract with highest expression in the duodenum and the lowest in the sigmoid colon (123). Oral administration of topotecan to Abcb1-/- mice in the presence of ABCG2 inibitor resulted in a six-fold increase in topotecan plasma concentration compared to the concentration in absence of inhibitor (124). Impact of ABCG2 on the bioavailability of drugs is greater for oral formulation but this not always the case. As an example, a report examining PK of oral and IV administration of imatinib, a good ABCG2 substrate, showed no increase in the CNS uptake in Abcg2-/- mice following oral dose of imatinib (125). The authors suggested that at high concentration imatinib inhibits ABCG2 whereas at low concentration, imatinib is a substrate of the transporter.

3.5.1.4. Mammary gland

Contrary to the proposed protective role of ABCG2 in several organs, several studies showed that ABCG2 in the mammary gland served to concentrate toxins into breast milk. Jonker *et al.* reported an upregulation of ABCG2 in the lactating mammary glands of mice compared to Abcg2 knock-out mice (126).

3.5.2. Substrates

Due to initial discovery in drug-resistant cells, a number of chemotherapeutic agents were first described to be transported by the protein. Resistance to mitoxantrone is the hallmark of ABCG2 expressing cells. However, BCRP can transport a wide range of substrates ranging from chemotherapeutic agents to organic anion conjugates (Table 8) (127). ABCG2 overexpressing cells have shown cross resistance to camptothecin derivatives (topotecan, irinotecan and SN38) (128, 129). Topotecan and CPT11 levels are markedly decreased in T8 resistant ovarian cancer overexpressing BCRP cells whereas these cells do not present any resistance to paclitaxel or CPT. Maliepaard *et al.* showed that the degree of resistance of T8 cells depends on level of BCRP expression (130). Experimental data suggest that the accumulation of camptothecin analogs in BCRP expressing cells is related to the polarity of the molecule. Nucleophilic groups at the 11th and 9th position of the camptothecin A ring ease the interaction with the transporter. As a demonstration, BCRP confers resistance to 9-aminocamptothecin but not to 9-nitrocamptothecin (131). The differences in structure of topoisomerase 1 inhibitor determine the specificity of BCRP substrates. To date, there is no clear structure-function relationship identified for ABCG2 substrates. However, ABCG2 displays a broad range of substrates that is partially overlapping with that of P-gp and MRP1.

Anticancer drugs	**Flavonoids**	**HMG CoA reductase inhibitors**
Mitoxantrone	Genestein	Rosuvastatin
Bisantrene	Quercetin	Pravastatin
Epipodophyllotoxins(etoposide, teniposide)	**Carcinogens**	Cerivastatin
Camptothecins (topotecan, irinotecan)	Aflatoxin B	**Antihypertensive**
Flavopiridol	PhiP	Reserpine
Anthracyclines (doxorubicin)	**Fungal toxins**	**Fluorescent compounds**
Antifolates	Fumitremorgin C	Hoechst 33342
Methotrexate	Ko143	BODIPY-prazosin
Porphyrins	**Drug and metabolite conjugates**	Rhodamin3 123
Pheophorbide A	Acetominaphen sulphate	**Antiviral drugs**
Protoporphyrin IX	Estrone-3 sulfate	Zidovudine
Hematoporphrin	Estradiol-17-β-d-glucuronide	Lamivudine
Tyrosine kinase inhibitors	Dinitrophenyl-S-glutathione	**Natural products**
Imatinib	**Antiobiotics**	Curcuminoids
Gefitinib	Ciprofloxacin	
	Norfloxacin	

Table 8: Clinically relevant drugs and others compounds that interact with BCRP (93)

3.5.3. Inhibitors

Even if substrate profiles of P-gp and BCRP overlap, BCRP is not inhibited by most of the P-gp inhibitors (132, 133). Fumitremorgin C (FTC) was the first BCRP inhibitor described even before that Abcg2 gene had been cloned (134). GF120918, an acridone derivative from the 2nd generation P-gp inhibitor is also able to inhibit BCRP (135). Acridone-deriatives have been studied as P-gp inhibitor and in a lesser extent as BCRP and MRP inhibitors. In that purpose, Boumendjel *et al.* has targeted new acridone-derivatives as inhibitors of ABCG2 (136). One acridone-derivative, MBLI87, was found to be as potent as GF120918 *in vitro* against mitoxantrone ABCG2-mediated efflux. A Proof-of-Concept (PoC) study has also been carried in mice xenografted with cells overexpressing the transporter and showed that MBLI87 is able to reverse CPT11 ABCG2-mediated resistance *in vivo* (137). Studies included in this thesis are focused on the mathematical modelling of the interaction between this new BCRP inhibitor and CPT11.

Compounds identified as BCRP inhibitors can also act as P-gp inhibitors, the possibility of using dual P-gp/BCRP inhibitors clinically appears thus to be a realistic goal. However, from all the ABCG2 modulators described in the literature (Table 9), none of them has been yet evaluated in patients.

P-gp inhibitors
GF120918 (elacridar)
XR9576 (tariquidar)
VX-710 (biricodar)
Tyrosine kinase inhibitors
Imatinib
Gefitinib
Acridone-derivatives
MBLI87
Others
Ko143
Pantoprazole

Table 9 : Clinically relevant modulators that interact with BCRP adapted from (93)

3.5.4. Role in anticancer drug resistance

Since its discovery in 1998, high levels of ABCG2 expression were found in a variety of drug-resistance cell lines that do not express P-gp nor MRP1. One of the first studies reporting the role of BCRP in tumour resistance was performed in leukemic cell lines. The role of BCRP in haematological tumour is controversial. Some studies reported a strong correlation between BCRP expression and poor prognosis or relapse whereas some others did not find any correlation (138, 139). The situation is clearer for solid tumours. Diestra *et al.* reported frequent ABCG2 expression in tumours of the digestive tract, endometrium, lung and skin (140). Breast cancer has been for instance the most studied with many reports that surprisingly conclude to poor BCRP expression in this cancer (135).

Larger studies are thus needed to determine the real contribution of BCRP to clinical drug resistance in order to avoid issues encountered with P-gp.

3.6. Multidrug Resistance Proteins

The last type of efflux described in drug resistance is the family of Multidrug Resistance Protein (MRP) and especially MRP1 and MRP2.

Compounds that enter into the body are often modified by oxidation (phase 1 metabolism) and/or become more water-soluble by conjugation to glutathione (GSH), sulfate or glucuronate (phase 2 metabolism). Resulting conjugates are too hydrophilic to diffuse out of the cell membrane and require specific transporters to support their efflux. Ishikawa *et al.* were the first to point the presence of a transporter different from P-gp to do this task (141). The first GS-X (glutathione-X conjugate) pump identified was the Multidrug Resistance Protein 1 (142). MRP family contains eight members (MRP1-8) that are all organic anion transporter that differ by their substrates specifity. Two structure types are found in this family, one with 17 TMD (MRP1, 2, 3, 6) and the other with 12 TMD (MRP4, 5, 7, 8). Contrary to P-gp and BCRP, the NBD is not essential for their catalytic function (143).

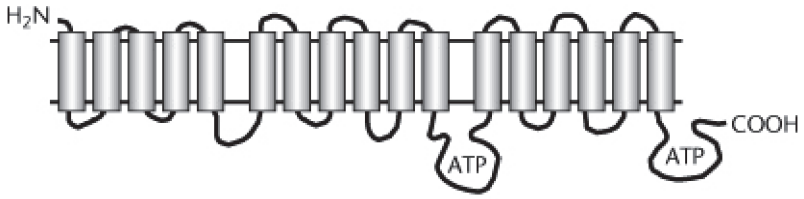

Figure 9: MRP1 and MRP2 structure (93)

In the following, we only present substrates specificity, physiological function and the role in anticancer drug resistance of the two main MRPs: MRP1 and MRP2.

3.6.1. Physiological roles

Contrary to P-gp and BCRP, MRP1 is expressed at the basolateral membrane of polarized epithelial cells, where it protects tissues such as the bone marrow, kidney collecting tubules and intestinal mucosa from toxins. MRP1 is also involved in drug clearance from the cerebrospinal fluid (144). MRP1 is the major high-affinity transporter of LTC4. Mrp1 knock-out mice exhibit more resistance to bacterial infection than wild type because of the inability of macrophages mast cells and granulocytes to secrete Lymphocytes TC4 cells and they also are deficient in the mobilization of dendritic cells (145).

The tissue distribution of MRP2 is more restricted than that of MRP1 and MRP2 is located at the apical cell membrane. This transporter has an important function in the biliary excretion of endogenous metabolites (146). MRP2 is mainly expressed in liver, kidney and intestine (147). Intestinal MRP2 excretes organic anions into the gut and reduces bioavailability of carcinogens (148). Mutations of the Mrp2 gene cause the Dubin-Johnson syndrome (inherited conjugated hyperbilirubemia). In these patients, bilirubin can enter into the hepatocytes but is not secreted into the bile.

3.6.2. Substrates

Initially, the substrate specificity of MRP1 seemed to be similar to that of P-gp. MRP1 can transport organic anions, such as glutathione conjugates without the help of free GSH, even though recent experiments depict a more complex picture (149). MRP2 has the same substrate specificity as MRP1 (150).

MRP1-2 can bind a large number of compounds (Table 10), their binding pockets are extremely flexible and numerous competition/cooperation between substrates and transporter can be envisaged (151, 152).

Anticancer drugs	Pesticides	Glucuronide conjugates
Vinca alkaloids (vinblastine, vincristine)	Fenitrothion	Glucuronosylbilirubin
Anthracyclines (doxorubicin)	Methoxychlor	Estradiol-17-β-D-glucuronide
Epipodophylltoxins (etoposide, teniposide)	**Glutathione conjugates**	Etoposide-glucuronide
Campothecins (topotecan, irinotecan)	Leukotrienes C4, D4 and E4	NS-38-glucuronide
Methotrexate	Prostaglandin A2-SG	**Tyrosine kinase inhibitors**
Metalloids	Hydroxynonenal-SG	Imatinib
Sodium arenate	Aflatoxin B1-epoxide-SG	Gefitinib
Sodium arsenite	Melphalan-SG	**Fluorescent compounds**
Potassium antimonite	Cyclophosphamide-SG	Calcein
Peptides	Doxorubicin-SG	Fluo-3
Glutathione (GSH)	Toxins	BCECF
Sulfate conjugates	Aflatoxin B1	**Antibiotics**
Etrone-3-sulfate	**HIV protease inhibitors**	Difloxacin
Dehydroepiandrosterone-3-sulfate	Ritonavir	Grepafloxicin
Sulfatolithocholyl taurine	Saquinavir	**Folates**
	Natural products	Folic acid
	Curcuminoids	L-leucovorin

Table 10 : Clinically relevant drugs and other compounds that interact with MRP1-2 (93)

Contrary to P-gp and BCRP, only a few inhibitors have been described for MRP1-2 including VX710 (biricodar), flavonoids and glutathione derivatives (153).

3.6.3. Role in anticancer drug resistance

Because MRP1 is ubiquitous in human tissues, it can be present in most of the tumour types to play a role in resistance. MRP1 expression was detected in almost every tumour types but there is no strong correlation reported between MRP1 expression levels and clinical resistance (154). In the absence of specific MRP1 inhibitors, it is difficult to evaluate the contribution of this transporter to clinical resistance.

No association between MRP2 expression and drug resistance was found in cell lines selected for multidrug resistance. However, MRP2 is found in 95% of renal clear-cell carcinomas and also detected in lung, gastric, colorectal and hepatocellular carcinomas (150).

Nevertheless, because of their ability to handle compounds associated with GSH, MRP1-2 can cause resistance to small molecules that form GSH complexes such as cisplatine. The importance of MRPs transporters in anticancer treatment is thus potentially high.

4. Pharmacometrics

4.1. Definitions

Pharmacometrics is a recent scientific discipline that has considerably been enriched since L.B. Sheiner introduced it 40 years ago. Pharmacometric research was firstly defined as "research focusing on non-linear mixed effects models, which describe response-time profiles observed in clinical trials with a focus on determining sources of variability within a studied population" (155). A broader definition of this field has recently been suggested which defined pharmacometrics as "the branch of science concerned with mathematical models of biology, pharmacology and diseases used to describe and quantify interactions between xenobiotic and patients including beneficial effects and side effects resultant from such interface" (156). Pharmacometrics thus integrates numerous quantitative disciplines with the main focus on developing predictive models of drug actions and diseases. Usually, pharmacometric models are used to quantitatively describe the time-profile of pharmacological responses, i.e. the interaction that occurs between a drug and an organism. It implies two main areas of interest: pharmacokinetics and pharmacodynamics. Pharmacokinetics (49) establishes the relationship between doses administered and resulting concentration in the organism following all the transformations of the drug. The main aim of PK is the characterization of drug absorption, distribution, metabolism and elimination. Pharmacodynamics (PD) establishes the relationship between drug concentrations and drug effects either beneficial or deleterious.

The final objective of pharmacometric models is the identification and quantification of the PKPD relationship, i.e. the identification of the causal chain:

Dose → Concentration → Effect

Data issued from PK and PD studies can be analysed using different types of pharmacometric models that can either be empirical or mechanistic in nature depending on the modeling question and information available.

4.2. Non-Linear Mixed Effects modeling (NLME)

4.2.1. Definitions

Mathematical models are a set of mathematical equations that describe the studied system. They establish the relationship between a variable of interest, dependent variable, and a set of known covariates, independent variables. In PK/PD modelling, the dependent variable can be the change over time of drug concentration in PK or tumour size evolution in PD. Independent variables in such models is often the time.

Population pharmacometric models, so called Non-Linear Mixed Effects models, focus on the population modelling in which data issued from all the individuals are simultaneously analysed (157). NLME accounts for the different sources of variability in the studied population and describes pharmacological responses in term of two parts: fixed and random. Fixed effects refer to the mean response within the population described by typical parameters, i.e. parameters describing the mean individual. Random effects refer to the variability around fixed effects. Usually three different levels of variability are included in pharmacometric models:

- Inter-Individual Variability (IIV) that quantifies the difference between the typical individual and the i^{th} individual in the population (158)
- Inter-Occasion Variability (IOV) that quantifies the difference in individual parameters between different occasions (159)
- Residual Variability (160) that quantifies the difference between the observed values and the individual predicted values.

The usual mathematical formulation of NLME models is the following:

$$y_{ij} = f(\theta_i, X_{ij}) + g(P_i, X_{ij}) \times \varepsilon_{ij} \quad \text{(Equation 1)}$$

Where y_{ij} is the j^{th} observation of the i^{th} individual in the population, f(…) is the individual model prediction described by X_{ij} variables and P_i the individual model parameters, $g(P_i, X_{ij}) \times \varepsilon_{ij}$ is the residual error where ε is assumed to be normally distributed with a 0 mean and σ^2 variance.

Any parameter included in the model is thus defined with a typical value (107) and with a random effect corresponding to the variability (IIV, IOV). In pharmacology, parameters are usually positive and a log-normal distribution is usually assumed to describe the variability:

$$P_i = \theta \times e^{\eta_i} \quad \text{(Equation 2)}$$

Where P_i is the individual parameter value, θ is the typical parameter value and η_i is a random variable describing the variability that is assumed to be normally distributed with a 0 mean and ω^2 variance.

4.2.2. Parameters estimations

Estimation methods used for fitting population models to data are generally based on the maximum likelihood principle. The individual likelihood in a mixed-effects model can be expressed as a function of marginal individual density:

$$L_i(y_i, \Psi) = \int P(y_i|\eta_i,\Psi) \times P(\eta_i, \Psi) d\eta_i \quad \text{(Equation 3)}$$

Where $P(y_i|\eta_i,\Psi)$ is the conditional density of observation given the individual random effects and $P(\eta_i, \Psi)$ is the population parameter density of the individuals random effects.

The product of the N individual likelihoods determines the likelihood of a population including N individuals:

$$L(y, \Psi) = \prod_{i=1}^{i=N} L_i(y_i, \Psi) \qquad \text{(Equation 4)}$$

Because of the random effects entering non-linearly in the model, there is no closed solution of Equation 3. Several algorithms are implemented in various software to estimate model parameters. The historical, and by far the most used, software for NLME models in PKPD is NONMEM which was developed originally by L.B. Sheiner and S. Beal whom first version has been released in 1979.

The projects included in this thesis used two main likelihood approximations methods that are implemented in NONMEM:

- First order method (FO) that consists in the linearization of the likelihood using 1st order Taylor expansion around 0, the mean of random effects. FO approximation can lead to biased estimation if IIV is important or model highly non-linear (158).
- First order conditional estimates method (FOCE) that consists in the linearization of the likelihood using a 1st Taylor expansion around the Bayesian estimates of random effects (161)

Recently, a new software was released, Monolix (162). Monolix does not use likelihood approximation as NONMEM but computes exactly the model likelihood using the SAEM algorithm coupled to MCMC. EM algorithm is more robust to handle missing data and is less sensitive to initial parameter estimates. It is important to note that the last release of NONMEM (NONMEM 7) contains also new estimation methods based on the EM algorithm.

4.2.3. Model evaluation

Once the model final structure is obtained and parameters are estimated, it is necessary to evaluate model performances (163). The gold standard is to externally evaluate the model using data issued from another study or in splitting the original dataset into one learning part and one confirming part. However, it is rare to get enough materials to perform such an evaluation and usually the models are internally evaluated, i.e. the same dataset is used for model building and evaluation.

In the following, three main types of model diagnostics that have been used throughout this thesis are presented:

- Goodness of Fit plots (164)
- Visual Predictive Check (VPC)
- Normalized Prediction Distribution Error (NPDE)

4.2.3.1. Goodness of fit plots

This evaluation tool graphically compared model predictions (population, individual) to the observations. Usually several diagnostic plots are generated (165):

- Individual and population model predictions versus observations
- Residuals plots over model predictions and independent variable (Hooker AC, CWRES)
- Observations, predictions over independent variable

GoF plots can be not sufficient to properly evaluate the model because they are highly impacted by the nature of the data (166). Simulation-based diagnostics are not impacted by the nature of the data and allow revealing some model misspecifications that are not easily diagnosed with classical GoF plots.

4.2.3.2. Visual Predictive Check

Visual Predictive Check consists in simulating the dependent variable based on model structure and parameter estimates (167). N simulations of the original dataset are performed by sampling in the distributions of the random effects. Simulations allow defining a confidence interval of model predictions that is then compared to observations. The model is considered as invalid when the confidence interval does not bracket the observations.

4.2.3.3. Normalized Prediction Distribution Error

Prediction errors are the quantile of each observation within its predictive distribution (168). NPDEs are obtained after decorrelation and normalization of predictions errors with respect to the empirical mean and variance obtained in simulations. The model is considered as invalid when NPDEs are not normally distributed with a 0 mean and a variance of 1.

4.2.4. PK data analysis

4.2.4.1. Non-compartmental analysis

This approach is not model-based but allows estimating some parameters related to the drug pharmacokinetics such as the Area Under the Curve (AUC), a metric of drug exposure, the maximal concentration (C_{max}) and its time of occurrence (T_{max}). Based on these parameters that are directly m from the observations, it is however possible to compute several others parameters such as the drug clearance (Cl=Dose/AUC), the volume of distribution, or the absorbed fraction which is the ratio of AUCs following IV administration and oral administration. This type of analysis remains quite basic and does not allow neither extrapolating results nor quantifying the variability between patients.

4.2.4.2. Compartmental analysis

This model-based approach assumes that drug is distributed in the organism within compartments. Drug concentration in each of the compartments is assumed to be homogeneous at any time and compartments do not have any physiological meanings. Drug kinetics, i.e. the rate of drug passage between one compartment to another, is governed by either a rate constant times the drug amount in the compartment (1st order kinetics) or constant independent of drug amount (0 order kinetics) or non-linear in case of saturable transport.

4.2.5. PD data analysis

4.2.5.1. Direct models

These models assume a direct relationship between the drug concentration and the effect, i.e. E=f(C(t)). This model implies that T_{max} fits with the maximal effect. Direct models are rarely used to describe PD of anticancer drugs because of the delay usual reported between drug administration and drug effect.

The drug effect can be proportional to the drug concentration in a limited range but in most of the cases it shows saturation for the highest concentrations that can be modelled using an E_{max} model (Equation 5).

$$E(t) = E_0 + \left(1 + \frac{E_{max} \times C(t)}{EC_{50} + C(t)}\right) \quad \text{(Equation 5)}$$

Where E_0 is the effect at baseline, i.e. without the drug, E_{max} is the maximal effect and EC_{50} is the drug concentration that produces half of the maximal effect.

4.2.5.2. Indirect models

As previously mentioned, most of anticancer agents show a delay between their administration and their effect on tumour size. It means that the drug does not act on the tumour size itself but on the effect kinetics, i.e. the tumour growth. Such features can be modelled using indirect response models (169). In their original forms, these models

assume that the response results from a zero order production and is "eliminated" with a first order elimination (Equation 6).

$$\frac{dR}{dt} = K_{in} - K_{out} \times R \qquad \text{(Equation 6)}$$

$$R_0 = \frac{K_{in}}{K_{out}}$$

Where R is the response, K_{in} is the production rate and K_{out} is the elimination rate constant.

Tumour growth is often modelled using such indirect models. In this particular case, K_{in} is the tumour growth rate and K_{out} is the tumour death rate constant (170).

Jusko *et al.* identified four main indirect effect models that are supposed to reflect all the possible drug effects (Figure 10): synthesis stimulation, synthesis inhibition, elimination stimulation and elimination inhibition.

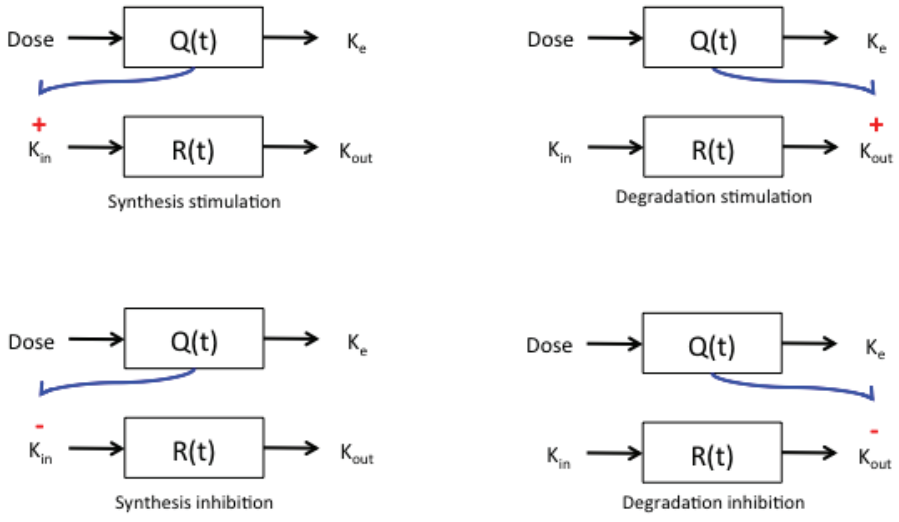

Figure 10: Indirect response models (169)

For chemotherapeutic drugs, the effect is often assumed to either stimulate the tumour degradation or inhibit the tumour growth according to their mechanisms of action. As an example, CPT11 is a topoisomerase 1 inhibitor that enhances tumour cells apoptosis and its action is more appropriately described using an enhancement of tumour degradation.

4.2.5.3. Effect compartment models

In some cases, the delay PK and PD kinetic profiles may be explained by the drug distribution into its site of action (Figure 11). Sheiner *et al.* proposed to introduce an effect compartment to differentiate plasma kinetics from site of action kinetics (171). Drug concentration in the effect compartment (also called biophase) is then linked to the effect.

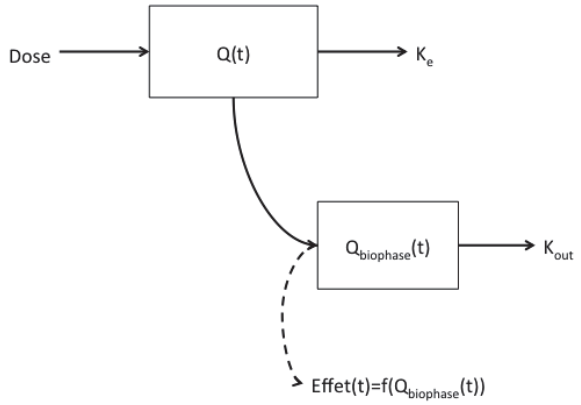

Figure 11: Effect compartment model

4.2.5.4. K-PD models

A K-PD model is a PKPD model in which drug concentrations are not measured and the PK model is thus reduced to its simplest form: a single compartment accounting for the kinetics in the biophase (172). Because no blood samples are required, K-PD models are very useful in preclinical studies by reducing the number of measurements to be performed.

K-PD models assume drug accumulation in one virtual compartment and mono-exponential elimination from this compartment (173). The PK model is thus reduced to its simplest form: bolus doses are directly input into the compartment and only a pseudo-elimination constant rate is estimated (Equation 7).

$$\begin{cases} \frac{dQ(t)}{dt} = -K_e \times Q(t) \\ Q_0(t) = Dose \end{cases} \quad \text{(Equation 7)}$$

Where K_e is the pseudo-elimination rate constant and Q(t) is the drug amount in the K-PD compartment at time t. The product $K_e \times Q(t)$ is analogous to an infusion rate and is called dose rate (DR).

Plasma PK of drugs does not need to follow a one-compartment model to be modeled using K-PD approach. K_e parameter is a composite parameter that reflects the elimination rate constant from the biophase and it accounts for the equilibrium between drug administration profile and drug amount profile in the biophase. Q(t) can thus be approximated by a one-compartment model in the biophase even if the concentration profile in plasma is multiphasic (174).

Then the K-PD compartment can be linked to response model (Figure 12).

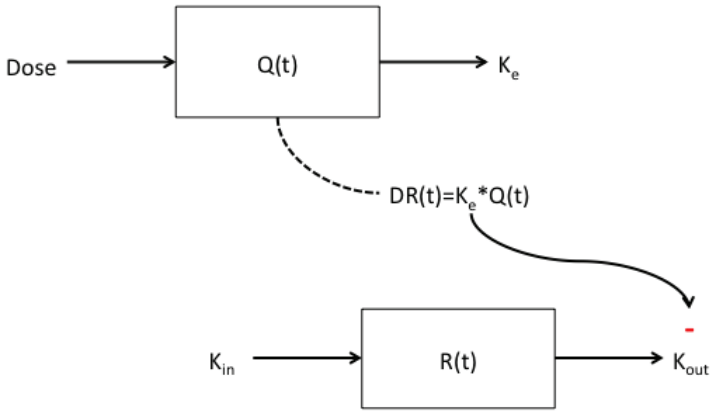

Figure 12: K-PD model linked to indirect response model

K-PD model only involves one parameter characterizing the drug kinetics, K_e. This approach must be used with caution. Since the PK information is missing it has to be compensated by the richness of the PD information with multiple times and/or doses observations to carry the information about the missing kinetic process.

4.2.6. Scaling

4.2.6.1. Interspecies scaling

Allometric scaling of animal data is the most widely used tool (although not necessarily the best) for the prediction of human pharmacokinetic parameters during drug development. The relationship between physiological parameters and body size or body weight has long been studied. In 1838 Sarrus and Rameaux postulated that in order to maintain constant internal temperature, mammals must produce energy as a constant rate proportional to their body surface area (BSA) (175). They demonstrated that the BSA is proportional to two thirds the power of the body mass and many physiological parameters can be related to the body weight according to Equation 8:

$$Y = a \times W^b \qquad \text{(Equation 8)}$$

Where a and b are the allometric coefficient and exponent respectively and W is the body weight.

The allometric scaling of PK parameters is based on Equation 8 assuming that there are anatomical, physiological and biochemical similarities among animals (176).

Clearance and physiological flow rates tend to have an allometric exponent of 0.75 indicating that they increase as species get larger but not as rapidly as body weight.

However, allometric exponents are not constant around 0.75 but tend to vary from 0.349 and 1.196 and simple allometry was shown to be inadequate to accurately predict human parameters from animal studies (177). Moreover, it is difficult to justify that a single allometric relationship may exist between body weight and all the PK parameters. If good correlations are reported for some compounds, there are also poor correlations for others that highlight the need of other approaches (178).

4.2.6.2. PBPK/PD models

Physiologically based pharmacokinetic models (PBPK) aim to describe the PK of drugs within the body in relation to the blood flows, tissue volume, routes of administration, biotransformation pathways and interaction with the tissues or organs (179). This type of models is derived from the anatomical and physiological structure of the organisms. In whole-body PBPK models, the drug enters the tissue compartment in the arterial blood and returns to the heart in the venous blood (Figure 13). PBPK models are mathematical models able to conduct extrapolations for dose-response and exposure assessments and to generate simulations of PK profiles under various physiological conditions (including different types of animals).

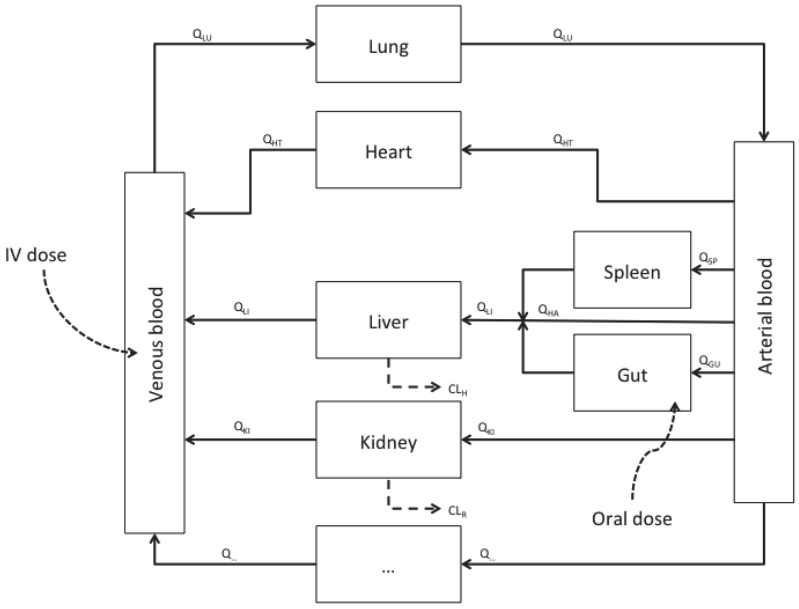

Figure 13: PBPK model structure

As opposed to empirical scaling, PBPK/PD models have richer information content and can integrate information from various sources including drug-dependent and physiological-dependent parameters as they vary between species. They can thus be used to accurately predict human PK before the first-in-human study.

In the particular case of oncology drugs, interspecies scaling is well established for PK parameters using PBPK models (180, 181). However it remains to scale PD models (182). This constitutes a largely unknown area. Even if some approaches have been proposed, there remain no generally accepted methodologies for extrapolating the anti-tumour effect measured in animal models to humans. Rocchetti *et al.* pointed that the lack of adequate metrics for drug efficacy may explain this deficiency. The evaluation of drugs in animals rely on the achievement of a certain tumour shrinkage relative to untreated animals (%T/C) that highly depends on dose, schedule, time and is thus irrelevant for scaling purposes. The authors suggested instead the use of parameters directly derived from tumour growth inhibition models that are drug-specific, i.e. drug potency and drug concentration at steady-state concentration, to scale between rodents and humans (183). Nevertheless, the assumption that drug-response in targeted tissues are analogous in animals and humans should be carefully examined with data from the relevant species.

5. Tumour growth modeling

Tumour growth modelling is an important task to support anti-cancer drug development. In 1999, Byrne *et al.* asserts that "in order to develop effective treatments, it is important to identify the mechanisms controlling cancer growth, how they interact and how they can easily be manipulated to control the disease. In order to gain such insights, it is usually necessary to perform large numbers of time-consuming and intricate experiments – but not always. Through the development of mathematical models that describe different aspects of tumour growth applied mathematics has the potential to prevent excessive experimentation and also to provide biologists and clinicians with complementary and valuable insights into the mechanisms that control the disease."(184)

Mathematical modelling is thus a powerful tool to develop and test hypotheses. It provides quantitative measure of the biological processes implied in the disease or drug mechanisms that can be used for predictions or diagnostics.

5.1. History

Mathematical models were first used to conceptualize the simple exponential growth of solid tumours, which shows constant accumulation over the time (185). Mayneord *et al.* were the first to point the reduced growth of solid tumours during the latest phases of growth. They conducted an experiment on the effect of X-rays on the growth of rat sarcomas and noticed a linear growth for the latest stages of the experiment. After histological examinations, which revealed that the active growth was restricted to a thin shell at the periphery of the tumour, Mayneord et al developed a mathematical model that investigated the effect of different distribution of dividing tissues. This model illustrated the rapid initial growth that gradually decreases as the region of active

growth progressively restricts to an outer shell of tissue. Observations conducted by the authors lead to the introduction of logistic tumour growth models that allow reduced growth in the later stages.

Mathematical models became more and more complex thanks to the experimental work on cellular kinetics in which growth fraction as well as cell cycle kinetics were analysed. After the initial work form Steel *et al.* (186) that revealed the differences between time scales involved in cellular and tumour kinetics, models started to account for physiologically relevant parameters such as the volume doubling times or the cell loss and growth fraction kinetics.

Recently, with the explosion of data issued from cellular and molecular biology, tumour growth models tend to integrate more complexity levels. Basically, models using this type of data can be classified in two categories:

- **Static models** that provide a framework for describing the expression of various cell cycle regulatory proteins. This type of models is useful because they allow understanding mechanisms at the molecular and cellular levels (187). In computational biology, such models are commonly used to analyse interaction networks and to simulate cellular components kinetics.
- **Dynamic models** that describe the functional properties of the biological system. Tumours are unstable systems and it is necessary to characterize and predict their changes in architecture, physiology and responses. This type of model supports the understanding of complex mechanisms such as carcinogenesis.

Carcinogenesis, i.e. the ability of a single cell to become a lethal lesion, was nicely modeled by Tan *et al.* with a k-stage Markov model (Figure 14).

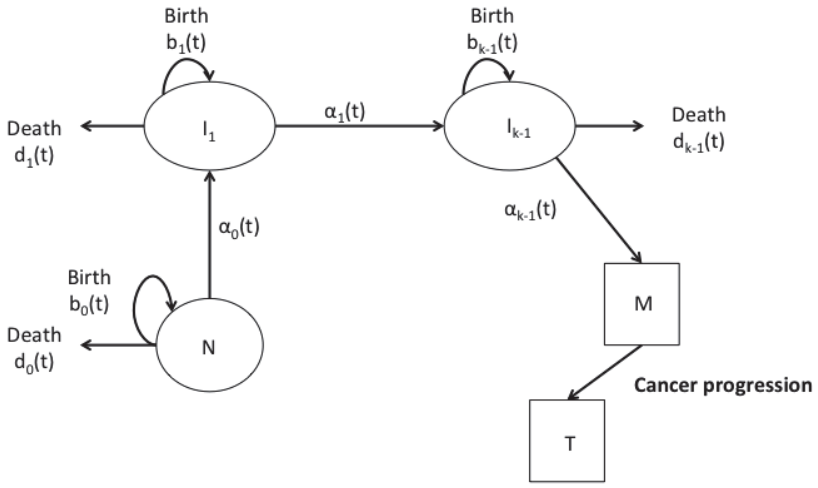

Figure 14: Schematic representation of a k-stage multilevel Markov model of carcinogenesis.

N = normal stem cell; I_i = the i^{th} stage initiated cell; i = 1, 2,.....,k ; M = proliferating cancer tumour cell; T = malignant tumour (188)

However, these complex models failed to extrapolate their results to patients and are unable to assess treatment outcomes. This is mainly due to the difficulty to parameterize these models using clinically relevant parameters and to estimate their parameters because most of them are not identifiable. These models derived from the system biology do not address one of the primary interests in oncology research: the prediction of treatment outcome.

A major challenge in oncology PK/PD modelling is the complexity of the system and the need for models to find a suitable balance between complexity and clinical relevance. Moreover, contrary to others therapeutic areas, the strict application of PK principles to target blood or plasma concentrations are not appropriate for anticancer drugs. Twenty years of PK studies have failed to improve cancer treatment for epirubicin attesting the limited utility of PK models alone as a surrogate of treatment efficacy. In oncology, much more than in others therapeutic areas, it is necessary to focus on the PD aspects.

5.2. Tumour growth models in preclinical drug development

Both *in vitro* and *in vivo* evaluations of anti-tumour drug effects are fundamental steps in the preclinical development of drugs in oncology.

In vitro models are used in order to characterize cellular effects of drugs. These models are often based on *in vitro* cellular growth experiments where cells are exposed to various concentrations of drugs in order to determine the drug potency, usually the IC_{50} value the drug concentration providing 50% of the drug effect. The range of complexity of *in vitro* models is large with the most basic ones only graphically estimating IC_{50} value and the most advanced ones accounting for the kinetics of drugs effect on cellular components. However, none of the models available in the literature account for the variability inherent to these experiments with a mixed effects approach so that their parameters only reflect the typical value.

The development of *in vivo* tumour growth models arose with the development of adequate animals' models such as syngeneic mouse and human xenografts that allow monitoring the entire growth time-course through the measurement of tumour size. The response to treatment can be easily evaluated in animals by directly comparing the tumour growth in treated animals and control animals. As it has been previously mentioned, those direct metrics depend on doses and study designs. Moreover, their biological interpretation is limited making difficult to predict quantitatively the activity of anticancer drugs in others conditions than those explored experimentally (different species, different dosing regimens).

In order to fully exploit the animal models, mathematical tumour growth models have been developed. Empirical models used well-known mathematical equations: logistic, Verhulst, Gompertz, von Bertalanffy without in-depth mechanistic description of the underlying physiological processes (189). Drug effects can thus be only evaluated in

terms of changes in the parameter values that describe the tumour growth. Such changes depend on the dose level and schedule so that these models can only be used retrospectively. The importance to differentiate system and drug-specific parameters has been illustrated by Levasseur *et al.* (190). They applied an exponential kill model to predict the shape of the dose-response curve based on the cell-cycle drug specificity, the cell cycle time and the duration of drug exposure at the site of action. Even if their model did not provide any insights on how drug and tumour characteristics can affect the dose-response curve, it highlights the importance for models to capture the time dependency, in separating drug and disease specific parameters, of the dose-response curve *in vivo*.

More complex models based on mechanistic descriptions of biological processes underlying tumour growth were recently proposed (191, 192). These models are built by making assumptions about tumour growth involving cell cycle kinetics and biochemical processes such as those related to angiogenesis or immunological responses. Because of their complexity their development is time-consuming and they involved more parameters than empirical models.

To date, the most widely used semi-mechanistic tumour growth models in preclinical drug development has been proposed by Simeoni *et al.* (191). This model links the drug plasma concentration to the effect on tumour growth in xenografted mice. It assumes that unperturbed tumour growth can be modelled with two phases: exponential followed by linear without reaching a plateau. It thus exists a threshold tumour mass at which tumour growth switches from exponential to linear (Equation 9):

$$\begin{cases} \frac{dw(t)}{dt} = \lambda_0 \times w(t) & w(t) \leq w_{th} \\ \frac{dw(t)}{dt} = \lambda_1 & w(t) > w_{th} \\ w(0) = w_0 \end{cases} \qquad \text{(Equation 9)}$$

Where w(t) is the tumour mass at time t; w_{th} is the tumour mass threshold, λ_0 is the exponential tumour growth rate and λ_1 is the linear growth rate.

To simplify model computations, it has been re-parameterized as follows (Equation 10):

$$\begin{cases} \frac{dw(t)}{dt} = \frac{\lambda_0 \times w(t)}{\left(1+\left(\frac{\lambda_0}{\lambda_1}\times w(t)\right)^{\psi}\right)^{\frac{1}{\psi}}} \\ w(0) = w_0 \end{cases} \quad \text{(Equation 10)}$$

For high values of ψ, Equation 10 is a good approximation of the original switching system.

When a drug is introduced into the system, it perturbs the natural tumour growth. At the beginning all the cells are assumed to proliferate according to Equation 9 and the drug affects a percentage of the original pool bringing them to death. Because of the delay usually observed between anticancer drugs administration and effects observed on the tumour, Simeoni *et al.* introduced a transit compartment model to mimic the progressive degree of cell damages leading to cell death (Equation 11, Figure 15).

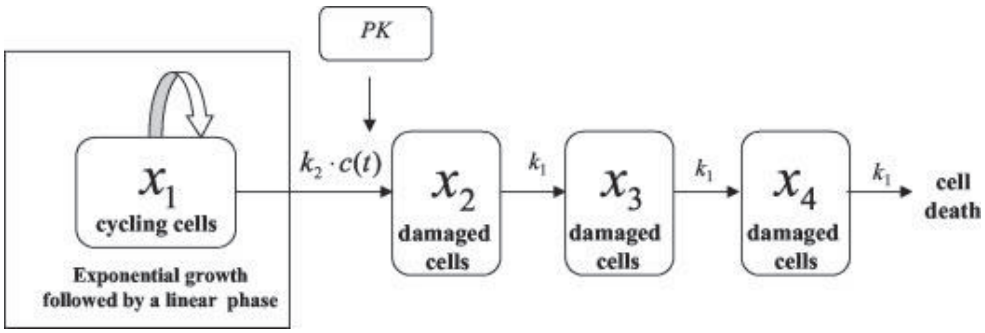

Figure 15: Scheme of the perturbed tumour growth model from Simeoni *et al.*(191)

k_1 is the first order rate constant of transit; k_2 is a measure of drug potency and c(t) is the plasma concentration of the anticancer agent.

$$\begin{cases} \dfrac{dx_1(t)}{dt} = \dfrac{\lambda_0 \times x_1(t)}{\left(1+\left(\frac{\lambda_0}{\lambda_1}\times x_1(t)\right)^{\psi}\right)^{\frac{1}{\psi}}} \\ \dfrac{dx_2(t)}{dt} = k_2 \times c(t) \times x_1(t) - k_1 \times x_2(t) \\ \dfrac{dx_3(t)}{dt} = k_1 \times \left(x_2(t) - x_3(t)\right) \\ \dfrac{dx_4(t)}{dt} = k_1 \times \left(x_3(t) - x_4(t)\right) \\ w(t) = x_1(t) + x_2(t) + x_3(t) + x_4(t) \\ \\ x_1(0) = w_0;\ x_2(0) = x_3(0) = x_4(0) = 0 \end{cases} \quad \text{(Equation 11)}$$

Where $x_1(t)$ is the fraction of proliferative cells at time t; $x_2(t)$, $x_3(t)$ and $x_4(t)$ are the fraction of cells affected by the drug; k_2 is the drug potency and k_1 is first order rate constant of transit.

This model was successfully applied to different drugs included new compounds. It thus successfully described the inhibition of tumour observed at different dose levels and schedules independently of the mechanism of drug action. Based on this model and single experiment in animals, it is possible to derive quantitative meaningful PD parameters that are drug specific: k_1 related to how rapidly the tumour cells are killed and k_2 related to the drug potency.

Some extensions of this model have been proposed. In particular, Rocchetti *et al.* extended the model for drug combinations. Even if the tumour growth model remains the same, they modified the drug potency parameter to account for the drug combinations (Figure 16).

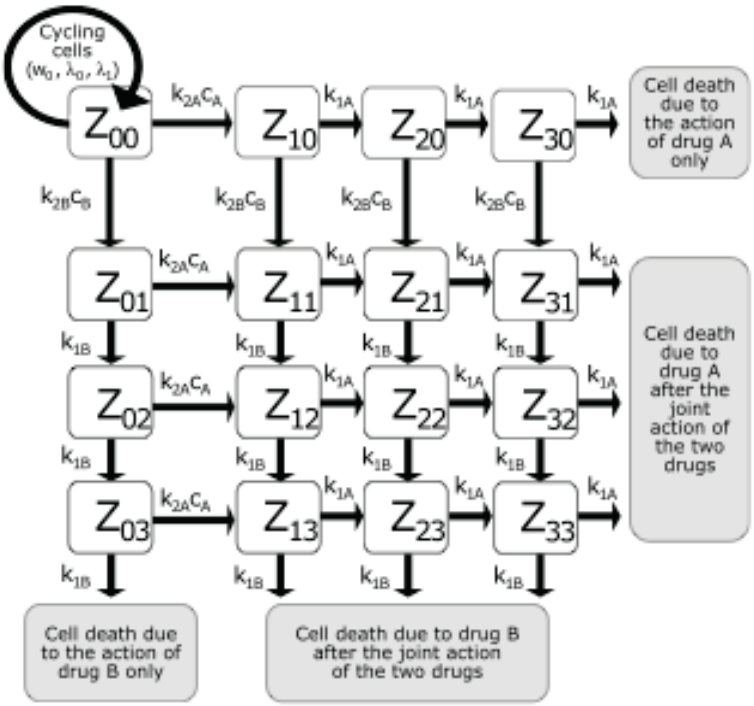

Figure 15: Scheme of the extended Simeoni's model for drug combinations (193)

In order to remove the discontinuity present in the model, Koch *et al.* rewrote the unperturbed tumour growth model as follows (194):

$$\frac{dw(t)}{dt} = \frac{2\times w(t)\times\lambda_0\times\lambda_1}{\lambda_1+2\times\lambda_0\times w(t)} \qquad \text{(Equation 12)}$$

Model parameters keep the same signification as in Simeoni's model and it is also possible to extend this model for drug combinations.

Hahnfeldt *et al.* has proposed another important tumour growth model in preclinical drug development (192). Their model focuses on the relationship between tumour growth and development of tumour vasculature. It accounts for the time-dependent carrying tumour capacity under angiogenic control.

The authors modified the usual Gompertz model in replacing the maximal capacity by a variable carrying capacity that whose rate of change depends on the tumour volume (Equation 13).

$$\frac{dV}{dt} = -\lambda_1 \times V \times log\left(\frac{V}{K}\right), K' = f(K,V,t) \qquad \text{(Equation 13)}$$

Where V is the tumour volume; λ_1 is the tumour growth rate and K is tumour carrying capacity that is a function of time and tumour volume.

The carrying capacity is now defined as the effective vascular support provided to the tumour as reflected by the tumour size. It comes that if K>V, the tumour vasculature supports tumour growth whereas if K<V it supports tumour shrinkage. The form of f(V, K, t) is based on the biological processes that control the size of the effective vascular network. Drug effect modifies the carrying tumour capacity function depending on the drug target. Hahnfeldt *et al.* successfully applied this model to data issued from experiments evaluated anti-angiogenic drugs.

This model has also been used as a basis for some others works such as the model proposed by Ribba *et al.* that accounts for the tumour composition on top of the varying tumour capacity (195)(Figure 16). Even if the model did not include any drug effect yet, authors used it to simulate effects of the accumulation of cytotoxic combined to anti-angiogenic compounds in order to optimize their times of delivery.

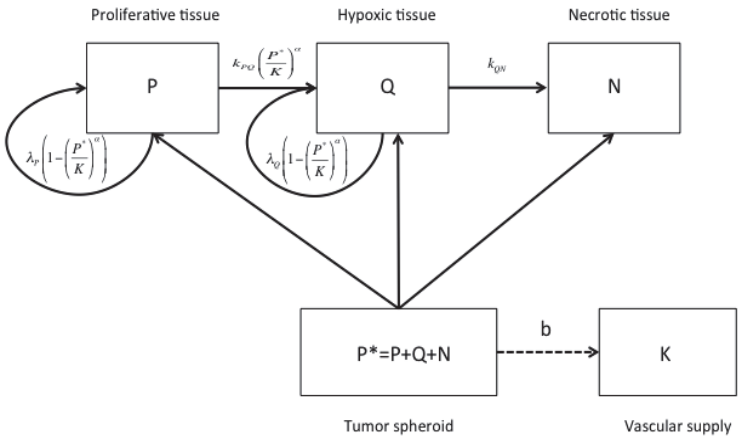

Figure 16: Scheme of Ribba's model

A limitation of the above models could be that, apart from Ribba's model, none of them include mixed-effects so that the variability observed between animals is never quantified reducing their extrapolation abilities.

However, it has been shown many times that the exploitation of this type of preclinical PKPD models reduced the risk of development failures in the later clinical phases with an important impact on the costs of late failure (196).

5.3. Tumour growth models in clinical drug development

Contrary to preclinical tumour growth inhibition models, it exists a lack of mechanistic tumour growth models in patients mainly explained by the difficulty to monitor as many variables as in animals. Moreover, the lack of mechanistic model in clinic creates a gap between what is learned during preclinical development and clinical outcomes. One example of translational model is the model developed by Tham *et al.* for NSCLC patients treated with gemcitabine and carboplatin (197). This model directly links drug plasma AUC to the tumour time course using an effect compartment that accounts for the drug distribution to the biophase (Figure 17).

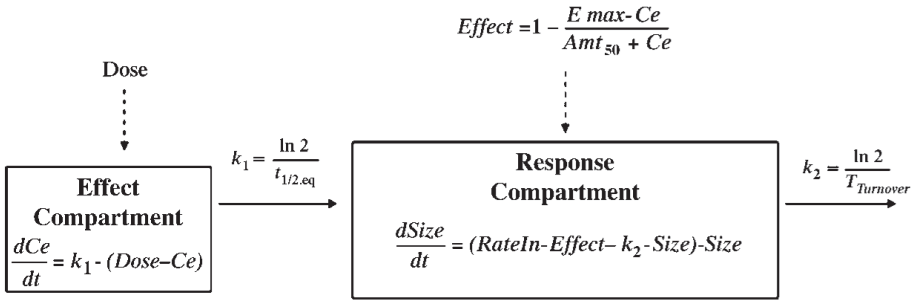

Figure 17: Scheme of the Tham's model

k_1 is a first order constant for effect equilibration ($k_1 = \frac{ln(2)}{t_{\frac{1}{2},eq}}$), k_2 is the second order rate constant for tumour loss ($k_2 = \frac{1}{T_{turnover}}$); Amt_{50} is gemcitabine dose required to produce 50% of the maximum inhibition in tumour growth and E_{max} is the maximal effect

Instead of using traditional clinical endpoints, the authors used a continuous scale to describe the time course of the tumour response relatively to the drug exposure. This AUC driven model thus predict changes in tumour size during and after multiple cycles of

chemotherapy. However, it does not fill the gap between anti-tumour activity and the main clinical endpoint in oncology, the overall survival.

From a drug development perspective, the ability to link anti-tumour activity in early phases of development to overall survival is critical for the progression of a molecule. As stated by the FDA in 2007 the only acceptable endpoint in oncology is the improvement of overall survival. Even with the discovery of new targets, the identification of relevant measure of drug efficacy other than overall survival remains a sensitive point.

The definition of a surrogate endpoint in oncology trials is not an easy task because a positive result in an early indication is not necessarily correlated to the final endpoint. Many examples show a correlation between progression free survival (PFS), antitumour efficacy and overall survival. However, this strong correlation between PFS and OS is not universal across tumour types (198).

In that sense, tumour growth models combined to survival analysis can be extremely powerful in order to predict overall survival at early stages of the study.

Recently, two publications showed how to predict patients' survival based on tumour growth models using modeled tumour size as a surrogate endpoint of patients' survival.

The most cited and used is the tumour growth inhibition (TGI) model from Claret *et al.* (170). This model was built on colorectal cancer patients treated with capecitabine. Based on capecitabine phase 2 data, they developed the following model:

$$\begin{cases} \frac{dy(t)}{dt} = K_L \times y(t) - K_D(t) \times y(t) \times Exposure(t) \\ K_D(t) = K_{D,0} \times e^{-\lambda \times t} \\ y(t=0) = y_0 \end{cases} \quad \text{(Equation 14)}$$

Where y(t) is the sum of the longest tumour diameter at time t, i.e. the tumour size; y_0 is tumour size at baseline; K_L is the tumour growth rate; $K_D(t)$ is the drug-constant cell kill rate that decreases exponentially with time from an initial value $K_{D,0}$ to account for the

development of drug resistance; Exposure(t) is the drug exposure at time t. Because no PK data were available, the daily dose was used as a metric for exposure to drive drug effect.

The model incorporates drug-specific ($K_{D,0}$, λ) and disease-specific (y_0, K_L) parameters. A survival model was then developed to describe the survival time distribution as a function of covariates derived from the model. The survival time described with a log-normal distribution ($Log(T) \sim logN(\alpha,\sigma^2)$) was found to be adequately predicted, using the relative change in tumour size observed at the first follow-up visit, around 7 weeks after the treatment onset. The survival model is thus drug-independent and relates a biomarker, the relative change in tumour size, to the clinical endpoint.

Claret *et al.* then used this modeling framework to predict patients' survival to be observed in a capecitabine phase 3 study. After realization of the study, the predicted and observed survivals were compared. As shown in Figure 17, the TGI model combined to the survival model adequately predicted the survival time in this study attesting the utility of this approach to early predict clinical endpoint.

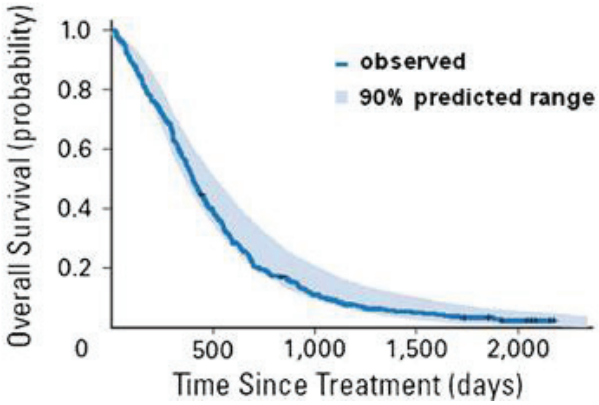

Figure 17: Prediction of patients' survival in capecitabine phase 3 study based on the modeling framework form Claret *et al.*
The light blue area represents the 90% prediction interval of the survival curve and the blue line represents the observed survival curve.

Because of its predictive capabilities and its flexibility this model was used in the following to optimize dose and dose schedule of capecitabine.

Pursuing the same objective, Wang *et al.* developed a TGI model for NSCLC patients treated with various therapy (199). Their model also describes the sum of the longest tumour diameters with a model combining mixed exponential decay and linear growth (Equation 15).

$$y(t) = y_0(t) \times e^{-SR \times t} + PR \times t \qquad \text{(Equation 15)}$$

Where SR is the tumour exponential shrinkage rate constant; PR is the linear tumour progression rate constant.

The tumour shrinkage characterizes the treatment effect on tumour growth and the linear growth is an approximation of the tumour growth under a specific treatment. Since data from different experiments were pooled to build this model, no drug PK was accounted for in the model.

The authors linked the TGI model to a survival model, three covariates were found to predict patients' overall survival: the baseline tumour size, the relative change in tumour size at week 8 (PTR_{W8}) and the ECOG score that is specific of NSCLC (Equation 16).

$$log(T) = \alpha_0 + \alpha_1 \times ECOG + \alpha_2 \times Baseline + \alpha_3 \times PTR_{W8} \qquad \text{(Equation 16)}$$

The authors used the survival model in order to predict the overall survival in patients from different studies. Model predictions were in accordance with the observations.

These models directly link the early change in tumour size to patient's overall survival. However, one can argues that it would be preferable to use biomarkers more easily measurable to predict clinical endpoints. In that purpose, You *et al.* proposed to use kinetic models of serum biomarkers that are over-produced during cancer (e.g. PSA for prostate cancers or CA125 for ovarian cancers). This type of approach can be extended

either to give more mechanistic insights through the modelling of biomarkers production or to link their kinetics to tumour growth (200, 201).

Another important part that is not detailed in this thesis concerns all the models for anticancer drugs side effects. Because of their narrow therapeutic window, old and new anticancer compounds display high toxicities that are necessary to model in order to limit their incidence and severity. The most common dose-limiting toxicity associated to chemotherapy drugs is febrile neutropenia that is thus the most studied toxicity. The reference model for neutropenia was proposed by Friberg *et al.* (202). This model can be used to identify patients with higher risk of toxicity which is particularly important in elderly and paediatric patients (Sostelly A, JGO, 2012).

6. Tumour response optimization

As it has been mentioned in the previous section, tumour growth models are very useful to predict clinical outcomes and to reduce drug development failures. One step ahead could be to optimize the design of upcoming oncology clinical trials based on tumour growth models in order to optimize the patients' response.

6.1. Population optimal design

A design may be optimized in many respects. Here, we consider how to optimize the design in order to reduce the expected uncertainty about the parameter of the model. In this kind of problem, optimal design methodology is typically based on the Cramer-Rao inequality that states that the inverse of the Fisher Information Matrix (FIM) is a lower bound of the variance-covariance matrix of any unbiased estimators of model parameters:

$$FIM^{-1}(q,\Theta) \leq COV(\hat{\Theta}) \qquad \text{(Equation 17)}$$

Where q is the vector of design parameters and Θ is the vector of model parameters.

The FIM is defined as the expectation of the second derivatives of the partial log-likelihood with respect to the model parameters (Equation 18):

$$FIM(q,\Theta) = -E\left(\frac{\partial^2}{\partial\Theta^2} Log\ L\right) \qquad \text{(Equation 18)}$$

Based on the Cramer-Rao inequality, the information in an experiment depends on the design. The design that maximizes the determinant of the FIM (i.e. maximizing the information) will give the most precise parameter estimates.

For NLME models, the FIM has to be approximated because there is no closed form for the marginal likelihood (see 4.2.2). Population optimal design was firstly introduced by Mentré *et al.* (203). They proposed to linearize the model to a linear mixed effects model to find a closed form for the FIM assuming normal distributions for the random effects.

This first attempt showed some limitations regarding the shape of the parameters distribution. Further extensions to this original approximated FIM were then proposed in order to refine the approximation (204).

Optimizing the upcoming experiment aims to maximize the information gained by the experiment. In order to use usual maximization methods, it is necessary to define a scalar function of the FIM. The most often used criteria assume that model parameters are known point values (local optimization). It means that unknown parameters are known without error to calculate the FIM. Two commonly used criteria are D-optimality that maximizes the determinant of the FIM, and A-optimality that maximizes the trace of the FIM.

To avoid issues inherent to local optimization, it is possible to use global criteria where parameter distribution is assumed. These criteria have been proven to get more robust optimal design. The most commonly used global optimal criteria are: ED-optimality that maximizes the average of the determinant of the FIM over the parameter distribution and EID-optimality that maximizes the determinant of the inverse of the FIM over the parameter distribution (205).

There are numerous of examples of applied optimal design. The main application of this mathematical theory is the optimization of the sample times in clinical trial with the objective to reduce the study costs. This has been demonstrated for ivabradine where sparse designs were shown to bring the same levels of information than the original design (206). However, any design parameters can be optimized and more clinically relevant designs have also been proposed in order to optimize trial duration or doses (207, 208).

6.2. Optimal control

Optimal control (OC) aims at optimizing a clinical criterion (target concentration, percentage of responders, tumour size reduction, …) within clinical constraints. Principles of OC are based on the optimization of a loss function that is defined based on the target to reach for the clinical criterion and clinical constraints. Any design variables can be optimized using OC but this approach is more often applied to optimize dose or dosing interval (209).

As an example, Gaillot *et al.* defined the following loss function to optimize the dosing schedule of lithium in order to reach a certain target concentration at steady state (210):

$$r(C) = 0 \; for \; 0.8mmol.L^{-1} \leq C \leq 2mmol.L^{-1} \qquad \text{(Equation 19)}$$

Where r(C) is the loss function for the lithium concentration C.

The thresholds were defined and related to the toxicity and efficacy. They choose the function so that it increases as a function of the square if the deviation between the unwanted concentration and the transgressed threshold.

$$r(C) = 100 \times (0.8 - C)^2 \; for \; C < 0.8mmol.L^{-1} \qquad \text{(Equation 20)}$$

$$r(C) = 100 \times (C - 2)^2 \; for \; C \geq 2mmol.L^{-1} \qquad \text{(Equation 21)}$$

The choice of the normalization coefficient is arbitrary.

The loss function assigns to each value taken by the criterion an assumed loss. To globally characterize its loss, the mean value of the loss function over the time is usually computed.

$$R_q(p_i) = \frac{1}{\tau} \times \int_0^\tau r(criterion, p_i)dt \qquad \text{(Equation 22)}$$

Where $R_q(p_i)$ is the risk function for the q design and for individual parameters p_i.

For a particular design, Equation 22 defines the total risk corresponding to the subject whose parameters are p_i.

The optimality criterion is the expected value of the total risk:

$$OC = E_p[R_q] \qquad \text{(Equation 23)}$$

The optimality criterion is a function only of the design parameter q. The design parameter obtained by minimization of the optimality criterion fulfils the optimality requirements because the risk is related to the clinical constraint to maintain the clinical criterion within the clinical constraints and the optimality criterion is computed over the whole population.

Contrary to population optimal design, the information content is not maximized with optimal control, only the clinical criterion is accounted for here.

6.3. Clinical trial simulation versus optimisation

A recent review highlighted the benefits of model-based clinical trial simulation (CTS) to optimize the efficiency of drug development process (211). The question of the benefits of population optimal design theory arises when experiments can be optimized using only simulations.

In CTS, data are simulated using a known model under a certain design and model parameters are then re-estimated with another design so that the performances of each design in terms of power or biased can be easily evaluated. CTS is a powerful tool because different types of data can simultaneously be handled and different models can be simultaneously used. However, it can become extremely computer-intensive because usually more than 1000 datasets have to be simulated and re-estimated to obtain relevant results. This is clearly a drawback when multiple design settings have to be optimized. Therefore, only a limited number of design candidates can be explored.

OD is thus preferable because it allows optimizing multiple design variables in one step in a shorter time (208). Moreover, the development of new optimal design methods such as adaptive optimal design will allow to better account for clinical constraints.

7. Mechanistic model-based drug development

7.1. Drug development process

Drug development process follows several steps form the target identification on cell cultures to the pharmacovigilance studies performed after drug approval. This process is largely recognized as inefficient, long and costly: from a set of compounds identified on cell cultures only one will eventually reach the market and the risk of development failure increases at late stage of development when clinical studies are the most long and costly (212). Historically, drug development is based on trial-and-error approaches, the information gained in the previous steps of development is never properly handled. With this approach each new step of development is a new beginning and the information issued from previous experiments is more or less omitted. In the critical path initiative to new medical products, the Food and Drug administration pointed the necessity of new methodologies to improve drug development (213). Among all the methodologies listed by the FDA, modelling and simulation has been recognized as a powerful tool to support decision making in drug development.

Modelling and simulation can be used at each step of the drug development process. In 1997, L.B. Sheiner suggested that drug development can be viewed as a succession of learning and confirming phases ("learn/confirm paradigm"). Learning from data results from preclinical and clinical studies with the development of models. These models allow defining new hypotheses that have to confirmed in future experiments (214). Model building consists in the structuration of all the information already available whereas simulation consists in projecting this information.

Pharmacometrics does not pursue the same objectives at the different steps of drug development but can always support the decision making in drug development (Figure 18).

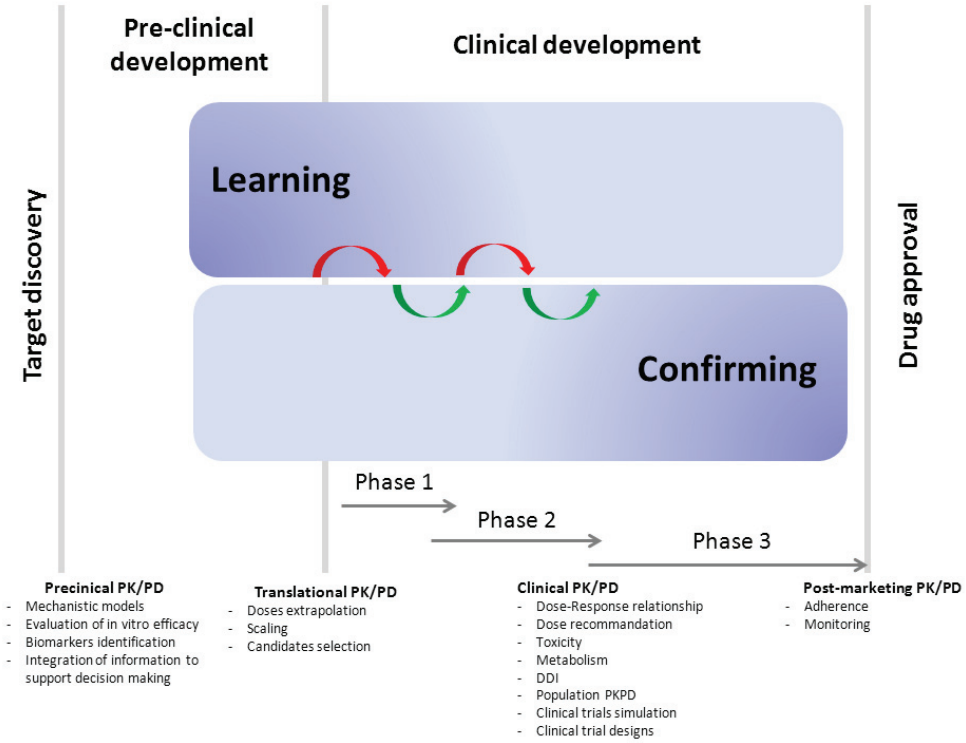

Figure 18: Potential applications of PK/PD modeling during drug development (215)

Modelling and simulation can thus accelerate the drug development process by anticipating all the upcoming steps and by early detecting the best candidates. It thus decreases the risk of development failure in phase 3 studies that are the longest and the most expensive ones since most of the development efforts can be moved to early phases for the most promising candidate. For all of these reasons, pharmacometrics is more and more integrated in pharmaceutical industry as a tool to support the decision-making at each step.

7.2. Current issues in oncology drug development

Drug development in oncology presents specific issues that are inherent to the complexity of the disease. Even if new compounds continuously reach the market, the drug

development in oncology can be considered as the most inefficient one compared to others therapeutic areas. Only 5% of oncology compounds show a successful development and more than 60% of compounds in phase 3 will never reach the market (196). Moreover, therapies currently available have a limited efficacy in the most common types of cancers and display significant toxicities (216).

Each step of oncology drug development displays some issues that require the development of innovative methodologies to improve it. In the following, only issues related to preclinical development and to phase 2 evaluation are presented since they constitute the core of this thesis.

The main reason of the inefficiency in oncology drug development lies in the lack of detailed knowledge in tumour cell biology even with the explosion of molecular biology, inadequate preclinical models to identify and test compounds and inappropriate analysis of results issued from preclinical and clinical studies.

Tumour cell lines used in *in vitro* models to screen anticancer agents are often selected on their ability to rapidly grow and do not reflect the genetic diversity of tumour cells *in vivo*. Moreover, data issued from *in vitro* experiments are rarely properly handled (see 5.2) and quantitative drug effects are thus usually known only approximately.

The ability of animal models to reflect the tumour growth in patients can also be questioned (217). If animal models can easily lead to discard an inactive compound, the predictive power of positive results in animals is less reliable. This is mainly due to the lack of adapted transition models between animals and humans. One consequence is the sub-optimality of phase I trials designed using traditional methods to extrapolate maximal tolerated dose from rodents to patients.

This inadequate preclinical development results in overall inefficient clinical development as it has been demonstrated with P-gp inhibitors: the strong efficacy of these compounds *in vitro* and in animals was never retrieved in patients.

Another critical point in oncology drug development concerns the evaluation of phase 2 trial. Typically, the decision to move a compound to the phase 3 is based on the achievement of a predefined objective response rate (ORR) calculated using RECIST criteria (Response Evaluation Criteria In Solid Tumours) at a certain time point (218). The problem of using ORR to evaluate compounds is that their estimation in small selected populations, such as these used in phase 2 study, is rather imprecise. In that sense, ORR cannot correctly inform the design of the upcoming phase 3 study. Moreover, RECIST criteria are computed at a certain time point and omit the entire tumour growth dynamics, they are thus unable to evaluate targeted therapies.

7.3. Benefits of mechanistic model-based drug development in oncology

As it has been previously mentioned, one of the main reasons for the lack of impact of models in preclinical development of anticancer compounds is the absence of appropriate mechanistic PKPD models in animals. However, this type of models can certainly fill the gap existing between animals and patients. Key issues that can be covered by mechanistic PKPD models are the following:

- Characterization of the entire time course of the disease progression in order to properly understand the drug mechanisms. This can be addressed with models separating drug and disease-specific parameters.
- Characterization of the intracellular and tumour drug PK and its relationship to plasma drug PK in order to obtain an indirect measure of drug concentrations at the site of action.

- Integration of information issued from *in vitro* and *in vivo* models through the development of mechanistic models in order to ease the translation between animals and patients.

Regarding the design and evaluation of phase 2 studies, modeling and simulation can be used to predict a clinical endpoint based on predictors issued from the model. Quantitative criterion derived from the model can also be used to optimize phase 2 design to improve patients response in terms of efficacy and safety.

Some anticancer drugs have already benefited of such approaches in their development. For example model-based CTS was performed for docetaxel in order to support the decision making (219) or a PBPK/PD model was developed for capecitabine based on preclinical data in order to predict the tissue exposure in patients (220).

In the particular case of efflux transporter inhibitors, mechanistic PKPD models have never been used during their preclinical and clinical development. To date, one mechanistic model, built a posteriori, that study the impact of tumour biology on P-gp inhibitors efficacy bas been reported (221). A model-based development would have increased the likelihood of a successful development, or helped to explain the reasons for a failure.

Objectives of the thesis

If the inhibition of P-gp failed to improve the management of drug resistance in cancer patients, the inhibition of others efflux transporters such as BCRP has rarely been addressed in preclinical and clinical studies. A new BCRP inhibitor, MBLI87 showed promising properties *in vitro* and *in vivo* and would allow retesting the benefit of efflux transporters inhibition in the management of anticancer drug resistance. To avoid the issues already encountered in the development of P-gp inhibitor, it was deemed necessary to develop mechanistic PK/PD models from the early development of this new molecule.

The overall objective of this thesis is to show the benefits of mechanistic model-based drug development applied to efflux transporter inhibitors for understanding their action (or lack of action).

Three specific objectives were thus identified:

- To show the benefits of non-linear mixed effects PK/PD models in the early preclinical development of efflux transporter inhibitors
- To develop template semi-mechanistic models to support the preclinical development of MBLI87 and future BCRP inhibitors.
- To show the benefits of non-linear mixed effects tumour growth model to optimize dose schedule in order to maximize tumour response in patients displaying drug resistance

Chapter II

Mechanistic model-based development applied to efflux transporter inhibitors

As it has been suggested in the introduction, the development of relevant mechanistic models to support preclinical drug development is important to ensure the future development of the compound.

This chapter deals with the development of mechanistic models of the interaction between efflux transporter inhibitors and cytotoxic drugs both *in vitro* and *in vivo*.

The first axis developed here concerns the construction of a NLME mechanistic model to study the cellular disposition of cytotoxic drugs in presence of efflux transporter inhibitors *in vitro* (Publication 1). The second axis re-uses the *in vitro* model in a multi-scale semi-mechanistic PKPD model where both the cellular dispositions of cytotoxic as well as the tumour composition are accounted for (Publication 2).

Throughout this chapter, the benefits of the NLME approach to analyze preclinical data will also be shown.

1. Modeling the interaction between cytotoxic and efflux transporter inhibitors *in vitro*

1.1. Introduction

Usually efflux transporters inhibitors are tested *in vitro* using competition experiments with cell transfected with the gene coding for the studied transporter. Data issued from *in vitro* experiments are analyzed with classical biochemistry methods in order to determine the interaction mechanism between the inhibitor and the substrate. This type of approach does not account for the competing processes such as passive diffusion and does not discriminate intra from inter experiment variability that result in biased parameter estimations. Mixed-effects approach combined to mechanistic model

accounting for all the processes occurring in the experimental system allow overcoming these previous issues.

In this study, we propose such a model to study the effect of MBLI87 on the cellular disposition of different BCRP substrates. The model was formulated as a function of meaningful parameters and in a fairly way to allow its use as a template for studying others efflux transporter inhibitors.

1.2. Methods

Human Embryonic Kidney 293 (HEK293) cell line transfected with either ABCG2 or empty vector was used to study the interaction between MBLI87 and well-established BCRP substrates (CPT11, SN38 and Mitoxantrone). The competition experiment was carried out by exposing cells for 30 minutes to fixed concentrations of substrates and various concentrations of inhibitors. Intracellular concentrations of substrates were monitored using HPLC-MSMS for CPT11 and SN38 and using flow cytometry for Mtx.

Data displays high inter-experiment variability and the expected transport saturation was not observed with the range of inhibitor concentrations used.

To model these data, a NLME transport inhibition model was developed. In this model, drugs cross cell membrane by passive diffusion; the active efflux is assumed to be only ABCG2 mediated and the interaction between substrates and inhibitor occurs within the transporter. In order to fit the data, several assumptions were included in the model to simplify its formulation. Substrates concentrations were measured up to a correction factor, which depends on experimental conditions such as extraction yielding or intracellular proteins binding which can vary between experiments. In order to model the "true" free intracellular substrate concentration, the correction factor was estimated for all the substrates.

Model parameters were estimated using NLME approach using the NONMEM software version 7.2.

1.3. Results

The final model expresses the intracellular substrates concentration as a function of extracellular concentration of substrates and inhibitor, ratio between intrinsic transport clearance and diffusion clearance, inhibitory constant and correction factor.

An inter-experiment variability was allowed for the correction factor and the clearance ratio and was found higher for CPT11 and SN38 than for Mtx. Model evaluation did not reveal any misspecifications.

The MBLI87 inhibitory constant (K_i) was estimated at 141nM for Mit, 289nM for CPT11 and 1160nM for SN38. The ratio of intrinsic transport clearance divided by diffusion clearance was estimated at 1.5 for Mit, 0.1 for CPT11 and 4.4 for SN38.

1.4. Discussion

Because of the assumptions included in the final model, it was not possible to distinguish between non-competitive and competitive interaction. However, it is possible to determine the nature of the interaction of CPT11 and SN38 with MBLI87 by considering their structure. As shown in Figure 2 both compounds get a close chemical structure meaning that they should bind to the same site on the transporter with thus a close MBLI87 K_i value. The model predicted different K_i values for CPT11 and SN38 attesting that inhibitors and substrates do not bind the same site on the transporter, which is in favour of a non-competitive interaction. This result is in accordance with the recent findings on ABCG2 structure that demonstrate that the transporter displays several binding sites (222).

The control experiment with non-transfected cells revealed that CPT11 and Mit were not transported in the absence of ABCG2. By contrast, an increased intracellular SN38 concentration was observed by increasing MBLI87 concentrations. This unexpected result indicated the presence of another transport mechanism occurring in these cells affecting only SN38 and being inhibited by MBLI87. This putative transporter can be ABCC2 (MRP2, cMOAT), which is known to specifically transport SN38 but not CPT11 and Mit (223). This result also raises the question of the relative expression of each efflux transporters *in vivo* and the necessity to use inhibitors targeting several transporters or a combination of several inhibitors as discussed in the first part.

Moreover, the clearance ratio indicates that active efflux is not equally important for all the substrates. This ratio can also be interpreted as the maximal intracellular concentration that is possible to achieve if the transporter is completely inhibited. This result indicates the importance of competing processes in the efficacy of efflux transporter inhibitors as it has been already suggested for P-gp inhibitors.

On top of the pharmacological results about ABCG2 inhibition and MBLI87 that will have future impact in animal studies, this work demonstrates the benefits of NLME approach to analyze *in vitro* data, an approach often dedicated to PK/PD data. Here each experiment was considered as an independent "individual" and each substrates concentration was considered as a repeated measurement of the same phenomenon. Making this allows the quantification of inter- and intra- variability, which is more important in experiments displaying large variability. Moreover, the model accounts for both passive and active transports in a mechanistic description allowing the quantification of both transport mechanisms. In case of non-competitive interaction IC_{50} value is equal to the K_i, but this is only true if there is no diffusion in the system. Traditional approaches to analyze *in vitro* competition experiments would have thus estimated a biased inhibitory constant. This biased estimate could have had significant repercussions on the next step of development. The combination of a mixed effects approach to a mechanistic model circumvents previous issues and allows estimating the "true" parameter values. In that sense this model can have a significant impact for the study of *in vitro* data.

Publication 1

A template model for studying anticancer drug efflux inhibitors *in vitro*

Alexandre SOSTELLY, Léa PAYEN, Jérôme GUITTON, Attilio DI PIETRO, Pierre FALSON, Mylène HONORAT, Glaucio VALDAMERI, Annabelle GEZE, Ahcène BOUMENDJEL, Gilles FREYER, Michel TOD

Accepted for publication in Fundamental and Clinical Pharmacology

Introduction

Several mechanisms contribute to cell resistance to anticancer drugs. One of these involves the alteration in cellular drug accumulation resulting in lower efficiency of drug-induced cell death.

ABC multidrug efflux pumps family is widely involved in the intracellular decrease of drug accumulation and thus in anticancer drug resistance. During the last decade, efforts were mainly focused on reversing the activity of ABCB1 transporter, so called P-glycoprotein (P-gp) (224-226). However, inhibition of P-gp essentially failed to improve clinical efficacy either because the transporter was not as prevalent as it was expected, or because the inhibition of P-gp was not complete. Only a few studies have addressed the question of the inhibition of others ABC transporters.

ABCG2, so called "Breast Cancer Resistance Protein" (BCRP), is a half-transporter that plays a tumour-protective role through its ability to pump out of the cells several anticancer drugs such as mitoxantrone, methotrexate, imatinib, topotecan, irinotecan and SN38 (111, 113, 227). Moreover, its substrate profile overlaps that of P-gp. Development of ABCG2 inhibitors may improve the efficacy of cytotoxic drugs on resistant tumours expressing BCRP.

Recently, new ABCG2 inhibitors have been developed, based on flavone and acridone derivatives that are non-toxic and specific (136). MBLI87, an acridone derivative, has shown favourable properties, both in-vitro and in-vivo as an ABCG2 inhibitor (137). Hence, MBLI87 is under further development.

In the context of preclinical drug development, these new inhibitors are often tested through competition experiments with cells transfected with the gene coding for one of these transporters. Data issued from these experiments are analysed with classical

biochemistry tools, in order to determine the interaction mechanism between inhibitor and drug. However, this approach does not account for competing processes; e.g. the passive diffusion of these compounds through cell membrane, and do not discriminate intra from inter-experiment variability, resulting in biased parameter estimations.

Development of mechanistic models taking into account all the processes occurring in the experimental system, together with the use of Non-Linear Mixed-Effects (NLME) technique may be a powerful approach for overcoming these issues.

In this study, we build such a model for studying the effect of a new ABCG2 inhibitor on the cellular accumulation of irinotecan, SN38 and mitoxantrone. This mathematical model describes two transport mechanisms involved in the system studied. It determines the nature and strength of the interaction between the inhibitor and cytotoxic drugs and quantifies parameters useful for characterizing the ABC pump inhibition. Moreover, the model was formulated as a function of biologically meaningful parameters and in a fairly general way in order to allow its use as a template.

Materials and Methods

Cell Culture

The Human Embryonic Kidney 293 (HEK293) cell line ABCG2-tranfected and the empty vector-transfected HEK293 (pcDNA KEH293 cells) were obtained as previously described (137). Cells were maintained in Dulbecco's modified Eagle's medium (DMEM high glucose), supplemented with 10% foetal bovine serum (FBS), 1% penicillin/streptomycin, and 1 $mg.mL^{-1}$ G418.

Quantification of *in-vitro* accumulation of irinotecan and SN38

Cells were first plated at 750,000 cells per well in 6-well plates. They were loaded with respectively 2µM irinotecan or SN-38 in DMEM medium without FBS in absence or presence of various concentrations of MBLI87, varying between 0.05 µM to 20 µM. After three washings with ice-cold PBS (to inhibit active efflux), cells were collected in 0.5 mL of ice-cold PBS, submitted to centrifugation (5 min at 1,500 x g) and lysed by 0.5 mL of pure methanol. Finally, intracellular concentrations of irinotecan and SN-38 were quantified by HPLC-MSMS according to the analytical procedure described (137). Specific transitions for metabolites APC and SN-38G were also monitored to assess potential metabolism of irinotecan in the cells. Results (expressed in ng of irinotecan or SN-38 / mg protein) were normalized to cellular protein content estimated by Bradford assay.

Quantification of *in-vitro* accumulation of Mitoxantrone

Cells were seeded at a 1.10^5 cells/well density into 24-well plates. After 48 hours, cells were exposed to 5 µM mitoxantrone (Mit) for 30 min at 37°C in the absence or presence of various concentrations of MBLI-87, varying between 0.1 to 10 µM. After medium removal and PBS washing, intracellular drug fluorescence was monitored with a FACS Calibur cytometer (Becton Dickinson) by collecting at least 10000 events. Control was done with 5 µM of GF120918 which fully inhibits ABCG2 drug-mediated efflux.

Modelling Technique

Mixed-effects modelling

The formulated model belongs to the family of non-linear mixed-effects models (NLME). NLME, so called population models, use information from all the experiments to estimate model parameters (228). The term "mixed-effects" is used because fixed and random effects are simultaneously estimated in the model. Fixed effects refer to the typical value (mean) of parameter estimates. Random effects are estimated on two levels: variability between experiments and variability within experiments. In their general form, such models are formulated as follows:

$$y_{ij} = f(X_{ij}, P_i) + g(X_{ij}, P_i) \times \varepsilon_{ij} \qquad \text{(Equation 1)}$$

Where y_{ij} is the j^{th} observation for the i^{th} experiment, f(…) is the individual prediction described by the individual variables X_{ij} and P_i the set of individual parameter.

The residual error $g(X_{ij}, P_i) \times \varepsilon_{ij}$ describes difference between individual predictions and the corresponding observed values. E_{ij}s are supposed to be normally distributed with a 0 mean and σ^2 variance. We used the proportional error model, $g(X_{ij}, P_i) = f(X_{ij}, P_i)$

Individual parameters, P_i, are expressed as a function of the typical value θ (which here represents the median) and deviation from this typical value:

$$P_i = \theta \times e^{\eta_i} \quad \text{(Equation 2)}$$

η_i is a random parameter that describes the difference between the population and the individual i. η_i values are expected to be normally distributed with 0 mean and ω^2 variance.

Parameters estimation was performed with NONMEM software, version 7.1.2 (229). NONMEM uses a parameter maximum likelihood method: the probability of the data under the model is maximized by minimizing the extended least squares objective function. Due to the random effects entering non-linearly in the model, the likelihood function cannot be calculated exactly. Several approximations are available in this software and we choose the First Order Conditional Estimates method with Interaction (FOCEI). This method linearizes the likelihood function with a 1st Taylor expansion around the Bayesian estimates of the random effects (161).

Model development

To model intracellular drug accumulation, we developed a non-linear mixed effects transport inhibition model. The model is composed of two ordinary differential equations (219) and the derivatives of our variables are expressed as balances between drug influx and efflux. The variables refer to extracellular and intracellular drug concentrations. The basic assumption underlying the model structure is the following: drugs, i.e. CPT11, SN38 and Mit, cross cell membrane in each direction by passive diffusion characterized by a diffusion clearance, Cl_{diff}. Active efflux is assumed to be mediated by a single transporter (say ABCG2) and, due to the nature of the transporter, a Michaelis-Menten behavior has been chosen to model its action. Interaction between drugs and MBLI87 occurs on ABCG2

and can either be competitive, non-competitive or uncompetitive. Both interaction type and active efflux are taken into account in the transport clearance parameter, Cl_{tran}. General scheme of the model is presented in Figure 1.

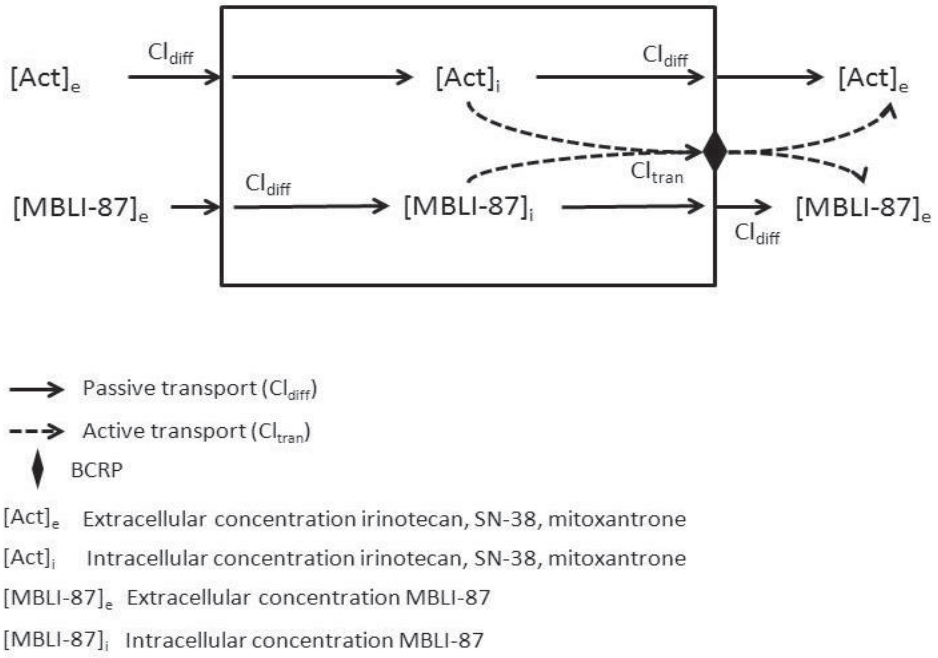

Figure 1: General Scheme of the model

Drugs can also be degraded through intracellular metabolism. Nevertheless, under our experimental conditions, the total drug amount remained constant during the time of experiment allowing us to neglect intracellular metabolism.

Preliminary analyses have shown that a kinetic equilibrium was achieved after 30 minutes of drug exposition. The ODE system can thus be considered at the equilibrium (Equation 3).

$$Cl_{diff} \times [Act]_e = \left(Cl_{tran} + Cl_{diff}\right) \times [Act]_i \qquad \text{(Equation 3)}$$

where Cl_{diff} is the diffusion clearance, Cl_{tran} is the transport clearance, $[Act]_e$ is the extracellular concentration of CPT11, SN38 and Mit and $[Act]_i$ is the intracellular concentration of either CPT11, SN38 or Mit.

After development and simplification of Equation 3, intracellular concentrations can be expressed as a function of extracellular concentration of drugs and MBLI87, and model parameters:

- In case of competitive interaction:

$$[Act]_i^{\,2} + [Act]_i \times \left(\frac{V_m}{Cl_{diff}} + K_m + K_m \times \frac{[MBLI87]_e}{K_i} - [Act]_e\right) - K_m \times \left(1 - \frac{[MBLI87]_e}{K_i}\right) = 0$$

(Equation 4)

- In case of non-competitive interaction

$$[Act]_i^{\,2} + [Act]_i \times \left(\frac{\frac{V_m}{Cl_{diff}}}{\left(1+\frac{[MBLI87]_e}{K_i}\right)} + \frac{K_m}{\left(1+\frac{[MBLI87]_e}{K_i}\right)} - [Act]_e\right) - [Act]_e \times \frac{K_m}{\left(1+\frac{[MBLI87]_e}{K_i}\right)} = 0$$

(Equation 5)

- In case of uncompetitive interaction

$$[Act]_i^{\,2} + [Act]_i \times \left(\frac{\frac{V_m}{Cl_{diff}}}{\left(1+\frac{[MBLI87]_e}{K_i}\right)} + \frac{K_m}{\left(1+\frac{[MBLI87]_e}{K_i}\right)} - [Act]_e\right) - [Act]_e \times \frac{K_m}{\left(1+\frac{[MBLI87]_e}{K_i}\right)} = 0$$

(Equation 6)

Equations 4-6 are in the shape of $AX^2+BX+C=0$ and their roots are easily found in the usual way.

We then assumed that the ABCG2-Michaelis constant (K_M) was much greater than the intracellular concentration, allowing to neglect this concentration in the expression of transport clearance. Model equations are considerably reduced since the relationship between intra- and extra-cellular concentrations becomes linear. Nevertheless, under this assumption, it was not possible to separately estimate V_{max}, Cl_{diff} and K_M. Equations were thus rearranged to instead estimate the ratio between intrinsic transport clearance ($Cl_i = V_{max}/K_M$) and diffusion clearance. Final equations of the linear model are the following:

- In case of competitive and non-competitive interaction

$$[Act]_i = \left(\frac{1}{1+\frac{\frac{Cl_i}{Cl_{diff}}}{\frac{[MBLI87]_e}{K_i}}} \right) \times [Act]_e \quad \text{(Equation 7)}$$

- In case of uncompetitive interaction

$$[Act]_i = \left(\frac{1}{\frac{Cl_i}{Cl_{diff}}+1} \right) \times [Act]_e \quad \text{(Equation 8)}$$

Equation 3 can be extended to multiple transporters inhibited by MBLI87:

$$Cl_{diff} \times [Act]_e = \left(\sum_{j=1}^{j=n} Cl_{tran_j} + Cl_{diff} \right) \times [Act]_i \quad \text{(Equation 9)}$$

After simplification and reduction of Equation 9, we obtained:

- In case of non-competitive and competitive interaction

$$[Act]_e = \left(\frac{1}{1+\sum_{j=1}^{j=n} \frac{\left(\frac{Cl_i}{Cl_{diff}}\right)_j}{\frac{[MBLI87]_e}{K_{i_j}}}} \right) \times [Act]_i \quad \text{(Equation 10)}$$

- In case of uncompetitive interaction

$$[Act]_e = \left(\frac{1}{1+\sum_{j=1}^{j=n} \left(\frac{Cl_i}{Cl_{diff}}\right)_j} \right) \times [Act]_i \quad \text{(Equation 11)}$$

Model assuming competitive and non-competitive interaction resulted in the same final expression. Model assuming uncompetitive interaction was independent of inhibitor concentration and, therefore was not further considered.

The model involves the free intracellular drug concentration, but this concentration is measured up to a factor α, which depends on experimental conditions, such as binding to intracellular components, extraction yield and dilutions which can vary between

experiments. The relationship between the true concentrations $[Act]_i$ and the apparent (experimentally measured) concentration X_i is:

$$[Act]_i \ or \ \bar{F}_i = \alpha \times X_i \qquad \text{(Equation 12)}$$

Where $[Act]_i$ is the intracellular concentration of either CPT11 or SN-38, $\bar{F}_i$ is the mean fluorescence intensity of mitoxantrone, and α is to be estimated.

The complete demonstration of model's equations is available in Appendix 1.

This approach was applied to data issued form the ABCG2-transfected and empty vector-transfected HEK293 cells.

Model building and diagnosis

Selection between models was based on the Objective Function Value, which is -2*log(likelihood) and Akaike Information Criterion (173), as well as goodness of fit, residual plots and precision of parameter estimates.

Simulation-based diagnostics could reveal model misspecifications that are not easily diagnosed with classical goodness-of-fit plots. Two methods were used: the Normalized Prediction Distribution Errors (NPDE) and the Visual Predictive Check (VPC).

Prediction errors were the quantile of each observation within its predictive distribution. NPDEs are obtained after decorrelation and normalization with respect to the empirical mean and variance obtained in simulations. The model was considered as invalid when NPDEs were not normally distributed with a 0 mean and a variance of 1 (230).

The VPC consisted of simulating intracellular drugs concentration based on model structure and parameter estimates (167). We simulated 1000 replications of the experimental datasets for each drug. The 90% non-parametric confidence interval of the simulated medians was then compared to the observed ones. The model was considered as invalid when the CI did not bracket the observed medians.

Model evaluation was performed with the R-based XPOSE4 program (231). PsN toolkit was used for executions of simulations and calculations for the VPC (232)

Comparison with standard approaches

A comparison of the model to standard approaches was performed in order to point the benefits of the NLME approach.

We compared our approach with two standard approaches. The first approach consists in naively pooling data and graphically estimating IC_{50} value, i.e. in this case the inhibitor concentration resulting in half-maximum substrate intracellular concentration.

The second approach consists also in naively pooling data and fitting the following model (Equation 13) to the data.

$$\frac{[Act]_i}{[Act]_{C_{inhib}=0}} = 1 - \left[\frac{I_{max} \times I}{I + IC_{50}}\right] \qquad \text{(Equation 13)}$$

Where $\frac{[Act]_i}{[Act]_{C_{inhib}=0}}$ is the efflux ratio of the probe substrate in the presence of inhibitor relative to the control in absence of inhibitor; I_{max} is the maximal inhibitory effect.

Results

Data

During the uptake period, CPT11 could have been metabolized but we were unable to detect SN38, and its metabolites SN38G and APC under our experimental conditions.

Figure 2.1 to 2.3 shows the change in intracellular Mit (N=5), CPT11 (N=8) and SN38 (N=12) concentrations as a function of MBLI87 concentrations in ABCG2-transfected cells. Figure 2.4 shows the change in intracellular SN38 (N=4) concentrations as a function of MBLI87 concentrations in pcDNA cells.

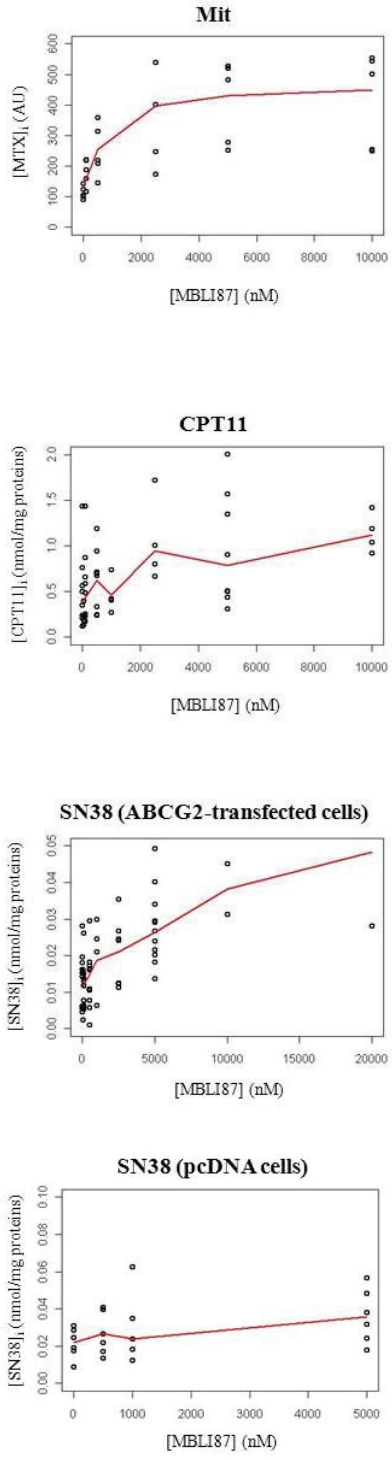

<u>Figure 2</u>: Intracellular drug concentrations versus MBLI87 concentrations
Figure 2 shows the changes in intracellular concentrations for Mit, CPT11, SN38 in ABCG2-transfected cells and SN38 in pcDNA cells. Each point represents one experiment and red line representes the median trend.

A maximal inhibition of drug transport was observed at high MBLI87 concentrations and the inter-experiment variability appeared to be either moderate for Mit or large for CPT11 and SN38.

A series of experiments with empty vector-transfected HEK293 (pcDNA HEK293) cells showed no increase in CPT11 and Mit intracellular concentrations with increasing MBLI87 concentrations. Surprisingly, SN38 intracellular concentrations increased with increasing MBLI87 concentrations in pcDNA cells. This result attests the presence of another transport mechanism affecting only SN38 and inhibited by MBLI87.

To account for these two mechanisms, the analysis was carried out in two steps. First, the data obtained with pcDNA cells were analyzed to estimate the parameters of the non-ABCG2 transport mechanism(s), using Equation 10. Then, the data obtained with ABCG2-transfected cells were analyzed using Equation 10, with the model parameters for the non-ABCG2 transport fixed to the values obtained in step 1. This analysis allowed us to estimate parameters related specifically to ABCG2.

Model evaluation

Basic diagnostic plots that evaluated model quality showed that the model could indeed adequately describe the data. The goodness-of-fit plots showed that model predictions (PRED, IPRED) were able to describe the observed concentrations (DV) for each drug (Figure 3, upper panel). At the individual level, model predictions were able to well describe the data for each experiment (not shown). NPDEs were normally distributed with a 0 mean and 1 variance, without a trend (Figure 3, lower panel).

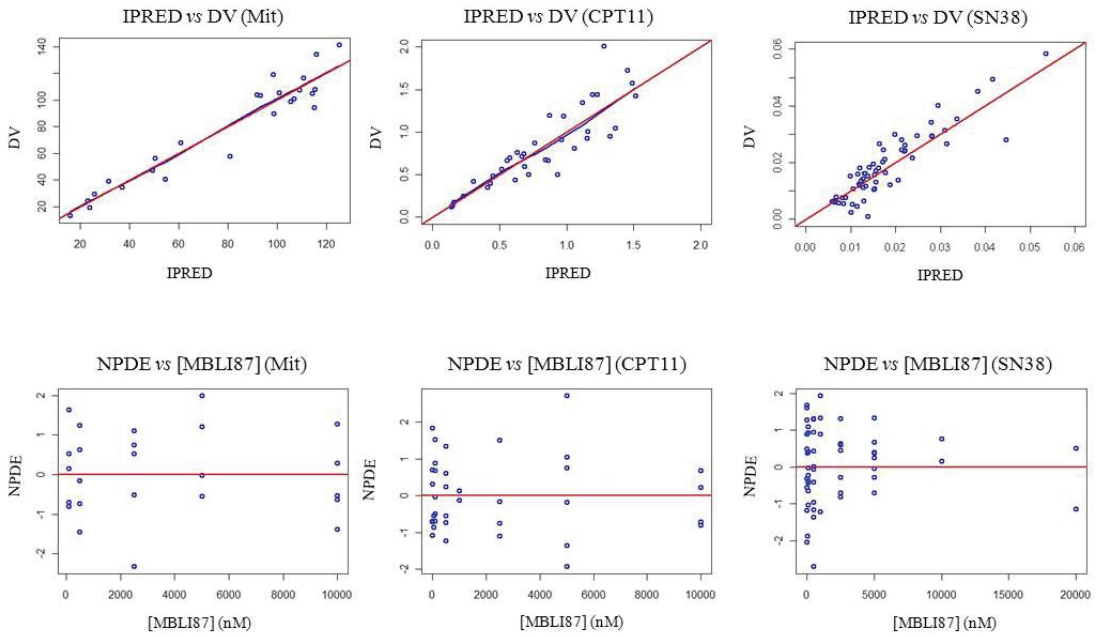

Figure 3: Goodness-of-Fit Plots

Upper panel: Individual Model Predictions versus Observations

Basic goodness of fits compare the individual model predictions to the observations (blue points) for Mit, CPT11 and SN38 in ABCG2-transfected cells. The black line is the identity line and the red line is a trend line.

Lower panel**:** Normalized Prediction Distribution Error (NPDE)

The normalized prediction distribution error (NPDE) versus MBLI87 concentrations is shown for Mit, CPT11 and SN38 in ABCG2-transfected cells. NPDEs follow a normal centered reduced distribution (heavy red line represents the 0 mean).

VPC revealed no invalidation of the mixed-effects model (Figure 4). The 90% non-parametric confidence intervals (CI) of the simulated medians were plotted over the observed intracellular median concentrations. The observed medians were enclosed within this CI, as required for model validation. Thus, a single model structure was able to adequately describe data from all the studies.

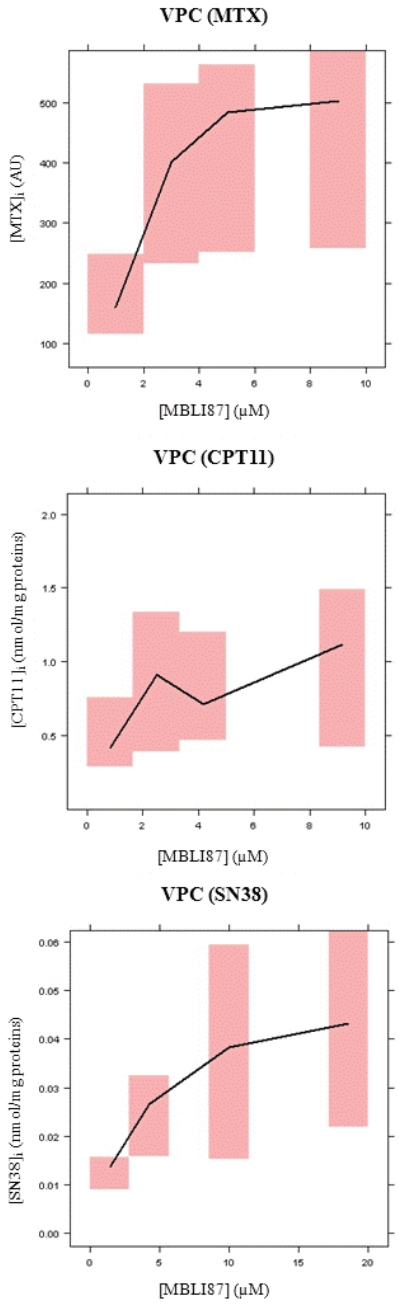

Figure 4: Visual Predictive Check (VPC)
Visual Predictive Check (VPC) plots compare the observed median intracellular drug concentrations (heavy black lines) over MBLI87 concentrations to the 90% non-parametric confidence interval (pink area) obtained after simulations. Observed medians and the 90% non-parametric interval are shown for Mit, CPT11 and SN38 in ABCG2-transfected cells.

Parameter estimates

Parameter estimates are presented in Table 1.

The final model for all drugs and both cellular types was the reduced model parameterized with Cl_i/Cl_{diff} incorporating either non-competitive or competitive

interaction (Equation 7). Full models incorporating non-competitive (Equation 5), competitive (Equation 4) and uncompetitive (Equation 6) interaction resulted in high parameter estimates uncertainty. Model incorporating uncompetitive interaction (Equation 8) reduced the quality of the model fit. Inter-experiment variability was added on α and Cl_i/Cl_{diff}. All model parameters were estimated quite precisely since standard error was low. Intrinsic transport clearance to diffusion clearance ratio was estimated at 1, 5.4 and 2.5 for CPT11, SN38, and Mit in ABCG2-transfected cells respectively, and 5.8 for SN38 in pcDNA cells. Values of MBLI87 ABCG2-inhibitroy constants were largely different between drugs: 289 nM, 1,160 nM and 141 nM for CPT11, SN38 and Mit in ABCG2-transfected cells respectively, and 7260 nM for SN38 in pcDNA cells. For SN38, MBLI87 Ki was found to be 6 fold lower for ABCG2 than for the other transporter. The parameters α and Cl_i/Cl_{diff} were allowed to vary between experiments, and their coefficient of variation was estimated around 30% for Mit and 60% for CPT11 and SN38.

		Typical Value (%RSE)	Inter-Experiment Variability (%CV)
Irinotecan	α (L/mg protein)	2460 (21%)	53%
	Cl_i/Cl_{diff}	1.01 (4%)	69%
	K_i (nM)	289 (53%)	-
	Residual Variability (%CV)	46,2%	-
SN38 (Non-transfected cells)	α (L/mg protein)	13200 (134%)	-
	Cl_i/Cl_{diff}	5.8 (175%)	47%
	K_i (nM)	7260 (56%)	-
	Residual Variability (%CV)	57.6%	-
SN38 (Transfected cells)	α (L/mg protein)	14600 (13%)	-
	Cl_i/Cl_{diff}	5.4 (36%)	72%
	K_i (nM)	1160 (20%)	-
	Residual Variability (%CV)	57.6%	-
Mitoxantrone	α (L/mg protein)	12.4 (18%)	36%
	Cl_i/Cl_{diff}	2.5 (17%)	29%
	K_i (nM)	141 (30%)	-
	Residual Variability (%CV)	34.2%	-

Table 1: Parameter estimates

Comparison with standard approaches

A comparison with standard approaches has been performed. The graphical analysis to estimate the MBLI87 IC_{50} value was only possible for Mit since it is the only case where the transport saturation was observed. The MBLI87 IC_{50} value was estimated at 500nM.

A model allowing the estimation of IC_{50} was also fitted to the data. Once again, the IC_{50} estimation was only possible for Mit (IC_{50}=35.1nM). For CPT11 and SN38, the confidence interval was very large precluding the use of this value.

Moreover, model evaluation (not shown) revealed a clear misspecification of this model.

Discussion

This study presents the construction of a template model for studying the intracellular disposition of drugs in presence of a new ABCG2 inhibitor, MBLI87. Data issued from in-vitro experiments were used to build this model.

This kind of data is rarely analyzed with a Non-Linear Mixed-Effects (NLME) approach. Here, we coupled the NLME approach to a mechanistic model that accounts for several mechanisms occurring in intracellular drug disposition. Moreover, experimental variability is here quantified and properly accounted for, avoiding the bias encountered with standard approaches. The developed model is formulated with generic equations and parameters that allow its use with different experimental conditions and different drugs. As a demonstration, we successfully applied this model for three different drugs under two experimental conditions. The model can thus be used as a template for studying the effects of efflux transporters inhibitors on the intracellular drug accumulation.

Our model did not account for cell death as due to drug cytotoxicity. Jang *et al.* have developed a model for studying the kinetics of P-glycoprotein efflux (233). In their

experiments, cells were exposed to various concentrations of drugs with different exposition times varying from 0 to 24 hours. The number of cells was thus affected by drug cytotoxicity and the cell count had to be introduced in their equation to correctly fit their data. In our experiments, cells were exposed to drugs for only 30 minutes, resulting in negligible drug cytotoxicity. Accounting for the variation of cell count was therefore not necessary.

ABCG2-transfected HEK293 cells have been used in this study. The use of transfected cells ensures that all the effects observed are related to ABCG2 and results can easily be translated to others biological system. However, since this type of cellular system does not represent the complex modifications of cell biology encountered in cancer, the efficacy of MBLI87 will have to be confirmed with selected tumour cells.

The same experiments have been carried out with empty vector-transfected HEK293 cells (pcDNA cells) and revealed that CPT11 and Mit intracellular concentration were independent of MBLI87 extracellular concentrations. By contrast, we observed an increase in SN38 intracellular concentration with increased MBLI87 concentrations. This unexpected result revealed the presence of another transport mechanism occurring in these cells affecting only SN38 and being inhibited by MBLI87. This putative transporter may be the ABCC2 efflux transporter (MRP2, cMOAT) that is known to specifically transport SN38 but not CPT11 and Mit (223).

To describe all the transport mechanisms occurring in our cellular system, it was necessary to account for both efflux transporters. Because pcDNA cells and ABCG2-transfected cells only differed in the expression of ABCG2, we first analyzed data issued from pcDNA cells to estimate parameters related to the efflux transporter in these cells. Then under the assumption that action of both transporters was additive, we fixed parameters related to the pcDNA cells transporter and only estimated parameters related

to ABCG2 using data issued from ABCG2-transfected cells. This analysis allowed us to quantify specifically ABCG2 transport.

Concerning the MBLI87 inhibitory effect on both transporters, we found that MBLI87 K_i value was 6 fold lower for ABCG2 attesting its better affinity for this transporter as expected. The clearance ratio was found to be equivalent between both cellular types attesting an equal contribution of both transporters in SN38 transport.

We introduced a correction factor in model equations that accounts for differences in binding to intracellular components, extraction yield and dilutions and allow us to model the "true" intracellular drug concentration. This factor was necessary to model data issued from different experimental conditions. It was thus not surprising to find different value of α for CPT11, SN38 and Mit. Although CPT11 and SN38 intracellular concentrations were measured with the same analytical method their intracellular protein binding may be different, as shown for their plasma protein binding (10).

In our analysis, the best model for Mit, CPT11 and SN38 was the model assuming intracellular concentrations negligible compared to drugs Michaelis constant (K_M). This assumption considerably simplified model's equations. According to the likelihood ratio test, the full model (Equations 4-6) was not significantly better than the reduced model that we retained and resulted in larger parameter confidence intervals. Data do not contain information about the transport saturation and only the lower part of the concentration-effect curve is observed. Our assumption was thus valid under our experimental conditions. However, it also indicates that parameter estimates are only valid when transport is far from saturation. Moreover, under this assumption, it was not possible to determine the nature of the interaction between drugs and MBLI87 since non-competitive and competitive interaction leads to the same model formulation. Nevertheless, the nature of interaction could be resolved here thanks to data from CPT11

and SN38 experiments. Because CPT11 and SN38 share similar chemical structures (SN38 is a direct metabolite of CPT11), both compounds should bind to the same site on ABCG2, resulting, in case of competitive interaction, in a similar value of K_i value for MBLI87. Analysis of the data from these experiments revealed different values of K_i (289 nM for CPT11 and 1,970 nM for SN38) attesting that MBLI87 did not bind to the drug site within the transporter. These arguments are thus in favor of a non-competitive interaction between CPT11, SN38 and MBLI87.

In case of non-competitive interaction, IC_{50} value is equal to K_i value in absence if diffusion (19). IC_{50} can be easily deduced from graphical analysis. In our case, this method can only be applied to Mit where the maximal inhibition was observed; the IC_{50} estimated with this method was around 500nM whereas our model predicted a K_i value of 140nM.

Another method to determine the IC_{50} consists in naively pooling data and fitting a non-linear regression. With this usual method, we also found an IC_{50} value largely different from the ones estimated in our model.

An explanation of such a difference is that graphical analysis and standard regression does not account for passive drug diffusion, and the estimated IC_{50} value is thus only an apparent value. Thanks to the mechanistic description of both transport mechanisms through cell membrane, our model allows estimating the true value of model parameters.

Disposition of MBLI87 in plasma has been assessed in mice after single drug administration of 0.12 µmoles by intraperitoneal route (137). We compared the mean free concentration in plasma over 24h ($C_{free,\ plasma\ [0\text{-}24h]}$= 2.97 nM) to the estimated K_i values. Concentration in plasma was at least ten-fold lower than the K_i, meaning that ABCG2 was poorly inhibited in-vivo. Nevertheless, an in-vivo study revealed that addition of MBLI87 to CPT11 treatment slowed down the growth of tumour overexpressing ABCG2, demonstrating the activity of MBLI87 (137). Two hypotheses can thus be

formulated on MBLI87 mechanism of action which can either be transformed in-vivo into an active metabolite or accumulate after repeated administrations.

Another parameter of interest in our model is the ratio between intrinsic transport clearance ($Cl_i = V_{max}/K_M$) and the diffusion clearance (Cl_{diff}). For all drugs analyzed in this study, we found that active transport was the major efflux mechanism. Ratio value was quite different between drugs (1.01, 5.4 and 2.5 for CPT11, SN38 and Mit in ABCG2-transfected cells respectively, and 5.8 for SN38 in pcDNA cells) resulting not only from their different affinity for the transporter, but also from their physico-chemical properties. All three drugs have similar molecular weight but their octanol to water distribution coefficient at pH 7 are log(D) = 2.29, 2.53, -2.68 for CPT11, SN38 and Mit respectively (234). Hence, passive diffusion is expected to be more important for CPT11 and SN38 than for Mit. CPT11 and SN38 are equally transported by passive diffusion but the difference in their clearance ratio may be explained by a greater affinity of ABCG2 for SN38 than for CPT11. This clearance ratio plus one is equal to the maximum increase in the intracellular concentration that is possible to achieve if the transporter is fully inhibited. Perego *et al.* have conducted a study in which they looked at the accumulation of topotecan (a drug akin to irinotecan) in cells overexpressing ABCG2 (235). They found that topotecan accumulation was was 2.25 lower in ABCG2 overexpressing cells (4 ng/10^7 cells in HT29/MIT cells versus 9 ng/10^7 cells in HT29 cells). This result is comparable with our Cl_i/Cl_{diff} parameter.

To conclude, a template model accounting for variability between experiments, has been derived and could be used for different drugs and experimental conditions. This approach provided some insights on the efficacy of MBLI87 and its mechanism of action, and identified critical points to be investigated in the future regarding the pharmacokinetics.

Appendix 1: Demonstration of model equations

Notations:

- ACT_e : extracellular quantity of Mtx, CPT11 or SN38
- ACT_i : intracellular quantity of Mtx, CPT11 or SN38
- $[ACT]_e$: extracellular concentration of Mtx, CPT11 or SN38
- $[ACT]_i$: intracellular concentration of Mtx, CPT11 or SN38
- $[MBLI87]_e$: extracellular concentration of MBLI87
- V_e: extracellular volume
- V_i: intracellular volume
- Cl_{diff}: diffusion clearance
- Cl_{tran}: transport clearance
- Cl_i: intrinsic transport clearance
- K_i: ABCG2 inhibitory constant
- K_m: ABCG2 Michaelis constant

ODE system:

$$\frac{dACT_e}{dt} = \frac{-Cl_{diff}}{V_e} \times ACT_e + \frac{Cl_{tran}}{V_i} \times ACT_i + \frac{Cl_{diff}}{V_i} \times ACT_i$$

$$\frac{dACT_e}{dt} = -\frac{dACT_i}{dt} \qquad \text{(Equation 11)}$$

$$\frac{dACT_e}{dt} = -Cl_{diff} \times [ACT]_i + Cl_{tran} \times [ACT]_i + Cl_{diff} \times [ACT]_i$$

At the kinetic equilibrium,

$$\frac{dACT_e}{dt} = 0 \Leftrightarrow Cl_{diff} \times [ACT]_e = Cl_{tran} \times [ACT]_i + Cl_{diff} \times [ACT]_i$$

$$\Leftrightarrow [ACT]_e = \frac{Cl_{tran}}{Cl_{diff}} \times [ACT]_i + [ACT]_i \qquad \text{(Equation 12)}$$

In case if non-competitive interaction:

$$[ACT]_e = [ACT]_i \times \left[\frac{\frac{V_m}{\left(1+\frac{[MBLI87]_e}{K_i}\right)}}{Cl_{diff} \times ([ACT]_i + K_m)} + 1 \right] \qquad \text{(Equation 13)}$$

$$[ACT]_e = [ACT]_i \times \left[\frac{\frac{\frac{V_m}{Cl_{diff}}}{\left(1+\frac{[MBLI87]_e}{K_i}\right)}}{[ACT]_i + K_m} + 1 \right] \qquad \text{(Equation 14)}$$

By developing and reducing Equation 14, we obtained:

$$\Leftrightarrow [ACT]_i^{\,2} \times \left(1 + \frac{[MBLI87]_e}{K_i}\right) + [ACT]_i \times \left(\frac{V_m}{Cl_{diff}} + K_m + K_m \times \frac{[MBLI87]_e}{K_i} - [ACT]_e - [ACT]_e \times \frac{[MBLI87]_e}{K_i}\right) - [ACT]_e \times K_m - [ACT]_e \times K_m \times \frac{[MBLI87]_e}{K_i} = 0$$

(Equation 15)

Let's denote: $[ACT]_i = \alpha \times X_i$ with X_i in AU and α in nmol.L^{-1}.AU^{-1} or in nml.L^{-1}.mg proteins^{-1}

$$\Leftrightarrow (\alpha^2 \times X_i^{\,2}) \times \left(1 + \frac{[MBLI87]_e}{K_i}\right) + (\alpha \times X_i) \times \left(\frac{V_m}{Cl_{diff}} + K_m + K_m \times \frac{[MBLI87_e]}{K_i} - [ACT]_e - [ACT]_e \times \frac{[MBLI87]_e}{K_i}\right) - K_m \times \left([ACT]_e + [ACT]_e \times \frac{[MBLI87]_e}{K_i}\right) = 0$$

(Equation 16)

Equation 16 is in the shape of $AX^2+BX+C=0$

Under the assumption of $K_m >> [ACT]_i$:

$$Cl_{tran} = \frac{\frac{V_m}{\left(1+\frac{[MBLI87]_e}{K_i}\right)}\times[ACT]_i}{K_m+[ACT]_i} \cong \frac{V_m\times[ACT]_i}{K_m\times\left(1+\frac{[MBLI87]_e}{K_i}\right)} \quad \text{(Equation 17)}$$

By replacing Equation 17 in Equation 12, we obtained

$$[ACT]_e = \frac{V_m\times[ACT]_i}{K_m\times\left(1+\frac{[MBLI87]_e}{K_i}\right)\times Cl_{diff}} + [ACT]_i \quad \text{(Equation 18)}$$

By developing Equation 18, we obtained

$$[ACT]_i \times \left(\frac{Cl_i}{Cl_{diff}} + 1 + \frac{[MBLI87]_e}{K_i}\right) - [ACT]_e \times \left(1 + \frac{[MBLI87]_e}{K_i}\right) = 0 \quad \text{(Equation 19)}$$

Let's denote: $[ACT]_i = \alpha \times X_i$ with X_i in AU and α in nmol.L^{-1}.AU^{-1} or in nml.L^{-1}.mg proteins^{-1}

$$(\alpha \times X_i) \times \left(\frac{Cl_i}{Cl_{diff}} + 1 + \frac{[MBLI87]_e}{K_i}\right) - [ACT]_e \times \left(1 + \frac{[MBLI87]_e}{K_i}\right) = 0 \quad \text{(Equation 20)}$$

Equation 20 is in the shape of AX+B = 0 and its solution is presented in Equation 8.

In case of competitive interaction:

$$[ACT]_e = [ACT]_i \times \left(\frac{V_m}{K_m\times\left(1+\frac{[MBLI87]_e}{K_i}\right)\times Cl_{diff}+[ACT]_i\times Cl_{diff}} + 1\right) \quad \text{(Equation 21)}$$

$$[ACT]_e = [ACT]_i \times \left(\frac{\frac{V_m}{Cl_{diff}}}{K_m\times\left(1+\frac{[MBLI87]_e}{K_i}\right)+[ACT]_i} + 1\right) \quad \text{(Equation 22)}$$

By reducing and developing Equation 22, we obtained:

$$[ACT]_i^2 + [ACT]_i \times \left(\frac{V_m}{Cl_{diff}} + K_m + K_m \times \frac{[MBLI87]_e}{K_i} - [ACT]_e\right) - K_m \times [ACT]_e \times \left(1 + \frac{[MBLI87]_e}{K_i}\right) = 0 \quad \text{(Equation 23)}$$

Let's denote: $[ACT]_i = \alpha \times X_i$ with X_i in AU and α in nmol.L^{-1}.AU^{-1} or in nml.L^{-1}.mg proteins^{-1}

$$(\alpha \times X_i)^2 + (\alpha \times X_i) \times \left(\frac{V_m}{Cl_{diff}} + K_m + K_m \times \frac{[MBLI87_e]}{K_i} - [Act_e]\right) - K_m \times [ACT]_e \times \left(1 + \frac{[MBLI87]_e}{K_i}\right) = 0 \quad \text{(Equation 24)}$$

Equation 24 is in the shape of AX^2+BX+C=0

Under the assumption of $K_m >> [Act]_i$

$$Cl_{tran} = \frac{V_m\times[ACT]_i}{K_m\times\left(1+\frac{[MBLI87]_e}{K_i}\right)+[ACT]_i} \cong \frac{V_m\times[ACT]_i}{K_m\times\left(1+\frac{[MBLI87]_e}{K_i}\right)} \quad \text{(Equation 25)}$$

By replacing Equation 25 in Equation 12, we obtained:

$$[ACT]_e = [ACT]_i \times \left(\frac{V_m}{K_m\times\left(1+\frac{[MBLI87]_e}{K_i}\right)\times Cl_{diff}} + 1\right) \quad \text{(Equation 26)}$$

By developing and reducing Equation 26, we obtained:

$$[ACT]_i \times \left(\frac{Cl_i}{Cl_{diff}} + 1 + \frac{[MBLI87]_e}{K_i}\right) - [ACT]_e \times \left(1 + \frac{[MBLI87]_e}{K_i}\right) = 0 \quad \text{(Equation 27)}$$

Lets denote: $[ACT]_i = \alpha \times X_i$ with X_i in AU and α in nmol.L^{-1}.AU^{-1} or in nml.L^{-1}.mg proteins^{-1}

$$(\alpha \times X_i) \times \left(\frac{Cl_i}{Cl_{diff}} + 1 + \frac{[MBLI87]_e}{K_i}\right) - [ACT]_e \times \left(1 + \frac{[MBLI87]_e}{K_i}\right) = 0 \quad \text{(Equation 28)}$$

Equation 28 is in the shape of AX+B = 0 and its solution is presented in Equation 9.

In case of uncompetitive interaction

$$[ACT]_e = [ACT]_i \times \left[\frac{\frac{V_m}{\left(1+\frac{[MBLI87]_e}{K_i}\right)}}{Cl_{diff}\times[ACT]_i+Cl_{diff}\times\frac{K_m}{\left(1+\frac{[MBLI87]_e}{K_i}\right)}} + 1\right]$$

(Equation 29)

$$[ACT]_e = [ACT]_i \times \left[\frac{\frac{V_m}{Cl_{diff}}}{\frac{\left(1+\frac{[MBLI87]_e}{K_i}\right)}{[ACT]_i+\frac{K_m}{\left(1+\frac{[MBLI87]_e}{K_i}\right)}}} + 1 \right]$$

(Equation 30)

By reducing and developing Equation 30, we obtained:

$$[ACT]_i{}^2 + [ACT]_i \times \left(\frac{\frac{V_m}{Cl_{diff}}}{\left(1+\frac{[MBLI87]_e}{K_i}\right)} + \frac{K_m}{\left(1+\frac{[MBLI87]_e}{K_i}\right)} - [ACT]_e \right) - [ACT]_e \times \frac{K_m}{\left(1+\frac{[MBLI87]_e}{K_i}\right)} = 0 \quad \text{(Equation 31)}$$

Let's denote: $[ACT]_i = \alpha \times X_i$ with X_i in AU and α in nmol.L^{-1}.AU^{-1} or in nml.L^{-1}.mg proteins^{-1}

$$(\alpha \times X_i)^2 + (\alpha \times X_i) \times \left(\frac{\frac{V_m}{Cl_{diff}}}{\left(1+\frac{[MBLI87]_e}{K_i}\right)} + \frac{K_m}{\left(1+\frac{[MBLI87]_e}{K_i}\right)} - [ACT]_e \right) - [ACT]_e \times \frac{K_m}{\left(1+\frac{[MBLI87]_e}{K_i}\right)} = 0 \quad \text{(Equation 32)}$$

Equation 26 is in the shape of $AX^2+BX+C=0$

Under the assumption of $K_m >> [ACT]_i$

$$Cl_{tran} = \frac{\frac{V_m}{1+\frac{[MBLI87]_e}{K_i}} \times [ACT]_i}{\frac{K_m}{1+\frac{[MBLI87]_e}{K_i}}+[ACT]_i} \cong \frac{V_m}{K_m} \times [ACT]_i \quad \text{(Equation 33)}$$

By replacing Equation 33 in Equation 12, we obtained:

$$\frac{Cl_i}{Cl_{diff}} \times [ACT]_i + [ACT]_i - [ACT]_e = 0 \quad \text{(Equation 34)}$$

Lets denote: $[ACT]_i = \alpha \times X_i$ with X_i in AU and α in nmol.L^{-1}.AU^{-1} or in nml.L^{-1}.mg proteins^{-1}

$$\frac{Cl_i}{Cl_{diff}} \times \alpha \times X_i + \times \alpha \times X_i - [ACT]_e = 0 \quad \text{(Equation 35)}$$

Equation 35 is in the shape of AX+B=0 and its solution is presented in Equation 10.

2. Modeling the interaction between cytotoxic and efflux transporter inhibitors *in vivo*

2.1. Introduction

The former model constitutes a first step to understand the cellular disposition of cytotoxic in presence of efflux transporters. By the quantification of physiologically relevant parameters, it shows the importance of competing mechanisms in the efficacy of efflux transporter inhibitors. However, these conclusions are based on *in vitro* experiments and one can argue that because of the complexity of tumour biology, the situation can be different *in vivo*. The following part deals with the construction of a semi-mechanistic PKPD model of the interaction between these compounds *in vivo* based on the *in vitro* mechanistic model. This model establishes the relationship between cytotoxic dosing regimens and tumour growth inhibition. It was applied to two animal studies testing the reversal effect of MBLI87 on CPT11 ABCG2-mediated resistance. Throughout this study, the benefits of the NLME approach in the construction of this type of model are also presented.

2.2. Methods

2.2.1. Experimental methods

Three different studies were used to build this model. The first one was the *in vitro* experiment studying the intracellular disposition of cytotoxic following different doses of MBLI87 that was presented in the previous section. The second study was a PK experiment carried out in tumour-free mice. CPT11 disposition was evaluated after single dose administration with either MBLI87 or alone to evaluate the potential PK interactions between these compounds. MBLI87 disposition was evaluated after multiple doses to assess the potential accumulation of the drug *in vivo*. CPT11, SN38 and

MBLI87 plasma concentrations were monitored during 24h using 5 animals per sample time. The last study was a PD experiment that aimed at evaluating the reversal effect of MBLI87 on CPT11 resistance. Mice xenografted with HEK293 cells overexpressing BCRP were treated with CPT11 alone or combined to MBLI87 and the tumour size was repetitively measured throughout the duration of the experiment. Two sets of experimental conditions were defined. In the first study (study 1, S1), 30 animals were randomized into the 3 treatment groups (control N=18, irinotecan N=6, irinotecan+MBLI87 N=3). In this study, irinotecan was administered IP at 30mg.kg^{-1} 3 days per week for 2 consecutive weeks, followed by a 2-week rest period and then 2 more weeks of treatment for a total of 6 weeks of treatment. MBLI87 was administered IP at 2.4mg.kg^{-1} 5 days per week with the same dose schedule. A 2-day delay between tumour cells implantation and first drug administration was applied.

In the second study (study 2, S2), 15 animals were randomized into the 3 treatment groups (control N=5, irinotecan N=5, irinotecan+MBLI87 N=5). Irinotecan was administered IP at 20mg.kg^{-1} 3 days per week for 4 weeks of treatment without any interruption. MBLI87 was administered IP at 2.4mg.kg^{-1} 5 days per week throughout the 4 weeks of treatment. A 7-day delay between tumour cells implantation and first drug administration was applied. Treatment intensity (total amount/treatment duration) was greater in S2 compared to S1 and treatment delay between cells inoculation and treatment onset was greater in S2.

2.2.2. Model development

The model includes four sub-models:

- The pharmacokinetic model describing the relationship between administered doses and drug concentration in plasma.

- The tumour accumulation model describing the relationship between drug concentration in plasma and in tumour cells. MBLI87 action is considered in this model because it increases the cellular concentration of cytotoxic.
- The tumour growth model incorporating three cell types and describing the natural evolution of the disease.
- The cytotoxic action model linking cytotoxic tumour concentration with inhibition of tumour growth

Plasma PK was modelled using compartmental analysis (see 4.2.4.2). The mechanistic *in vitro* model was used to model the tumour disposition of CPT11 and SN38 in presence of MBLI87. In order to ruse the former model which assumes a kinetic equilibrium *in vitro*, the tumour compartment was modelled as a receptor compartment (see 4.2.5.3) that allows writing the change in tumour concentration as a function of active efflux and passive transport (Equation 19):

$$\frac{dC_{tumour}}{dt} = K_{trans} \times \left(C_{plasma} - C_{tumour}\right) - \frac{K_{act} \times C_{tumour}}{1 + \frac{C_{MBLI87,plasma}}{K_i}} \qquad \text{(Equation 19)}$$

Where C_{tumour} and C_{plasma} are the tumour and plasma drug concentration, K_{trans} is the rate constant governing the passive transport (from tumour to plasma), K_{act} is rate constant governing the active efflux and K_i is the MBLI87 inhibitory constant.

Contrary to the *in vitro* model, parameters of Equation 19 are expressed using rate constants, alleviating the need to estimate the volume of the tumour compartment.

Tumour growth was modelled using a model similar to the one proposed by Ribba *et al.* Three different cell types composed the tumour spheroid: proliferative, hypoxic and necrotic. Cells moved from one type to another according to some rate constants.

The final sub-model is the cytotoxic action model. This model links the tumour concentration of CPT11 and SN38 to the effect on tumour growth. Because of their

mechanisms of action, CPT11 and SN38 were assumed to only affect proliferative cells and their effect was modelled as a decrease of the tumour growth rate.

The model was sequentially built: the PK parameters were first estimated from data issued from PK experiments and their typical values were fixed in the subsequent steps. Then parameters governing the natural tumour growth were estimated on data issued from control group in S1 and S2 and their typical values were fixed thereafter. MBLI87 inhibitory constant was fixed to the value estimated in the *in vitro* model and corrected to account for plasma protein binding. Finally the 4 sub-models were linked and the remaining parameters were estimated from data issued from treatment groups in S1 and S2.

Model parameters were estimated using NLME approach with the NONMEM software version 7.2.

2.2.3. Simulation study

Based on the final model structure and parameter estimates, a simulation study was performed to evaluate the impact of different properties of the system and MBLI87 on the tumour accumulation of CPT11 and SN38 and treatment outcomes. Three different axes were explored: the MBLI87 reversal effect, the tumour cell line and the tumour biology.

2.3. Results

Model evaluation did not reveal any misspecifications; the final model was able to correctly predict the effect of MBLI87 combined to CPT11 in mice xenografted with HEK293 cells overexpressing ABCG2. PK analysis did not reveal any interaction between CPT11, SN38 and MBLI8 based on plasma concentrations $AUC_{CPT11+MBLI87}$=30.9±4µmol.L^{-1}.h^{-1}, $AUC_{CPT11-MBLI87}$=34.3±22µmol.L^{-1}.h^{-1}; $AUC_{SN38+MBLI87}$=9.5±2µmol.L^{-1}.h^{-1}, $AUC_{SN38-MBLI87}$=8.3±2µmol.L^{-1}.h^{-1}). There was also no evidence for MBLI87 accumulation *in vivo* and MBLI87 half-life was estimated at 0.43d. Parameters governing the natural tumour growth were comparable between both studies attesting the reproducibility of the experiment. Even if the tumour growth was comparable, the tumour size at day 40 was 8 times greater in S2 despite a greater treatment intensity indicating thus a difference of treatment efficacy. Because of the small number of animals used, some parameters are associated to a high uncertainty because of the too small number of animals used. It was thus not possible to compare parameters between both studies. Nevertheless, the comparison of parameters point estimates indicates some differences. Parameter governing the cytotoxic passive diffusion in tumour was lower in S2 (K_{trans}=0.099d^{-1} in S1 and 0.048d^{-1} in S2 for CPT11) and the active efflux rate was greater in S2 (K_{act}=0.0578d^{-1} in S1 versus 0.98d^{-1} in S2 for CPT11). It suggests a different tumour biology between both studies leading to a decreased accumulation of cytotoxic in S2. In addition the proportion

of drug sensitive cells was lower at treatment onset in S2 (68% and 85% of proliferative cells in S1 and S2 respectively at treatment onset).

2.4. Discussion

This model includes a mechanistic description of the cellular interaction between efflux inhibitor and cytotoxic as well as a semi-mechanistic model tumour growth model that accounts for the repartition of tumour cells into proliferative, hypoxic and necrotic cells. To date this is the first model that establishes the relationship between the intracellular disposition of cytotoxic in presence of an efflux inhibitor to tumour growth.

The methodology developed in this section combined the NLME approach and a semi-mechanistic model. Building such an advanced model using data issued from studies containing minimum information, large variability and unbalanced design was a modelling challenge. Thanks to the sequential building, it has been possible to combine all the studies together even it has led to several assumptions in the complete model such as the dose independency of PK parameters. The NLME approach allows using all the information available to fully quantify all the model parameters. Nevertheless, due to the complexity of the model and the paucity of the data, some of the parameters were estimated with a high imprecision making impossible to compare them between both studies. The model was applied to study the reversal properties of MBLI87 on CPT11 ABCG2-mediated resistance. The tumour growth experiment contains two sets of experimental conditions. Even if in S2, mice received a treatment more intense and the delay of treatment onset was longer. Based only on the amount of drugs received, the tumour size should has been more important in this study, whereas the tumour size was 8 times greater at day 40 in S2. Thanks to our model, it was possible to identify and quantify parameters explaining this unexpected difference. Since the PK was the same for all the animals and the natural tumour growth comparable between both studies, the

observed difference is necessarily associated to a different tumour biology. Indeed, the equilibration between plasma and tumour due to passive diffusion was faster in S1. This parameter reflects the tumour environment and vasculature and was found to impact the treatment outcomes. Another factor contributing to the difference is the active efflux rate representing the transporter activity and found higher in S2. There is thus a lower accumulation of cytotoxic in the tumour compartment that is associated to a lower drug effect (Figure 19). In addition, the proportion of drug sensitive cells was also lower at treatment onset in S2 (68% and 85% of proliferative cells at treatment onset in S1 and S2 respectively).

Regarding MBLI87 efficacy, the model predicts a relatively small benefit of the inhibitor to reverse CPT11 ABCG2-mediated resistance (Figure 19). Interestingly, this finding is contradictory to the observations made *in vitro* where MBLI87 was shown to efficiently inhibit CPT11 and SN38 efflux.

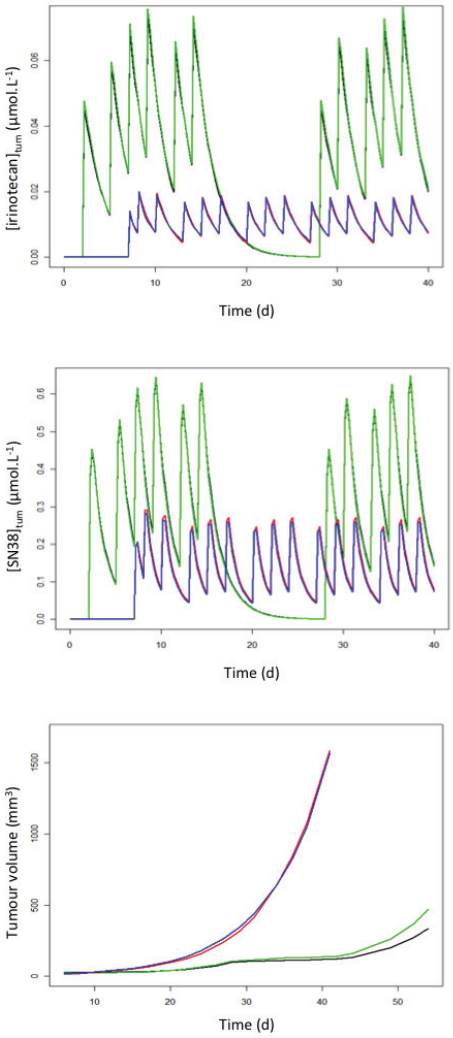

Figure 19: CPT11/SN38 tumour concentration prediction
CPT11 (upper panel), SN38 (center panel) tumour accumulation and tumour growth (lower panel) in Study 1 and Study 2 in presence and absence of MBLI87 (green: +MBLI87 Study 1, black: -MBLI87 Study 1, red: +MBLI87 Study 2, blue: -MBLI87 Study 2) predicted from the final model.

This poor effect arose from the low inhibition of ABCG2 *in vivo* by MBLI87 ($\frac{C_{moy,plasma}(MBLI87)}{K_i(MBLI87|CPT11)} = 10^{-2}, \frac{C_{moy,plasma}(MBLI87)}{K_i(MBLI87|SN38)} = 10^{-3}$). Moreover, MBLI87 clearance is too high to ensure an accumulation of MBLI87 *in vivo* and a prolonged inhibition of the transporter.

In the simulation study, we demonstrated that a 1000 times increase of MBLI87 dose using the same dose schedule as in S2 allows increasing its reversal effect ($\frac{Tumour\ size\ (day\ 40)_{+MBLI87}}{Tumour\ size\ (day\ 40)_{-MBLI87}}$=1.18, Figure 20)

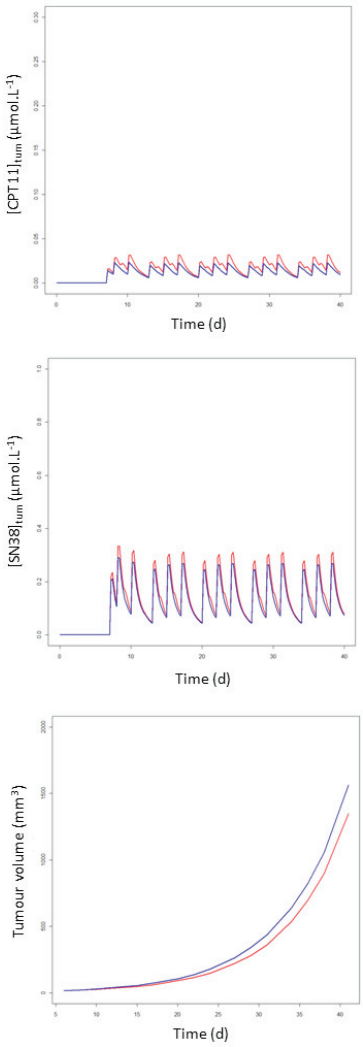

Figure 20: CPT11/SN38 tumour concentration prediction with 1000 times MBLI87 dose and dose schedule from S2

CPT11 (upper panel), SN38 (center panel) tumour accumulation and tumour growth (lower panel) in Study 2 in presence and absence of MBLI87 (red: +MBLI87 Study 2, blue: -MBLI87 Study 2)

Using a continuous infusion of MBLI87, a 100 times increase of MBLI87 dose was necessary to increase MBLI87 reversal effect ($\frac{Tumour\ size\ (day\ 40)_{+MBLI87}}{Tumour\ size\ (day\ 40)_{-MBLI87}}$=1.12, Figure 21). It means that if the transporter is constantly inhibited, a better effect can reached.

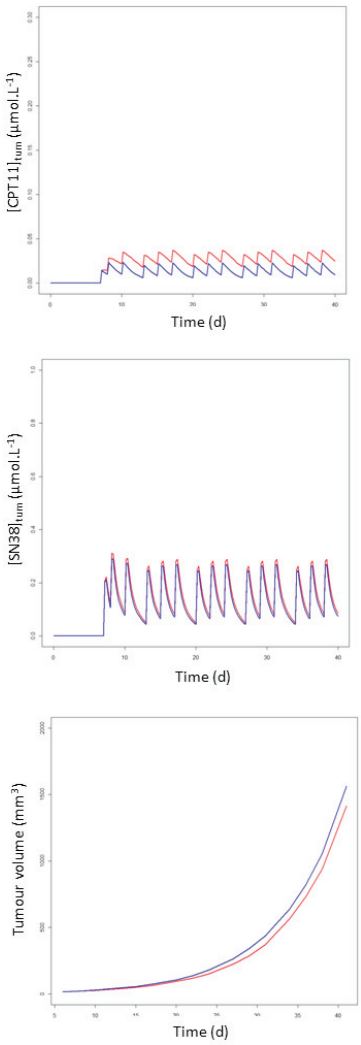

Figure 21: CPT11/SN38 tumour concentration prediction with 100 times MBLI87 dose and continuous infusion

CPT11 (upper panel), SN38 (center panel) tumour accumulation and tumour growth (lower panel) in Study 2 in presence and absence of MBLI87 (red: +MBLI87 Study 2, blue: -MBLI87 Study 2)

Even if a greater effect of MBLI87 was observed when its dose was increased, the effect on the tumour size remained relatively small. It thus indicates that its poor effect was due either to its inhibitory constant or to its too short half-life. In that sense, we simulated a scenario where MBLI87 Ki was decreased in order to obtain a ratio $\frac{C_{moy,plasma}(MBLI87)}{K_i(MBLI87)} = 100$. In that case, the ratio of the tumour size at day 40 was predicted at 1.54 demonstrating the significant impact of this parameter in MBLI87 efficacy, as expected (Figure 22).

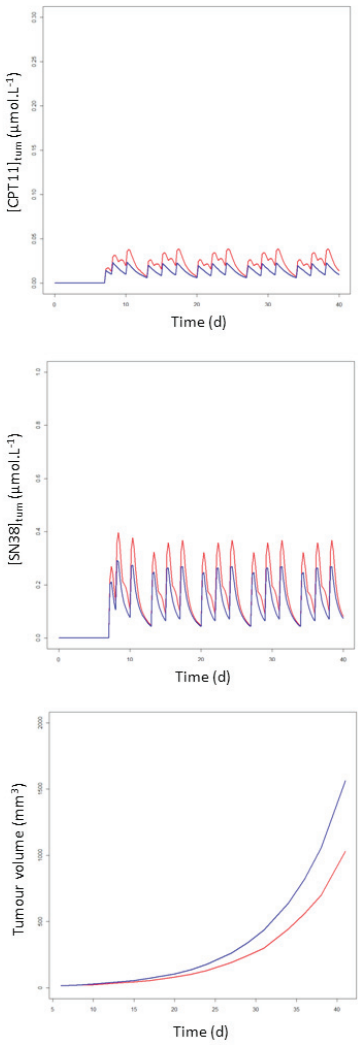

Figure 22: CPT11/SN38 tumour concentration prediction with MBLI87 K_i (K_i(MBLI87|CPT11)=0.0005784µM, K_i(MBLI87|SN38)=0.000394µM) decreased and dose schedule from S2
CPT11 (upper panel), SN38 (center panel) tumour accumulation and tumour growth (lower panel) in Study 2 in presence and absence of MBLI87 (red: +MBLI87 Study 2, blue: -MBLI87 Study 2)

In the same way, an increase of MBLI87 half-life ($t_{1/2}$(MBLI87)=4.8d) allows a significant gain of MBLI87 effect due to the prolonged inhibition of the transporter Indeed, if both MBLI87 K_i and clearance are decreased simultaneously, the reversal effect of MBLI87 is maximized with a tumour size ratio predicted equal to 4.2 (Figure 23). This result corroborates the result obtained with P-gp inhibitor where the question of the adequate inhibition of the transporter appeared crucial to ensure an effect of the inhibitor.

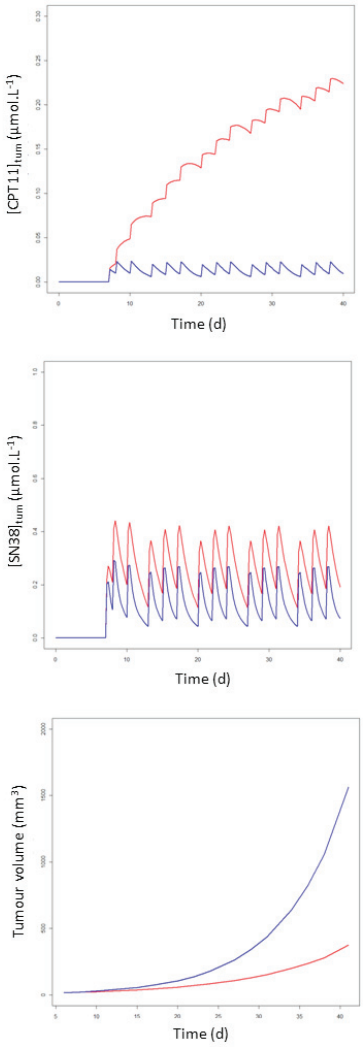

Figure 23: CPT11/SN38 tumour concentration prediction with a decrease MBLI87 K_i (K_i(MBLI87|CPT11)=0.0005784µM, K_i(MBLI87|SN38)=0.000394µM) and a decrease MBLI87 clearance (Cl(MBLI87)=0.162) using dose schedule from S2
CPT11 (upper panel), SN38 (center panel) tumour accumulation and tumour growth (lower panel) in Study 2 in presence and absence of MBLI87 (red: +MBLI87 Study 2, blue: -MBLI87 Study 2)

We also investigated the impact of the system parameters on the treatment outcomes. We showed that if the active transport rate constant was increased, the difference observed between animals receiving the inhibitor and those that do not received the inhibitor was potentiated (Figure 24). However, if the active efflux becomes more important, the cytotoxic tumour concentration decreases leading to a lower effect of cytotoxic on the tumour growth. It also demonstrated the need to choose a cell line where the transporter is well expressed in order to see the impact of its inhibition. Even if HEK293 cells were

interesting because of their simplicity, we showed in the 1st part that the maximum increase in cytotoxic intracellular concentration was moderate in this cell line. Better results of ABCG2 inhibition by MBLI87 could thus have been observed with a different cell line.

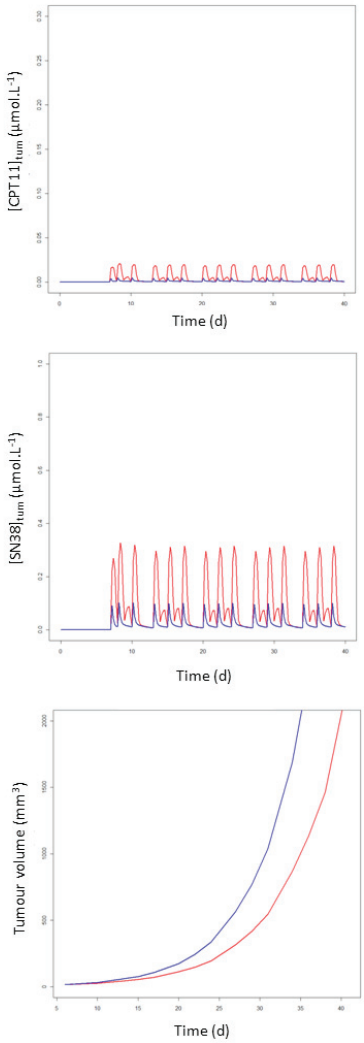

Figure 24: CPT11/SN38 tumour concentration prediction with a decrease MBLI87 K_i (K_i(MBLI87|CPT11)=0.0005784µM, K_i(MBLI87|SN38)=0.000394µM) and an increase of active transport rate constant (K_{act}(CPT11)=9.8d^{-1}, K_{act}(SN38)=10.3d^{-1}) using dose schedule from S2
CPT11 (upper panel), SN38 (center panel) tumour accumulation and tumour growth (lower panel) in Study 2 in presence and absence of MBLI87 (red: +MBLI87 Study 2, blue: -MBLI87 Study 2)

The last axis investigated in the simulation study concerns the tumour biology where both the proportion of drug sensitive cells at treatment onset and the cytotoxic diffusion were studied. As expected, if less drug sensitive cells composed the tumour tissue at treatment onset, a lower effect of cytotoxic was observed. However, this result largely depends on

the nature of the tumour growth model. Different behaviours could have been simulated if the model incorporated a growth of hypoxic cells for example. More interestingly, we demonstrated the importance of cytotoxic diffusion in the tumour on the treatment outcomes. This has already been demonstrated by Patel *et al.* for doxorubicin and P-gp inhibitors. (236). Here, the tumour size was minimized when MBLI87 Ki and clearance where decreased as previously and also when the passive diffusion constant rate was increased by 10. In that case, the tumour size at day 40 was predicted at 320.5mm^3 for animals receiving the combination CPT11-MBLI87 and at 470.3mm^3 for animals receiving CPT11 alone (Figure 25). It also raised the question of combining an antiangiogenic agent in order to normalize the tumour vasculature at treatment onset to ensure a sufficient diffusion of the cytotoxic drug (237).

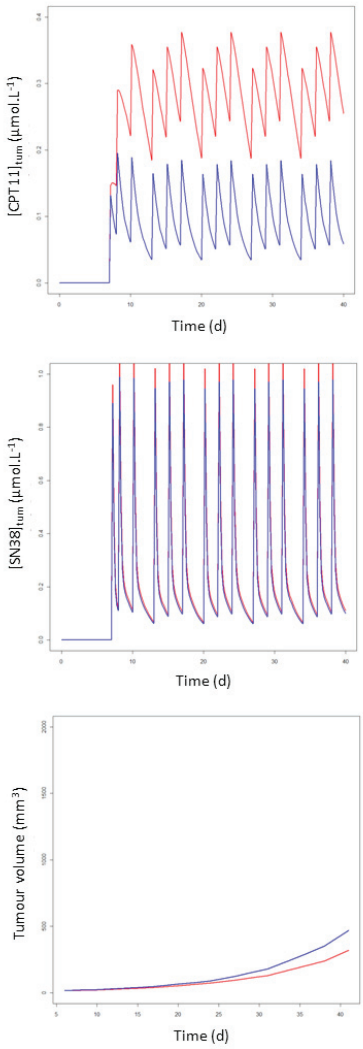

Figure 25: CPT11/SN38 tumour concentration prediction with a decrease MBLI87 K_i (K_i(MBLI87|CPT11)=0.0005784µM, K_i(MBLI87|SN38)=0.000394µM) and an increase of passive diffusion rate constant (K_{trans}(CPT11)=0.48d^{-1}, K_{trans}(SN38)=11d^{-1}) using dose schedule from S2
CPT11 (upper panel), SN38 (center panel) tumour accumulation and tumour growth (lower panel) in Study 2 in presence and absence of MBLI87 (red: +MBLI87 Study 2, blue: -MBLI87 Study 2)

This last scenario does not allow maximizing MBLI87 effect since the tumour sizes ratio was predicted at 1.47, whereas it was predicted at 4.24 when only its K_i and its clearance were decreased. Our results indicate that it is thus not possible to simultaneously maximize the inhibitor effect and minimize the tumour size. Since the final aim of this type of study is to minimize the tumour size, it can explain why the addition of an efflux inhibitor never led to a significant amelioration of patients response (237).

Publication 2

Characterization of the interaction between cytotoxic and efflux transporter inhibitors with a multiscale semi-mechanistic PKPD model

Alexandre SOSTELLY, Léa PAYEN, Jérôme GUITTON, Attilio DI PIETRO, Pierre FALSON, Mylène HONORAT, Annabelle GEZE, Ahcène BOUMENDJEL, Gilles FREYER, Michel TOD

In manuscript

Introduction

Effective systemic treatment of solid tumours requires that tumour cells are exposed to sufficient concentrations of drugs to cause cytotoxicity. The ability of anticancer drugs to reach tumour cells depends on efficient delivery of drugs through the vascular system and penetration into tumours (238). One of the mechanisms of anticancer drug resistance relies on the decrease of intracellular drug concentration mediated by efflux pumps from the ATP Binding Cassette family (ABC). ABC transporters are known to play an important role in drug absorption, distribution and elimination (88). Many anticancer drugs are high-affinity substrates of these transporters that are thus involved in the resistance of tumours (239). In the past, many attempts were made to overcome the anticancer drug resistance by inhibiting ABCB1, P-gp, so far the best characterized efflux transporters (240). Three generations of P-gp inhibitors have been developed to inhibit the chemoresistance in patients. Despite, promising results obtained in animals, none of the clinical trials that evaluated P-gp inhibitors concluded to their positive effect in patients (42, 43, 241-244). Several points have to be made regarding the methodology used in these trials so that their ability to adequately address the question of overcoming drug resistance through efflux inhibition can be questioned. None of the trials assessed P-gp expression in tumours and there was no selection of patients based on the transporter expression. Moreover, enrolled patients had already received several lines of chemotherapy and the drug resistance was certainly multifactorial. Others factors were advocated to explain the clinical failure of P-gp inhibitors such as the insufficient penetration of cytotoxic drugs in the tumour (236), the prevalence of the target *in vivo* (245), the occurrence or development of others resistance mechanisms (246), or the insufficient inhibition of the transporter *in vivo* (247).

Because of the clinical failure of P-gp inhibitors, the question of overcoming drug resistance by inhibiting others efflux transporters are rarely been addressed in preclinical and clinical trials (247). ABCG2, Breast Cancer Resistance Protein (BCRP), is one of the latest ABC transporter discovered (111). This efflux transporter plays a tumour-protective role by decreasing the tumour accumulation of several anticancer drugs such as topotecan, mitoxantrone, irinotecan and its active metabolite, SN38 (135). Moreover, ABCG2 substrates' profile overlaps that of P-gp. This transporter is thus a promising target for re-testing the benefits of the efflux inhibition in the management of anticancer drug resistance. New ABCG2 inhibitors non-toxic have been recently developed (136). One acridone derivative, MBLI87, was able to inhibit mitoxantrone ABCG2-mediated efflux *in vitro*. *In vivo*, this compound was able to reverse irinotecan (CPT11) ABCG2-mediated resistance in mice (137).

To overcome issues already encountered in the development of P-gp inhibitors it is necessary to identify and quantify the key steps of efflux inhibitors action from the beginning of their development. Mechanistic drug disease models may be an efficient tool to disentangle the influence of several pharmacokinetic and pharmacodynamic factors on the efficacy of these compounds. In a drug development perspective, *in silico* modelling and simulation can help to optimize recommendations about the formulation or dosing schedule of the developed compound. This approach has already been successfully applied to cytotoxic and anti-angiogenic compounds (191) (192) but such models have never been applied to efflux transporter inhibitors.

In this work, we developed a model for studying MBLI87 reversal effect on CPT11 ABCG2-mediated resistance *in vivo*. This mathematical model establishes the relationship between the efflux transporter activity, the cytotoxic accumulation into tumour and the tumour growth.

Materials and methods

Experimental methods

Cell Culture

The Human Embryonic Kidney 293 (HEK293) cell line ABCG2-transfected were obtained as described in (137). Cells were maintained in Dulbecco's modified Eagle's medium (DMEM high glucose) supplemented with 10% foetal bovine serum (FBS), 1% penicillin/streptomycin, and 1mg.mL^{-1} G418.

Animals

Female Severe Combined Immuno-Deficient (SCID) mice, 8-week old, were obtained from the Charles River Company. Animals were handled in accordance with the Guide for the Care and Use of Laboratory Animals and all procedures followed protocols approved by the Animal Facility veterinarian board.

Pharmacokinetic studies

Drug disposition was evaluated in tumour-free mice. Irinotecan (CPT11) was provided by the MAP company (France). CPT11 pharmacokinetics was evaluated after single dose (20mg.kg^{-1}) administered intra-peritoneally (IP) either alone or with MBLI87 to evaluate potential pharmacokinetic interactions. Concentrations of CPT11 and its active metabolite in plasma, SN38, were monitored during 24h using 5 mice per sampling times. MBLI87 pharmacokinetics was evaluated after multiple doses (3.45mg.kg^{-1}) administered IP. To evaluate the potential accumulation of MBLI87 in animals, three groups of animals were used: Group 1 received a single dose of MBLI87 at t=0 and concentrations were measured at t=1, 2, 4 and 6h; Group 2 received 2 doses of MBLI87 at t=0, 4h and concentrations were measured at t=5 and 8h; Group 3 received 3 doses of MBLI87 at t=0, 4, 8h and concentrations were measured at t=9 and 12h.

Tumour growth studies

SCID mice were subcutaneously inoculated with the HEK293 cells overexpressing ABCG2 cells ($8.2.10^6$ cells in 100µL PBS/inoculation) on the right and left flanks. Time 0 was the time of cells inoculation. Mice were randomized into treatment groups the day following cells implantation. Three groups of treatment were defined:

- 1 control group
- 1 group receiving irinotecan alone
- 1 group receiving irinotecan combined to MBLI87

Two studies with 2 sets of experimental conditions were defined.

In the first study (study 1, S1), 30 animals were randomized into the 3 treatment groups (control N=18, irinotecan N=6, irinotecan+MBLI87 N=3). In this study, irinotecan was administered IP at $30mg.kg^{-1}$ 3 days per week for 2 consecutive weeks, followed by a 2-week rest period and then 2 more weeks of treatment for a total of 6 weeks of treatment. MBLI87 was administered IP at $2.4mg.kg^{-1}$ 5 days per week with the same dose schedule. A 2-day delay between tumour cells implantation and first drug administration was applied.

In the second study (study 2, S2), 15 animals were randomized into the 3 treatment groups (control N=5, irinotecan N=5, irinotecan+MBLI87 N=5). Irinotecan was administered IP at $20mg.kg^{-1}$ 3 days per week for 4 weeks of treatment without any interruption. MBLI87 was administered IP at $2.4mg.kg^{-1}$ 5 days per week throughout the 4 weeks of treatment. A 7-day delay between tumour cells implantation and first drug administration was applied.

Main designs set-ups are summarized in Table 1. Treatment intensity (total amount/treatment duration) was greater in S2 than in S1 and treatment delay between cells inoculation and treatment onset was greater in S2.

	Study 1	Study 2
Total amount - irinotecan (µmol)	11.25	10.91
Total amount – MBLI87 (µmol)	2.16	2.84
Treatment intensity – irinotecan ($\mu mol.d^{-1}$)	0.24	0.28
Treatment intensity – MBLI87 ($\mu mol.d^{-1}$)	0.05	0.07
Treatment delay (d)	2	7
Wash-out period	Yes	No

Table 1: Tumour growth experiments design settings

Mice were clinically evaluated daily. Tumour dimensions (length, width) were measured with a calliper 3 times per week from day 5 and mice were euthanized when the tumour volume exceeded 1,800mm^3.

Four measurements per animals were available (tumour length and width on each flank) at each measuring time point. The mean tumour volume over the 2 flanks was defined as a metric of tumour size.

Model development

Model structure

Complete model includes four sub-models (Figure 1):

- The pharmacokinetic model describing the relationship between administered doses and drug concentration in plasma.
- The tumour accumulation model describing the relationship between drug concentration in plasma and in tumour cells, and the action of MBLI87 leading to increase the cellular concentration of the cytotoxic

- The tumour growth model incorporating three cell types and describing the natural evolution of the disease.
- The cytotoxic action model linking cytotoxic tumour concentration with inhibition of tumour growth

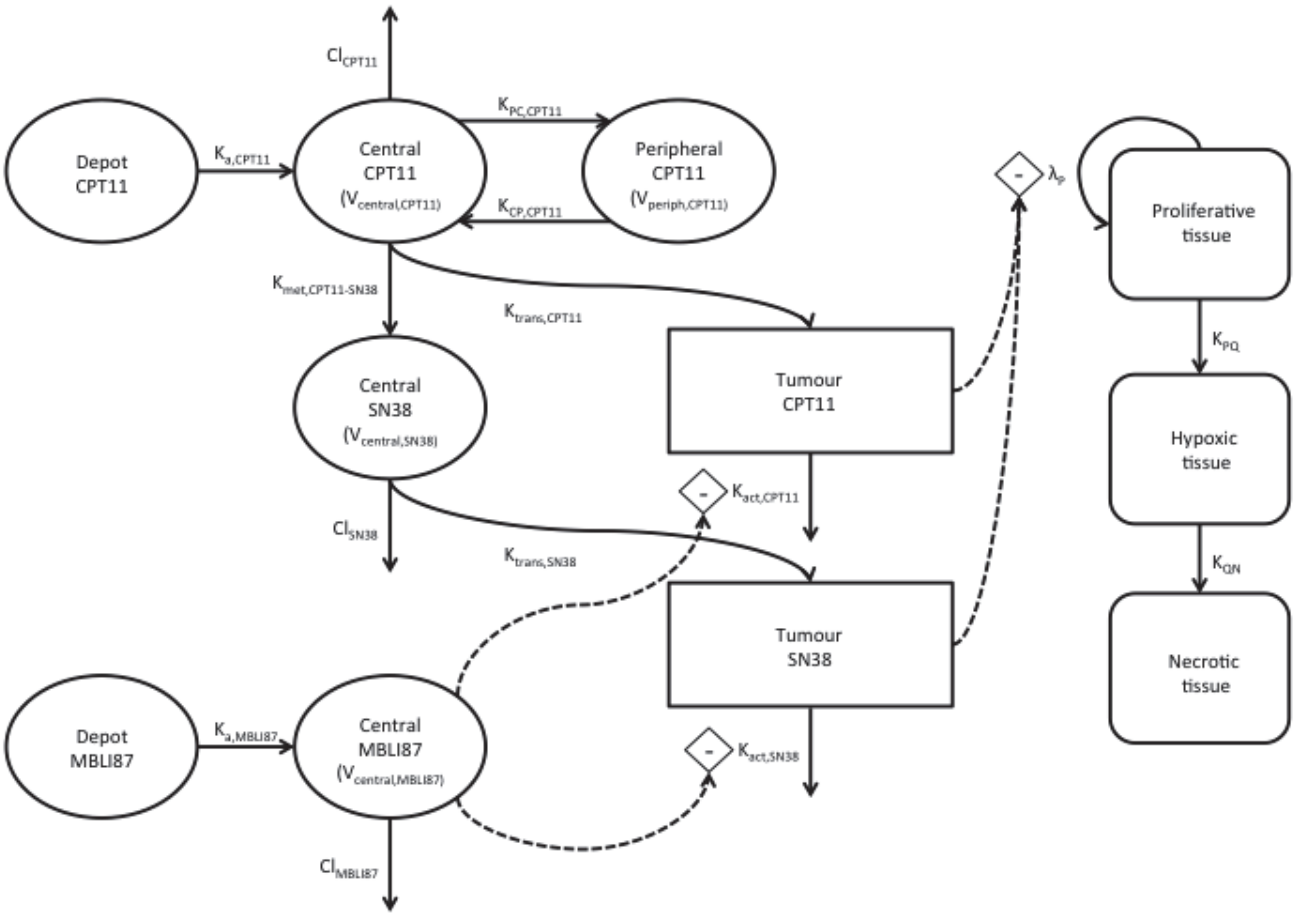

Figure 1: Figure 1: Scheme of the final model structure
Schematic representation of the multiscale semi-mechanistic PKPD model.

Pharmacokinetic models

For practical reasons, animals were euthanized after blood sampling and no repeated measurement of drug concentration was available. PK data was thus pooled together and analysed using compartmental models.

Concentrations of CPT11 and SN38 in plasma were simultaneously analysed since CPT11 is metabolized in SN38 in vivo (248). CPT11 disposition was best described using a 2-compartment linear model, CPT11 metabolization occurring from the central compartment. SN38 disposition was best described with a 1-compartment linear model. MBLI87 disposition in plasma was best described with a 1-compartment model with first-order absorption and elimination rates.

Tumour accumulation model

To account for the accumulation kinetics of CPT11 and SN38 in tumours and ABCG2 inhibition by MBLI87, a previously developed model was used (SOSTELLY, 2012 #323). The assumption underlying this model was the following: CPT11 and SN38 cross the cell membrane in each direction by passive diffusion, characterized by a diffusion clearance (Cl_{diff}). Active efflux is assumed to be ABCG2-mediated and due to the nature of the transporter, a Michaelis-Menten behaviour has been chosen to model its action. Interaction between cytotoxic and efflux inhibitor occurs within the transporter and is non-competitive. Both interaction and active efflux are accounted for in the transport clearance parameter (Cl_{tran}). At equilibrium, the following equation holds:

$$Cl_{diff} \times [Drug]_e = \left(Cl_{diff} + Cl_{tran}\right) \times [Drug]_i \qquad \text{(Equation 1)}$$

Where $[Drug]_i$ and $[Drug]_e$ are respectively the intracellular and extracellular concentrations of CPT11 and SN38.

To be able to use this model developed on in vitro data, the tumour compartment was assimilated to a receptor compartment at the kinetic equilibrium at any times. This assumption allows re-using Equation 1 in vivo and lead to the following equation which governed the CPT11/SN38 kinetic accumulation in the tumour cells.

$$\frac{dC_{tumour}}{dt} = K_{trans} \times \left(C_{plasma} - C_{tumour}\right) - \frac{K_{act} \times C_{tumour}}{1 + \frac{C_{MBLI87,plasma}}{K_i}} \qquad \text{(Equation 2)}$$

Where C_{tumour} is the tumour concentration of CPT11/SN38; C_{plasma} is the concentration of CPT11/SN38 in plasma; K_{trans} is the rate constant governing the accumulation of CPT11/SN38 in the tumour due to passive diffusion relatively to the tumour compartment volume; K_{act} is the rate constant governing the active efflux of CPT11/SN38 relatively to the plasma compartment volume; $C_{MBLI87,plasma}$ is the concentrations of MBLI87 in plasma. This model assumed a linear interaction between cytotoxic and efflux inhibitor, i.e. the Michaelis constant is assumed to be greater compared to the intracellular concentration of cytotoxic.

Tumour growth model

The tumour growth model includes 3 cell compartments: proliferative cells (P), hypoxic cells (Q) and necrotic cells (N). The sum of the volumes of the 3 compartments was directly fitted to the observed tumour volume (195). The tumour growth model assumes an exponential growth of proliferative cells. A part of proliferative cells becomes hypoxic (Q) and hypoxic degrade into necrotic cells (N). Hypoxic and necrotic cells do not divide. Passage from one stage to another is governed by transfer rate constants as described in Equation 3:

$$\begin{cases} \frac{dP}{dt} = \lambda_P \times P - k_{PQ} \times P \\ \frac{dQ}{dt} = k_{PQ} \times P - k_{QN} \times Q \\ \frac{dN}{dt} = k_{QN} \times Q \\ P(t=0) = P_0 \\ Q(t=0) = 0 \\ N(t=0) = 0 \end{cases} \quad \text{(Equation 3)}$$

Where P is the volume of proliferative cells; λ_P is the exponential growth rate; k_{PQ} is the transfer rate between proliferative and hypoxic cells; Q is the volume of hypoxic cells; k_{QN} is the transfer rate between hypoxic and necrotic cells; N is the volume of necrotic cells.

Cytotoxic action model

CPT11 and SN38 enhance tumour cells apoptosis by inhibiting the topoisomerase 1 (249). Because cytotoxic agents preferentially target tumour cells that grow rapidly, their effect was modelled as a decrease of the exponential growth rate (249). Because the parent and the metabolite are both active, an additive interaction of both compounds was considered to account for their cooperation. In order to reduce the number of parameters to be estimated in the model, the ratio of their cytotoxic potencies was fixed to 11 because SN38 is expected to be 11 times more potent in vivo than CPT11 after accounting for plasma protein binding (249, 250). Finally, their effect was directly proportional to their concentration in the tumour compartment normalized by their relative cytotoxic potencies (K_p, Equation 4)

$$\frac{dP}{dt} = \lambda_P \times \left(1 - \frac{\alpha}{K_P} \times \left(C_{tumour,CPT11} + \frac{C_{tumour,SN38}}{11}\right)\right) - k_{PQ} \times P \quad \text{(Equation 4)}$$

Where α is the cooperative coefficient, $C_{tumour,\ CPT11}$ is the CPT11 tumour concentration; $C_{tumour,\ SN38}$ is the SN38 tumour concentration; K_p is the cytotoxic potency.

Population modelling

Data were all analysed using non-linear mixed effects (NLME) approach that enables the simultaneous estimation of fixed and random effects in the model (228). Fixed effects refer to the typical value (median) of parameters (P) in the population. Random effects are estimated on 2 levels: variability between individuals (Inter-Individual Variability, IIV) and within an individual (Residual Variability, RV). Each observation of an individual in the population can be described as follows:

$$y_{ij} = f(X_{ij}, P_i) + g(X_{ij}, P_i) \times \varepsilon_{ij} \qquad \text{(Equation 5)}$$

Where y_{ij} is the j^{th} observation for the i^{th} individual, f(…) is the individual model prediction described by X_{ij} variables and P_i the individual parameter, $g(X_{ij}, P_i) \times \varepsilon_{ij}$ is the residual error describing the difference between the individual model prediction and the corresponding observed value. Residual error is assumed to be normally distributed with 0 mean and g(…) standard deviation. In the following, we will only consider the so-called combined error model, $g(X_{ij}, P_i) = f(X_{ij}, P_i) + k$ where k is a constant.

The individual parameter, P_i, is expressed as a function of the typical value for the population and the deviation from this typical value:

$$P_i = \theta \times e^{\eta_i} \qquad \text{(Equation 6)}$$

Where P_i is the individual parameter value for the i^{th} individual; θ is the parameter typical value (the median); η_i is a random parameter that described the difference between the median and the parameter value in individual i; η_is values are assumed to be normally distributed with 0 mean and ω^2 variance. In such a model the parameters to be estimated are the fixed effects (θs), the random effects (ω^2) and the variances of the residual error.

Model evaluation

Parameter estimation was performed by likelihood maximization using NONMEM software, version 7.2 (229).

Selection between models was based on the Objective Function Value (-2log(likelihood)), which is the criterion minimized by NONMEM, and Akaike Information Criterion (173), as well as goodness of fit, residual plots, simulation-based diagnostics and precision of parameter estimates.

Simulation-based diagnostics were performed to reveal model misspecifications that are not easily diagnosed with classical goodness-of-fit plots. Two methods were used here: the Normalized Prediction Distribution Errors (NPDE) and the Visual Predictive Check (VPC).

Prediction errors were the quantile of each observation within its predictive distribution. NPDEs are obtained after decorrelation and normalization of prediction error with respect to the empirical mean and variance obtained in simulations (251). The model was considered as invalid when NPDEs were not normally distributed with a 0 mean and a variance of 1 (230).

Visual Predictive Check consists of simulating dependant variable based on model structure and parameter estimates (167). 1000 simulations of the original datasets were simulated and the 90% non-parametric confidence interval of the simulated medians was then compared to the observed ones. The model was considered as invalid when the confidence interval did not bracket the observed medians.

Model evaluation was performed with the R-based XPOSE4 program (231). PsN toolkit was used for simulations and calculations for the VPC (232).

Model building

Model was sequentially built. First, typical parameters of the PK models were estimated using data from the PK experiment and were then fixed in the final model. Second, tumour growth parameters were estimated on data issued from control group in S1 and S2 and their typical value was then fixed in the final model. MBLI87 inhibitory constant value (K_i) was fixed based on the value estimated in (252) and then corrected to account for the plasma protein binding in vivo (f_u(MBLI87)=5%).

Thus, in the complete model, only parameters K_{trans}, K_{act}, α/K_p and tumour growth parameters variability were estimated in S1 and S2.

Simulation study

Based on the final model structure and parameter estimates, a simulation study was performed in order to explore different properties of MBLI87 and of the system on the efficacy of the CPT11-MBLI87 outcomes. Three axes were investigated: the reversal effect of MBLI87, the tumour cell line and the tumour biology. Five hundred Monte Carlo simulations were performed for each of the simulated scenario. The mean tumour concentration of CPT11 and SN38 as well as the tumour size at day 40 were computed to evaluate the performances of each scenario.

Results

Data

Data obtained in S1 and S2 are presented in the supplementary file 1. In both S1 and S2, the addition of CPT11 slows significantly the tumour growth and the effect of MBLI87 is low. The tumour growth was more significantly more rapid in S2 than in S1 with a tumour size 8 times greater for animals receiving both CPT11 and MBLI87 at the day 40 (113.2mm^3 versus 1448.3mm^3 in S1 and S2 respectively).

Model evaluation

Model evaluation was performed separately for PK, tumour growth and complete models. VPCs (Figure 2) compared the 90% non-parametric confidence interval of the predicted medians to the observed ones. For all the sub-models as well as for the complete models, the observed medians lie within the confidence interval as required for model validation. NPDEs were normally distributed with a 0 mean and 1 variance without any trends (not shown). There was thus no misspecification of the final mixed effects model.

A

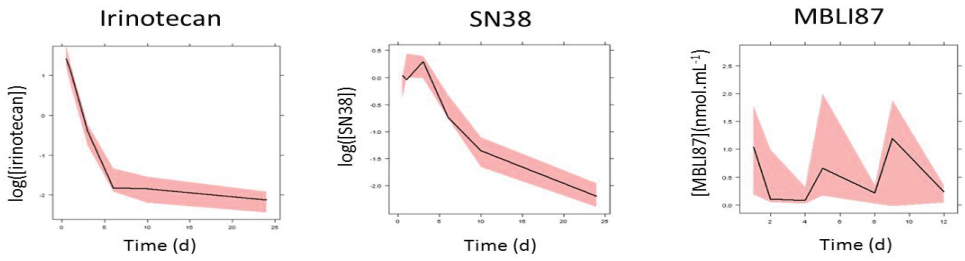

B

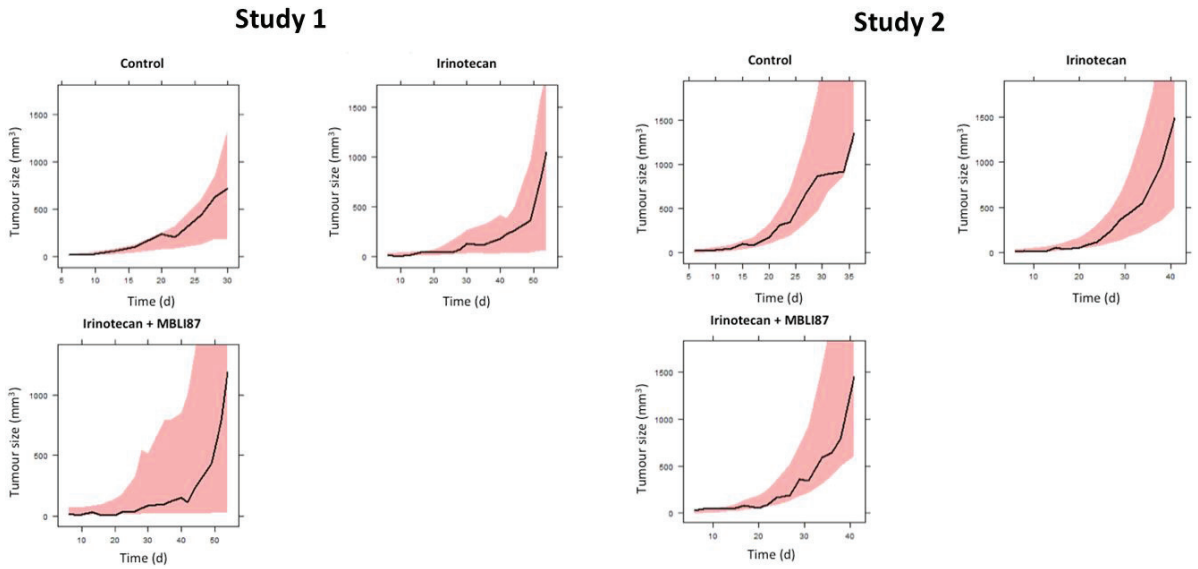

Figure 2: Visual Predictive Check

A. Visual Predictive Check (VPC) plot of the PK models compare the 90% non-parametric confidence interval of median (pink area) of plasmatic concentrations for CPT11 and SN38 on the log-scale (left and center panel) and for MBLI87 (right panel) obtained after simulations to the observed ones.

B. Visual Predictive Check (VPC) plot of the complete model compare the 90% non-parametric confidence interval of median (pink area) of tumour volume obtained after simulations to the observed ones.

Left panel: Study 1

Control: Control group; CPT11: Animals receiving CPT11 alone, CPT11+MBLI87: Animals receiving CPT11 combined to MBLI87

Right panel: Study 2

Control: Control group; CPT11: Animals receiving CPT11 alone, CPT11+MBLI87: Animals receiving CPT11 combined to MBLI87

PK model

No repeated measurement of the drug concentration in plasma was available and only the typical value of parameters was estimated. Parameter estimates of CPT11 and SN38 disposition plasma are presented in Table 2. Volumes of CPT11 peripheral compartment and SN38 central compartment were not identifiable and were fixed to 1mL.

Parameter estimates of MBLI87 pharmacokinetic model are presented in Table 2. MBLI87 absorption rate was estimates at $900d^{-1}$ attesting the rapid absorption of the drug.

MBLI87 clearance was estimated at 900L.d^{-1} attesting also of the quite rapid disappearance of the drug from the system.

Effect of MBLI87 on plasmatic disposition of CPT11 and SN38 in plasma was assessed by comparing CPT11 and SN38 AUCs in presence and absence of MBLI87. The medians AUCs were similar for the different conditions ($AUC_{CPT11+MBLI87}$=30.9±4µmol.L^{-1}.h^{-1}, $AUC_{CPT11-MBLI87}$=34.3±22µmol.L^{-1}.h^{-1}; $AUC_{SN38+MBLI87}$=9.5±2µmol.L^{-1}.h^{-1}, $AUC_{SN38-MBLI87}$=8.3±2µmol.L^{-1}.h^{-1}). Consequently, MBLI87 had no effect on CPT11 and SN38 disposition in plasma.

Tumour growth model

The tumour growth parameters (Table 2) were separately estimated on data issued from control group in S1 and S2. Exponential tumour growth rate was estimated at 0.187mm^3.d^{-1} in S1 and to 0.179mm^3.d^{-1} in S2. The transfer rate between proliferative and hypoxic cells was associated to a high relative standard error; it was thus not possible to conclude about its difference between both studies. Apart for this parameter, all the tumour growth parameters were comparable attesting the reproducibility of the experiment. At t=0, tumour was assumed to be only constituted of proliferative cells because cells were inoculated just after reaching confluence. Initial volume of proliferative cells was estimated at 16.3mm^3 in S1 and 15.4 mm^3 in S2.

Complete model

Parameter estimated separately on S1 and S2 treatment groups' (K_{trans}, K_{act}, α/K_i) are presented in Table 2. Rate constant governing the accumulation of CPT11 and SN38 in tumour due to passive diffusion (K_{trans}) was estimated at 0.099d^{-1} in S1, 0.048d^{-1} in S2 for CPT11 and at 1.3d^{-1} in S1, 1.12d^{-1} in S2 for SN38. Rate constant governing active efflux (K_{act}) was estimated at 0.89d^{-1} in S1, 0.98d^{-1} in S2 for CPT11 and 0.058d^{-1} in S1, 1.03d^{-1} in S2 for SN38. CPT11 and SN38 cytotoxic potency was less important in S2 than in S1

(0.19µmol.d^{-1} versus 0.15µmol.d^{-1} in S1 and S2 respectively) that is in accordance with the difference observed in tumour growth (tumour size was 8 times greater in S2 than in S1 at day 40). Because of the small number of animals used in S1 and S2, some parameters are associated to high relative standard errors. It was thus not possible to conclude about the difference between parameter estimates between both studies. However, the comparison of parameter point estimates suggest a different accumulation of cytotoxic in the tumour compartment (passive diffusion rate constant lower in S2 and active efflux rate constant higher in S2) that is associated to a lower effect on the tumour growth (Figure 3A)

The ratio of the mean MBLI87 concentration in plasma by its inhibitory constant was estimated at 10^{-2} for CPT11 and 10^{-3} for SN38 indicating the low inhibition of the ABCG2 by MBLI87. This is corroborated by the low effect of the inhibitor on the tumour growth in both studies ($\frac{Tumour\ Size\ (day\ 40)_{+MBLI87}}{Tumour\ size\ (day\ 40)_{-MBLI87}} = 0.98\ in\ S2$, Figure 3A).

PK CPT11/SN38	
	Typical value (%RSE)
Clearance CPT11 ($L.d^{-1}$)	1.01 (24.6%)
K_a CPT11 (d^{-1})	21.7 (14.7%)
$K_{CPT11\text{-}SN38}$ (d-1)	20.9 (28.3%)
$K_{central\text{-}peripheral}$ CPT11 (d^{-1})	3024 (50.4%)
$K_{peripheral\text{-}central}$ CPT11 (d^{-1})	1.11 (44.2%)
$V_{central}$ CPT11 (L)	0.004 (15.2%)
Clearance SN38 ($L.d^{-1}$)	0.009 (9.1%)

PK MBLI87	
	Typical value (%RSE)
Clearance MBLI87 ($L.d^{-1}$)	1.62 (90%)
K_a MBLI87 (d^{-1})	900 (44.8%)
$V_{central}$ MBLI87 (L)	0.12 (33.3%)

Tumour growth parameters				
	Study 1		**Study 2**	
	Typical Value (%RSE)	**IIV (%CV)**	**Typical Value (%RSE)**	**IIV (%CV)**
λ_P ($mm^3.d^{-1}$)	0.19 (26%)	27%	0.18 (6%)	26%
k_{PQ} (d^{-1})	0.05 (128%)	12%	0.001 (90%)	80%
k_{QN} (d^{-1})	0.09 (2%)	33%	0.09 (14%)	25%
P_0 (mm^3)	16.2 (19%)	41%	15.4 (26%)	63%
Q_0, N_0 (mm^3)	0*	-	0*	-

Complete model parameters				
	Study 1		**Study 2**	
	Typical Value (%RSE)	**IIV (%CV)**	**Typical Value (%RSE)**	**IIV (%CV)**
K_{trans} CPT11 (d^{-1})	0.099 (70.5%)	33%	0.048 (63.1%)	38%
K_{trans} SN38 (d^{-1})	1.4 (33.8%)	60%	1.1 (36.1%)	34%
K_{act} CPT11 (d^{-1})	0.89 (35%)	35%	0.98 (24.9%)	-
K_{act} SN38 (d^{-1})	0.058 34.6%	59%	1.03 (33.4%)	19%
α/K_p ($\mu mol.d^{-1}$)	0.19 (19.8%)	32%	0.15 (17.3%)	25%

Table 2: Parameters estimates

K_a: absorption constant rate; $K_{metabolism}$: metabolization rate constant CPT11-SN38; $K_{central\text{-}peripheral}$: transfer constant rate central compartment – peripheral compartment; $K_{peripheral\text{-}central}$: transfer constant rate peripheral compartment-central compartment; $V_{central}$: central compartment distribution volume; $V_{peripheral}$: peripheral compartment distribution volume

λ_P: Exponential tumour growth rate; k_{PQ}: Transfer constant rate proliferative tissue – hypoxic tissue; k_{QN}: Transfer constant rate hypoxic tissue – necrotic tissue; P_0: Initial volume of proliferative tissue; Q_0: Initial volume of hypoxic tissue; N_0: Initial volume of necrotic tissue

K_{trans}: Cytotoxic accumulation rate into tumour compartment; K_{act}: Cytotoxic active efflux rate from tumour compartment;

α/K_p: Cytotoxic potency of CPT11 and SN38

*: Fixed value; %RSE: Relative Standard Error of parameter estimates; IIV(%CV): Coefficient of variation of the Inter-Individual Variability

Simulation study

A simulation study was carried out to determine the impact of several factors on MBLI87 reversal effect and treatment outcomes. Seven different scenarios were simulated and compared based on the tumour size at day 40 and the mean CPT11 and SN38 tumour concentration to evaluate their performances. Simulations have only been performed for S2 where the maximum increase in treatment efficacy can be achieved. Performances of the different scenarios are presented in Table 3.

Scenario	Tumour size (day 40) (mm^3)	Ration tumour size	$C_{moy,tum}$(CPT11) ($\mu mol.L^{-1}$)	$C_{moy,tum}$(SN38) ($\mu mol.L^{-1}$)
Normal	1564.8	0.98	0.0114	0.118
	1585.6		0.0108	0.115
$P_0=Q_0=N_0$				
+ MBL87	1678.5	1.01	-	-
-MBLI87	1700.4			
1000 times dose MBLI87 (S2 dosing regimen)		1.18		
+ MBL87	1349.2		0.0156	0.131
-MBLI87	1700.4		0.0108	0.115
100 times dose MBLI87 (Continuous infusion)		1.12		
+ MBL87	1415.5		0.0227	0.131
-MBLI87	1585.6		0.0108	0.115
MBLI87 K_i decreased				
+ MBL87	1031.6	1.54	0.0192	0.157
-MBLI87	1585.6		0.0108	0.115
MBLI87 K_i decreased + MBLI87 clearance decreased		4.24		
+ MBL87	374.1		0.122	0.224
-MBLI87	1585.6		0.0108	0.115
MBLI87 K_i decreased + K_{act} increased		2.36		
+ MBL87	2343.4		0.00578	0.0882
-MBLI87	5532.05		0.000986	0.0203
MBLI87 K_i decreased + K_{trans} increased		1.19		
+ MBL87	394.2		0.115	0.211
-MBLI87	470.3		0.0793	0.198
MBLI87 K_i decreased + MBLI87 clearance decreased + K_{trans} increased		1.47		
+ MBL87	320.5		0.231	0.218
-MBLI87	470.3		0.0793	0.198

Table 3: Performances of the different scenarios simulated

Normal: Normal conditions using parameter estimates and dosing schedule from S2

$P_0=Q_0=N_0$: modification of the tumour initial composition to obtain as many proliferative, hypoxic and necrotic cells proportions

1000 times dose MBLI7 using parameter estimates from S2 (S2 dosing regimen): Increase of MBLI87 doses 1000 times using parameter estimates and dosing schedule from S2

100 times dose MBLI87 (Continuous infusion): Increase of MBLI87 100 times with a continuous infusion of MBLI87 (constant concentration) using parameter estimates from S2

MBLI87 Ki decreased: Decrease of MBLI87 Ki for CPT11 and SN38 active transport (K_i(MBLI87|CPT11)=0.000578 µM, K_i(MBLI87|SN38)=0.000394µM) using dosing schedule and parameter estimates from S2

MBLI87 K_i decreased + MBLI87 clearance decreased: Decrease of MBLI87 Ki as previously and decrease MBLI87 clearance by 10 (Cl(MBLI87)=0.162L.d^{-1}) using dosing schedule and parameter estimates from S2

MBLI87 K_i decreased + K_{act} increased: Decrease of MBLI87 K_i as previously and increase active efflux constant rate by 10 (K_{trans} CPT11=9.8d^{-1}; K_{trans} SN38=10.3d^{-1}) using the dosing schedule and parameter estimates from S2

MBLI87 K_i decreased + K_{trans} increased: Decrease of MBLI87 K_i as previously and increase passive diffusion constant rate by 10 (K_{trans} CPT11=0.48d^{-1}, K_{trans} SN38=11d^{-1}) using dosing schedule and parameter estimates from S2

MBLI87 K_i decreased + MBLI87 clearance decreased + K_{trans} increased: Decrease of MBLI87 K_i, clearance and increase of passive diffusion constant rate as previously

MBLI87 was maximized when its inhibitory constant was decreased to obtain a ratio between its mean plasma concentration and its inhibitory constant equal at 100 (K_i(MBLI87$_{SN38}$)=0.000578µM, Ki(MBLI87$_{CPT11}$)=0.000394µM) and when its clearance

was decreased by 10 leading to an half life at 4.3d. This scenario leads to a ratio of tumour concentration with and without MBLI87 predicted at 11 for CPT11 and 2 for SN38 (Table 3, Figure 3B). Surprisingly, the scenario that minimizes the tumour size at day 40 was not the same. In this case, MBLI87 clearance and inhibitory constant have also to be decreased as previously but the diffusion rate constant (K_{trans}) of cytotoxic drugs in the tumour compartment has to be increased. This scenario leads to a tumour size at day 40 predicted at 320.5mm^3 with MBLI87 and 470.3mm^3 without MBLI87 (Table 3, Figure 3C).

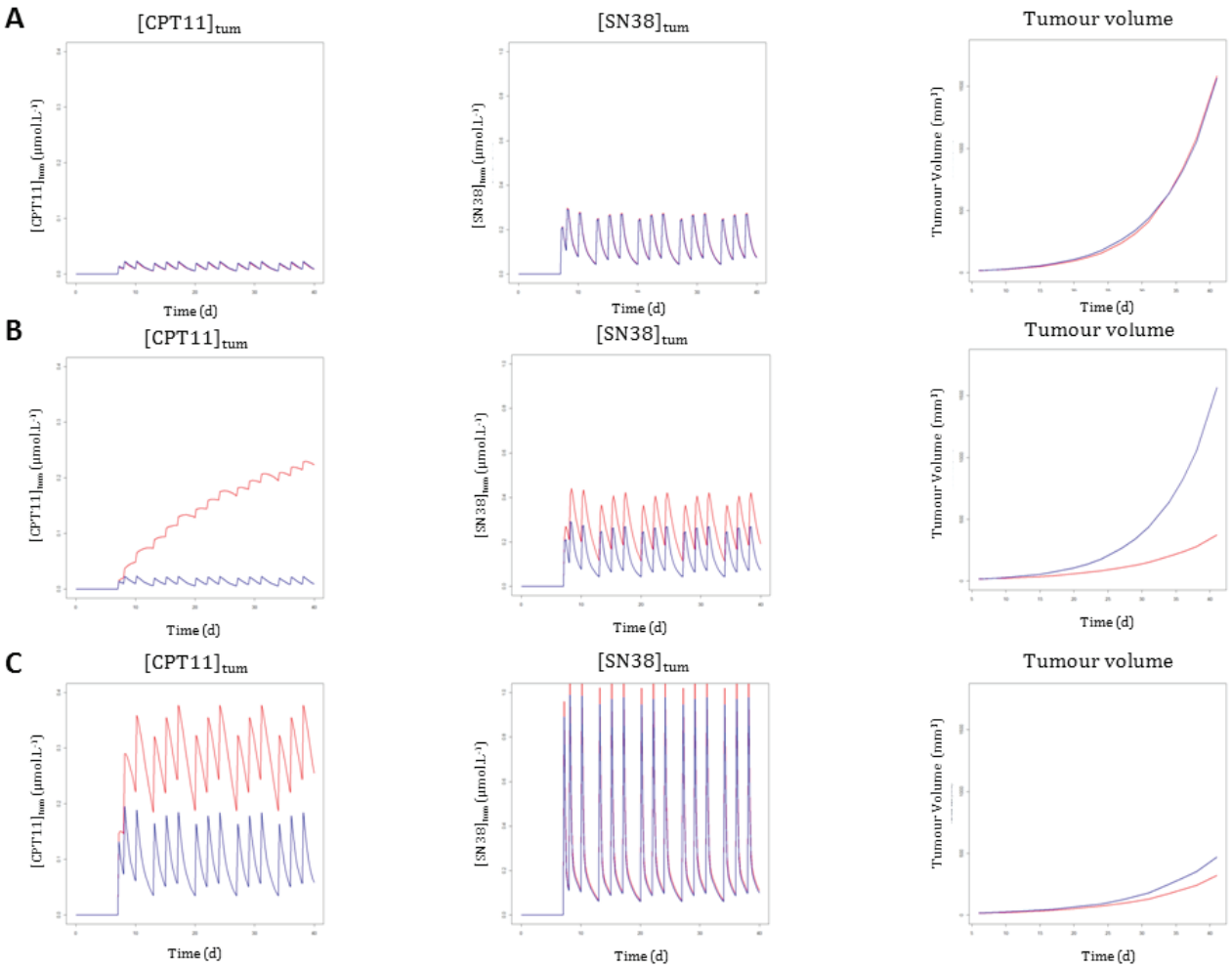

Figure 3: Performances of the simulated scenarios

The mean tumour concentration of CPT11 (left) and SN38 (center) over the time and the tumour growth (right) are presented in presence (red curve) or absence (blue curve) of MBLI87

- **A. Normal conditions:** Normal conditions using parameter estimates and dosing schedule from S2
- **B. MBLI87 K_i decreased + MBLI87 clearance decreased:** Decreased of MBLI87 Ki for CPT11 and SN38 active transport (K_i(MBLI87|CPT11)=0.000578 µM, K_i(MBLI87|SN38)=0.000394µM) and decreased MBLI87 clearance by 10 (Cl(MBLI87)=0.162L.d^{-1}) using dosing schedule and parameter estimates from S2
- **C. MBLI87 K_i decreased + MBLI87 clearance decreased + K_{trans} increased:** Decreased of MBLI87 Ki for CPT11 and SN38 active transport (K_i(MBLI87|CPT11)=0.000578 µM, K_i(MBLI87|SN38)=0.000394µM), decreased MBLI87 clearance by 10 (Cl(MBLI87)=0.162L.d^{-1}) and increased passive diffusion constant rate by 10 (K_{trans} CPT11=0.48d^{-1}, K_{trans} SN38=11d^{-1}) using dosing schedule and parameter estimates from S2

Discussion

This study presented the construction and use of a semi-mechanistic PKPD model of the interaction between efflux transporter inhibitors and cytotoxic drugs. The model includes a mechanistic description of the cellular interaction between both compounds as well as a semi-mechanistic tumour growth model that accounts for the proliferative, hypoxic and necrotic cells proportions. To our knowledge, this is the first model that establishes the relationship between the cellular effects of efflux inhibitors to the tumour growth. We applied this model to a new ABCG2 inhibitor, MBLI87, co-administered with the cytotoxic agent irinotecan, CPT11.

In order to combine all the information available about MBLI87, the model was sequentially built. PK studies were performed independently of tumour growth studies, the same PK profile was thus assumed for S1 and S2. Moreover, doses of CPT11 and MBLI87 used in PK experiments were different from the ones used in S1 and S2 and PK parameters were assumed to be dose-independent.

The cytotoxic accumulation kinetics in the tumour cells was based on a previously developed model (252). This model assumed that Michaelis constant of cytotoxic was greater than their intracellular concentration leading to a linear interaction between compounds. The model is thus unable to predict the saturation of the active transport expected for high doses. Sigmoid interaction models could have been used but would have required to test several doses of cytotoxic and inhibitors.

The tumour growth model includes three types of cells. Contrary to the model from Ribba et al. (195), only the proliferative cells grow in our model according to an exponential growth rate. A generalized logistic tumour growth model as used by Ribba et al. has been tested but failed to converge because our data did not contain enough information about

the maximum tumour capacity. Under this formulation, the model is not able to predict a decrease of the tumour size because tumour cells do not eliminate but accumulate into the necrotic compartment. The addition of such a constant reduced the quality of the model fit. Moreover, in xenografted animals necrotic cells accumulate in the tumour central core that is consistent with our assumption (195).

The last assumption included in the complete model concerns the cytotoxic action model where a linear effect of CPT11 and SN38 was used. Here again, the model is not able to predict the saturation of cytotoxic effect expected for high doses of CPT11.

Despite all these assumptions, the complete model was successfully applied to both tumour growth experiments. However, because of the small number of animals used, some of the model parameters are associated to a high uncertainty. It was not possible to conclude about the significance of their differences between both studies. Nevertheless, the comparison of parameters point estimates indicates some differences between both studies. K_{trans} represents the kinetics of drug accumulation into tumour cells due to passive diffusion; through this parameter it is the tumour environment and vasculature that are accounted for. K_{trans} was found lower in S2 than in S1 suggesting a lower cytotoxic accumulation in tumour cells. In addition, the active efflux rate representing the transporter activity (K_{act}) was found greater in S2. In addition the delay between tumour cells implantation and treatment onset was longer in S2 so that the proportion of drug sensitive cells was lower in S2 at treatment onset (68% in S2 versus 85% in S1 at respective treatment onset). All these results suggest a different tumour biology between both studies mainly due to a different tumour development status at treatment onset.

In both studies, MBLI87 effect was low. One of the reason of this low effect can be attributed to the lower inhibition of active transport for SN38 compared to that of CPT11 ($\frac{C_{moy(MBLI87)}}{K_i\,(MBLI87|CPT11)} = 10^{-2}, \frac{C_{moy(MBLI87)}}{K_i\,(MBLI87|SN38)} = 10^{-3}$). SN38 being around 11 times more

potent than CPT11 in vivo, a better inhibition of its active transport would allow a better effect on the tumour growth. In a general way, ABCG2 inhibition by MBLI87 is too weak to ensure a sufficient effect on the tumour growth ($\frac{Tumour\ Size\ (day\ 40)_{+MBLI87}}{Tumour\ size\ (day\ 40)_{-MBLI87}} = 0.98\ in\ S2$). This can due to the chemical properties of MBLI87 such as its short half-life or its weak inhibitory constant. In the simulation study, MBLI87 properties were artificially modified to find some recommendations to enhance its efficacy. Using the same dosing regimen as in S2, a 1000 times increase of MBLI87 dose was necessary to increase the mean tumour concentration of CPT11 by 1.4 and by 1.1 for SN38. However, effects on the tumour growth were still low ($\frac{Tumour\ Size_{day\ 40,+MBLI87}}{Tumour\ Size_{day\ 40,-MBLI87}} = 1.2$). Better results were achieved by using a continuous infusion with a 100 times increase of MBLI87 dose that leads to a constant inhibition of the transporter. In that case, the increase of CPT11 and SN38 mean tumour concentration was slightly better but still associated to a low effect on the tumour growth (Table 3). These first results indicate that MBLI87 K_i and clearance are too high to ensure a sufficient inhibition of the transporter. As a demonstration, MBLI87 reversal effect was maximized when its K_i value was decreased to obtain a ratio between MBLI87 mean plasma concentration and K_i equal to 100 and when its clearance was 10 times decreased (Figure 3B).

The active efflux rate (K_{act}) is a characteristic of tumour cells. We modified its value to evaluate its impact on the inhibitor efficacy (while decreasing MBLI87 K_i to ensure a sufficient inhibition of the transporter). In that case, MBLI87 was potentiated demonstrating the necessity to choose a cell line where the transporter is enough expressed to prove the benefits of active efflux inhibition. In a previous work, we established that the maximum increase of CPT11 and SN38 intracellular concentration was moderate in HEK293 cells even when ABCG2 was fully inhibited (252). Better results

could thus have been observed with a cell line overexpressing more the transporter. The last axis explored in the simulation study concerns the tumour biology. As already found for S1 and S2, the percentage of drug sensitive cells impacts treatment outcomes. Here the initial tumour volume was changed to get the same initial volume of proliferative, necrotic and hypoxic cells. As expected, treatment efficacy was lower with larger tumour volumes observed at day 40 in that case (Table 3). These results need to be interpreted with caution since they depend on the tumour growth model, different finding could have been obtained with a different model. The last point investigated concerns the diffusion of cytotoxic in the tumour. This system-dependent parameter was found crucial for the drug efficacy. Indeed, the smallest tumour size at day 40 was obtained with increased cytotoxic diffusion. Surprisingly, the scenario maximizing the treatment outcomes was different of the one maximizing MBLI87 effect. If a better inhibition of ABCG2 is necessary by decreasing both MBLI87 Ki and clearance, it appeared also necessary to ensure a good diffusion of cytotoxic in the tumour to minimize the tumour size as already shown by Patel and Tanock (236). This last result raises the question of combining an anti-angiogenic at treatment onset to normalize the tumour vasculature and ensure a better drug diffusion (253).

It is thus not possible to simultaneously maximize the inhibitor reversal effect and minimizes the tumour size. In one case, it is important to use a system where the efflux transporter is well expressed that is necessarily associated to a lower effect on the tumour growth and to ensure a sufficient inhibition of the transporter, whereas it is preferable to focus on the cytotoxic penetration into the tumour to minimize the tumour size

Chapter III

Quantitative evaluation of the interaction between cytotoxic and efflux transporter inhibitors: a tool to support early preclinical drug development

1. Introduction

If mechanistic models are the "gold standard" approach to identify the key drug mechanism, they require a lot of data that are not always available at early stages of preclinical drug development. First studies in animals are relatively poorly designed since their aim is just to demonstrate the relevance of the target. Usually, only one dose level is tested using small number of animals so that their results are difficult to extrapolate. Moreover, usual methods to analyse these so-called Proof-of-Concept (PoC) studies can lead to biased interpretation of the results.

In this chapter, we propose to illustrate the benefits of the NLME approach and quantitative longitudinal modelling to support the early development of the efflux transporter inhibitors – cytotoxic combination.

In this study, a minimal tumour growth inhibition model of the interaction between efflux transporter inhibitor and cytotoxic is presented based on data issued from a preclinical PoC study, in which no PK data were collected. Our aim was to develop a suitable modelling approach to characterize tumour growth inhibition under various treatments, in spite of the lack of PK data. The model was applied to the MBLI87 - CPT11 combination in order to evaluate the reversal effect of MBLI87 on CPT11 BCRP-mediated resistance.

2. Materials and Methods

Twenty mice xenografted with HEK293 cells overexpressing BCRP were randomized into four treatment groups: Control, MBLI87, CPT11 and MBLI87+CPT11. CPT11 was IP administered at $20mg.kg^{-1}$ 3 days per week for 4 consecutive weeks and MBLI87 was IP administered at $2.4mg.kg^{-1}$ 5 days per week for 4 consecutive weeks. Tumour size was repetitively measured throughout the length of the experiment. Four measures per

animals were available (tumour length and width on each flank) and the geometric mean of these four measures relative to the baseline tumour size was used as the dependent variable in the model. No PK data were available.

Three tumour growth models with increasing shape complexity were tested to model the unperturbed tumour growth (exponential, Gompertz, Simeoni). Since no PK data were available, a K-PD approach was used to account for the drug kinetics in the biophase.

In the case of single drug administration, i.e. CPT11 and MBLI87 groups, the drug effect was assumed to be directly proportional to the accumulated amount of drug accumulated in the K-PD compartment.

The interaction between CPT11 and MBLI87 was considered at the tumour growth level. In the interaction model, it was assumed that the efflux transporter inhibitor was not cytotoxic and only increased CPT11 cytotoxicity relatively to the accumulated amount of inhibitor in the K-PD compartment. MBLI87 was thus excluded from the interaction model. However, this parameter was still estimated for animals receiving MBLI87 alone to check the assumption made in the interaction model.

Model parameters have been estimated by NLME approach using the NONMEM software version 7.1.2. To maximize the advantages of the NLME approach, all the treatment groups are simultaneously analysed. Drug potencies were estimated for each drug and the interaction parameter for the co-administration group. Individual tumour growth rates were assumed to arise from a single distribution.

3. Results

Among the three tumour growth models tested, the most appropriate one was the Simeoni's model that assumes two growth phases (exponential followed by linear, see 5.2). Model evaluation did not reveal any misspecifications and all the parameters were

estimated with an adequate precision. The model thus correctly described and predicted the tumour growth dynamics in all the treatment groups.

Elimination half-life from the biophase was estimated at 8.5h and at 491d for CPT11 and MBLI87 repsectively. The latter value indicates that the MBLI87-induced inhibition is nearly constant during the time of the experiment. MBLI87 cytotoxic potency was estimated at $1.4.10^{-6}\mu mol^{-1}.d^{-1}$, a value 3500 times lower than that of CPT11 confirming its lack of-cytotoxicity. The PD interaction parameter was estimated at $10^{-2}\mu mol^{-2}.d$.

4. Discussion

A Kinetic-Pharmacodynamic tumour growth inhibition model that includes a pharmacodynamic drug-drug interaction was presented in this study. The model was applied to the CPT11-MBLI87 combination and was able to correctly describe and predict the effects of the drug combination on the tumour growth.

Contrary to the models presented in Part 2, this model includes several simplifications while retaining enough complexity to simultaneously quantify the tumour growth and the effect of a new drug combination.

The major assumption includes in the model is the absence of cytotoxicity of the efflux inhibitor. The analysis of the tumour growth in animals treated by MBLI87 alone give substantiation to this assumption since MBLI87 potency was found to be 3500 times lower than that of CPT11. This drug only act by increasing CPT11 potency, which is consistent with its mechanism of action as demonstrated in Part 2. MBLI87 was found to increase CPT11 potency of $0.01\mu mol^{-1}$ per µmol of MBLI87, so its effect is potentially strong.

Another simplification in the model concerns the linear interaction between compounds, the model is thus unable to predict the expected saturation of MBLI87 effect at high doses.

Drug effect was modelled using a direct model (see 4.2.5.1) so that the delay between drug administration and observed effects usually reported for anticancer drugs was not accounted for here.

Because of the absence of PK data, a K-PD approach was used to model the kinetics of the effect. Even if the K-PD approach shows large benefits to analyse this type of study by reducing the study costs and length, it also shows some limitations. As an example, CPT11 PK in mice is known to be non-linear with a saturable elimination (Chatelut), that cannot be accounted for with the K-PD model. The linearity assumption included in the K-PD model also reduces the extrapolation properties of the model because the assumption is violated for higher doses.

Traditionally, animals PoC studies are analysed using simple statistical tests that compare the outcome in the treatment and control groups. These tests can lead to biased results is the study is unbalanced because the power to detect a drug effect is decreased. Moreover, to account for all the tumour growth, it is necessary to include some corrections of the tests significance to account for the multiple testing and for the correlation between two successive tumour size measurements. The approach developed here circumvents all these issues. The time dependent-nature of the data is accounted for through the longitudinal model allowing the analysis of sparse data and the inter- and intra-individual variability is quantified. Moreover, the NLME approach enables to combine all the information available to fully quantify model parameters in a single step. Finally the model separates both drug and disease specific parameters in order to properly quantify the drug effects as suggested previously.

This model thus constitutes an alternative to usual analysis methods for PoC studies. Moreover, its equations are drug-independent allowing its use as a template for early evaluation of efflux transporter inhibitors *in vivo*.

Publication 3

Quantitative evaluation of the combination between cytotoxic drug and efflux transporter inhibitors based on a tumour growth inhibition model

Alexandre SOSTELLY, Léa PAYEN, Jérôme GUITTON, Attilio DI PIETRO, Pierre FALSON, Mylène HONORAT, Annabelle GEZE, Ahcène BOUMENDJEL, Gilles FREYER, Michel TOD

Acceptable for publication in Fundamental and Clinical Pharmacology

Introduction

Several multidrug efflux pumps that belong to the ATP Binding Cassette (ABC) are known to play a crucial role in drug absorption, distribution and elimination. Under normal conditions, one primary function of these pumps is to protect healthy tissues against xenobiotics by decreasing the intracellular retention of endogenous and exogenous molecules and by altering the cellular response to drugs. Tumour cells that overexpress these pumps act in the same way and thus exhibit a resistance to anticancer agents.

In the last few years, efforts have been mainly focused on reversing the activity of ABCB1, or P-glycoprotein (P-gp) (224-226). P-gp inhibition has essentially failed either because the transporter was not as prevalent as expected or because P-gp inhibition was insufficient. Clinical and preclinical studies are rarely addressed the inhibition of others ABC transporters to overcome drug resistance (254).

The present work focused on one of the latest ABC efflux transporter discovered ABCG2, so called Breast Cancer Resistance, BCRP. This transporter plays a tumour-protective role against several anticancer drugs including mitoxantrone, irinotecan and SN38, the active metabolite of irinotecan (111, 113, 227). Moreover, its substrate profile partially overlaps that of P-gp. Development of ABCG2 inhibitors may thus improve the efficiency of cytotoxic drugs on tumour overexpressing this efflux transporter.

Various ABCG2 inhibitors were already described in the literature, including imatinib and gefitinib (125, 255). These drugs are efficient tyrosine kinase inhibitors but not ABCG2 specific. Inhibition of ABCG2 with these drugs would require very high doses associated to intolerable toxicities which preclude their clinical use for this purpose (256). Recently, new ABCG2 inhibitors that are non-toxic and transporter specific have been synthetized (136). One acridone derivative, MBLI87, has shown favourable properties against

mitoxantrone-ABCG2 mediated efflux in-vitro. A proof-of-concept (PoC) study has also been successfully carried out in-vivo and MBLI87 is undergoing further preclinical development (137).

The objective of preclinical drug development is to investigate drug efficiency and safety as earlier as possible. When development is based on trial-and-error approaches, it is quite inefficient, costly and results in high attrition rates (212, 213). Model-based drug development has been advocated to overcome previous issues but, surprisingly, there is still a paucity of studies using models for preclinical drug evaluation (191, 193, 194, 257). Moreover, information derived from preclinical studies can be largely increased with this approach. New hypotheses about the drug mechanism can also be generated (214). We decided to apply this approach to MBLI87 preclinical development.

Based on preliminary data from PoC study, we developed a minimal tumour growth inhibition template model of the efflux transporter inhibitors effect on cytotoxic potency. Using this model, we quantified the reverting effect of MBLI87 on irinotecan ABCG2-mediated resistance *in vivo*.

Materials and Methods

Experimental method

Proof-Of-Concept animal study

The Human Embryonic Kidney 293 (HEK293) cell line ABCG2-transfected were cultured as described in (137). Cells were maintained in Dulbecco's modified Eagle's medium (DMEM high glucose), supplemented with 10% foetal bovine serum (FBS), 1% penicillin/streptomycin, and 1mg.mL^{-1} G418.

8-week old Severe Combined Immuno-Deficient (SCID) female mice (Charles River laboratories) were subcutaneously inoculated with these ABCG2-overexpressing cells (8.6.10^{6} cells in 100µL PBS/inoculation). Each mouse was implanted on the right and left flanks with the same tumour cell type.

Time 0 was the time of cell inoculation. Twenty mice were randomized the day after cell implantation into 4 treatment groups (control N=5, irinotecan N=5, MBLI87 N=5, irinotecan+MBLI87 N=5).

All the procedures were approved by the Animal Facility veterinarian board.

Drug treatment

Irinotecan was provided by MAP-France company. It was injected intra-peritoneally (IP) at 20 mg.kg^{-1} 3 days per week. MBLI87, which was not soluble in either water or saline vehicle, was formulated in enzymatically modified-cyclodextrin-based colloidal suspension obtained by solvent displacement method as described in (137). MBLI87-loaded nanoparticles size, estimated by quasi-elastic light scattering, was around 185-195nm. The final suspension loaded at 0.16mg.mL^{-1} of MBLI87 was IP administered at 2.4mg.kg^{-1} 5 days per week. The treatment began 7 days after cells implantation and was pursued during 4 weeks.

In-vivo tumour growth experiments

Mice were clinically evaluated daily. Tumour dimensions (length, width) were measured with a caliper 3 times per week starting on day 5. Mice were sacrificed when the tumour volume exceeded 1800 mm^3.

Four measurements per mouse (tumour length and width on each flank) were available at each observation time point. The geometric mean of the 4 measures, normalized to baseline tumour size, was the dependent variable of the regression model.

Model development

Non-Linear mixed-effects modelling

The data was analysed using Non-Linear Mixed Effects (NLME) approach which enables simultaneous estimation of fixed and random effects in the model. Fixed effects refer to the typical value (mean) of a parameter (P) in the population. Random effects are estimated on two levels: variability between individuals (Inter-Individual Variability, IIV), and variability within an individual (Residual Variability, RV). Each observation of an individual can be described as follows (228):

$$y_{ij} = f(X_{ij}, P_i) + g(X_{ij}, P_i) \times \varepsilon_{ij} \qquad \text{(Equation 1)}$$

Where y_{ij} is the j^{th} observation for the i^{th} individual, f(…) is the individual prediction described by X_{ij} the individual variables and P_i the individual parameter, $g(X_{ij}, P_i) \times \varepsilon_{ij}$ is the residual error that describes the difference between the individual model prediction and the corresponding observed value. The residual error is supposed to be independently and identically normally distributed with 0 mean and σ^2 variance. In the following, we will consider a proportional error model, $g(X_{ij}, P_i) = f(X_{ij}, P_i)$.

The individual parameter, P_i, is expressed as a function of the typical value for the population (θ) and the deviation from this typical value:

$$P_i = \theta \times e^{\eta_i} \quad \text{(Equation 2)}$$

η_i is a random value that describes the difference between the population and the individual i. η_i values are assumed to be independently and identically normally distributed with 0 mean and ω^2 variance.

Unperturbed tumour growth modelling

To describe the tumour growth in animals in the absence of drug effect, we tested three different tumour growth models (exponential, Gompertz and Simeoni unperturbed (191)) of increasing shape complexity:

- Exponential model

$$\frac{d\phi_i(t)}{dt} = \lambda_i \times \phi_i(t) \quad \text{(Equation 3)}$$

- Gompertz model

$$\frac{d\phi_i(t)}{dt} = \lambda_i \times \phi_i(t) \times \left(1 - \left(\frac{\phi_i(t)}{K_{lim_i}}\right)\right) \quad \text{(Equation 4)}$$

- Simeoni unperturbed model

$$\frac{d\phi_i(t)}{dt} = \frac{\lambda_{0,i} \times \phi_i(t)}{\left(1 + \left(\frac{\lambda_{0,i}}{\lambda_{1,i}} \times \phi_i(t)\right)^{\psi}\right)^{\frac{1}{\psi}}} \quad \text{(Equation 5)}$$

Where the subscript i designate the i^{th} individual, $\Phi_i(t)$ is the mean tumour diameter at time t relative to baseline ($\Phi_i(t=0)=1$), λ_i is the tumour growth rate, $K_{lim,i}$ is the maximum tumour capacity, $\lambda_{0,i}$ and $\lambda_{1,i}$ are the exponential and linear growth rate and ψ is the switching parameter allowing the transition between both growth phases.

The number of parameters estimated in each of these models was the following: one (λ_P) for the exponential model, two (λ_i, K_{lim}) for the Gompertz model and two (λ_0, λ_1) for the Simeoni's unperturbed model, ψ being fixed to a high value allowing the rapid switch between both growth phases.

Drug action modelling

No pharmacokinetic (49) information was available in this study. It was thus impossible to build a usual PK-PD model. To overcome this difficulty, we used a Kinetic-Pharmacodynamic (K-PD) approach (173). This approach assumed drug accumulation in one virtual compartment and mono-exponential elimination from this compartment. The PK model is thus reduced to its simplest form: bolus doses are directly input into the compartment and only a pseudo-elimination rate constant is estimated (Equation 6).

$$\frac{dA_{X,i}(t)}{dt} = -K_{X,i} \times A_{X,i}(t) \qquad \text{(Equation 6)}$$

Where $K_{X,i}$ is the pseudo-elimination constant for drug X and in the i^{th} individual, $A_{X,i}(t)$ is the drug amount for drug X at time t. The product $K_{X,i}$ by $A_{X,i}(t)$ is the dose rate.

In the case of single drug treatment, drug effect was assumed to be directly proportional to the drug amount in an individual at time t, the rate of tumour shrinkage due to the drug action was described as follows:

$$\text{Drug action} = P_X \times A_{X,i}(t) \qquad \text{(Equation 7)}$$

$$\text{With } P_X = \frac{E_{max_X}}{ED_{50_X}}$$

Where P_X is the potency of drug X in $\mu mol^{-1}.d^{-1}$ that is the ratio between maximal drug X effect ($E_{max,X}$) divided by the amount of drug amount resulting in half the maximal effect ($ED_{50,X}$); $A_{X,i}(t)$ is the drug amount of drug X at time t.

For those groups, Equation 7 is directly subtracted from tumour growth equation (Equation 3-5).

The interaction between drugs was considered at the level of tumour growth. We assumed that efflux transporter inhibitor was not cytotoxic and increased directly irinotecan cytotoxicity as described in Equation 8.

$$P_X = P_{cytotoxic} + \beta_{cytotoxic|inhibitor} \times A_{inhibitor,i}(t) \qquad \text{(Equation 8)}$$

Where $P_{cytotoxic}$ is the cytotoxic potency of irinotecan, $\beta_{cytotoxic|inhibitor}$ is the pharmacodynamic interaction parameter between irinotecan and MBLI87, and $A_{inhibitor,i}(t)$ is the amount of MBLI87 in individual i at time t. According to Equation 8, strength of the interaction increased with $\beta_{cytotoxic|inhibitor}$ and also with amount of inhibitors.

MBLI87 potency was not included in the interaction model. However, this parameter was still estimated for animals receiving MBLI87 alone in order to check the non-cytotoxicity assumption of this compound.

All treatment groups were analysed simultaneously. Drug potencies were estimated for each drug and interaction parameter for irinotecan and MBLI87 combination. Individual tumour growth rates were assumed to arise from a single distribution.

Parameter estimation and model diagnosis

Parameters estimation was performed with NONMEM software, version 7.1.2 (229). NONMEM uses a parametric maximum likelihood method: the probability of the data under the model is maximized by minimizing the extended least squares objective function.

Selection between tumour growth models was based on the likelihood ratio test and Akaike Information Criteria (173) as well as on goodness-of-fits plots and simulation-based diagnostics.

To evaluate the model fit, we used classical goodness-of-fits plots, based on the model predictions and observations, and simulation-based diagnostics. The latter could reveal model misspecifications that were not easily diagnosed with classical goodness-of-fit plots and allowed to test the model's predictive performances. Two of these methods were used here: the Normalized Prediction Distribution Errors (NPDE) and the Visual Predictive Check (VPC).

NPDEs should follow a standard normal distribution (230, 251). The model was considered as invalid when NPDEs are not normally distributed with a 0 mean and 1 variance.

The VPC consists of simulating tumour growth profiles of each treatment groups based on model structure and parameter estimates (167). We simulated 1000 replications of the experimental data set. The 90% non-parametric confidence interval (CI) of the simulated medians was computed and then compared to the observed medians. The model was considered as invalid when the CI did not bracket the observed medians.

The model evaluation was performed with the R-based XPOSE4 program (231) and the PsN toolkit for the VPC calculations (232).

Results

The geometric mean of tumour diameters correlated best with tumour volumes and was thus chosen as the dependent variable.

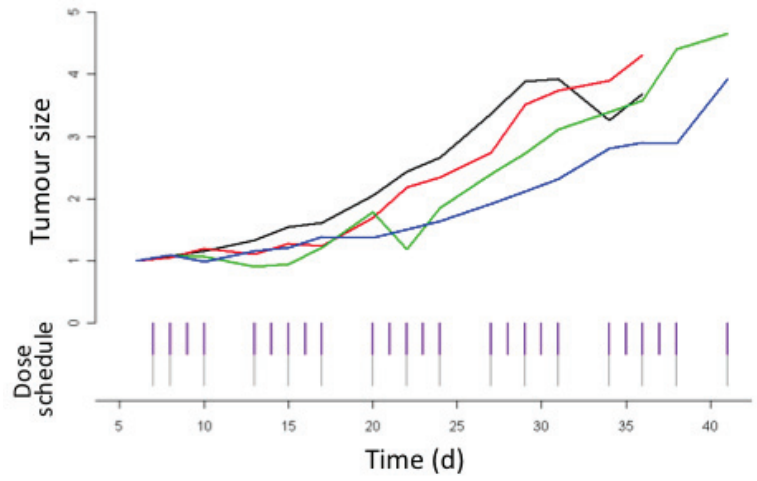

Figure 1: Data representation
Median tumour size is represented for each treatment groups (black: control group; red: MBLI87 group; green: irinotecan group; blue: irinotecan+MBLI87 group). Dose schedule is also represented in segment (purple: MBLI87 dose schedule; grey: irinotecan dose schedule).

Among the three tumour growth models, the most appropriate was the Simeoni's unperturbed model. The Gompertz model failed to converge and the exponential model resulted in an increase of 85 points in the AIC value (Table 1, Figure 2).

	Exponential model	Gompertz model	Simeoni model
AIC	-193.6	Failed to converge	-278.6
Goodness-of-Fit plots	Does not capture the biphasic tumour growth		Capture the biphasic tumour growth
NPDE	Does not follow a normal reduced distribution		Follows a normal reduced distribution
VPC	Simulations are not in agreement with the tendency observed in data		Simulations are in agreement with the observed tendency in data

Table 1: Model selection procedure

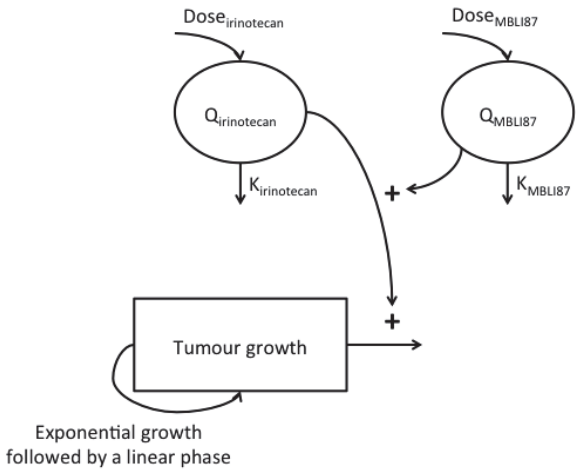

Figure 2**:** Model Structure
Schematic representation of the model structure

Basic diagnostic plots of the model revealed no model misspecification. The model predictions (PRED, IPRED) were able to capture the observed tumour growth distributions (DV) (Figure 3).

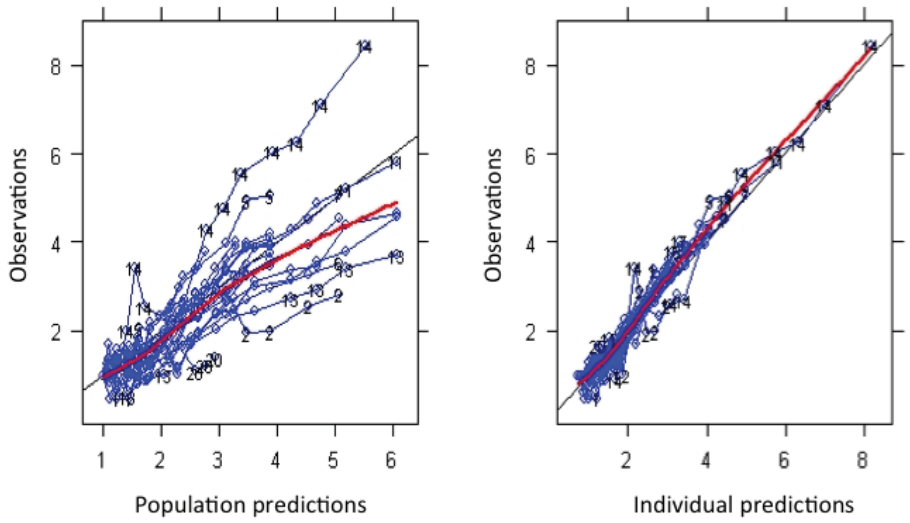

Figure 3: Basic goodness of fit plots
Basic goodness of fit plots compares the population predictions (left) and individual predictions (right) to the observations. The red line indicates the trend in the distributions and the black line is the identity line.

The NPDEs were normally distributed with 0 mean and 1 variance without a trend (Figure 4 and 5).

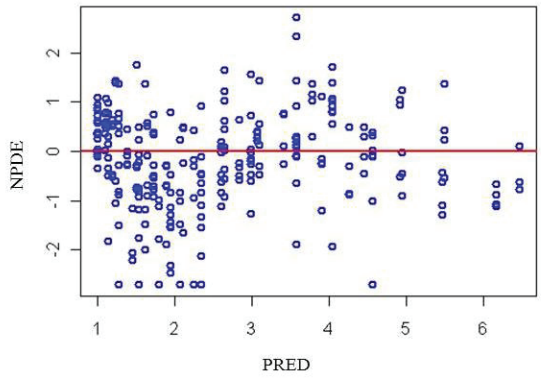

Figure 4: Normalized Prediction Distribution Error (NPDE) over population predictions
The normalized prediction distribution error (NPDE) versus population model predictions (PRED) is shown. NPDEs follow a normal centred reduced distribution (heavy line represents the 0 mean).

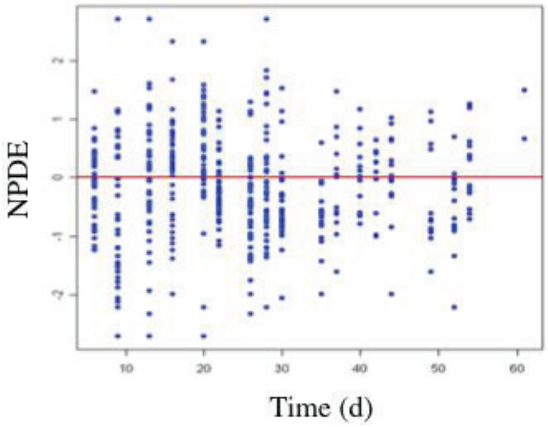

Figure 5: Normalized Prediction Distribution Error (NPDE) over time
The normalized prediction distribution error (NPDE) versus population model predictions (PRED) is shown. NPDEs follow a normal centred reduced distribution (heavy line represents the 0 mean).

The VPC results showed the predictive abilities of the model (Figure 6). The observed tumour growth medians for each treatment group were enclosed within the 90% CI of the simulated medians as required for model validation. The model structure was thus able to adequately describe the data and had adequate predictive performances.

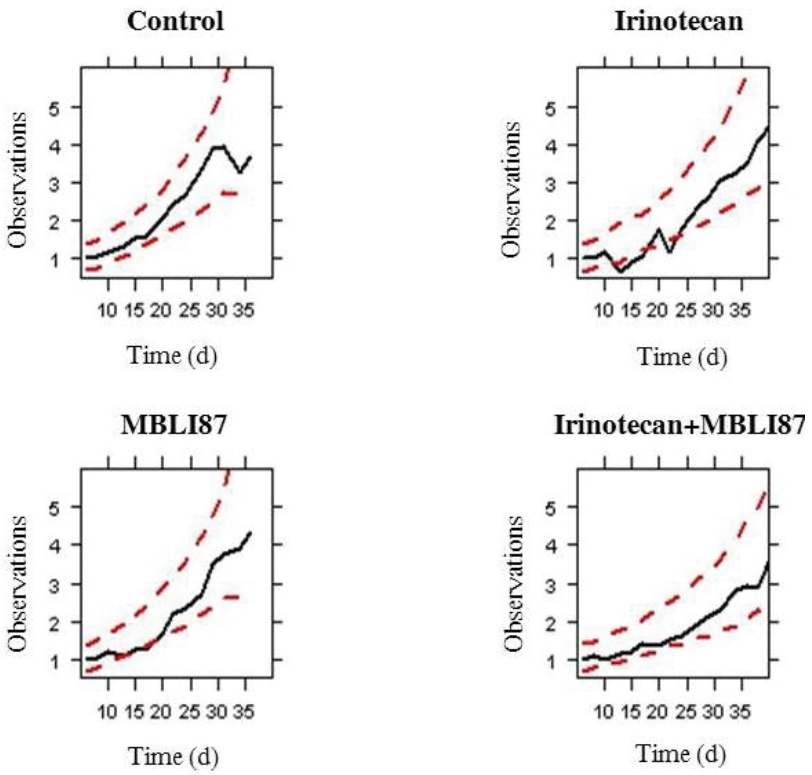

Figure 6: Visual Predictive Check (VPC)
Visual Predictive Check (VPC) plot compare the observed median tumour size (mm, heavy lines) over time (d) to the 90% non-parametric confidence interval of the median (dashed lines) obtained after simulations. Observed median and 90% non-parametric confidence interval are shown in each treatment group.

Parameter estimates are presented in Table 1. Inter-Individual Variability (IIV) was estimated on four parameters: $K_{irinotecan}$, λ_0, λ_1 and baseline. Inter-Individual Variability was estimated with a shrinkage not greater than 30% and residual variability with a 4% shrinkage.

The exponential growth rate (λ_0) was estimated at $0.06d^{-1}$ and the linear growth rate (λ_1) at $0.069d^{-1}$ with an IIV at 49% corresponding to an exponential tumour doubling time estimated at 11.5d. Pseudo-elimination constants (K) were estimated at $1.9d^{-1}$ with an IIV coefficient of variation at 25% for CPT11 and $0.00141d^{-1}$ with IIV coefficient of variation at 31% for MBLI87 that correspond to elimination half-life from the biophase at 8.5h and 491d for CPT11 and MBLI87 respectively. The latter value indicates that in our conditions, the MBLI87-induced inhibition was nearly constant during the course of the

study.MBLI87 potency was estimated at $1.4.10^{-6}$µmol^{-1}.d^{-1}, a value 3500 times lower than irinotecan potency. It confirmed the assumption of absence of MBLI87 cytotoxicity made in the pharmacodynamic interaction model. This result was in accordance with the absence of measurable difference in tumour growth between control and MBLI87 groups. Absence of difference was assessed in simultaneously fitting both groups to the unperturbed tumour growth model to test the group effect; the increase of λ_0 and λ_1 under MBLI87 treatment compared to control was 0.1% and 0.001% respectively. The interaction parameter, β, was estimated at 10^{-2} µmol^{-2}.d^{-1}.

Precision in parameter estimates, expressed as 95% confidence interval, was obtained after 50 bootstraps. All the model parameters were estimated with an adequate precision.

Parameters	Typical Value [95% confidence interval]	IIV (%CV)
$K_{irinotecan}$ (d^{-1})	1.98 [1.55; 2.41]	25.2
K_{MBLI87} (d^{-1})	$1.41.10^{-3}$ [$1.55.10^{-4}$; $2.66.10^{-3}$]	-
λ_0 (d^{-1})	$6.06.10^{-2}$ [$3.57.10^{-2}$; $8.55.10^{-2}$]	0.3
λ_1 (d^{-1})	$6.87.10^{-2}$ [$5.98.10^{-2}$; $7.56.10^{-2}$]	48.3
$P_{irinotecan}$ (µmol^{-1}.d^{-1})	$4.95.10^{-2}$ [$1.67.10^{-2}$; $8.21.10^{-2}$]	-
P_{MBLI87} (µmol^{-1}.d^{-1})	$1.41.10^{-6}$ [1.10^{-8}; $2.4.10^{-6}$]	-
$\beta_{irinotecan\|MBLI87}$ (µmol^{-2}.d^{-1})	1.10^{-2} [$1.26.10^{-3}$; $1.87.10^{-2}$]	-
Baseline of tumour size	1*	-
Variance of residual error	0.235	-

Table 1: Model parameters estimates
*: Fixed value

Discussion

This study presented the construction of a Kinetic-Pharmacodynamic Tumour Growth Inhibition model including a pharmacodynamic drug-drug interaction. The model describes and predicts the effects of a new ABCG2 inhibitor, MBLI87, co-administered with irinotecan on tumour growth in xenografted animals.

Proof-of-Concept studies are designed to give preliminary evidences of treatment efficacy and thus contain minimum information. Classical methods to analyze such studies are usually based on simple statistical tests that compare the outcome in control and treatment arms. Despite their attractive simplicity, these tests can lead to biased results if study design is unbalanced, as it is the case here, since the power to detect drug effect decreases.

Moreover, to account for all the tumour growth, it is necessary to include some correction of the tests significance to account for the multiple testing and for the correlation between two successive tumour size measurements. The Non-Linear Mixed Effects (NLME) approach circumvents all these issues. The time-dependent nature of the data and the variability between and within individuals are accounted for, allowing the analysis of sparse data. The whole tumour growth dynamics is described that allows to properly estimating the drug effect. Moreover, since the different sources of variability are taken into account, the drug effect is estimated with less bias.

The major assumption in our model was that ABCG2 inhibitor was not cytotoxic. No previous study has demonstrated the absence of MBLI87 cytotoxicity *in vivo*, it was thus necessary to quantify its potency to give substantiation for the assumption made in the interaction model. Analysis of the tumour growth in animals receiving MBLI87 alone

supported this assumption. In this group of treatment, MBLI87 potency was estimated at $1.4.10^{-6}\mu mol^{-1}$, a value 3500 times lower than that of irinotecan.

This drug only acts in modifying irinotecan cytotoxic potency, which is consistent with the mechanism of action of this drug. MBLI87 competes with irinotecan within the transporter leading to an increase of irinotecan intracellular concentration and, enhancing its cytotoxicity. Our pharmacodynamic interaction model describes MBLI87 action on irinotecan potency but does not account for the expected saturation of MBLI87 effect at high doses. A sigmoidal interaction model was also tested but failed to converge, while no model misspecification was found with the linear interaction model.

Interaction between irinotecan and MBLI87 was characterized by a β value of $10^{-2}\mu mol^{-2}.d^{-1}$; i.e. a 0.01 $\mu mol^{-1}.d^{-1}$ increase of irinotecan potency per µmol of MBLI87.

The cytotoxic potency of irinotecan ($P_{irinotecan}$) was estimated at 0.025 μmol^{-1} and the impact of MBLI87 is thus potentially strong. However, this impact depends on the active drug efflux rate, and thus on the cell line used in xenografted tumours.

The cytotoxic effect was described using a direct effect model assuming an absence of delay between cytotoxic administration and effects on the tumour growth. Usually, cytotoxic effects are described with indirect effect models to account for this delay, which depends on both the tumour type and the drug at hand. However, our data did not support the estimation of such a model.

Previous studies showed that irinotecan triggers the up-regulation of the efflux transporter leading to a possible decrease of irinotecan effect with time (12). It could have been interesting to incorporate such a phenomenon in the model structure. However, since the model relies on a small number of animals (5 per group), the data cannot support the estimation of one more parameter with reasonable precision.

Tumour growth in our data followed two phases; Simeoni's unperturbed tumour growth model was thus the most appropriate. Due to the absence of observable plateau, the maximal tumour capacity (K_{lim}) cannot be estimated, explaining why the Gompertz-like model failed to converge. The exponential model was not able to capture both growth phases and thus resulted in an increase of the AIC value. Simeoni's unperturbed model was thus the most appropriate model, with minimal complexity.

Due to the absence of drug concentration measurement, a K-PD approach was used: the drug kinetics was governed by a rate constant whose estimation was derived from observations of tumour growth dynamics. Using K-PD approach to analyze such studies reduce costs and length of study since no independent PK study has to be performed. The K-PD approach is a compromise between the classical "intent-to-treat" analysis where the PK in not accounted for and the full "pharmacokinetic" approach where individual PK profiles are assessed. The pseudo-elimination (K) cannot be interpreted as a pure pharmacokinetic parameter derived from real concentration measurements. This parameter has to be interpreted as the rate constant that governed the kinetics of active drugs in the biophase (i.e, the effect site) (174). The possible impact of MBLI87 formulation was thus accounted for since the pseudo-elimination constant describes the elimination of MBLI87-loaded nanoparticles from the biophase.

This rate constant can be transformed into an half-life ($t_{1/2}=\ln(2)/K$). For irinotecan, its half-life in the biophase was estimated at 8.4 hours, a value longer than its half-life observed in mouse plasma (0.8-1.1 hour). However, irinotecan pharmacokinetic in mice is non-linear with a saturable elimination (11), this feature cannot be represented with the K-PD approach and can limit the extrapolation of our results with various dosing regimens. Assumptions of linearity included in both K-PD and interaction models thus reduce the extrapolation properties of the model since these assumptions would be

violated for high doses of irinotecan or MBLI87. However, the model can be used to simulate the effects associated with lower doses or with different dosing schedules assuming the same total dose amount. Figure 7 shows that if irinotecan and MBLI87 doses are equally distributed within the cycle, there is a trend for an increased drug effect. Moreover, in the context of early preclinical development, this model can be used to choose the most potent inhibitor based only on a single tumour growth study.

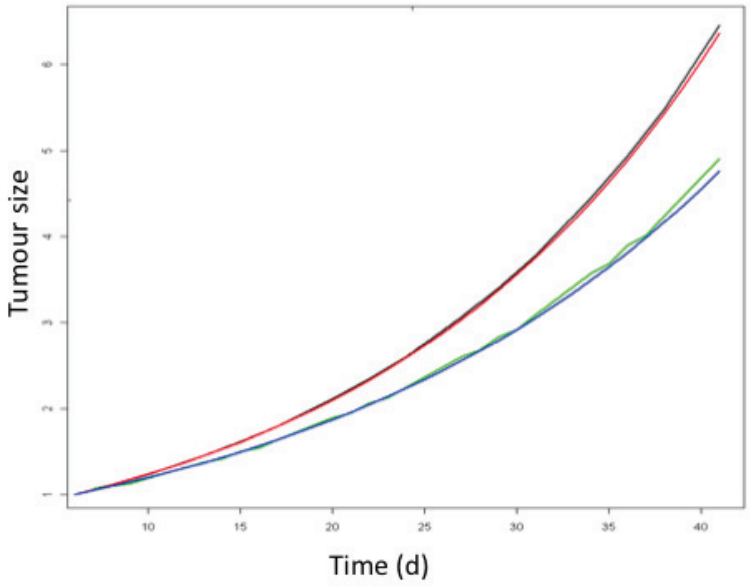

Figure 7: Tumour growth simulation under equally distributed irinotecan and MBLI87 dose schedule obtained after 1000 simulations from the model.
Tumour growth simulations are presented for current and modified dose schedule, e.g. doses equally distributed throughout the treatment period (0.31µmol of irinotecan and 0.0807µmol of MBLI87 given every day).
Black line represents the median tumour growth profile under current irinotecan dose schedule; red line represents the median tumour growth profile under irinotecan updated dose schedule, green line represents the median tumour growth profile under irinotecan+MBLI87 current dose schedule and blue line represents the median tumour growth profile under irinotecan+MBLI87 updated dose schedule.

This model includes several assumptions and simplification while retaining enough complexity to quantify simultaneously tumour growth and action of an efflux transporter inhibitor combined to cytotoxic. Moreover, NLME approach enables to combine all the available information in a single step. Model equations are drug-independent, allowing their use as a template for early evaluation of efflux transporter inhibitors in-vivo. In a

drug development context, it is also possible to reduce experimental effort based on experimental design optimisation derived from this model.

Chapter IV

Benefits of tumour growth inhibition models to optimize anticancer drugs regimens

1. Introduction

The two previous parts dealt with the benefits of the NLME approach and tumour growth models to evaluate oncology drugs during preclinical development. In patients, the model-based approach is much more established but it remains some challenges to meet. As mentioned in the first chapter, one critical point concerns the design and evaluation of phase 2 studies. These studies are usually evaluated using Objective Response Rates (ORRs) that omit the whole tumour growth dynamics. ORRs are unable to establish the link between patients' response and their survival, the ultimate clinical endpoint in oncology.

However, the change in tumour size has been characterized as a predictor of patients' overall survival (198, 258). Moreover, the relationship between tumour response and patients' overall survival has already been characterized and the benefits of the tumour size modelling have thus been already demonstrated.

Although the use of these tumour growth inhibition models is well established to evaluate oncology drugs, there is still a lack of attempts to design oncology trials based on tumour growth inhibition models.

This is the purpose of this chapter, to optimize dose schedule of an oncology phase 2 trial based on TGI model to maximize the patients' response. In addition, the effects of both the dose-effect relationship and the tumour resistance on the optimization outputs were investigated.

2. Methods

The context of f this study was a theoretical phase 2 study of the oral prodrug of 5-FU, capecitabine (see 1.3.5.). Capecitabine was subject to intensive modelling during its development. One of the models developed establishes the link between modelled tumour response and patients' overall survival (170). Claret's model accounts for both the natural disease progression and the drug effects and shows adequate predictive performances as well as flexibility so that it fits the purposes for this optimal design problem.

The same study design as the ones used in capecitabine phase 2 study were used here. A user-defined penalty function was implemented to optimize both dose and dose schedule on the individual tumour growth. The different optimal criteria consist all in maximizing the change in tumour size from baseline. To account for the natural variability existing between patients, the criterion was computed using individual parameter values sampled from their distribution and the mean of the individualcriteria was maximized to obtain the optimal design. Optimizations were performed within a set of clinical constraints to obtain the most clinically relevant dose schedule and to limit the risk of toxicity.

Then the impact of both dose-effect relationship and tumour resistance development rate was investigated on the optimization outputs. The impact of the dose-effect relationship was assessed by modifying the drug exposure function in the model. Both E_{max} and linear dose-effect relationship were investigated. The impact of the tumour resistance development rate was assessed by modifying the value of the resistance parameter in the TGI model. Optimal dose schedules were compared using the mean dose time (MDT) that reflects the dose intensity within the cycle.

3. Results

The optimal criterion selected was the following:

$$X_{optimal} = Argmax_{\vec{x}} \left[E_{\vec{\eta}} \left(\frac{1}{N} . \left[\sum_{i=1}^{i=N} \left[\frac{y_i(\vec{\theta},\vec{\eta}_i,\vec{x})_{\vec{\varepsilon_i}=0,t_i}}{y_i(\vec{\theta},\vec{\eta}_i,\vec{x})_{\vec{\varepsilon_i}=0,t_i=0}} \right] \right] \right) \right] \quad \text{(Equation 20)}$$

Where i refers to the i^{th} individual parameter values in the population including N individual values, y_i refers to the tumour size ($y_i(t_i=0)$=71mm) $\vec{x}$ refers to the vector of design parameters, $\vec{\theta}$ refers to the vector of parameters typical values, $\vec{\eta}$ refers to the vector of parameters inter-individual variability and $\vec{\varepsilon}$ refers to the vector of the residual variability.

The criterion shows good stability when computed with 500 Latin Hypercube Samples samples taken in the parameter distribution. Since the survival model from Claret *et al.* identified the tumour size at week 6 as a predictor of the overall survival, the optimal criterion was computed using the modelled tumour size at this time point and the modelled tumour size at baseline.

In case of a linear dose-effect relationship, the optimal dose schedule frontloads all the doses in the first week of the cycle independently of the value of the tumour resistance development rate. When the tumour resistance increase, the optimal criterion value decreased attesting the decrease of the drug effect. The situation is more complex in case of E_{max} type dose-effect relationship; the optimal dose schedule depends on both the ED_{50} and tumour resistance development rate values. For high values of ED50, the optimal dose schedule equally distributes the doses in the cycle for medium and low values of tumour resistance development rate. For low ED_{50} values, the optimal dose schedule frontloads doses within the first week of the cycle for any degrees of tumour resistance development rate.

In all the cases, the optimal dose schedule performs better than the current dose schedule in terms of tumour response.

4. Discussion

This study aimed at developing a population OD methodology to optimize tumour response and by extension anticancer drug efficacy. In that purpose, a clinically relevant optimal design criterion was defined based on the change in tumour size allowing the optimization of anticancer drug dose and dose schedule. The optimal criterion used the modelled tumour size derived from TGI model from Claret *et al.*, which was linked to the changes in tumour size to overall survival in patients treated with capecitabine.

A user-defined clinically relevant optimality criterion was used to ensure the clinical relevance of the optimization outputs, optimizations were conducted within a set of clinical constraints. Moreover, the optimal criterion used the same variables as those used in the survival model of Claret *et al.*, so by extension the design should also maximize patient's overall survival.

All the optimized dose schedules performed better than the current dose schedule indicating that the tumour response could be improved. However, these results have to be nuanced because optimizations do not account for drug toxicity, even if the same boundaries as those used in clinical practice were used.

In the context of oncology phase 2 studies, the choice of the most relevant dose schedule remains a critical point. The use of ORRs has already shown its limits and new approaches are necessary to better design these studies in order to reduce the risk of development failure. This study demonstrated that the use of quantitative TGI models allows the optimization of the expected patients' response. However, this work will require additional features such as the consideration of the drug toxicity to ensure the feasibility of the optimal dose schedule.

Publication 4

Dose and dose schedule optimization of anticancer drugs

Alexandre SOSTELLY, Joakim NYBERG, Mats O. KARLSSON, Andrew C. HOOKER

Submitted

Introduction

The drug development process in oncology suffers from inefficiency with more than 60% of anticancer drugs that reach phase 3 failing (196, 216). This clearly implies that improvement of current methodologies to evaluate oncology compounds can result in substantial benefits.

Typically, in oncology, the decision to move compounds to phase 3 is based on the achievement of a predefined Objective Response Rate (ORR) calculated using the Response Criteria In Solid Tumours (RECIST) criteria. One of the issues in using ORRs to evaluate a phase 2 study are that their estimations are relatively imprecise and they cannot be used to predict the most informative design for phase 3 studies (164, 259). Moreover, RECIST criteria do not account for tumour growth dynamics and are thus unable to evaluate targeted therapies (260).

The use of tumour response to evaluate oncology compounds has been proposed (261, 262). Tumour response has been characterized as a surrogate of patients' survival which is the main endpoint in oncology studies (258). Recently, three publications demonstrated that it was possible to predict patients' survival from tumour response (170, 197, 199). These publications were focused on the development of quantitative tumour growth inhibition models linked to survival models. Results from these publications showed that the tumour growth dynamics models were much more informative than observing ORR and highly predictive of patients' survival. The papers also showed that building quantitative models for tumour size allows for more informative designs in the next phase of drug development. Tumour growth inhibition models establish the relationship between the natural evolution of the disease and the drug effect. In the phase 2 context, they enable a quantitative comparison of different

therapeutic regimens in order to obtain a stronger rational to design the phase 3 study. It is thus reasonable to use these quantitative models not only to evaluate different regimens but also to optimize regimens.

Optimal experimental design theory using non-linear mixed effects models (NLMEM) was first introduced by Mentré *et al.* (263, 264). The primary aim is to maximize the information content of an upcoming experiment. Often, this is accomplished by changing sample times (design parameters) to achieve the highest possible precision in model parameter estimates (measured using the Fisher Information Matrix, FIM) when fitting a model to study data. However, the methodology is not limited to these types of optimizations. Specifically, any design variables of interest can be optimized (trial treatment length, dose and dose schedule for example) (265) and the optimization criterion must not be based on the FIM.

The aim of this work was to illustrate how a population optimal design framework can be used to optimize the dose schedule of anticancer drugs for maximal tumour response. Different dose-effect relationships and different tumour resistance development rates were explored to illustrate how these phenomena impact dose scheduling.

Methods

We used the example of capecitabine (Xeloda®, Hoffman La Roche) applied to a theoretical phase 2 study. Capecitabine is an oral pro-drug of 5-Fluorouracile (5-FU) that is clinically established in the management of metastatic and advanced breast and colorectal cancers (266).

Tumour growth inhibition model

The tumour growth inhibition (TGI) model from Claret *et al.* was used as a basis to develop our optimal design approach (170). This model, built on capecitabine data phase 2 data,

accounts for tumour dynamics, anti-tumour effect and resistance to the drug effect. It describes the tumour size (i.e. the sum of the longest tumour diameters according to the RECIST criteria) as a function of time and drug exposure. The natural tumour growth is described using a first order growth rate. A resistance process has also been introduced to describe the decrease of the drug effect with time. The model is described with the following differential equation:

$$\begin{cases} \frac{dy_i(t_i)}{dt} = K_{L_i} \cdot y_i(t_i) - K_{D_i}(t_i) \cdot y_i(t_i) \cdot Exposure(t_i) \\ y_i(t=0) = y_{0_i} \\ K_D(t_i) = K_{D,0_i} \cdot e^{-\lambda_i \cdot t_i} \end{cases} \quad \text{(Equation 1)}$$

Where subscript i refers to the i^{th} individual, $y_i(t)$ is the tumour size at time t, y_{0_i} is the baseline tumour size, K_{L_i} is the 1^{st} order tumour growth rate, $K_{D_i}(t_i)$ is the drug-constant cell kill rate that decreases exponentially with time from an initial value $K_{D,0_i}$ to account for the progressive development of resistance; λ_i is the tumour resistance development rate; Exposure(t) is the drug exposure at time t. This model incorporates both drug-specific ($K_{D,0}$, λ) and disease-specific parameters (K_L, y_0). Since no pharmacokinetic data was available, the daily dose (dose-response) was driving the drug effect as in Claret *et al.* instead of concentrations (concentration-response). Inter-individual variability (IIV) has been introduced in model parameters (K_L, $K_{D,0}$, λ) and the parameters were assumed to be log-normally distributed. Residual error was described using an additive residual error model.

The relative change in tumour size from baseline after 2 treatment cycles, i.e. change in tumour size from baseline to 7 weeks has been identified as predictor of patients' survival (Equation 3):

$$\frac{y_i(t=0) - y_i(t=7)}{y_i(t=0)} \quad \text{(Equation 3)}$$

Claret *et al.* used both the TGI and a survival model to predict the outcomes of a capecitabine phase 3 study. Simulations confirmed that the modelling framework, TGI and survival models, was able to predict patients' survival in the phase 3 based on phase 2 data. In the present work, optimizations of the dose schedule were performed using this TGI model and parameter estimates derived from the capecitabine phase 2 study (parameter estimates are presented in Table 1).

Parameter	Estimate
Tumour growth rate, K_L ($week^{-1}$)	0.021
Cell kill rate, $K_{D,0}$ ($g^{-1}.week^{-1}$)	0.025
Resistance appearance, λ ($week^{-1}$)	0.053
Inter-Individual Variability	
$\omega^{2,\ KL}$	0.499
$\omega^{2,\ KD,0}$	0.388
$\omega^{2,\ \lambda}$	1.26
Residual error	
σ (mm)	11.83

Table 1: Parameter estimates of Claret *et al.*'s model

"Standard" phase 2 study design

The current regimen of capecitabine consists of $1250 g.m^{-2}$ twice daily for 14 days followed by a 7-day rest period (3-week treatment period). This regimen has been established based on a phase 2 study comparing different dosing regimens and its efficacy in terms of tumour response was confirmed in a phase 3 study (267, 268). In this work, the same design as the one used in the phase 2 study was used with one group of 34 patients. Tumour size was measured at treatment initiation (basal value) and every 6 weeks for a total of 42 weeks. In addition, since capecitabine dose is adjusted to body surface area (BSA) we assumed a normal distribution of BSA with a mean and variance of $1.9 m^2$ and 0.2 respectively in our design calculations.

Optimal design approach

Optimal design methodology is typically based on the minimization of model parameter uncertainty (269). However, in the context of optimizing dose and dose schedule in a phase 2 study, parameter precision if not the main criterion of interest. At this stage of

development, efforts should be made to optimize drug effects and alternatives to FIM-based criteria can be used.

For this reason, a user-defined criterion function was implemented to optimize dose schedule on the individual tumour growth profile. For cytotoxic drugs such as capecitabine, a natural criterion to judge the drug efficacy is tumour shrinkage. All the investigated criteria thus consist of minimizing tumour size at the end of the second cycle to remain related to the survival predictors used in the survival model from Claret *et al.* Minimizing the tumour size can also be viewed as maximizing the change in tumour size from baseline, as defined, for example, in criterion 1 (Equation 4).

$$Criterion_1 = Argmax_{\vec{x}}\left[E_{\vec{\eta}}\left(\frac{1}{N}.\left[\sum_{i=1}^{i=N}\left[\frac{y_i\left(\vec{\theta},\vec{\eta}_i,\vec{x}\right)_{\vec{\varepsilon_i}=0,t_i=0}}{y_i\left(\vec{\theta},\vec{\eta}_i,\vec{x}\right)_{\vec{\varepsilon_i}=0,t_i}}\right]\right]\right)\right] \quad \text{(Equation 4)}$$

Where i refers to the ith individual parameter values in the population including N individual values, $\vec{x}$ refers to the vector of design parameters, $\vec{\theta}$ refers to the vector of parameters typical values, $\vec{\eta}$ refers to the vector of parameters inter-individual variability and $\vec{\varepsilon}$ refers to the vector of the residual variability.

To account for the natural variability in tumour response, this criteria is computed using individual parameter values (η_{P_i}) sampled from individual parameter distributions ($\eta_{X_i} \sim N(0, \omega_{P_i}^2)$), thus the expected value of the sum of the relative change in tumour size is calculated. The ratio of the tumour sizes in criterion 1 can vary from 0 for patients that have infinite tumour size at the end of the second cycle to infinity for patients in which the tumour is completely eradicated. However, the objective is to maximize (Argmax) this criterion by changing the design parameters X and good responders can thus be overly influential in the optimizations, which will cause the design to focus almost entirely on these good responders. We thus defined another criterion (criterion 2, Equation 5).

$$Criterion_2 = Argmax_{\vec{x}}\left[E_{\vec{\eta}}\left(\frac{1}{N}.\left[\sum_{i=1}^{i=N}\left[\frac{y_i\,(\vec{\theta},\vec{\eta}_i,\vec{x})_{\vec{\varepsilon_i}=0,t_i}}{y_i\,(\vec{\theta},\vec{\eta}_i,\vec{x})_{\vec{\varepsilon_i}=0,t_i=0}}\right]\right]\right)\right] \qquad \text{(Equation 5)}$$

The ratio of the tumour sizes included in criterion 2 varies between minus (–) infinity for patients that do not respond to the drug and 0 for a good responder.

For both criteria an expectation calculation was needed and was computed using Monte-Carlo (sampling) based techniques. Latin Hypercube samples (LHS) were used to increase the stability of the calculation and to ensure sampling over the entire multi-dimensional parameter distribution. A stability analysis was performed for both criteria to determine the number of samples needed to accurately compute the expectations; 50 evaluations of both criteria were performed with different numbers of samples (100-1000) from the individual parameter distributions were taken. The mean and the variance of the 50 criteria were then computed to select the most stable criterion.

Clinical constraints

Optimizations of the dose schedule were performed within a set of clinical constraints to obtain the most clinically relevant dose schedules; the cumulative capecitabine dose within a treatment cycle (3 weeks) was fixed to 35g.m^{-2} corresponding to the cumulative dose used in clinical practice (267); daily doses were not allowed to exceed 5g.m^{-2}. To reduce the optimization search space, daily doses ranged between 0 and 5g.m^{-2} with a 0.5g.m^{-2} dose step size.

Capecitabine is orally administered and in order to limit the number of doses; the dose interval was fixed to 1 day for all optimizations. This implies that during one cycle, patients can take at most 21 doses and at least 1 dose. Since patients take medications at home, dose variations during the cycle have to be reduced and doses were constrained to be the same within each week of the cycle. The two cycles were also assumed to have the same design pattern. All these constraints not only allow finding a clinically relevant dose

schedule but also reduce the complexity of the optimal design problem since only 3 discrete doses have to be optimized (the dose to be given each week of a three week cycle of treatment).

Impact of dose-effect relationship

The shape of the dose-effect relation, linear or non-linear, is of interest when optimizing the dose schedule. To evaluate the impact of the dose-effect relationship on dose schedule optimizations the dose-effect relation in the tumour growth inhibition model has been modified. Both linear and non-linear (E_{max}) dose-effect relationships have been evaluated. In case of linear dose-effect relationship, the daily dose was taken as a metric of drug exposure to drive the drug effect according to Equation 6.

$$Exposure(t_i) = Dose(t_i) \cdot BSA_i \qquad \text{(Equation 6)}$$

In case of an E_{max} type dose-effect relationship, the drug exposure parameter was modified according to Equation 7. Fifteen ED_{50} values (0.0125-1000g) reflecting different levels of drug exposure were tested to investigate the impact of the tumour response and dose schedule optimizations.

$$Exposure(t_i) = \frac{K_{D,0_i} \cdot Dose(t_i) \cdot BSA_i}{D_{50_i} + Dose(t_i) \cdot BSA_i} \qquad \text{(Equation 7)}$$

Impact of tumour resistance development rate

Another important parameter in the anticancer therapy outcome is the development of tumour resistance. Tumour resistance can develop in many different ways but always results in a decrease of the drug effect. To evaluate the impact of tumour resistance development rate, the value of the tumour resistance appearance (λ) was modified. Seven degrees of tumour resistance development rates were tested (0.001-100 times the value estimated in Claret *et al.* model). Dose schedule optimizations were performed for both

linear and E_{max} dose-effect relationships and for each value of tumour resistance development rates.

Design comparison

In addition to the optimization criteria (tumour size at week 7), other metrics were employed to compare the "standard" and optimized dose schedules. The mean dose time (MDT) was computed according to Equation 8.

$$MDT = \frac{1}{Total\ Dose}\sum_{j=1}^{j=21} Dose_j \cdot Day_j \qquad \text{(Equation 8)}$$

Where Total Dose refers to the maximal dose tolerated in the cycle ($35 g.m^{-2}$), $Dose_j$ refers to the j^{th} dose on the cycle and Day_j refers to the j^{th} day of the cycle. MDT reflects the timing of doses in the treatment cycle. For instance, if the optimal schedule gives all the doses within the 1^{st} week of the cycle, the MDT value will be low and if the optimal dose schedule gives all the doses during the last week of the cycle, the MDT value will be high. Dose schedules were also compared by plotting the typical tumour response over time given various dose schedules. Finally, schedules were compared by calculating the typical area under the tumour growth curve given the different dose schedules.

Algorithms settings

The tumour growth model was implemented in Matlab version R2009b and all the optimizations were performed in the optimal experimental design software PopED version 2.11, implementing the optimization criterion using the "user defined criterion" functionality (270-272). Discrete optimizations of doses were performed using the Random Search algorithms with 2000 iterations (RS) followed by Line Search (LS) algorithm. For more details regarding the description of the optimization algorithms, please refer to (272).

Results

Stability of the criterion

Stability analyses of both optimality criteria were performed to identify the most stable one. As shown in Figure 1, criterion 1 (Equation 4) shows an unstable mean and variance compared to criterion 2 (Equation 5). Criterion 2, on the other hand, becomes more stable when the number of samples increases. 500 samples appear to be good compromise between computational costs and criterion stability, therefore, criterion 2 computed using 500 LHS samples was selected as the optimal criterion for use in the rest of the following work.Sa

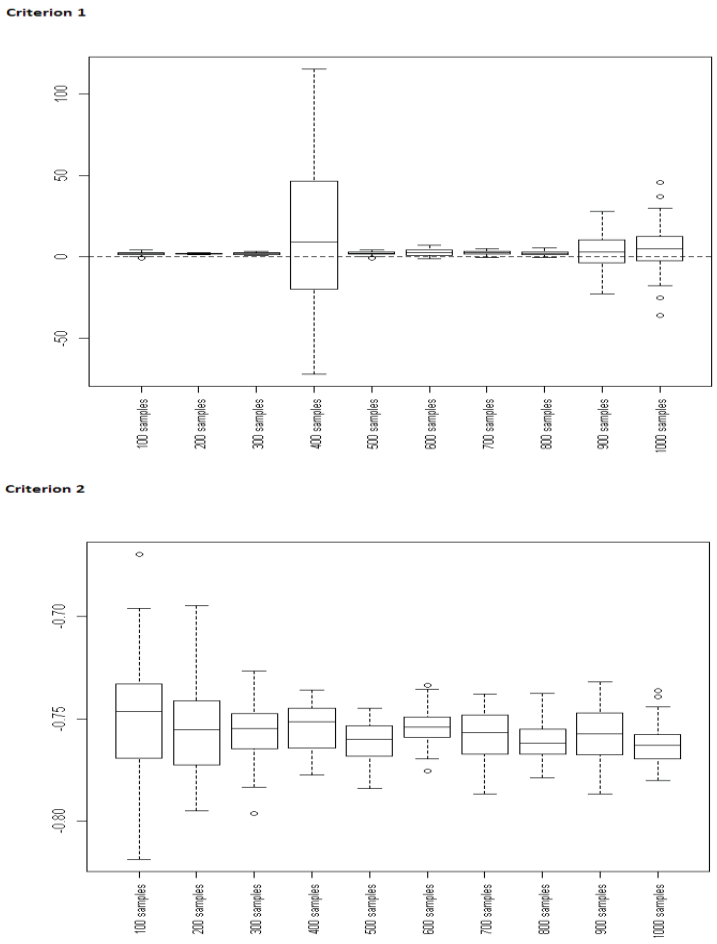

Figure 1: Stability of the optimal criteria

Linear dose-effect relationship

In case of linear dose-effect relationship, the optimal schedule frontloads doses within the 1st week of the treatment cycle (Table 2). The MDT associated with all designs is equal to 4d, implying that to maximize the tumour response; patients have to take $5g.m^{-2}$ of capecitabine for 7 days followed by a 14-day rest period. The value of the optimality criterion (OC) decreases when the tumour resistance development rate increases (OC = -0.685 with $\lambda = 0.00053w^{-1}$ and OC = -1.06 with $\lambda = 5.3w^{-1}$). The drug effect thus decreases when the tumour resistance appears more rapidly. However, the same optimal dose schedule is found for all the tumour resistance development rates. Figure 2 shows the typical values of the tumour response rate over time for the optimized and standard regimens for various resistance development rates. The curves themselves as well as the computed AUC under these curves show that the "standard" regimen is always worse than the optimized regimen in terms of tumour shrinkage.

λ ($week^{-1}$)	0.00053	OC	-0.685
		Dose schedule ($g.m^{-2}$)	
		1st week	5
		2nd week	0
		3rd week	0
		MDT (d)	4
	0.0053	OC	-0.713
		Dose schedule ($g.m^{-2}$)	
		1st week	5
		2nd week	0
		3rd week	0
		MDT (d)	4
	0.053	OC	-0.731
		Dose schedule ($g.m^{-2}$)	
		1st week	5
		2nd week	0
		3rd week	0
		MDT (d)	4
	0.265	OC	-0.830
		Dose schedule ($g.m^{-2}$)	
		1st week	5
		2nd week	0
		3rd week	0
		MDT (d)	4
	0.53	OC	-0.891
		Dose schedule ($g.m^{-2}$)	
		1st week	5
		2nd week	0
		3rd week	0
		MDT (d)	4
	2.65	OC	-1.02
		Dose schedule ($g.m^{-2}$)	
		1st week	5
		2nd week	0
		3rd week	0
		MDT (d)	4
	5.3	OC	-1.06
		Dose schedule ($g.m^{-2}$)	
		1st week	5
		2nd week	0
		3rd week	0
		MDT (d)	4

Table 2: Optimal schedule for linear dose-effect relationship

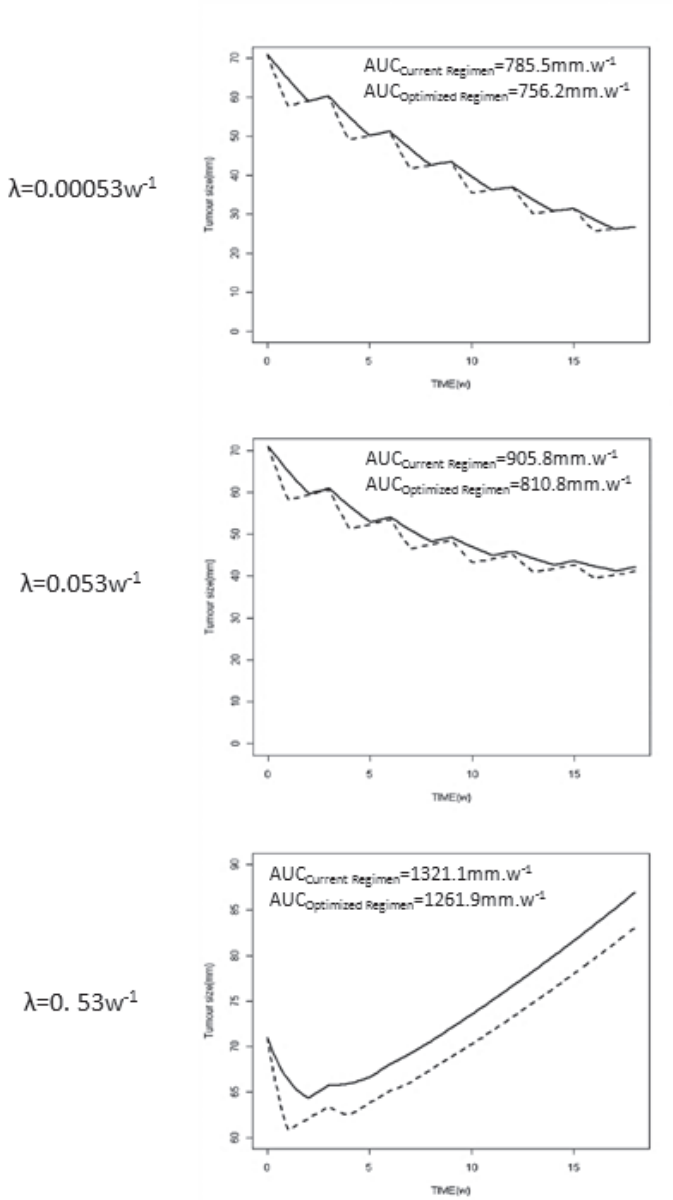

Figure 2: Typical value plot

These figures represent the median tumour growth profile (y axis) over the time (x axis) incase of linear dose-effect relationship. Tumour growth profiles were represented for 3 different values of λ (0.00053, 0.053 and 0.53 week^{-1}) for the current dose schedule (i.e. 2.5g.m^{-2} for 14 days followed by a 7-day rest period, solid line) and for the optimized regiment (dashed line).

E_{max} type dose-effect relationship

Results of the dose schedule optimization in case of E_{max} type dose-effect relationship is presented in Table 3 and summarized in Figure 3. The situation is more complex than the linear case since optimizations outputs are affected by both ED_{50} and λ values. For low and intermediate values of ED_{50}, i.e. maximal effect, the optimal dose schedule equally

distributes doses within the cycle for low rates of tumour resistance development leading to a MDT equal to 10.3d. For high rates of tumour resistance development, the MDT decreases to 4.7d meaning that the optimal dose schedule frontloads doses at the beginning of the cycle. Thus for low rates of resistance development, patients take 21 doses during the cycle and for high rates of resistance development, patients take most of the doses during the 1st week of the cycle. For high values of ED_{50}, the relationship is essentially linear and the resulting dose schedules are the same, i.e. MDT equal to 4d. Figure 4 shows the typical values of the tumour response rate over time for the optimized and standard regimens for various resistance development rates and various ED_{50} values. The curves themselves as well as the computed AUC under these curves show that the "standard" regimen is always worse than the optimized regimen in terms of tumour shrinkage.

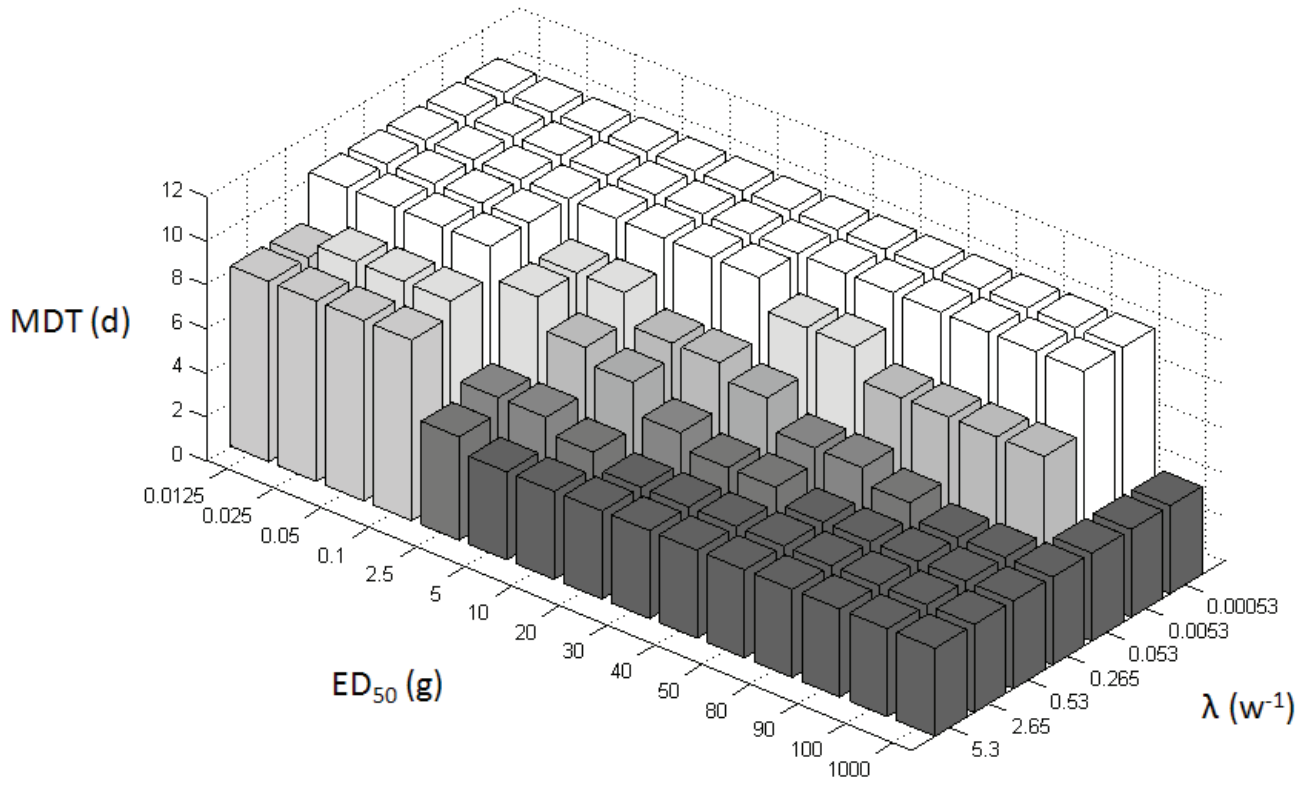

Figure 3: Optimization outputs for Emax dose-effect relationship
This figure illustrates Table 4. The MDT (z axis) is represented as a function of λ (x axis) and ED50 (y axis). The colours are scaled to represent the MDT value, from light (high MDT) to dark (low MDT) colour.

			ED50 (g)														
			0.0125	0.025	0.05	0.1	2.5	5	10	20	30	40	50	80	90	100	1000
λ (week^{-1})	0.00053	OC	-1.019	-1.002	-0.999	-1.021	-0.0951	-0.181	-0.344	-0.518	-0.635	-0.704	-0.792	-0.890	-0.919	-0.942	-1.154
		Dose schedule (g.m^{-2})															
		1st week	2	2	2	2	2	2	2	2	2	2	2	2	2	2	5
		2nd week	1.5	1.5	1.5	1.5	1.5	1.5	1.5	1.5	1.5	1.5	1.5	1.5	1.5	1.5	0
		3rd week	1.5	1.5	1.5	1.5	1.5	1.5	1.5	1.5	1.5	1.5	1.5	1.5	1.5	1.5	0
		MDT (d)	10.3	10.3	10.3	10.3	10.3	10.3	10.3	10.3	10.3	10.3	10.3	10.3	10.3	10.3	4
	0.0053	OC	-0.993	-1.003	-1.001	-1.005	-0.105	-0.211	-0.333	-0.525	-0.656	-0.738	-0.783	-0.908	-0.924	-0.943	-1.148
		Dose schedule (g.m^{-2})															
		1st week	2	2	2	2	2	2	2	2	2	2	2	2	2	2	5
		2nd week	1.5	1.5	1.5	1.5	1.5	1.5	1.5	1.5	1.5	1.5	1.5	1.5	1.5	1.5	0
		3rd week	1.5	1.5	1.5	1.5	1.5	1.5	1.5	1.5	1.5	1.5	1.5	1.5	1.5	1.5	0
		MDT (d)	10.3	10.3	10.3	10.3	10.3	10.3	10.3	10.3	10.3	10.3	10.3	10.3	10.3	10.3	4
	0.053	OC	-1.028	-1.02	-1.026	-1.047	-0.155	-0.262	-0.417	-0.601	-0.712	-0.781	-0.834	-0.939	-0.957	-0.990	-1.165
		Dose schedule (g.m^{-2})															
		1st week	2	2	2	2	2	2	2	2	2.5	2.5	3	3	3	3	5
		2nd week	1.5	1.5	1.5	1.5	1.5	1.5	1.5	1.5	1.5	1.5	1.5	1.5	1.5	1.5	0
		3rd week	1.5	1.5	1.5	1.5	1.5	1.5	1.5	1.5	1	1	0.5	0.5	0.5	0.5	0
		MDT (d)	10.3	10.3	10.3	10.3	10.3	10.3	10.3	10.3	8.9	8.9	7.5	7.5	7.5	7.5	4
	0.265	OC	-1.092	-1.08	-1.089	-1.086	-0.345	-0.442	-0.579	-0.732	-0.842	-0.882	-0.930	-1.0095	-1.022	-1.013	-1.168
		Dose schedule (g.m^{-2})															
		1st week	2	2	2	2	2.5	2.5	3	3	3.5	4	4	4.5	5	5	5
		2nd week	1.5	1.5	1.5	1.5	1.5	1.5	1.5	1.5	1	1	1	0.5	0	0	0
		3rd week	1.5	1.5	1.5	1.5	1	1	0.5	0.5	0.5	0	0	0	0	0	0
		MDT (d)	10.3	10.3	10.3	10.3	8.9	8.9	7.5	7.5	6.8	5.4	5.4	4.7	4	4	4
	0.53	OC	-1.125	-1.09	-1.115	-1.119	-0.481	-0.582	-0.701	-0.836	-0.880	-0.931	-0.993	-1.039	-1.042	-1.069	-1.161
		Dose schedule (g.m^{-2})															
		1st week	2	2	2	2	2.5	3	3.5	4	4.5	4.5	5	5	5	5	5
		2nd week	1.5	1.5	1.5	1.5	1.5	1.5	1	1	0.5	0.5	0	0	0	0	0
		3rd week	1.5	1.5	1.5	1.5	1	0.5	0.5	0	0	0	0	0	0	0	0
		MDT (d)	10.3	10.3	10.3	10.3	8.9	7.5	6.8	5.4	4.7	4.7	4	4	4	4	4
	2.65	OC	-1.159	-1.15	-1.160	-1.162	-0.790	-0.859	-0.902	-1.005	-1.037	-1.005	-1.076	-1.115	-1.107	-1.111	-1.160
		Dose schedule (g.m^{-2})															
		1st week	3	2.5	2.5	2.5	4	4	4.5	5	5	5	5	5	5	5	5
		2nd week	1	1.5	1.5	1.5	1	1	0.5	0	0	0	0	0	0	0	0
		3rd week	1	1	1	1	0	0	0	0	0	0	0	0	0	0	0
		MDT (d)	8.2	8.9	8.9	8.9	5.4	5.4	4.7	4	4	4	4	4	4	4	4
	5.3	OC	-1.177	-1.17	-1.171	-1.160	-0.863	-0.961	-0.991	-1.037	-1.085	-1.037	1.109	-1.135	-1.135	-1.127	-1.175
		Dose schedule (g.m^{-2})															
		1st week	3	3	3	3	4.5	5	5	5	5	5	5	5	5	5	5
		2nd week	1	1	1	1	0.5	0	0	0	0	0	0	0	0	0	0
		3rd week	1	1	1	1	0	0	0	0	0	0	0	0	0	0	0
		MDT (d)	8.2	8.2	8.2	8.2	4.7	4	4	4	4	4	4	4	4	4	4

Table 3: Optimal dose schedule for E_{max} dose-effect relationship

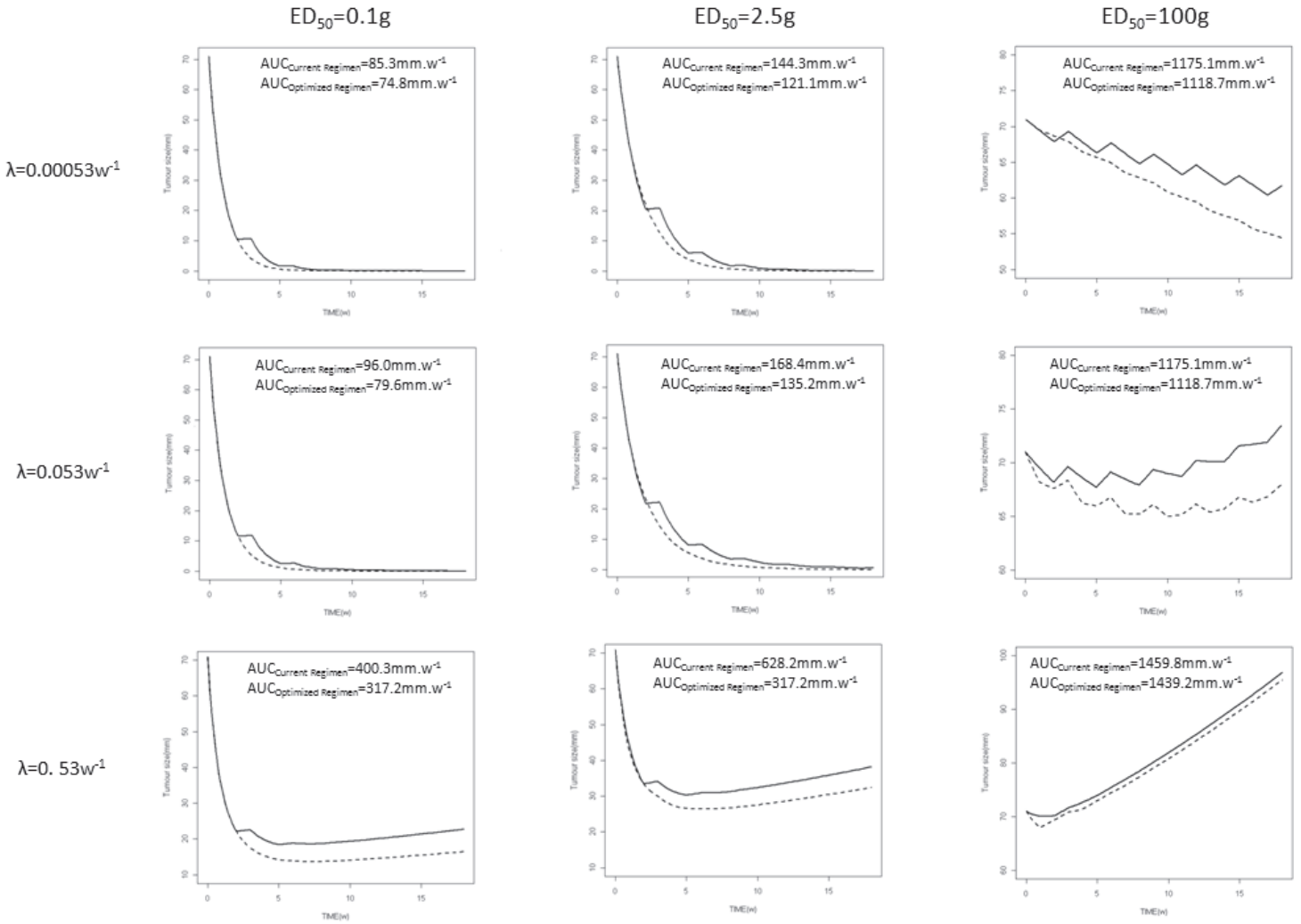

Figure 4: Typical value plot

These figures represent the median tumour growth profile (y axis) over the time (x axis) in case of E_{max} type dose-effect relationship. Tumour growth profiles were represented for 3 different values of λ (0.00053, 0.053 and 0.53 week^{-1}) for the current dose schedule (i.e. 2.5g.m^{-2} for 14 days followed by a 7-day rest period, solid line) and for the optimized regiment (dashed line).

Discussion

The aim of this work was to develop a population optimal design methodology to allow more informed dose schedule selection. For that purpose, a clinically relevant optimal criterion was defined based on the change in tumour size allowing the optimization of dose schedules. The tumour growth inhibition (TGI) model from Claret *et al.* was used and applied to a theoretical phase 2 study of capecitabine. The tumour growth inhibition model was developed on data from a capecitabine phase 2 study. It accounts for both the natural evolution of the disease and the drug effect. This model was shown to correctly predict treatment outcome of the phase 3 study only based in data coming from the phase 2 study. Because of its predictive capabilities and its flexibility, this model fitted the purposes for this optimal design problem. To our knowledge, there is no previous work aimed at optimizing dose schedules for maximal tumour response using TGI models. In the context of oncology phase 2 trials, the choice of the most relevant dose schedule remains a critical point. Usually this choice is based on the achievement of a predefined ORR. It has already been demonstrated that ORR cannot easily be used for an optimization of a phase 3 study because no quantitative measurements are considered. Instead, the use of TGI models combined with a population criterion to optimize dose schedule allows for a quantitative way to maximize the drug effect.

Optimizations of doses have already been attempted in oncology using clinical trial simulations (273), an approach that may be used to investigate relatively few possible scenarios using model-based simulations and re-estimations (211). However, if several variables are to be optimized, the number of design scenarios will grow and therefore the clinical trial simulation methodology will become extremely computer-intensive. Optimal design methodology, on the other hand, is generally faster than clinical trial simulations and allows for investigation of a far larger design space. Thus, a reasonable approach

seems to be optimizations of designs with optimal design methodology and then exploration of these optimized designs with clinical trial simulations. To obtain clinically relevant dose schedules, optimizations were performed within a set of clinical constraints. Capecitabine toxicity is related to the accumulated amount of drug. Therefore, to reduce the risk of developing high toxicity, the total amount of drug within the cycle was fixed to the same amount as currently used in clinical practice. This optimal design problem thus aims at optimizing the dose partitioning within the cycle with a fixed total dose. Previous studies have shown that a 100% increase of the capecitabine dose currently used was tolerable for patients' in terms of toxicity (273). Therefore, in this study, the maximal daily dose was fixed to $5 g.m^{-2}$, two times larger than the current daily dose used in clinical practice. In addition, the dose interval was fixed to 1 day and the daily doses were constrained to be the same for each week of the treatment cycle. This last constraint greatly reduced the number of possible doses combinations since only 3 dose levels have to be optimized.

One of the most important points in optimizing dose schedule is the dose-effect relationship. The impact of the dose-effect relationship was thus investigated by modifying the exposure parameter in the TGI model. Contrary to the linear dose-effect relationship, the non-linear (E_{max}) dose-effect relationship leads to different optimum according to the value of the ED_{50}. In case of large ED_{50} values, the optimal schedule frontloads doses within the 1st week of the cycle whereas it tends to equally distribute the doses within the cycle when ED_{50} value is low. In case of linear dose-effect relationship, all the dose schedule optimizations conclude that a loading dose is necessary to optimize the tumour response. Another critical point when developing a cytotoxic therapy concerns the development of tumour resistance. For many cytotoxic compounds, tumour resistance development is associated with a decreasing drug effect over time and is

responsible of patients' relapse. Here, the impact of tumour resistance development was investigated by modifying the value of the resistance development parameter (λ). As expected, when tumour resistance development is faster, the optimality criterion value decreases indicating that the therapy becomes less efficient. Regarding the optimal dose schedule, the tumour resistance does not change the scheduling of the regimen if the dose-effect relationship is linear. However, in case of non-linear dose-effect relationships, tumour resistance development has an impact on optimized regimens; for high rates of resistance development and low to intermediate ED_{50} values the optimized designs tend to frontload doses at the beginning of the cycle whereas it tends to equally distribute doses within the cycle for low rates of resistance. This means that in the case of rapid tumour resistance development rate, a loading dose is needed to ensure a tumour response whereas in case of slow tumour resistance development rate, it seems better to maintain drug exposure throughout the cycle. This study shows how both the dose-effect relationship and tumour resistance development rate interplay and impact the tumour response. Optimizations appear to be mostly driven by the dose-effect relationship. However, the tumour resistance development rate has a greater impact in case of low to intermediate ED_{50} values. The characterization of both parameters is thus needed to optimize dose schedule. In this work the first two cycles were optimized. The main motivation to base the optimal criterion on only the first two cycles was that the tumour size after two treatment cycles was a predictor of patients' survival in Claret *et al.* This time point also corresponds to the 1st follow-up visit after treatment initiation; it thus gives the opportunity to adapt the dose schedule in case of toxicity appearance or disease progression. Moreover, in the optimal design perspective, using the tumour size after two cycles enables the opportunity for the use of adaptive optimal design. In that case, data

collected at this time point can be used to inform the model and the design in order to adapt doses (274, 275).

One limitation of this study is directly related to the optimal design methodology. To optimize design parameters, it is necessary to trust the model structure and parameter estimates derived from the model. Here, this assumption implied that no pharmacokinetic (49) parameters were incorporated in the optimizations because the model stated that the daily dose drove the drug effect. However, it would have been relevant to introduce some PK into the optimizations in order to account for the delay between drug administration and effects on the tumour or to account for drug accumulation.

Moreover, in the context if early preclinical development, the assumption of certain model parameter values may be questioned since models are built on small cohorts and parameter estimates may be relatively imprecise. One option to account for parameter imprecision can be to use a global design approach, such as ED-optimality (205). Global optimal design techniques assume that the parameters come from distributions instead of unique point vales and hence allows for incorporation of uncertainty in parameter estimates. This method is considered more robust than local optimal design methods since it tries to make designs that are optimal for a whole range of parameter values. The method was not used here because of the increased computing power needed in the computations decreases the ability to investigate many scenarios. Another limitation of this work is that the optimal design criterion was only defined in terms of drug efficacy. Some clinical constraints were used to reduce the risk for a patient to develop high toxicities. Nevertheless, if no clinical constraints were defined, the favoured dose schedule in order to maximize the tumour response is to repeatedly take doses of infinite amount. On the other hand, if the optimal criterion was only based on toxicity, optimal results would have stated that, to avoid toxicity, patients should receive no dose. For drugs with

a narrow therapeutic window such as cytotoxics, it is necessary to account for both drug efficacy and toxicity in order to obtain the relevant dose schedule. This can be done simultaneously by combining both criteria in a utility function. Unfortunately, to our knowledge there is no such example in oncology.

Conclusions

This is the first study presenting the use of optimal design methodology to tumour growth inhibition models to date. The method presented allows optimization of dose schedules of anticancer drugs using a clinically relevant optimality criterion. It was demonstrated that the current dose schedule of capecitabine was predicted to be sub-optimal in terms of tumour shrinkage. The shape of the dose-effect relationship and the tumour resistance development rate were both found to impact the optimal dose scheduling.

Chapter 5:

General discussion

Throughout all the studies included in this thesis, the benefits of the (mechanistic) model-based approach applied to evaluate oncology compounds in early preclinical development and to optimize dose regimens in patients were demonstrated.

Since the recommendations edited by the Food and Drug Administration in 2004 that recognized the usefulness of this approach to support the drug development, pharmacometrics is more and more integrated in pharmaceutical companies to support the decision making and drug development programs. Mechanistic model-based drug development might be even more powerful to support the development of compounds in complex diseases such as cancer. Current anticancer drugs development is quite inefficient and regarding the progression of the disease incidence, there are urgent needs to improve the methodology used in the drug development in oncology.

The example used throughout this thesis concerns the preclinical development of a new efflux transporter inhibitor. The history of the development of this type of molecules illustrates some of the drawbacks associated to the usual development of oncology compounds. When the role of P-gp in tumour cells, so far the most intensively studied efflux transporter, has been discovered and the first inhibitors described, the concept of the reversion of multidrug resistance using P-gp inhibitors was directly moved from animals to patients with the hope of finding the same benefits in both species. The clinical failure of these inhibitors was primarily explained by their toxicity and their low affinity for P-gp. The second and third generation of P-gp inhibitors were more specific and had greater affinity and lower toxicity. However, they still failed to improve cancer treatment. This in part because all the information obtained with the development failure of the first generation was not analysed in depth, due to the lack of suitable tools to disentangle the influence of factors pertaining to PK, PD and tumour biology. The first explanation of the discrepancy between animal results and human results came after the development

arrest of P-gp inhibitor. This type of trial-and-error development has thus shown its limits.

In order to overcome issues already encountered for P-gp inhibitors, a model-based approach was used to evaluate the effect of the inhibition of BCRP inhibition on multidrug resistance using the new BCRP inhibitor, MBLI87.

1. MBLI87, a good BCRP inhibitor ?

One of the main conclusions of this thesis regards the compound MBLI87. If preliminary results, before the modelling work, indicated the good performances of the compound, our conclusions are more nuanced.

It is undeniable that MBLI87 inhibits the active efflux of various BCRP substrates such as CPT11, SN38 and Mit *in vitro*. However, the MBLI87 inhibitory constant (K_i) varies from 141nM for Mit to 1160nM for SN38 so the efflux inhibition is not as potent for all the substrates. In addition, the *in vitro* model demonstrated the importance of competing processes such as passive diffusion. If in this cellular system, the active efflux is greater than passive diffusion ($Cl_i/Cl_{diff}>1$), the ratio between both varies from 1.01 for CPT11 to 5.4 for SN38. This indicates that the maximal increase in intracellular substrates concentration is not the same across substrates (1% for CPT11 and 440% for SN38). These results may of course vary depending on the cell line. One question at this stage concerns the choice of the cellular system to demonstrate MBLI87 properties. HEK293 cells are at first sight interesting for studying the efflux inhibition because no metabolism occurs in these cells. However, regarding these first results, it would be necessary to investigate a range of cell lines to potentiate substrates efflux and thus MBLI87 effect.

The situation is more complex *in vivo*. The predicted tumour concentration of CPT11/SN38 in presence or absence of MBLI87 did not allow concluding about MBLI87 reversal effect. The discrepancy observed between *in vitro* and *in vivo* results can be explained by several points identified by the model. Thanks to the contradictory results obtained in both tumour growth experiments, some processes appeared to play a major role in the efficacy of MBLI87/CPT11 combination. Equilibration between plasma and tumour due to passive diffusion is lower in the second study. Results obtained by simulation attested that this parameter was crucial to minimize the tumour growth. Several works were conducted to study doxorubicin distribution and penetration in tumour spheroids in presence of P-gp inhibitors (236, 276). As an example, Patel *et al.* concluded to a paradoxical effect of P-gp inhibitors that lead to an increased uptake of doxorubicin in cells close to blood vessels but that have no effect on cells at high distance from blood vessels (236). Therefore, it exists a trade-off between uptake into proximal cells and penetration to distal cells, the effect of efflux inhibitors can be limited. It is thus important to consider factors that affect drug distribution into solid tumour to ensure a sufficient effect of efflux inhibitors. This can be addressed by modelling the tumour growth in 3D using spatial model and partial derivatives equations. These findings with doxorubicin and P-gp inhibitors corroborate our conclusions regarding MBLI87 differential effect between S1 and S2. In this purpose, it would be of great interest to use the normalization of tumour vasculature observed at the beginning of treatment by antiangiogenic drugs in combination to efflux inhibitors and cytotoxic to validate the role of drug diffusion (24, 253). Another difference found between both tumour growth experiments was the differential active efflux rate attributed to a different transporter activity. This factor is directly linked to the cell line used. As already found *in vitro*, the active efflux in HEK293 cells was not sufficient to observe a significant effect of ABCG2

inhibition. This has been corroborated in the simulation study where an increase of this parameter potentiated the reversal effect of MBLI87. The direct consequence of these two factors is a different cytotoxic tumour concentration between both studies resulting in a different efficacy on tumour growth. In addition, the tumour composition was shown to also impact cytotoxic efficacy since the percentage of drug sensitive cells at treatment onset was found significantly different between S1 and S2.

The nuanced results obtained for MBLI87 in this cellular system and under these experimental conditions could however be increased as shown in the simulation study since a higher dose of MBLI87 allows increasing its effect. Some further work has to be done regarding MBLI87 formulation. MBLI87 is encapsulated into nanoparticles because it is not soluble in water or saline vehicle; there are thus still some questions to be addressed by chemists and pharmacists in order to increase the drug content in the vehicle. The modest effect of the inhibitor *in vivo* is also attributable to the different inhibition of CPT11 and SN38 efflux. *In vivo*, SN38 is around 10 times more potent than CPT11, so if the SN38 BCRP-mediated efflux could be better inhibited, it will lead to an increase effect on the tumour growth. As shown in simulations, MBLI87 reversal effect was maximized if both MBLI87 K_i and clearance were decreased attesting the necessity of a sufficient inhibition of the transporter to ensure an effect on the tumour growth as already shown for P-gp inhibitor (247). These results indicate that further improvement of MBLI87 chemical structure and formulation have to be done.

However, even if a low effect of MBLI87 was found through the semi-mechanistic model, the K-PD model predicts that the inhibitor potentiated CPT11 potency by 20% per µmol. The K-PD model predicts a long half-life of the compound in the biophase whereas there was no evidence of an accumulation of MBLI87 in the plasma. Since the semi-mechanistic model does not indicate an accumulation of MBLI87, this finding may be interpreted as a

delayed and prolonged antitumoral effect due to the mechanism of action of CP11 and SN38. To address this question, it would be worth to investigate the tumour concentration of MBLI87 and CPT11. Such additional data would allow enriching the semi-mechanistic model.

Another point to discuss here concerns the relevance of BCRP inhibition. As it has been pointed in the first part of this document, BCRP is less widely expressed than P-gp but still expressed at important natural barriers where it plays its protective role. As for P-gp, its inhibition could be associated to high toxicity that could preclude the use of BCRP inhibitors in clinical practice. An answer to this would be the development of formulation that preferentially target the tumour tissues through the development of pegylated liposomal formulations as for doxorubicin.

In addition, the determination of the part of drug resistance due to BCRP has to be clearly determined in order to know is it is preferable to develop specific inhibitors such as MBLI87 or if it is preferable to develop inhibitors that target several transporters. Finally, in order to obtain, a real improvement of the management of clinical multidrug resistance, it is necessary to adopt adaptive strategies because multidrug resistance is multifactorial. As an example, it has been demonstrated that if one efflux transporter is inhibited, tumour cells will overexpress others efflux transporters in order to escape from the treatment.

2. Benefits of the mechanistic model-based drug development in the development of efflux transporter inhibitors

The second axis developed throughout this thesis concerns the use of NLME PK/PD models to evaluate preclinical oncology studies and to design oncology clinical studies.

The development of a new drug relies heavily on *in vitro* and animals studies that provide a framework for clinical trials. In some cases, such as for P-gp inhibitors, a drug can be

highly effective in animals and inefficient in humans. This issue can arise if the translation between both species is not correctly handled. The development of PK/PD models to ensure an appropriate translation between preclinical and clinical studies was shown to overcome this type of issue especially in the case of antibiotics. Here, in addition to PK/PD model, the benefits of the NLME approach coupled to these models was demonstrated.

Regarding the *in vitro* study of MBLI87, the NLME mechanistic model accounting for both passive and active cytotoxic transport was shown to be superior to the usual analysis tool to analyse competition *in vitro* data.

A great advantage of the model-based development is that information gained in an experiment can be used to analyse another experiment. As an example, the former model and some of these parameters were re-used in a semi-mechanistic PK/PD model of the interaction between CPT11 and MBLI87. This second model combines all the information available at this stage of development about this drug combination. One of the challenges with the model was to develop an advanced model based on sparse data gained in an experiment not originally designed for modelling purposes. Thanks to the sequential building and the use of NLME approach, it was possible to combine all the studies together and to quantify all the model parameters; although the precision of some of them was limited. This model constitutes an important step in MBLI87 development because it allows the identification of the limiting features of MBI87. In addition, it can generate some target values to be reached regarding the future development of similar compound in terms of inhibitory constant, protein binding, tota clearance, drug content in the vehicle, ect… If more data are coming, a natural extension of this semi-mechanistic model would be the development of a PBPK/PD model to translate the results observed in animals to patients. If CPT11 and MBLI87 pKa, log(P) and unbound fraction are known, a PBPK model can be easily developed (277). Regarding the tumour growth parameters,

West *et al.* demonstrated that the same scaling law as for PK parameter can be applied (278, 279). Parameters of the semi-mechanistic model can thus be scaled as follows:

$$Volume_{human}(L) = Volume_{animal} \times \left(\frac{m_{animal}}{m_{human}}\right) \quad \text{(Equation 21)}$$

$$Concentration_{human}(\mu mol.L^{-1}), = Concentration_{animal} \quad \text{(Equation 22)}$$

$$K_{human}\ (d^{-1}) = K_{animal} \times \left(\frac{m_{animal}}{m_{human}}\right)^{-\frac{1}{4}} \quad \text{(Equation 23)}$$

$$t_{human}\ (d^{-1}) = t_{animal} \times \left(\frac{m_{animal}}{m_{human}}\right)^{\frac{1}{4}} \quad \text{(Equation 24)}$$

$$Cl_{human}\ (L.d^{-1}) = Cl_{animal} \times \left(\frac{m_{animal}}{m_{human}}\right)^{\frac{3}{4}} \quad \text{(Equation 25)}$$

Where m_{human} and m_{animal} are the typical animal and human mass respectively (*e.g.* 30 g for a mouse and 70 kg for a human).

All the model parameters getting the same units as parameters defined in Equation 21-25 are scaled using the same law. It is also important to mention that the dose interval (in day) has also to be scaled between species, according to equation 24.

However, the development of such advanced model is not always possible when only data issued from PoC studies are available. In these cases, it is still possible to use the advantage of the model-based development as it has been shown with the minimal TGI model. This model was used in order to structure the information derived from animal PoC study. Here, the use of the NLME approach was shown to be even more important to quantify model parameters. Of course this type of models cannot pretend to pursue the same objectives as the mechanistic models but we showed that the model is useful to early identify the most promising candidates or to decrease the experimental effort.

Optimally design experiment is also a benefit of the model-based approach. In the last study included in this thesis, the clinical TGI model was used to optimize the tumour response in patients. The design of oncology phase 2 study remains a critical point of

oncology drug development because historical approaches showed recently their limits to evaluate new targeted therapies.

Even if cancer research had undergone some radical changes in the last decade, there is thus still some challenges to meet. Exploring the tumour dynamics and disease processes using quantitative models at clinical levels is becoming routine. However, this approach has to be more applied to preclinical study to ensure the translation between animals and human. The use of mathematical models is now essential to integrate the huge amount of data produced and to quantitatively assess the properties of new compound *in vitro* and *in vivo*. There is thus a great opportunity to integrate knowledge to address clinical questions and to improve the decision making in oncology drug development.

Overall conclusion

The question of the management of anticancer drug resistance is primordial because most of the treatment failures in cancer patients are associated to the development of this phenomenon.

In this thesis, the management of anticancer drug resistance was addressed through the study of a new BCRP inhibitor, MBLI87. To overcome issues already encountered in the development of P-gp inhibitor, a mechanistic model-based approach was used to support its preclinical development. The power of this approach was demonstrated in all the studies included in this work not only to evaluate preclinical studies but also to optimize patients' response in clinical trials. Since the current paradigm of oncology drug development is quite inefficient, this type of approach can thus be applied from the early beginning of anticancer drug development to avoid the risk and costs of development failure.

Résumé substantiel en français

La résistance aux chimiothérapies anticancéreuses constitue l'une des raisons principales de l'échec des traitements anti-tumoraux. Ce phénomène multifactoriel peut être associé à la physiologie tumorale ou aux cellules tumorales elles-mêmes (31). L'un des mécanismes de résistance les plus étudié consiste en l'efflux actif des médicaments des cellules cancéreuses résultant en l'altération de la concentration intracellulaire des médicaments (31). Les transporteurs de la famille ABC (ATP Binding Cassette). sont les effecteurs de ce mécanisme de résistance (74). Parmi les 48 transporteurs ABC contenus dans le génome humain, trois sont principalement associé à la manifestation clinique du phénomène de résistance aux anticancéreux : ABCB1/P-gp, ABCG2/BCRP et ABCC1/MRP1 (239). P-gp a été le transporteur d'efflux le plus étudié dans le passé de par son expression ubiquitaire et sa capacité à transporter de nombreuses molécules différentes (280). L'inhibition de P-gp dans la problématique de la résistance aux anticancéreux a toujours échoué en clinique malgré des résultats prometteurs *in vitro* et chez l'animal (247). Plusieurs critiques peuvent être faites à l'égard de la méthodologie employée lors du développement des inhibiteurs de P-gp, notamment l'absence de modèles quantitatifs permettant la translation des résultats précliniques à l'homme. L'échec des inhibiteurs de P-gp a mené à l'arrêt du développement de ces molécules, cependant la question du bénéfice de l'inhibition d'autres transporteurs d'efflux, notamment de BCRP, n'a que très rarement été testée (135). Comme P-gp, BCRP joue un rôle important dans la résistance aux traitements anticancéreux par sa capacité à effluer de nombreuses molécules anticancéreux dont une partie des substrats de P-gp tout en présentant l'avantage de ne pas être inhibé par les principaux inhibiteurs de P-gp. BCRP constitue donc une cible intéressante pour tester l'hypothèse du bénéfice de l'inhibition d'autres transporteurs d'efflux dans la résistance aux traitements anticancéreux. De

nouveaux inhibiteurs de BCRP ont récemment été synthétisés (136). Un dérivé d'acridone, MBLI87, a montré des propriétés intéressantes contre l'efflux d'irinotecan, CPT11, *in vitro* et *in vivo*. Cette nouvelle molécule étant en phase de développement préclinique, il apparaît nécessaire d'utiliser de nouvelles approches afin d'éviter les écueils rencontrés pour les inhibiteurs de P-gp.

L'objectif de cette thèse est de montrer les bénéfices de la modélisation appliquée au développement préclinique des inhibiteurs de transporteur d'efflux. Les objectifs spécifiques sont les suivants :

- Montrer les bénéfices des modèles à effets mixtes d'inhibition de la croissance tumorale dans le développement préclinique des inhibiteurs de transporteur d'efflux.
- Développer des modèles semi-mécanistiques de l'interaction entre cytotoxiques et inhibiteurs de transporteur d'efflux.
- Montrer les bénéfices des modèles à effets mixtes d'inhibition de la croissance tumorale pour optimiser la réponse tumorale chez les patients montrant une résistance.

Chacune des parties incluses dans ce document présente les publications associées aux travaux présentés.

La première partie de cette thèse présente le développement et l'utilisation de modèles semi-mécanistiques de l'interaction entre cytotoxiques et inhibiteurs d'efflux. Le premier axe développé concerne l'utilisation de ces modèles couplés à l'approche non-linéaire à effets mixtes (NLME) pour analyser les données issues d'expériences de compétition *in vitro*. Ce type de données est habituellement analysé avec des méthodes graphiques ou de régression simple qui ne prennent pas en compte les différents mécanismes intervenant dans le système étudié. De plus ces méthodes ne permettent pas de distinguer la

variabilité inter- et intra- expérience. Les modèles NLME mécanistiques permettent de répondre aux manquements des approches usuelles. Ici, un modèle NLME d'inhibition du transport a été construit et appliqué au MBLI87 permettant de quantifier son effet sur l'accumulation intracellulaire de différents cytotoxiques. Ce modèle permet également de quantifier d'autres paramètres pharmacologiques importants de l'interaction entre ces molécules. Ce modèle a été appliqué avec succès à trois différents cytotoxiques et deux types de données différents démontrant sa capacité à être appliqué pour étudier différentes combinaisons de traitements. En prenant en compte les différents mécanismes en présence ainsi que les différentes sources de variabilité, ce modèle permet d'estimer la vraie valeur des paramètres et non une valeur apparente comme c'est le cas avec les méthodes habituelles.

Le second axe abordé dans cette partie concerne le développement d'un modèle PKPD semi-mécanistique de l'interaction entre inhibiteurs d'efflux et cytotoxiques. En effet les leçons tirées du développement des inhibiteurs de P-gp ont montré la nécessité de comprendre les mécanismes de ces molécules mis en jeu *in vivo* afin d'assurer une translation efficace des résultats précliniques à l'homme. Le modèle développé ici établit la relation entre l'accumulation intracellulaire des cytotoxiques en présence d'inhibiteurs de transporteur d'efflux et la croissance tumorale. Dans ce cas, l'approche NLME combinée au modèle semi-mécanistique permet de tirer un maximum partie des données disponibles. Ce modèle a été appliqué a deux études de preuve du concept chez l'animal présentant des designs différents en termes d'intensité et de délai de traitement. Plusieurs facteurs impactant l'efficacité de cette combinaison de traitement ont pu être identifiés. En effet, la cinétique d'accumulation tumorale due à la diffusion passive de cytotoxiques dans la tumeur ainsi que la cinétique d'efflux actif apparaissent comme deux éléments importants de l'efficacité de cette combinaison. De plus le pourcentage de

cellules sensibles à l'agent anticancéreux impacte également l'efficacité de la combinaison. Ce dernier facteur met en avant le rôle possible de l'hypoxie comme facteur de résistance secondaire rappelle que la résistance aux traitements anticancéreux est multifactorielle et qu'il peut s'avérer nécessaire de combiner plusieurs stratégies pour la surmonter. De plus, cette étude a permis de mettre en avant via une étude par simulation plusieurs facteurs permettant d'optimiser l'effet révertant du MBLI87.

Ce type d'approche semi-mécanistique n'est cependant pas toujours envisageable aux stades précoces de développement précliniques où très peu de données sont disponibles. Les études de première administration chez l'animal sont généralement pauvres car elles ne servent uniquement à démontrer la pertinence de la cible et de son inhibiteur. Un seul niveau de dose est en général testé sur un faible nombre d'animaux rendant difficile l'extrapolation des résultats obtenus dans ces études. Les méthodes classiques d'analyse de ces études sont basées sur de simples tests statistiques comparant les effets de la molécule étudiée par rapport à une référence. La seconde partie de ce travail se propose d'illustrer les bénéfices des modèles NLME pour aider le développement préclinique des inhibiteurs de transporteurs d'efflux. Le modèle développé dans cette partie est un modèle minimal d'inhibition de la croissance tumorale de l'interaction entre cytotoxiques et inhibiteurs d'efflux. Il appartient aux modèles K-PD et ne prend pas en compte la pharmacocinétique du cytotoxique et de l'inhibiteur. De ce fait, l'interaction est considérée au niveau de la croissance tumorale où l'inhibiteur d'efflux augmente la cytotoxicité de l'anticancéreux. Le modèle final comporte plusieurs simplifications tout en retenant suffisamment de complexité pour caractériser simultanément la croissance tumorale et l'interaction entre ces molécules. Il a été appliqué avec succès à une étude de première administration chez l'animal du MBLI87 combiné à l'irinotecan. L'approche NLME a permis ici d'utiliser toute l'information disponible dans cette étude afin de

quantifier les paramètres du modèle. De plus l'analyse longitudinale des données a permis de séparer les paramètres relatifs au système et aux molécules, ce qui n'est pas envisageable avec les approches classiques.

Ces deux premières parties ont permis d'illustrer les bénéfices de l'approche NLME et des modèles d'inhibition de la croissance tumorale dans l'évaluation de préclinique des inhibiteurs de transporteurs d'efflux combinés aux cytotoxiques dans la problématique de la résistance aux chimiothérapies anticancéreuses. Si ce type d'approche n'est pas encore complètement établi en développement préclinique, il l'est davantage pour évaluer les essais cliniques en oncologie. Cependant, les modèles NLME d'inhibition de la croissance tumorale ne sont que très peu utilisés pour optimiser la réponse des patients aux traitements. La dernière partie de ce travail propose une approche de design optimal utilisant les modèles d'inhibition de la croissance tumorale pour optimiser les régimes de doses des cytotoxiques afin de maximiser la réponse tumorale. La question du choix du régime de dose optimal pour les études de phase 3 en oncologie demeure un point critique du développement clinique des anticancéreux. Les outils couramment utilisés ne prennent pas en compte la dynamique tumorale et mènent souvent à des erreurs de développement comme en témoignent le taux d'échec des molécules anticancéreuses en phase 3. Cette étude montre que l'utilisation des modèles quantitatifs permet d'optimiser de façon rationnelle les régimes de doses pour les études de phase 3. Néanmoins, ce travail reste théorique puisqu'il ne se préoccupe que de l'efficacité des traitements en oubliant les aspects liés à leur toxicité.

Au travers de cette thèse, la prise en charge de la résistance aux traitements anticancéreux a été étudiée par l'étude d'un nouvel inhibiteur de transporteur d'efflux, MBLI87. Le développement passé de ce type de molécules a présenté plusieurs lacunes qui peuvent être en partie compensées par le développement de modèles quantitatifs de l'interaction

entre les cytotoxiques et les inhibiteurs de transporteurs d'efflux et ce depuis le début de leur développement préclinique. L'utilité de la modélisation et notamment des modèles à effets mixtes d'inhibition de la croissance tumorale a été montrée dans toutes les études incluses dans ce travail non seulement pour évaluer ce type d'interaction de façon précoce mais aussi pour optimiser la réponse tumorale dans les essais cliniques. Les méthodes usuelles d'évaluation des médicaments en oncologie font du développement de ces molécules l'un des plus inefficaces. Les approches présentées dans cette thèse peuvent donc permettre d'améliorer le développement des médicaments en oncologie et diminuer les risques d'échec de développement ainsi que les coûts qui y sont associés.

References

1. Organization WH. Cancer. Fact Sheet N°297
2012.
2. Campone M, Fumoleau P, Bourbouloux E, Kerbrat P, Roche H. Taxanes in adjuvant breast cancer setting: which standard in Europe? Critical reviews in oncology/hematology. 2005 Sep;55(3):167-75.
3. Danesi R, Di Paolo A. Chemoembolization is effective as second-line therapy in patients with colorectal carcinoma metastatic to the liver. Clinical colorectal cancer. 2002 Nov;2(3):180-1.
4. Fisher B, Jeong JH, Bryant J, Anderson S, Dignam J, Fisher ER, et al. Treatment of lymph-node-negative, oestrogen-receptor-positive breast cancer: long-term findings from National Surgical Adjuvant Breast and Bowel Project randomised clinical trials. Lancet. 2004 Sep 4-10;364(9437):858-68.
5. Wolpin BM, Meyerhardt JA, Mamon HJ, Mayer RJ. Adjuvant treatment of colorectal cancer. CA: a cancer journal for clinicians. 2007 May-Jun;57(3):168-85.
6. Kawato Y, Aonuma M, Hirota Y, Kuga H, Sato K. Intracellular roles of SN-38, a metabolite of the camptothecin derivative CPT-11, in the antitumor effect of CPT-11. Cancer Res. 1991 Aug 15;51(16):4187-91.
7. Rivory LP, Riou JF, Haaz MC, Sable S, Vuilhorgne M, Commercon A, et al. Identification and properties of a major plasma metabolite of irinotecan (CPT-11) isolated from the plasma of patients. Cancer Res. 1996 Aug 15;56(16):3689-94.
8. Dodds HM, Haaz MC, Riou JF, Robert J, Rivory LP. Identification of a new metabolite of CPT-11 (irinotecan): pharmacological properties and activation to SN-38. J Pharmacol Exp Ther. 1998 Jul;286(1):578-83.
9. Pommier Y, Pourquier P, Urasaki Y, Wu J, Laco GS. Topoisomerase I inhibitors: selectivity and cellular resistance. Drug resistance updates : reviews and commentaries in antimicrobial and anticancer chemotherapy. 1999 Oct;2(5):307-18.
10. Stewart CF, Zamboni WC, Crom WR, Houghton PJ. Disposition of irinotecan and SN-38 following oral and intravenous irinotecan dosing in mice. Cancer Chemother Pharmacol. 1997;40(3):259-65.
11. Guichard S, Chatelut E, Lochon I, Bugat R, Mahjoubi M, Canal P. Comparison of the pharmacokinetics and efficacy of irinotecan after administration by the intravenous versus intraperitoneal route in mice. Cancer Chemother Pharmacol. 1998;42(2):165-70.
12. Gupta E, Mick R, Ramirez J, Wang X, Lestingi TM, Vokes EE, et al. Pharmacokinetic and pharmacodynamic evaluation of the topoisomerase inhibitor irinotecan in cancer patients. J Clin Oncol. 1997 Apr;15(4):1502-10.
13. Xie R, Mathijssen RH, Sparreboom A, Verweij J, Karlsson MO. Clinical pharmacokinetics of irinotecan and its metabolites: a population analysis. J Clin Oncol. 2002 Aug 1;20(15):3293-301.

14. Chau I, Cunningham D. Adjuvant therapy in colon cancer--what, when and how? Ann Oncol. 2006 Sep;17(9):1347-59.
15. Fujita A, Takabatake H, Tagaki S, Sekine K. Phase I study of cisplatin, ifosfamide and CPT11 with granulocyte colony-stimulating factor support in advanced non-small cell lung cancer. Gan To Kagaku Ryoho. 1996 Sep;23(10):1285-90.
16. Rothenberg ML, Eckardt JR, Kuhn JG, Burris HA, 3rd, Nelson J, Hilsenbeck SG, et al. Phase II trial of irinotecan in patients with progressive or rapidly recurrent colorectal cancer. J Clin Oncol. 1996 Apr;14(4):1128-35.
17. Kawahara M. Irinotecan in the treatment of small cell lung cancer: a review of patient safety considerations. Expert Opin Drug Saf. 2006 Mar;5(2):303-12.
18. Blesch KS, Gieschke R, Tsukamoto Y, Reigner BG, Burger HU, Steimer JL. Clinical pharmacokinetic/pharmacodynamic and physiologically based pharmacokinetic modeling in new drug development: the capecitabine experience. Invest New Drugs. 2003 May;21(2):195-223.
19. Miwa M, Ura M, Nishida M, Sawada N, Ishikawa T, Mori K, et al. Design of a novel oral fluoropyrimidine carbamate, capecitabine, which generates 5-fluorouracil selectively in tumours by enzymes concentrated in human liver and cancer tissue. Eur J Cancer. 1998 Jul;34(8):1274-81.
20. Rustum YM, Harstrick A, Cao S, Vanhoefer U, Yin MB, Wilke H, et al. Thymidylate synthase inhibitors in cancer therapy: direct and indirect inhibitors. J Clin Oncol. 1997 Jan;15(1):389-400.
21. Biedler JL, Riehm H. Cellular resistance to actinomycin D in Chinese hamster cells in vitro: cross-resistance, radioautographic, and cytogenetic studies. Cancer Res. 1970 Apr;30(4):1174-84.
22. Larsen AK, Skladanowski A. Cellular resistance to topoisomerase-targeted drugs: from drug uptake to cell death. Biochim Biophys Acta. 1998 Oct 1;1400(1-3):257-74.
23. Teicher BA, Herman TS, Holden SA, Wang YY, Pfeffer MR, Crawford JW, et al. Tumor resistance to alkylating agents conferred by mechanisms operative only in vivo. Science. 1990 Mar 23;247(4949 Pt 1):1457-61.
24. Dewhirst MW, Tso CY, Oliver R, Gustafson CS, Secomb TW, Gross JF. Morphologic and hemodynamic comparison of tumor and healing normal tissue microvasculature. Int J Radiat Oncol Biol Phys. 1989 Jul;17(1):91-9.
25. Ma J, Waxman DJ. Modulation of the antitumor activity of metronomic cyclophosphamide by the angiogenesis inhibitor axitinib. Mol Cancer Ther. 2008 Jan;7(1):79-89.
26. Wilson WR, Hay MP. Targeting hypoxia in cancer therapy. Nat Rev Cancer. 2011 Jun;11(6):393-410.
27. Bedford JS, Mitchell JB. The effect of hypoxia on the growth and radiation response of mammalian cells in culture. Br J Radiol. 1974 Oct;47(562):687-96.

28. Durand RE, LePard NE. Modulation of tumor hypoxia by conventional chemotherapeutic agents. Int J Radiat Oncol Biol Phys. 1994 Jun 15;29(3):481-6.
29. Conley BA, Taube SE. Prognostic and predictive markers in cancer. Dis Markers. 2004;20(2):35-43.
30. Shanafelt TD, Witzig TE, Fink SR, Jenkins RB, Paternoster SF, Smoley SA, et al. Prospective evaluation of clonal evolution during long-term follow-up of patients with untreated early-stage chronic lymphocytic leukemia. J Clin Oncol. 2006 Oct 1;24(28):4634-41.
31. Rochat B. Importance of influx and efflux systems and xenobiotic metabolizing enzymes in intratumoral disposition of anticancer agents. Curr Cancer Drug Targets. 2009 Aug;9(5):652-74.
32. Holzer AK, Manorek GH, Howell SB. Contribution of the major copper influx transporter CTR1 to the cellular accumulation of cisplatin, carboplatin, and oxaliplatin. Mol Pharmacol. 2006 Oct;70(4):1390-4.
33. Okabe M, Szakacs G, Reimers MA, Suzuki T, Hall MD, Abe T, et al. Profiling SLCO and SLC22 genes in the NCI-60 cancer cell lines to identify drug uptake transporters. Mol Cancer Ther. 2008 Sep;7(9):3081-91.
34. Hu S, Franke RM, Filipski KK, Hu C, Orwick SJ, de Bruijn EA, et al. Interaction of imatinib with human organic ion carriers. Clin Cancer Res. 2008 May 15;14(10):3141-8.
35. Kaufman Y, Ifergan I, Rothem L, Jansen G, Assaraf YG. Coexistence of multiple mechanisms of PT523 resistance in human leukemia cells harboring 3 reduced folate carrier alleles: transcriptional silencing, inactivating mutations, and allele loss. Blood. 2006 Apr 15;107(8):3288-94.
36. Fotoohi K, Jansen G, Assaraf YG, Rothem L, Stark M, Kathmann I, et al. Disparate mechanisms of antifolate resistance provoked by methotrexate and its metabolite 7-hydroxymethotrexate in leukemia cells: implications for efficacy of methotrexate therapy. Blood. 2004 Dec 15;104(13):4194-201.
37. Crossman LC, Druker BJ, Deininger MW, Pirmohamed M, Wang L, Clark RE. hOCT 1 and resistance to imatinib. Blood. 2005 Aug 1;106(3):1133-4; author reply 4.
38. Szakacs G, Annereau JP, Lababidi S, Shankavaram U, Arciello A, Bussey KJ, et al. Predicting drug sensitivity and resistance: profiling ABC transporter genes in cancer cells. Cancer Cell. 2004 Aug;6(2):129-37.
39. Mignogna C, Staibano S, Altieri V, De Rosa G, Pannone G, Santoro A, et al. Prognostic significance of multidrug-resistance protein (MDR-1) in renal clear cell carcinomas: a five year follow-up analysis. BMC Cancer. 2006;6:293.
40. Seiden MV, Swenerton KD, Matulonis U, Campos S, Rose P, Batist G, et al. A phase II study of the MDR inhibitor biricodar (INCEL, VX-710) and paclitaxel in women with advanced ovarian cancer refractory to paclitaxel therapy. Gynecol Oncol. 2002 Sep;86(3):302-10.
41. Chico I, Kang MH, Bergan R, Abraham J, Bakke S, Meadows B, et al. Phase I study of infusional paclitaxel in combination with the P-glycoprotein antagonist PSC 833. J Clin Oncol. 2001 Feb 1;19(3):832-42.

42. Fox E, Bates SE. Tariquidar (XR9576): a P-glycoprotein drug efflux pump inhibitor. Expert Rev Anticancer Ther. 2007 Apr;7(4):447-59.
43. Cripe LD, Uno H, Paietta EM, Litzow MR, Ketterling RP, Bennett JM, et al. Zosuquidar, a novel modulator of P-glycoprotein, does not improve the outcome of older patients with newly diagnosed acute myeloid leukemia: a randomized, placebo-controlled trial of the Eastern Cooperative Oncology Group 3999. Blood. 2010 Nov 18;116(20):4077-85.
44. Shimada T, Yamazaki H, Mimura M, Inui Y, Guengerich FP. Interindividual variations in human liver cytochrome P-450 enzymes involved in the oxidation of drugs, carcinogens and toxic chemicals: studies with liver microsomes of 30 Japanese and 30 Caucasians. J Pharmacol Exp Ther. 1994 Jul;270(1):414-23.
45. Mackenzie PI, Bock KW, Burchell B, Guillemette C, Ikushiro S, Iyanagi T, et al. Nomenclature update for the mammalian UDP glycosyltransferase (UGT) gene superfamily. Pharmacogenet Genomics. 2005 Oct;15(10):677-85.
46. Nebert DW, Vasiliou V. Analysis of the glutathione S-transferase (GST) gene family. Hum Genomics. 2004 Nov;1(6):460-4.
47. Cai L, Yu SZ, Zhan ZF. Cytochrome P450 2E1 genetic polymorphism and gastric cancer in Changle, Fujian Province. World J Gastroenterol. 2001 Dec;7(6):792-5.
48. Hida T, Kozaki K, Ito H, Miyaishi O, Tatematsu Y, Suzuki T, et al. Significant growth inhibition of human lung cancer cells both in vitro and in vivo by the combined use of a selective cyclooxygenase 2 inhibitor, JTE-522, and conventional anticancer agents. Clin Cancer Res. 2002 Jul;8(7):2443-7.
49. Petros WP, Hopkins PJ, Spruill S, Broadwater G, Vredenburgh JJ, Colvin OM, et al. Associations between drug metabolism genotype, chemotherapy pharmacokinetics, and overall survival in patients with breast cancer. J Clin Oncol. 2005 Sep 1;23(25):6117-25.
50. DeMichele A, Aplenc R, Botbyl J, Colligan T, Wray L, Klein-Cabral M, et al. Drug-metabolizing enzyme polymorphisms predict clinical outcome in a node-positive breast cancer cohort. J Clin Oncol. 2005 Aug 20;23(24):5552-9.
51. Goetz MP, Rae JM, Suman VJ, Safgren SL, Ames MM, Visscher DW, et al. Pharmacogenetics of tamoxifen biotransformation is associated with clinical outcomes of efficacy and hot flashes. J Clin Oncol. 2005 Dec 20;23(36):9312-8.
52. Katragadda S, Budda B, Anand BS, Mitra AK. Role of efflux pumps and metabolising enzymes in drug delivery. Expert Opin Drug Deliv. 2005 Jul;2(4):683-705.
53. Hu R, Shen G, Yerramilli UR, Lin W, Xu C, Nair S, et al. In vivo pharmacokinetics, activation of MAPK signaling and induction of phase II/III drug metabolizing enzymes/transporters by cancer chemopreventive compound BHA in the mice. Arch Pharm Res. 2006 Oct;29(10):911-20.
54. Ishikawa T, Tamura A, Saito H, Wakabayashi K, Nakagawa H. Pharmacogenomics of the human ABC transporter ABCG2: from functional evaluation to drug molecular design. Naturwissenschaften. 2005 Oct;92(10):451-63.

55. Lahaye T, Riehm B, Berger U, Paschka P, Muller MC, Kreil S, et al. Response and resistance in 300 patients with BCR-ABL-positive leukemias treated with imatinib in a single center: a 4.5-year follow-up. Cancer. 2005 Apr 15;103(8):1659-69.
56. Shah NP, Sawyers CL. Mechanisms of resistance to STI571 in Philadelphia chromosome-associated leukemias. Oncogene. 2003 Oct 20;22(47):7389-95.
57. Al-Ali HK, Heinrich MC, Lange T, Krahl R, Mueller M, Muller C, et al. High incidence of BCR-ABL kinase domain mutations and absence of mutations of the PDGFR and KIT activation loops in CML patients with secondary resistance to imatinib. Hematol J. 2004;5(1):55-60.
58. Soverini S, Colarossi S, Gnani A, Rosti G, Castagnetti F, Poerio A, et al. Contribution of ABL kinase domain mutations to imatinib resistance in different subsets of Philadelphia-positive patients: by the GIMEMA Working Party on Chronic Myeloid Leukemia. Clin Cancer Res. 2006 Dec 15;12(24):7374-9.
59. Corbin AS, La Rosee P, Stoffregen EP, Druker BJ, Deininger MW. Several Bcr-Abl kinase domain mutants associated with imatinib mesylate resistance remain sensitive to imatinib. Blood. 2003 Jun 1;101(11):4611-4.
60. Marsh S, McLeod HL. Thymidylate synthase pharmacogenetics in colorectal cancer. Clin Colorectal Cancer. 2001 Nov;1(3):175-8; discussion 9-81.
61. Martin LP, Hamilton TC, Schilder RJ. Platinum resistance: the role of DNA repair pathways. Clin Cancer Res. 2008 Mar 1;14(5):1291-5.
62. Cobo M, Isla D, Massuti B, Montes A, Sanchez JM, Provencio M, et al. Customizing cisplatin based on quantitative excision repair cross-complementing 1 mRNA expression: a phase III trial in non-small-cell lung cancer. J Clin Oncol. 2007 Jul 1;25(19):2747-54.
63. Welsh C, Day R, McGurk C, Masters JR, Wood RD, Koberle B. Reduced levels of XPA, ERCC1 and XPF DNA repair proteins in testis tumor cell lines. Int J Cancer. 2004 Jun 20;110(3):352-61.
64. Selvakumaran M, Pisarcik DA, Bao R, Yeung AT, Hamilton TC. Enhanced cisplatin cytotoxicity by disturbing the nucleotide excision repair pathway in ovarian cancer cell lines. Cancer Res. 2003 Mar 15;63(6):1311-6.
65. Reed JC. Dysregulation of apoptosis in cancer. J Clin Oncol. 1999 Sep;17(9):2941-53.
66. Korsmeyer SJ. Bcl-2 initiates a new category of oncogenes: regulators of cell death. Blood. 1992 Aug 15;80(4):879-86.
67. Chiarugi V, Ruggiero M. Role of three cancer "master genes" p53, bcl2 and c-myc on the apoptotic process. Tumori. 1996 May-Jun;82(3):205-9.
68. Youle RJ, Strasser A. The BCL-2 protein family: opposing activities that mediate cell death. Nat Rev Mol Cell Biol. 2008 Jan;9(1):47-59.
69. Levine AJ. p53, the cellular gatekeeper for growth and division. Cell. 1997 Feb 7;88(3):323-31.
70. Zuckerman V, Wolyniec K, Sionov RV, Haupt S, Haupt Y. Tumour suppression by p53: the importance of apoptosis and cellular senescence. J Pathol. 2009 Sep;219(1):3-15.
71. Dassa E, Schneider E. The rise of a protein family: ATP-binding cassette systems. Res Microbiol. 2001 Apr-May;152(3-4):203.

72. Saurin W, Hofnung M, Dassa E. Getting in or out: early segregation between importers and exporters in the evolution of ATP-binding cassette (ABC) transporters. J Mol Evol. 1999 Jan;48(1):22-41.
73. Higgins CF. ABC transporters: physiology, structure and mechanism--an overview. Res Microbiol. 2001 Apr-May;152(3-4):205-10.
74. Dean M, Rzhetsky A, Allikmets R. The human ATP-binding cassette (ABC) transporter superfamily. Genome Res. 2001 Jul;11(7):1156-66.
75. Sheps JA, Ralph S, Zhao Z, Baillie DL, Ling V. The ABC transporter gene family of Caenorhabditis elegans has implications for the evolutionary dynamics of multidrug resistance in eukaryotes. Genome Biol. 2004;5(3):R15.
76. Schneider E, Hunke S. ATP-binding-cassette (ABC) transport systems: functional and structural aspects of the ATP-hydrolyzing subunits/domains. FEMS Microbiol Rev. 1998 Apr;22(1):1-20.
77. Rees DC, Johnson E, Lewinson O. ABC transporters: the power to change. Nat Rev Mol Cell Biol. 2009 Mar;10(3):218-27.
78. Mourez M, Hofnung M, Dassa E. Subunit interactions in ABC transporters: a conserved sequence in hydrophobic membrane proteins of periplasmic permeases defines an important site of interaction with the ATPase subunits. EMBO J. 1997 Jun 2;16(11):3066-77.
79. Biemans-Oldehinkel E, Doeven MK, Poolman B. ABC transporter architecture and regulatory roles of accessory domains. FEBS Lett. 2006 Feb 13;580(4):1023-35.
80. Schmitt L, Benabdelhak H, Blight MA, Holland IB, Stubbs MT. Crystal structure of the nucleotide-binding domain of the ABC-transporter haemolysin B: identification of a variable region within ABC helical domains. J Mol Biol. 2003 Jul 4;330(2):333-42.
81. Davidson AL. Mechanism of coupling of transport to hydrolysis in bacterial ATP-binding cassette transporters. J Bacteriol. 2002 Mar;184(5):1225-33.
82. Senior AE, al-Shawi MK, Urbatsch IL. The catalytic cycle of P-glycoprotein. FEBS Lett. 1995 Dec 27;377(3):285-9.
83. Callaghan R, Ford RC, Kerr ID. The translocation mechanism of P-glycoprotein. FEBS Lett. 2006 Feb 13;580(4):1056-63.
84. Gao M, Cui HR, Loe DW, Grant CE, Almquist KC, Cole SP, et al. Comparison of the functional characteristics of the nucleotide binding domains of multidrug resistance protein 1. J Biol Chem. 2000 Apr 28;275(17):13098-108.
85. Tombline G, Bartholomew LA, Urbatsch IL, Senior AE. Combined mutation of catalytic glutamate residues in the two nucleotide binding domains of P-glycoprotein generates a conformation that binds ATP and ADP tightly. J Biol Chem. 2004 Jul 23;279(30):31212-20.
86. Dong J, Yang G, McHaourab HS. Structural basis of energy transduction in the transport cycle of MsbA. Science. 2005 May 13;308(5724):1023-8.
87. Szakacs G, Paterson JK, Ludwig JA, Booth-Genthe C, Gottesman MM. Targeting multidrug resistance in cancer. Nat Rev Drug Discov. 2006 Mar;5(3):219-34.
88. Borst P, Elferink RO. Mammalian ABC transporters in health and disease. Annu Rev Biochem. 2002;71:537-92.

89. Juliano RL, Ling V. A surface glycoprotein modulating drug permeability in Chinese hamster ovary cell mutants. Biochim Biophys Acta. 1976 Nov 11;455(1):152-62.
90. Szakacs G, Varadi A, Ozvegy-Laczka C, Sarkadi B. The role of ABC transporters in drug absorption, distribution, metabolism, excretion and toxicity (ADME-Tox). Drug Discov Today. 2008 May;13(9-10):379-93.
91. Gottesman MM, Ling V. The molecular basis of multidrug resistance in cancer: the early years of P-glycoprotein research. FEBS Lett. 2006 Feb 13;580(4):998-1009.
92. Hermann DM, Bassetti CL. Implications of ATP-binding cassette transporters for brain pharmacotherapies. Trends Pharmacol Sci. 2007 Mar;28(3):128-34.
93. Sharom FJ. ABC multidrug transporters: structure, function and role in chemoresistance. Pharmacogenomics. 2008 Jan;9(1):105-27.
94. Schinkel AH. P-Glycoprotein, a gatekeeper in the blood-brain barrier. Adv Drug Deliv Rev. 1999 Apr 5;36(2-3):179-94.
95. Terao T, Hisanaga E, Sai Y, Tamai I, Tsuji A. Active secretion of drugs from the small intestinal epithelium in rats by P-glycoprotein functioning as an absorption barrier. J Pharm Pharmacol. 1996 Oct;48(10):1083-9.
96. Keller RP, Altermatt HJ, Donatsch P, Zihlmann H, Laissue JA, Hiestand PC. Pharmacologic interactions between the resistance-modifying cyclosporine SDZ PSC 833 and etoposide (VP 16-213) enhance in vivo cytostatic activity and toxicity. Int J Cancer. 1992 May 28;51(3):433-8.
97. Sparreboom A, van Asperen J, Mayer U, Schinkel AH, Smit JW, Meijer DK, et al. Limited oral bioavailability and active epithelial excretion of paclitaxel (Taxol) caused by P-glycoprotein in the intestine. Proc Natl Acad Sci U S A. 1997 Mar 4;94(5):2031-5.
98. Meijer OC, de Lange EC, Breimer DD, de Boer AG, Workel JO, de Kloet ER. Penetration of dexamethasone into brain glucocorticoid targets is enhanced in mdr1A P-glycoprotein knockout mice. Endocrinology. 1998 Apr;139(4):1789-93.
99. Lankas GR, Wise LD, Cartwright ME, Pippert T, Umbenhauer DR. Placental P-glycoprotein deficiency enhances susceptibility to chemically induced birth defects in mice. Reprod Toxicol. 1998 Jul-Aug;12(4):457-63.
100. Ambudkar SV, Dey S, Hrycyna CA, Ramachandra M, Pastan I, Gottesman MM. Biochemical, cellular, and pharmacological aspects of the multidrug transporter. Annu Rev Pharmacol Toxicol. 1999;39:361-98.
101. Zheleznova EE, Markham P, Edgar R, Bibi E, Neyfakh AA, Brennan RG. A structure-based mechanism for drug binding by multidrug transporters. Trends Biochem Sci. 2000 Feb;25(2):39-43.
102. Ling V. Charles F. Kettering Prize. P-glycoprotein and resistance to anticancer drugs. Cancer. 1992 May 15;69(10):2603-9.
103. Polgar O, Bates SE. ABC transporters in the balance: is there a role in multidrug resistance? Biochem Soc Trans. 2005 Feb;33(Pt 1):241-5.
104. Ford JM, Hait WN. Pharmacology of drugs that alter multidrug resistance in cancer. Pharmacol Rev. 1990 Sep;42(3):155-99.

105. Faneyte IF, Kristel PM, van de Vijver MJ. Determining MDR1/P-glycoprotein expression in breast cancer. Int J Cancer. 2001 Jul 1;93(1):114-22.
106. Smith AJ, Mayer U, Schinkel AH, Borst P. Availability of PSC833, a substrate and inhibitor of P-glycoproteins, in various concentrations of serum. J Natl Cancer Inst. 1998 Aug 5;90(15):1161-6.
107. Fracasso PM, Brady MF, Moore DH, Walker JL, Rose PG, Letvak L, et al. Phase II study of paclitaxel and valspodar (PSC 833) in refractory ovarian carcinoma: a gynecologic oncology group study. J Clin Oncol. 2001 Jun 15;19(12):2975-82.
108. Baekelandt M, Lehne G, Trope CG, Szanto I, Pfeiffer P, Gustavssson B, et al. Phase I/II trial of the multidrug-resistance modulator valspodar combined with cisplatin and doxorubicin in refractory ovarian cancer. J Clin Oncol. 2001 Jun 15;19(12):2983-93.
109. Sonneveld P. Multidrug resistance in acute myeloid leukaemia. Baillieres Clin Haematol. 1996 Mar;9(1):185-203.
110. Goldstein LJ. Clinical reversal of drug resistance. Curr Probl Cancer. 1995 Mar-Apr;19(2):65-124.
111. Doyle LA, Yang W, Abruzzo LV, Krogmann T, Gao Y, Rishi AK, et al. A multidrug resistance transporter from human MCF-7 breast cancer cells. Proc Natl Acad Sci U S A. 1998 Dec 22;95(26):15665-70.
112. Allikmets R, Schriml LM, Hutchinson A, Romano-Spica V, Dean M. A human placenta-specific ATP-binding cassette gene (ABCP) on chromosome 4q22 that is involved in multidrug resistance. Cancer Res. 1998 Dec 1;58(23):5337-9.
113. Miyake K, Mickley L, Litman T, Zhan Z, Robey R, Cristensen B, et al. Molecular cloning of cDNAs which are highly overexpressed in mitoxantrone-resistant cells: demonstration of homology to ABC transport genes. Cancer Res. 1999 Jan 1;59(1):8-13.
114. Maliepaard M, Scheffer GL, Faneyte IF, van Gastelen MA, Pijnenborg AC, Schinkel AH, et al. Subcellular localization and distribution of the breast cancer resistance protein transporter in normal human tissues. Cancer Res. 2001 Apr 15;61(8):3458-64.
115. Fetsch PA, Abati A, Litman T, Morisaki K, Honjo Y, Mittal K, et al. Localization of the ABCG2 mitoxantrone resistance-associated protein in normal tissues. Cancer Lett. 2006 Apr 8;235(1):84-92.
116. Zhang Y, Wang H, Unadkat JD, Mao Q. Breast cancer resistance protein 1 limits fetal distribution of nitrofurantoin in the pregnant mouse. Drug Metab Dispos. 2007 Dec;35(12):2154-8.
117. Pollex E, Lubetsky A, Koren G. The role of placental breast cancer resistance protein in the efflux of glyburide across the human placenta. Placenta. 2008 Aug;29(8):743-7.
118. Gedeon C, Anger G, Piquette-Miller M, Koren G. Breast cancer resistance protein: mediating the trans-placental transfer of glyburide across the human placenta. Placenta. 2008 Jan;29(1):39-43.
119. Cooray HC, Blackmore CG, Maskell L, Barrand MA. Localisation of breast cancer resistance protein in microvessel endothelium of human brain. Neuroreport. 2002 Nov 15;13(16):2059-63.

120. Cisternino S, Mercier C, Bourasset F, Roux F, Scherrmann JM. Expression, up-regulation, and transport activity of the multidrug-resistance protein Abcg2 at the mouse blood-brain barrier. Cancer Res. 2004 May 1;64(9):3296-301.
121. Breedveld P, Pluim D, Cipriani G, Wielinga P, van Tellingen O, Schinkel AH, et al. The effect of Bcrp1 (Abcg2) on the in vivo pharmacokinetics and brain penetration of imatinib mesylate (Gleevec): implications for the use of breast cancer resistance protein and P-glycoprotein inhibitors to enable the brain penetration of imatinib in patients. Cancer Res. 2005 Apr 1;65(7):2577-82.
122. de Vries NA, Zhao J, Kroon E, Buckle T, Beijnen JH, van Tellingen O. P-glycoprotein and breast cancer resistance protein: two dominant transporters working together in limiting the brain penetration of topotecan. Clin Cancer Res. 2007 Nov 1;13(21):6440-9.
123. Gutmann H, Hruz P, Zimmermann C, Beglinger C, Drewe J. Distribution of breast cancer resistance protein (BCRP/ABCG2) mRNA expression along the human GI tract. Biochem Pharmacol. 2005 Sep 1;70(5):695-9.
124. Allen JD, Schinkel AH. Multidrug resistance and pharmacological protection mediated by the breast cancer resistance protein (BCRP/ABCG2). Mol Cancer Ther. 2002 Apr;1(6):427-34.
125. Oostendorp RL, Buckle T, Beijnen JH, van Tellingen O, Schellens JH. The effect of P-gp (Mdr1a/1b), BCRP (Bcrp1) and P-gp/BCRP inhibitors on the in vivo absorption, distribution, metabolism and excretion of imatinib. Invest New Drugs. 2009 Feb;27(1):31-40.
126. Jonker JW, Merino G, Musters S, van Herwaarden AE, Bolscher E, Wagenaar E, et al. The breast cancer resistance protein BCRP (ABCG2) concentrates drugs and carcinogenic xenotoxins into milk. Nat Med. 2005 Feb;11(2):127-9.
127. Doyle LA, Ross DD. Multidrug resistance mediated by the breast cancer resistance protein BCRP (ABCG2). Oncogene. 2003 Oct 20;22(47):7340-58.
128. Kawabata S, Oka M, Shiozawa K, Tsukamoto K, Nakatomi K, Soda H, et al. Breast cancer resistance protein directly confers SN-38 resistance of lung cancer cells. Biochem Biophys Res Commun. 2001 Feb 9;280(5):1216-23.
129. Yang CH, Schneider E, Kuo ML, Volk EL, Rocchi E, Chen YC. BCRP/MXR/ABCP expression in topotecan-resistant human breast carcinoma cells. Biochem Pharmacol. 2000 Sep 15;60(6):831-7.
130. Maliepaard M, van Gastelen MA, de Jong LA, Pluim D, van Waardenburg RC, Ruevekamp-Helmers MC, et al. Overexpression of the BCRP/MXR/ABCP gene in a topotecan-selected ovarian tumor cell line. Cancer Res. 1999 Sep 15;59(18):4559-63.
131. Rajendra R, Gounder MK, Saleem A, Schellens JH, Ross DD, Bates SE, et al. Differential effects of the breast cancer resistance protein on the cellular accumulation and cytotoxicity of 9-aminocamptothecin and 9-nitrocamptothecin. Cancer Res. 2003 Jun 15;63(12):3228-33.
132. Schinkel AH, Jonker JW. Mammalian drug efflux transporters of the ATP binding cassette (ABC) family: an overview. Adv Drug Deliv Rev. 2003 Jan 21;55(1):3-29.

133. Ahmed-Belkacem A, Pozza A, Macalou S, Perez-Victoria JM, Boumendjel A, Di Pietro A. Inhibitors of cancer cell multidrug resistance mediated by breast cancer resistance protein (BCRP/ABCG2). Anticancer Drugs. 2006 Mar;17(3):239-43.
134. Rabindran SK, Ross DD, Doyle LA, Yang W, Greenberger LM. Fumitremorgin C reverses multidrug resistance in cells transfected with the breast cancer resistance protein. Cancer Res. 2000 Jan 1;60(1):47-50.
135. Robey RW, Polgar O, Deeken J, To KW, Bates SE. ABCG2: determining its relevance in clinical drug resistance. Cancer Metastasis Rev. 2007 Mar;26(1):39-57.
136. Boumendjel A, Macalou S, Ahmed-Belkacem A, Blanc M, Di Pietro A. Acridone derivatives: design, synthesis, and inhibition of breast cancer resistance protein ABCG2. Bioorg Med Chem. 2007 Apr 15;15(8):2892-7.
137. Arnaud O, Boumendjel A, Geze A, Honorat M, Matera EL, Guitton J, et al. The acridone derivative MBLI-87 sensitizes breast cancer resistance protein-expressing xenografts to irinotecan. Eur J Cancer. 2010 Jan 7.
138. Benderra Z, Faussat AM, Sayada L, Perrot JY, Chaoui D, Marie JP, et al. Breast cancer resistance protein and P-glycoprotein in 149 adult acute myeloid leukemias. Clin Cancer Res. 2004 Dec 1;10(23):7896-902.
139. Ross DD, Karp JE, Chen TT, Doyle LA. Expression of breast cancer resistance protein in blast cells from patients with acute leukemia. Blood. 2000 Jul 1;96(1):365-8.
140. Diestra JE, Scheffer GL, Catala I, Maliepaard M, Schellens JH, Scheper RJ, et al. Frequent expression of the multi-drug resistance-associated protein BCRP/MXR/ABCP/ABCG2 in human tumours detected by the BXP-21 monoclonal antibody in paraffin-embedded material. J Pathol. 2002 Oct;198(2):213-9.
141. Ishikawa T, Li ZS, Lu YP, Rea PA. The GS-X pump in plant, yeast, and animal cells: structure, function, and gene expression. Biosci Rep. 1997 Apr;17(2):189-207.
142. Cole SP, Bhardwaj G, Gerlach JH, Mackie JE, Grant CE, Almquist KC, et al. Overexpression of a transporter gene in a multidrug-resistant human lung cancer cell line. Science. 1992 Dec 4;258(5088):1650-4.
143. Bakos E, Evers R, Szakacs G, Tusnady GE, Welker E, Szabo K, et al. Functional multidrug resistance protein (MRP1) lacking the N-terminal transmembrane domain. J Biol Chem. 1998 Nov 27;273(48):32167-75.
144. Leslie EM, Deeley RG, Cole SP. Multidrug resistance proteins: role of P-glycoprotein, MRP1, MRP2, and BCRP (ABCG2) in tissue defense. Toxicol Appl Pharmacol. 2005 May 1;204(3):216-37.
145. Robbiani DF, Finch RA, Jager D, Muller WA, Sartorelli AC, Randolph GJ. The leukotriene C(4) transporter MRP1 regulates CCL19 (MIP-3beta, ELC)-dependent mobilization of dendritic cells to lymph nodes. Cell. 2000 Nov 22;103(5):757-68.
146. Panwala CM, Jones JC, Viney JL. A novel model of inflammatory bowel disease: mice deficient for the multiple drug resistance gene, mdr1a, spontaneously develop colitis. J Immunol. 1998 Nov 15;161(10):5733-44.

147. Gotoh Y, Suzuki H, Kinoshita S, Hirohashi T, Kato Y, Sugiyama Y. Involvement of an organic anion transporter (canalicular multispecific organic anion transporter/multidrug resistance-associated protein 2) in gastrointestinal secretion of glutathione conjugates in rats. J Pharmacol Exp Ther. 2000 Jan;292(1):433-9.
148. Dietrich CG, de Waart DR, Ottenhoff R, Schoots IG, Elferink RP. Increased bioavailability of the food-derived carcinogen 2-amino-1-methyl-6-phenylimidazo[4,5-b]pyridine in MRP2-deficient rats. Mol Pharmacol. 2001 May;59(5):974-80.
149. Sakamoto H, Hara H, Hirano K, Adachi T. Enhancement of glucuronosyl etoposide transport by glutathione in multidrug resistance-associated protein-overexpressing cells. Cancer Lett. 1999 Jan 8;135(1):113-9.
150. Konig J, Nies AT, Cui Y, Leier I, Keppler D. Conjugate export pumps of the multidrug resistance protein (MRP) family: localization, substrate specificity, and MRP2-mediated drug resistance. Biochim Biophys Acta. 1999 Dec 6;1461(2):377-94.
151. Ito K, Oleschuk CJ, Westlake C, Vasa MZ, Deeley RG, Cole SP. Mutation of Trp1254 in the multispecific organic anion transporter, multidrug resistance protein 2 (MRP2) (ABCC2), alters substrate specificity and results in loss of methotrexate transport activity. J Biol Chem. 2001 Oct 12;276(41):38108-14.
152. Leslie EM, Ito K, Upadhyaya P, Hecht SS, Deeley RG, Cole SP. Transport of the beta -O-glucuronide conjugate of the tobacco-specific carcinogen 4-(methylnitrosamino)-1-(3-pyridyl)-1-butanol (NNAL) by the multidrug resistance protein 1 (MRP1). Requirement for glutathione or a non-sulfur-containing analog. J Biol Chem. 2001 Jul 27;276(30):27846-54.
153. Boumendjel A, Baubichon-Cortay H, Trompier D, Perrotton T, Di Pietro A. Anticancer multidrug resistance mediated by MRP1: recent advances in the discovery of reversal agents. Med Res Rev. 2005 Jul;25(4):453-72.
154. Hipfner DR, Deeley RG, Cole SP. Structural, mechanistic and clinical aspects of MRP1. Biochim Biophys Acta. 1999 Dec 6;1461(2):359-76.
155. Barrett JS, Fossler MJ, Cadieu KD, Gastonguay MR. Pharmacometrics: a multidisciplinary field to facilitate critical thinking in drug development and translational research settings. J Clin Pharmacol. 2008 May;48(5):632-49.
156. Ette EWPJ. Pharmacometrics: The science of quantitative pharmacology. Wiley; 2007.
157. Sheiner LB, Rosenberg B, Melmon KL. Modelling of individual pharmacokinetics for computer-aided drug dosage. Computers and biomedical research, an international journal. 1972 Oct;5(5):411-59.
158. Sheiner LB, Ludden TM. Population pharmacokinetics/dynamics. Annu Rev Pharmacol Toxicol. 1992;32:185-209.
159. Karlsson MO, Sheiner LB. The importance of modeling interoccasion variability in population pharmacokinetic analyses. Journal of pharmacokinetics and biopharmaceutics. 1993 Dec;21(6):735-50.
160. Orloff J, Douglas F, Pinheiro J, Levinson S, Branson M, Chaturvedi P, et al. The future of drug development: advancing clinical trial design. Nat Rev Drug Discov. 2009 Dec;8(12):949-57.

161. Beal SL. Population pharmacokinetic data and parameter estimation based on their first two statistical moments. Drug Metab Rev. 1984;15(1-2):173-93.
162. Lavielle M, Mentre F. Estimation of population pharmacokinetic parameters of saquinavir in HIV patients with the MONOLIX software. J Pharmacokinet Pharmacodyn. 2007 Apr;34(2):229-49.
163. Dartois C, Brendel K, Comets E, Laffont CM, Laveille C, Tranchand B, et al. Overview of model-building strategies in population PK/PD analyses: 2002-2004 literature survey. Br J Clin Pharmacol. 2007 Nov;64(5):603-12.
164. Goffin J, Baral S, Tu D, Nomikos D, Seymour L. Objective responses in patients with malignant melanoma or renal cell cancer in early clinical studies do not predict regulatory approval. Clin Cancer Res. 2005 Aug 15;11(16):5928-34.
165. Ette EI, Ludden TM. Population pharmacokinetic modeling: the importance of informative graphics. Pharmaceutical research. 1995 Dec;12(12):1845-55.
166. Karlsson MO, Savic RM. Diagnosing model diagnostics. Clin Pharmacol Ther. 2007 Jul;82(1):17-20.
167. Yano Y, Beal SL, Sheiner LB. Evaluating pharmacokinetic/pharmacodynamic models using the posterior predictive check. J Pharmacokinet Pharmacodyn. 2001 Apr;28(2):171-92.
168. Brendel K, Comets E, Laffont C, Laveille C, Mentre F. Metrics for external model evaluation with an application to the population pharmacokinetics of gliclazide. Pharmaceutical research. 2006 Sep;23(9):2036-49.
169. Dayneka NL, Garg V, Jusko WJ. Comparison of four basic models of indirect pharmacodynamic responses. Journal of pharmacokinetics and biopharmaceutics. 1993 Aug;21(4):457-78.
170. Claret L, Girard P, Hoff PM, Van Cutsem E, Zuideveld KP, Jorga K, et al. Model-based prediction of phase III overall survival in colorectal cancer on the basis of phase II tumor dynamics. J Clin Oncol. 2009 Sep 1;27(25):4103-8.
171. Sheiner LB, Stanski DR, Vozeh S, Miller RD, Ham J. Simultaneous modeling of pharmacokinetics and pharmacodynamics: application to d-tubocurarine. Clin Pharmacol Ther. 1979 Mar;25(3):358-71.
172. Verotta D, Sheiner LB. Semiparametric analysis of non-steady-state pharmacodynamic data. Journal of pharmacokinetics and biopharmaceutics. 1991 Dec;19(6):691-712.
173. Jacqmin P, Snoeck E, van Schaick EA, Gieschke R, Pillai P, Steimer JL, et al. Modelling response time profiles in the absence of drug concentrations: definition and performance evaluation of the K-PD model. J Pharmacokinet Pharmacodyn. 2007 Feb;34(1):57-85.
174. Tod M. Evaluation of drugs in pediatrics using K-PD models: perspectives. Fundam Clin Pharmacol. 2008 Dec;22(6):589-94.
175. White CR, Seymour RS. Allometric scaling of mammalian metabolism. The Journal of experimental biology. 2005 May;208(Pt 9):1611-9.
176. Muraszko K, Sung C, Walbridge S, Greenfield L, Dedrick RL, Oldfield EH, et al. Pharmacokinetics and toxicology of immunotoxins administered into the subarachnoid space in nonhuman primates and rodents. Cancer Res. 1993 Aug 15;53(16):3752-7.

177. Barrett JS, Shi J, Xie HT, Huang XH, Fossler MJ, Sun RY. Globalization of quantitative pharmacology: first international symposium of quantitative pharmacology in drug development and regulation. J Clin Pharmacol. 2008 Jul;48(7):787-92.
178. Mahmood I. Critique of prospective allometric scaling: does the emperor have clothes? J Clin Pharmacol. 2000 Apr;40(4):341-4; discussion 5-6.
179. Brown RP, Delp MD, Lindstedt SL, Rhomberg LR, Beliles RP. Physiological parameter values for physiologically based pharmacokinetic models. Toxicology and industrial health. 1997 Jul-Aug;13(4):407-84.
180. Himmelstein KJ, Lutz RJ. A review of the applications of physiologically based pharmacokinetic modeling. Journal of pharmacokinetics and biopharmaceutics. 1979 Apr;7(2):127-45.
181. Mordenti J. Pharmacokinetic scale-up: accurate prediction of human pharmacokinetic profiles from animal data. Journal of pharmaceutical sciences. 1985 Oct;74(10):1097-9.
182. Zamboni WC, Stewart CF, Thompson J, Santana VM, Cheshire PJ, Richmond LB, et al. Relationship between topotecan systemic exposure and tumor response in human neuroblastoma xenografts. J Natl Cancer Inst. 1998 Apr 1;90(7):505-11.
183. Rocchetti M, Simeoni M, Pesenti E, De Nicolao G, Poggesi I. Predicting the active doses in humans from animal studies: a novel approach in oncology. Eur J Cancer. 2007 Aug;43(12):1862-8.
184. Byrne HM. A weakly nonlinear analysis of a model of avascular solid tumour growth. Journal of mathematical biology. 1999 Jul;39(1):59-89.
185. W.P. C. J Roetgenal Radium Ther Nucl Med. 1956.
186. Steel GG, Courtenay VD, Peckham MJ. The response to chemotherapy of a variety of human tumour xenografts. Br J Cancer. 1983 Jan;47(1):1-13.
187. Laing JH, Rew DA, Wilson GD. Cell kinetics of human solid tumours. BJR supplement / BIR. 1992;24:163-7.
188. Tan WY, Singh KP. A mixed model of carcinogenesis with applications to retinoblastoma. Mathematical biosciences. 1990 Mar;98(2):211-25.
189. Marusic M, Bajzer Z, Vuk-Pavlovic S, Freyer JP. Tumor growth in vivo and as multicellular spheroids compared by mathematical models. Bulletin of mathematical biology. 1994 Jul;56(4):617-31.
190. Levasseur LM, Slocum HK, Rustum YM, Greco WR. Modeling of the time-dependency of in vitro drug cytotoxicity and resistance. Cancer Res. 1998 Dec 15;58(24):5749-61.
191. Simeoni M, Magni P, Cammia C, De Nicolao G, Croci V, Pesenti E, et al. Predictive pharmacokinetic-pharmacodynamic modeling of tumor growth kinetics in xenograft models after administration of anticancer agents. Cancer Res. 2004 Feb 1;64(3):1094-101.
192. Hahnfeldt P, Panigrahy D, Folkman J, Hlatky L. Tumor development under angiogenic signaling: a dynamical theory of tumor growth, treatment response, and postvascular dormancy. Cancer Res. 1999 Oct 1;59(19):4770-5.

193. Rocchetti M, Del Bene F, Germani M, Fiorentini F, Poggesi I, Pesenti E, et al. Testing additivity of anticancer agents in pre-clinical studies: a PK/PD modelling approach. Eur J Cancer. 2009 Dec;45(18):3336-46.
194. Koch G, Walz A, Lahu G, Schropp J. Modeling of tumor growth and anticancer effects of combination therapy. J Pharmacokinet Pharmacodyn. 2009 Apr;36(2):179-97.
195. Ribba B, Watkin E, Tod M, Girard P, Grenier E, You B, et al. A model of vascular tumour growth in mice combining longitudinal tumour size data with histological biomarkers. Eur J Cancer. 2011 Feb;47(3):479-90.
196. Kola I, Landis J. Can the pharmaceutical industry reduce attrition rates? Nat Rev Drug Discov. 2004 Aug;3(8):711-5.
197. Tham LS, Wang L, Soo RA, Lee SC, Lee HS, Yong WP, et al. A pharmacodynamic model for the time course of tumor shrinkage by gemcitabine + carboplatin in non-small cell lung cancer patients. Clin Cancer Res. 2008 Jul 1;14(13):4213-8.
198. Burzykowski T, Buyse M, Piccart-Gebhart MJ, Sledge G, Carmichael J, Luck HJ, et al. Evaluation of tumor response, disease control, progression-free survival, and time to progression as potential surrogate end points in metastatic breast cancer. J Clin Oncol. 2008 Apr 20;26(12):1987-92.
199. Wang Y, Sung C, Dartois C, Ramchandani R, Booth BP, Rock E, et al. Elucidation of relationship between tumor size and survival in non-small-cell lung cancer patients can aid early decision making in clinical drug development. Clin Pharmacol Ther. 2009 Aug;86(2):167-74.
200. M.O. SAHEYBGPK, editor. Simultaneous modelling of PSA production in Prostatic Benign Hyperplasia (PBH) and prostatic adenocarcinoma patients treated by prostate surgery. Population Approach Group Europe; 2009; Saint Petersburg. PAGE. Abstracts of the Annual Meeting of the Population Approach Group in Europe.
ISSN 1871-6032
201. M. WMYBHECOFGT, editor. Population K-PD joint modeling of tumor size and CA 125 kinetics after chemotherapy in relapsed ovarian cancer (ROC) patients. Population Approache Group Europe; 2012; Venice. PAGE. Abstracts of the Annual Meeting of the Population Approach Group in Europe.
ISSN 1871-6032
202. Friberg LE, Henningsson A, Maas H, Nguyen L, Karlsson MO. Model of chemotherapy-induced myelosuppression with parameter consistency across drugs. J Clin Oncol. 2002 Dec 15;20(24):4713-21.
203. Mentre F., Baccar D. Optimal design in random-effects regression models. Biometrika. 1997;84:429-42.
204. Retout S, Mentre F. Further developments of the Fisher information matrix in nonlinear mixed effects models with evaluation in population pharmacokinetics. Journal of biopharmaceutical statistics. 2003 May;13(2):209-27.

205. Tod M, Rocchisani JM. Comparison of ED, EID, and API criteria for the robust optimization of sampling times in pharmacokinetics. Journal of pharmacokinetics and biopharmaceutics. 1997 Aug;25(4):515-37.
206. Duffull SB, Mentre F, Aarons L. Optimal design of a population pharmacodynamic experiment for ivabradine. Pharmaceutical research. 2001 Jan;18(1):83-9.
207. Hennig S, Nyberg J, Fanta S, Backman JT, Hoppu K, Hooker AC, et al. Application of the optimal design approach to improve a pretransplant drug dose finding design for ciclosporin. J Clin Pharmacol. 2012 Mar;52(3):347-60.
208. Nyberg J, Karlsson MO, Hooker AC. Simultaneous optimal experimental design on dose and sample times. J Pharmacokinet Pharmacodyn. 2009 Apr;36(2):125-45.
209. Park K, Verotta D, Gupta SK, Sheiner LB. Use of a pharmacokinetic/pharmacodynamic model to design an optimal dose input profile. Journal of pharmacokinetics and biopharmaceutics. 1998 Aug;26(4):471-92.
210. Gaillot J, Steimer JL, Mallet AJ, Thebault JJ, Bieder A. A priori lithium dosage regimen using population characteristics of pharmacokinetic parameters. Journal of pharmacokinetics and biopharmaceutics. 1979 Dec;7(6):579-628.
211. Holford N, Ma SC, Ploeger BA. Clinical trial simulation: a review. Clin Pharmacol Ther. 2010 Aug;88(2):166-82.
212. Sheiner LB, Steimer JL. Pharmacokinetic/pharmacodynamic modeling in drug development. Annu Rev Pharmacol Toxicol. 2000;40:67-95.
213. FDA. Challenge and Opportunity on Critical Path to New Medical Products. Department of Health and Human Services (US). Food and Drug Administration. Available from:[http://www.fda.gov/oc/initiatives/criticalpath/whitepaper.pdf]. 2004.
214. Sheiner LB. Learning versus confirming in clinical drug development. Clin Pharmacol Ther. 1997 Mar;61(3):275-91.
215. Meibohm B, Derendorf H. Pharmacokinetic/pharmacodynamic studies in drug product development. Journal of pharmaceutical sciences. 2002 Jan;91(1):18-31.
216. Kopetz S, Overman M, Chang DZ, Glover KY, Shureiqi I, Wolff RA, et al. Systematic survey of therapeutic trials for metastatic colorectal cancer: room for improvement in the critical pathway. J Clin Oncol. 2008 Apr 20;26(12):2000-5.
217. Yang J, Liu A, Dougherty C, Chen X, Guzman R, Nandi S. Beware of contaminating mouse cells in human xenografts from nude mice. Anticancer research. 2000 May-Jun;20(3A):1635-9.
218. Eisenhauer EA, Therasse P, Bogaerts J, Schwartz LH, Sargent D, Ford R, et al. New response evaluation criteria in solid tumours: revised RECIST guideline (version 1.1). Eur J Cancer. 2009 Jan;45(2):228-47.
219. Veyrat-Follet C, Bruno R, Olivares R, Rhodes GR, Chaikin P. Clinical trial simulation of docetaxel in patients with cancer as a tool for dosage optimization. Clin Pharmacol Ther. 2000 Dec;68(6):677-87.
220. Tsukamoto Y, Kato Y, Ura M, Horii I, Ishikawa T, Ishitsuka H, et al. Investigation of 5-FU disposition after oral administration of capecitabine, a triple-prodrug of 5-FU, using a

physiologically based pharmacokinetic model in a human cancer xenograft model: comparison of the simulated 5-FU exposures in the tumour tissue between human and xenograft model. Biopharmaceutics & drug disposition. 2001 Jan;22(1):1-14.

221. Lankelma J, Fernandez Luque R, Dekker H, Schinkel W, Pinedo HM. A mathematical model of drug transport in human breast cancer. Microvasc Res. 2000 Jan;59(1):149-61.

222. Honorat M, Falson P, Terreux R, Di Pietro A, Dumontet C, Payen L. Multidrug resistance ABC transporter structure predictions by homology modeling approaches. Current drug metabolism. 2011 Mar;12(3):268-77.

223. Salphati L, Plise EG, Li G. Expression and activity of the efflux transporters ABCB1, ABCC2 and ABCG2 in the human colorectal carcinoma cell line LS513. Eur J Pharm Sci. 2009 Jun 28;37(3-4):463-8.

224. Sandler A, Gordon M, De Alwis DP, Pouliquen I, Green L, Marder P, et al. A Phase I trial of a potent P-glycoprotein inhibitor, zosuquidar trihydrochloride (LY335979), administered intravenously in combination with doxorubicin in patients with advanced malignancy. Clin Cancer Res. 2004 May 15;10(10):3265-72.

225. Lancet JE, Baer MR, Duran GE, List AF, Fielding R, Marcelletti JF, et al. A phase I trial of continuous infusion of the multidrug resistance inhibitor zosuquidar with daunorubicin and cytarabine in acute myeloid leukemia. Leuk Res. 2009 Aug;33(8):1055-61.

226. Rubin EH, de Alwis DP, Pouliquen I, Green L, Marder P, Lin Y, et al. A phase I trial of a potent P-glycoprotein inhibitor, Zosuquidar.3HCl trihydrochloride (LY335979), administered orally in combination with doxorubicin in patients with advanced malignancies. Clin Cancer Res. 2002 Dec;8(12):3710-7.

227. Ross DD, Yang W, Abruzzo LV, Dalton WS, Schneider E, Lage H, et al. Atypical multidrug resistance: breast cancer resistance protein messenger RNA expression in mitoxantrone-selected cell lines. J Natl Cancer Inst. 1999 Mar 3;91(5):429-33.

228. Davidian M, Giltinan D, Cox DR. Nonlinear models for repeated measurements data. 1995.

229. Beal S, Sheiner LB, Boeckmann A, & Bauer RJ. NONMEM User's Guides. (1989-2009), . Icon Development Solutions, Ellicott City, MD, USA,. 2009.

230. Mentre F, Escolano S. Prediction discrepancies for the evaluation of nonlinear mixed-effects models. J Pharmacokinet Pharmacodyn. 2006 Jun;33(3):345-67.

231. Jonsson EN, Karlsson MO. Xpose--an S-PLUS based population pharmacokinetic/pharmacodynamic model building aid for NONMEM. Comput Methods Programs Biomed. 1999 Jan;58(1):51-64.

232. Lindbom L, Pihlgren P, Jonsson EN. PsN-Toolkit--a collection of computer intensive statistical methods for non-linear mixed effect modeling using NONMEM. Comput Methods Programs Biomed. 2005 Sep;79(3):241-57.

233. Jang SH, Wientjes MG, Au JL. Kinetics of P-glycoprotein-mediated efflux of paclitaxel. J Pharmacol Exp Ther. 2001 Sep;298(3):1236-42.

234. Chem Spider. http://wwwchemspidercom/.

235. Perego P, De Cesare M, De Isabella P, Carenini N, Beggiolin G, Pezzoni G, et al. A novel 7-modified camptothecin analog overcomes breast cancer resistance protein-associated resistance in a mitoxantrone-selected colon carcinoma cell line. Cancer Res. 2001 Aug 15;61(16):6034-7.
236. Patel KJ, Tannock IF. The influence of P-glycoprotein expression and its inhibitors on the distribution of doxorubicin in breast tumors. BMC Cancer. 2009;9:356.
237. Tunggal JK, Cowan DS, Shaikh H, Tannock IF. Penetration of anticancer drugs through solid tissue: a factor that limits the effectiveness of chemotherapy for solid tumors. Clin Cancer Res. 1999 Jun;5(6):1583-6.
238. Baguley BC, Finlay GJ. Pharmacokinetic/cytokinetic principles in the chemotherapy of solid tumours. Clin Exp Pharmacol Physiol. 1995 Nov;22(11):825-8.
239. Gottesman MM, Fojo T, Bates SE. Multidrug resistance in cancer: role of ATP-dependent transporters. Nat Rev Cancer. 2002 Jan;2(1):48-58.
240. Juranka PF, Zastawny RL, Ling V. P-glycoprotein: multidrug-resistance and a superfamily of membrane-associated transport proteins. FASEB J. 1989 Dec;3(14):2583-92.
241. Friedenberg WR, Rue M, Blood EA, Dalton WS, Shustik C, Larson RA, et al. Phase III study of PSC-833 (valspodar) in combination with vincristine, doxorubicin, and dexamethasone (valspodar/VAD) versus VAD alone in patients with recurring or refractory multiple myeloma (E1A95): a trial of the Eastern Cooperative Oncology Group. Cancer. 2006 Feb 15;106(4):830-8.
242. Baer MR, George SL, Dodge RK, O'Loughlin KL, Minderman H, Caligiuri MA, et al. Phase 3 study of the multidrug resistance modulator PSC-833 in previously untreated patients 60 years of age and older with acute myeloid leukemia: Cancer and Leukemia Group B Study 9720. Blood. 2002 Aug 15;100(4):1224-32.
243. Greenberg PL, Lee SJ, Advani R, Tallman MS, Sikic BI, Letendre L, et al. Mitoxantrone, etoposide, and cytarabine with or without valspodar in patients with relapsed or refractory acute myeloid leukemia and high-risk myelodysplastic syndrome: a phase III trial (E2995). J Clin Oncol. 2004 Mar 15;22(6):1078-86.
244. Saeki T, Nomizu T, Toi M, Ito Y, Noguchi S, Kobayashi T, et al. Dofequidar fumarate (MS-209) in combination with cyclophosphamide, doxorubicin, and fluorouracil for patients with advanced or recurrent breast cancer. J Clin Oncol. 2007 Feb 1;25(4):411-7.
245. Rottenberg S, Nygren AO, Pajic M, van Leeuwen FW, van der Heijden I, van de Wetering K, et al. Selective induction of chemotherapy resistance of mammary tumors in a conditional mouse model for hereditary breast cancer. Proc Natl Acad Sci U S A. 2007 Jul 17;104(29):12117-22.
246. Franke RM, Sparreboom A. Drug transporters: recent advances and therapeutic applications. Clin Pharmacol Ther. 2010 Jan;87(1):3-7.
247. Robey RW, Massey PR, Amiri-Kordestani L, Bates SE. ABC transporters: unvalidated therapeutic targets in cancer and the CNS. Anticancer Agents Med Chem. 2010 Oct 1;10(8):625-33.

248. Kaneda N, Nagata H, Furuta T, Yokokura T. Metabolism and pharmacokinetics of the camptothecin analogue CPT-11 in the mouse. Cancer Res. 1990 Mar 15;50(6):1715-20.
249. Hertzberg RP, Caranfa MJ, Hecht SM. On the mechanism of topoisomerase I inhibition by camptothecin: evidence for binding to an enzyme-DNA complex. Biochemistry. 1989 May 30;28(11):4629-38.
250. Tanizawa A, Fujimori A, Fujimori Y, Pommier Y. Comparison of topoisomerase I inhibition, DNA damage, and cytotoxicity of camptothecin derivatives presently in clinical trials. J Natl Cancer Inst. 1994 Jun 1;86(11):836-42.
251. Comets E, Brendel K, Mentre F. Computing normalised prediction distribution errors to evaluate nonlinear mixed-effect models: the npde add-on package for R. Comput Methods Programs Biomed. 2008 May;90(2):154-66.
252. Sostelly A, Payen L, Guitton J, Di Pietro A, Falson P, Honorat M, et al. A template model for studying anticancer drug efflux transporter inhibitors in-vitro. Fundamental and Clinical Pharmacology. 2012.
253. Sato Y. Persistent vascular normalization as an alternative goal of anti-angiogenic cancer therapy. Cancer Sci. 2011 Jul;102(7):1253-6.
254. Sostelly A, Payen L, Guitton J, Di Pietro A, Falson P, Boumendjel A, et al. A template model for studying anticancer drug efflux inhibitors in vitro. Groupe de Métabolisme et Pharmacocinétique; 2011; Paris. GMP; 2011.
255. Yanase K, Tsukahara S, Asada S, Ishikawa E, Imai Y, Sugimoto Y. Gefitinib reverses breast cancer resistance protein-mediated drug resistance. Mol Cancer Ther. 2004 Sep;3(9):1119-25.
256. Elkind NB, Szentpetery Z, Apati A, Ozvegy-Laczka C, Varady G, Ujhelly O, et al. Multidrug transporter ABCG2 prevents tumor cell death induced by the epidermal growth factor receptor inhibitor Iressa (ZD1839, Gefitinib). Cancer Res. 2005 Mar 1;65(5):1770-7.
257. Goteti K, Garner CE, Utley L, Dai J, Ashwell S, Moustakas DT, et al. Preclinical pharmacokinetic/pharmacodynamic models to predict synergistic effects of co-administered anti-cancer agents. Cancer Chemother Pharmacol. 2010
Jul;66(2):245-54.
258. Buyse M, Burzykowski T, Carroll K, Michiels S, Sargent DJ, Miller LL, et al. Progression-free survival is a surrogate for survival in advanced colorectal cancer. J Clin Oncol. 2007 Nov 20;25(33):5218-24.
259. El-Maraghi RH, Eisenhauer EA. Review of phase II trial designs used in studies of molecular targeted agents: outcomes and predictors of success in phase III. J Clin Oncol. 2008 Mar 10;26(8):1346-54.
260. Ratain MJ, Eckhardt SG. Phase II studies of modern drugs directed against new targets: if you are fazed, too, then resist RECIST. J Clin Oncol. 2004 Nov 15;22(22):4442-5.
261. Lavin PT. An alternative model for the evaluation of antitumor activity. Cancer Clin Trials. 1981 Winter;4(4):451-7.

262. Karrison TG, Maitland ML, Stadler WM, Ratain MJ. Design of phase II cancer trials using a continuous endpoint of change in tumor size: application to a study of sorafenib and erlotinib in non small-cell lung cancer. J Natl Cancer Inst. 2007 Oct 3;99(19):1455-61.
263. Mentre FM, A.; Baccar, D. Optimal design in random-effects regression models. Biometrika. 1997;84:429-42.
264. Retout S, Mentre F, Bruno R. Fisher information matrix for non-linear mixed-effects models: evaluation and application for optimal design of enoxaparin population pharmacokinetics. Stat Med. 2002 Sep 30;21(18):2623-39.
265. Hennig S, Nyberg J, Hooker AC, Karlsson MO. Trial treatment length optimization with an emphasis on disease progression studies. J Clin Pharmacol. 2009 Mar;49(3):323-35.
266. Hoff PM, Ansari R, Batist G, Cox J, Kocha W, Kuperminc M, et al. Comparison of oral capecitabine versus intravenous fluorouracil plus leucovorin as first-line treatment in 605 patients with metastatic colorectal cancer: results of a randomized phase III study. J Clin Oncol. 2001 Apr 15;19(8):2282-92.
267. Van Cutsem E, Twelves C, Cassidy J, Allman D, Bajetta E, Boyer M, et al. Oral capecitabine compared with intravenous fluorouracil plus leucovorin in patients with metastatic colorectal cancer: results of a large phase III study. J Clin Oncol. 2001 Nov 1;19(21):4097-106.
268. Van Cutsem E, Findlay M, Osterwalder B, Kocha W, Dalley D, Pazdur R, et al. Capecitabine, an oral fluoropyrimidine carbamate with substantial activity in advanced colorectal cancer: results of a randomized phase II study. J Clin Oncol. 2000 Mar;18(6):1337-45.
269. Retout S, Duffull S, Mentre F. Development and implementation of the population Fisher information matrix for the evaluation of population pharmacokinetic designs. Comput Methods Programs Biomed. 2001 May;65(2):141-51.
270. MATLAB. MATLAB. Natick, MA: The Mathworks Inc; 2011.
271. Nyberg JU, S.; Karllson, M.O.; Hooher, A.C. popED v2.11. In: http://poped.souceforge.net, editor.; 2011.
272. Nyberg J, Ueckert S, Stromberg EA, Hennig S, Karlsson MO, Hooker AC. PopED: An extended, parallelized, nonlinear mixed effects models optimal design tool. Comput Methods Programs Biomed. 2012 May 26.
273. Paule I, Tod M, Henin E, You B, Freyer G, Girard P. Dose adaptation of capecitabine based on individual prediction of limiting toxicity grade: evaluation by clinical trial simulation. Cancer Chemother Pharmacol. 2011 Feb;69(2):447-55.
274. Maloney A, Karlsson MO, Simonsson US. Optimal adaptive design in clinical drug development: a simulation example. J Clin Pharmacol. 2007 Oct;47(10):1231-43.
275. Zamuner S, Di Iorio VL, Nyberg J, Gunn RN, Cunningham VJ, Gomeni R, et al. Adaptive-optimal design in PET occupancy studies. Clin Pharmacol Ther. 2010 May;87(5):563-71.
276. Jackson TL. Intracellular accumulation and mechanism of action of doxorubicin in a spatio-temporal tumor model. J Theor Biol. 2003 Jan 21;220(2):201-13.

277. Rowland M, Balant L, Peck C. Physiologically based pharmacokinetics in Drug Development and Regulatory Science: a workshop report (Georgetown University, Washington, DC, May 29-30, 2002). AAPS J. 2004;6(1):56-67.
278. West GB, Brown JH, Enquist BJ. The fourth dimension of life: fractal geometry and allometric scaling of organisms. Science. 1999 Jun 4;284(5420):1677-9.
279. Herman AB, Savage VM, West GB. A quantitative theory of solid tumor growth, metabolic rate and vascularization. PLoS One. 2011;6(9):e22973.
280. Bradley G, Ling V. P-glycoprotein, multidrug resistance and tumor progression. Cancer Metastasis Rev. 1994 Jun;13(2):223-33.